HAMBURGER WASSERBAU-SCHRIFTEN
Herausgegeben von Prof. Dr.-Ing. Peter Fröhle
2025

Yohannis Birhanu Tadesse

Integrated Modelling of Riverine Levee Breaches and Subsequent Inundation of Protected Areas

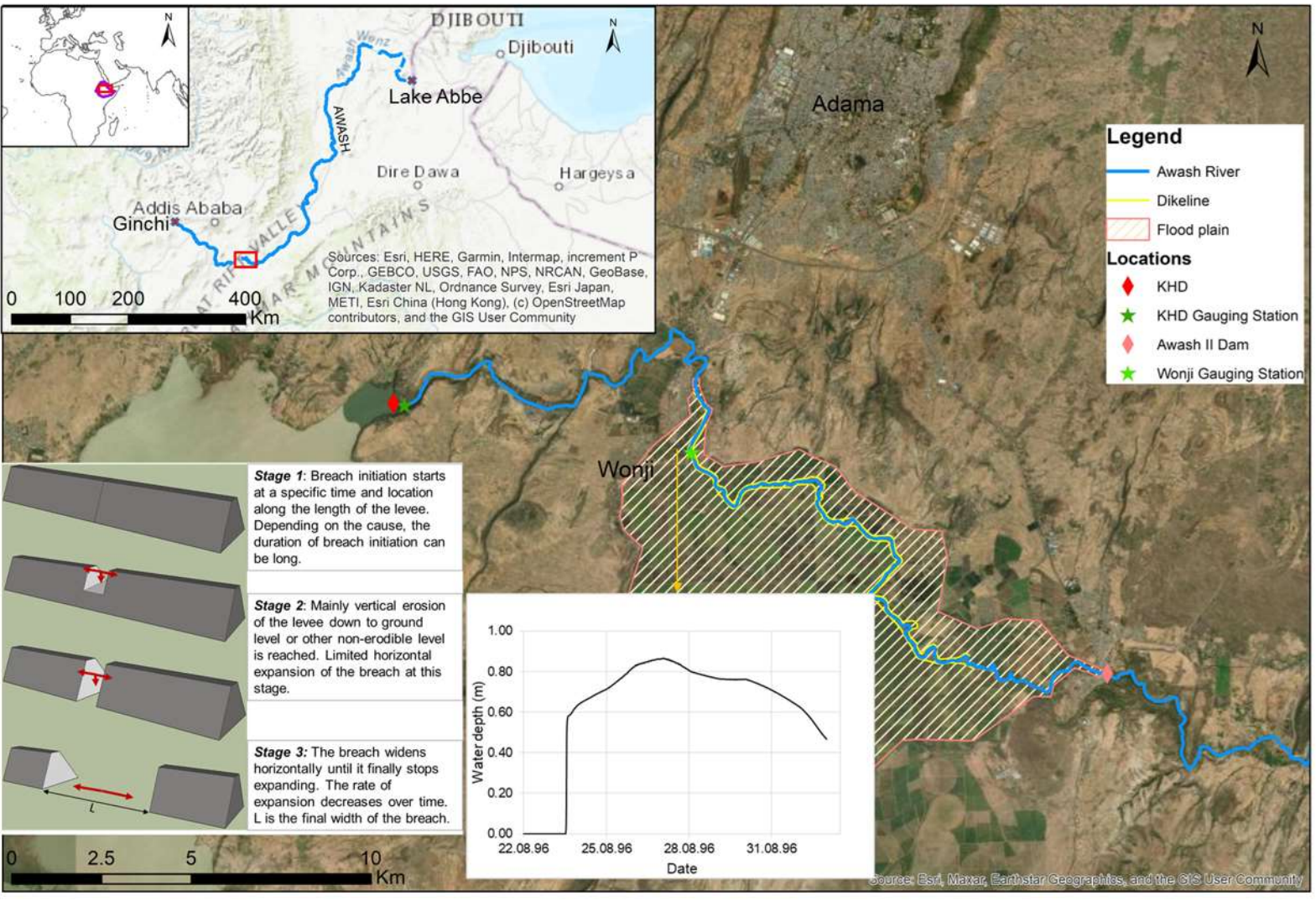

WASSERBAU
River and Coastal Engineering

Integrated Modelling of Riverine Levee Breaches and Subsequent Inundation of Protected Areas

Dissertation (monograph) approved by the
Doctoral Degree Committee of
Hamburg University of Technology
in pursuit of the academic degree of

Doctor of Engineering (Dr.-Ing.)

written by
Yohannis Birhanu Tadesse

from

Arsi Robe (Ethiopia)

2025

1. Reviewer: Prof. Dr.- Ing. Peter Fröhle
2. Reviewer: Prof. Dr.-Ing Reinhard Hinkelmann

Date of the oral examination: 17.05.2024

DOI: https://doi.org/10.15480/882.14128

Yohannis Birhanu Tadesse https://orcid.org/0000-0002-1514-7270

Integrated Modelling of Riverine Levee Breaches and Subsequent Inundation of Protected Areas

By

Yohannis Birhanu Tadesse

Edited by

P. Fröhle

Hamburg University of Technology

Institute of River and Coastal Engineering

Vorwort des Herausgebers

Die Besiedlung durch Menschen entwickelt sich seit Urzeiten entlang von Gewässern. Hier fanden und finden die Menschen, was sie zum Leben benötigen: Wasser und Nahrung durch fruchtbare Böden und Tiere. Zudem bieten Flüsse ideale Möglichkeiten zum Transport von Waren. Daher entwickelten sich mit der Zeit kleine und große Städte an Flüssen.

Zum Schutz der besiedelten und / oder anderweitig vom Menschen genutzten Flächen vor den Folgen von Hochwasserabflüssen wurden und werden entlang der Flüsse vielfach Dammbauwerke / Deiche gebaut. Heutzutage werden Deiche gegen festzulegende Bemessungsgrößen bemessen und bestehen meist aus lokal verfügbaren Materialien (Böden). Die Deich-Deckschicht wird in vielen Länder begrünt und häufig nicht besonders konstruktiv befestigt beispielsweise durch ein Deckwerk. Zudem treten an Deichen wie an jedem anderen Bauwerk auch Alterungsprozesse und Abnutzungserscheinungen auf. Daher müssen Deiche entsprechend unterhalten werden.

Trotz des Schutzes durch Deiche kommt es immer wieder zu mehr oder weniger verheerenden Überschwemmungen, wie Beispiele weltweit immer wieder zeigen. Auslöser sind i) Ereignisse, die von den Abflüssen und Wasserständen her oberhalb der angesetzten Werte für das Bemessungshochwasser liegen, ii) die Unterschätzung der resultierenden hydraulischen und hydrodynamischen Belastungen und/oder iii) Schäden an den Deichen, die nicht erkannt oder nicht repariert wurden. Beispiele hierfür gibt es zuhauf.

An diesem Punkt setzt die im 27. Band der Hamburger Wasserbauschriften veröffentlichte Arbeit von Herrn Dr. Yohannis Birhanu Tadesse mit dem Titel „Integrated Modelling of Riverine Levee Breaches and Subsequent Inundation of Protected Areas“ an. Herr Dr. Tadesse verfolgt mit seiner Arbeit das Ziel, einen integrierten Ansatz zur Modellierung von Überschwemmungen als Folge von Deichbrüchen zu entwickeln und die Anwendbarkeit des Ansatzes exemplarisch an einem real-world Beispiel zu erproben. Dazu war es erforderlich, ein geeignetes Deichbruchmodell zu entwickeln und dieses Deichbruchmodell in ein hydrodynamisches numerisches Modell zu integrieren. Hierbei muss das hydrodynamisch-numerische Modell natürlich in der Lage sein, die komplexen Strömungsbedingungen beim Deichbruch und bei der Überflutung des Hinterlands hinreichend genau abzubilden. Zudem soll das integrierte Modell ein breites Anwendungsspektrum abdecken.

Herr Dr. Tadesse hat eine äußerst runde Dissertation mit sehr schönen Ergebnissen abgeliefert und die Kenntnisse in einem der wesentlichen Themengebiete im Zusammenhang mit Hochwasserschutz und Risikomanagement in überschwemmungsgefährdeten Gebieten – die integrierte Modellierung extremer Lastfälle unter Einschluss der Simulation von Deichbrüchen – deutlich verbessert. Die Arbeit enthält viele wichtige Aspekte zu den Themen Deichversagen sowie integrierte Modellierung von

Deichbrüchen und resultierenden Überschwemmungen und wird sicher auf ein breites Interesse in der Fachwelt stoßen.

Hamburg, 02. Januar 2025

Peter Fröhle
Leiter des Instituts für Wasserbau der Technischen Universität Hamburg

Foreword by the editor

Human settlement has developed along rivers and lakes since time immemorial. Here were the places where people found and still find what they need to live: Water and food through fertile soils and animals. Rivers also offer ideal opportunities for the transportation of goods. This is the reason why small and large towns developed along rivers over time.

To protect populated and/or other areas used by humans from the consequences of flood run-off, dams / dikes were and are widely built along rivers. Dikes are usually made of locally available materials (soils) and are nowadays frequently designed against specified design events. In many countries, the dike surface layer is vegetated with grasses and is often not particularly structurally reinforced, for example by a revetment. In addition, dikes, like any other structure, are subject to ageing processes and wear and tear. Dikes must therefore be maintained accordingly.

Despite the protection provided by dikes, more or less devastating floods occur again and again, as examples worldwide repeatedly show. The causes are i) events with discharges and water levels above the values estimated for the design event, ii) underestimation of the resulting hydraulic and hydrodynamic loads and/or iii) damage to the dikes has not been detected and repaired. There are plenty of examples of such cases.

This is where the work of Dr. Yohannis Birhanu Tadesse entitled “Integrated Modelling of Riverine Levee Breaches and Subsequent Inundation of Protected Areas”, published in the 27th volume of the Hamburger Wasserbauschriften, comes in. The aim of Dr. Tadesse's work is to develop an integrated approach to modelling floods as a result of levee breaches and to test the applicability of the approach using a real-world example. For this purpose, it was necessary to develop an appropriate dike breach model and to integrate this dike breach model into a hydrodynamic numerical model. Of course, the hydrodynamic-numerical model must be able to reproduce the complex flow conditions during dike breaches and the flooding of the hinterland with sufficient accuracy. In addition, the integrated model should cover a wide range of applications.

Dr. Tadesse has delivered an extremely comprehensive dissertation with very important results and has significantly improved the knowledge in one of the essential topics related to flood protection and risk management in flood-prone areas - the integrated modeling of extreme load cases including the simulation of dike breaches. The work contains many important aspects on the topics related to dike failures as well as on topics related to the integrated modelling of dike breaches and resulting floods and will certainly be of great interest to experts.

Hamburg, 02 January 2025

Peter Fröhle

Institute of River and Coastal Engineering, Hamburg University of Technology

Acknowledgment

This PhD endeavor began with an IPSWaT[1] scholarship from BMBF[2], and I am deeply grateful to the BMBF for providing me with this invaluable opportunity.

My sincere thanks go to Prof. Dr.-Ing Peter Fröhle for funding my work and keeping me in the group after my scholarship ended – without which it would have been impossible to complete this thesis. Furthermore, your constant guidance, encouragement and support have been invaluable.

I am also sincerely grateful to Prof. Dr.-Ing Reinhard Hinkelmann for agreeing to be my second examiner and for thoroughly reading the final version of the manuscript. Your thoughtful and detailed feedback has greatly improved the readability of this thesis.

To my current and former colleagues, I thank you for the good times, the coffee and tea breaks, and your helpful comments during our PhD workshops and other discussions. These exchanges have been both enjoyable and intellectually enriching.

I would also like to thank my friends near and far for their encouragement and support. Special thanks go to Anju for reading my draft manuscript and providing invaluable insights.

My infinite gratitude also goes to my family – my wife Serki, my daughter Fenet and my son Ben – for their unwavering support, constant encouragement and for being my source of motivation. Your love and presence have brought balance to my work and life, and I am deeply grateful for everything you have done to make this journey possible.

Finally, my deepest thanks go to my parents, especially my mother, for ensuring that I received an education, a privilege not always guaranteed in the part of the world where I was born. Your sacrifices have made this achievement possible and I am forever grateful.

Hamburg, January 2025

Yohannis Birhanu Tadesse

[1] International Postgraduate Studies in Water Technologies
[2] Bundesministerium für Bildung und Forschung (German Federal Ministry of Education and Research)

Abstract

Levees are earthen embankments, often constructed from locally available soil material, used to contain floodwaters in rivers. Levee design standards have improved over time, contributing to their reliability in providing flood protection. However, levees never provide absolute flood protection. The preparation of flood hazard maps for areas behind levees is therefore indispensable. Flood hazard maps can be produced using hydrodynamic numerical models that simulate flood inundation. The modelling of flood inundation due to levee breaching involves the modelling of two processes: i) the breaching of the levee and ii) the propagation of the flood through the resulting opening into the hinterland.

This thesis proposes the modelling of flood inundation due to levee breach with a 2D hydrodynamic numerical model with an integrated parametric levee breach model. To model levee breaching, a parametric levee breach model is developed, which is based on analyses of physical levee breaching experiments and of real levee breaches. The breach model is then integrated into the hydrodynamic numerical model Telemac-2D, a publicly available code for modelling flood propagation.

The thesis also developed methods for estimating the parameters of the parametric breach model based on historical (available) levee breach data. Regression fitting for the final breach width is performed using multiple linear regression, multiple non-linear regression and artificial neural networks. In addition, an approach is developed to estimate a possible breach location based on flood characteristics (water level and flood duration), geometric and geological characteristics of the levee in question and its foundation, the cause of the breach, and information from historical levee breaches on their breach location.

By re-modelling physical laboratory tests simulating levee breaching, this work has demonstrated that the hydrodynamic numerical model, Telemac-2D, is a suitable tool for modelling flood inundation due to levee breaching. The flood inundation caused by the levee breach on the Awash River at Wonji, Ethiopia in August 1996 could be reproduced using the proposed integrated approach. Furthermore, the determination of the breach location for this levee breach case using the approach proposed in this thesis resulted in the same location as the actual breach location, demonstrating the general applicability of the approach.

The uncertainties associated with the models used are also discussed. To demonstrate the uncertainty associated with the breach model, the sensitivity of flood inundation depth and breach discharge to variation of the levee breach parameters is systematically analysed using the August 1996 Awash River levee breach flood event at Wonji, Ethiopia.

Zusammenfassung

Deiche sind Erddämme, die häufig aus lokal verfügbarem Bodenmaterial errichtet werden und dazu dienen, Hochwasser von Flüssen zurückzuhalten. Die Baunormen für Deiche haben sich im Laufe der Zeit verbessert, was zu ihrer Zuverlässigkeit beim Hochwasserschutz beigetragen hat. Deiche bieten jedoch keinen absoluten Hochwasserschutz. Die Erstellung von Hochwassergefahrenkarten für Gebiete hinter Deichen ist daher unerlässlich. Hochwassergefahrenkarten können mit Hilfe von hydrodynamischen numerischen Modellen erstellt werden, die die Überflutung simulieren. Bei der Modellierung von Überflutungen infolge eines Deichbruchs werden zwei Prozesse modelliert: (i) der Deichbruch und (ii) die Ausbreitung des Hochwassers durch die entstandene Öffnung ins Hinterland.

In dieser Arbeit wird die Modellierung von Überflutungen infolge von Deichbrüchen mit einem 2D-hydrodynamischen numerischen Modell mit einem integrierten parametrischen Deichbruchmodell vorgeschlagen. Für die Modellierung von Deichbrüchen wird ein parametrisches Deichbruchmodell entwickelt, das auf der Analyse von physikalischen Deichbruchexperimenten und realen Deichbrüchen basiert. Das Bruchmodell wird dann in das hydrodynamische numerische Modell Telemac-2D integriert. Telemac-2D ist ein frei verfügbarer Code zur Modellierung der Hochwasserausbreitung.

Im Rahmen dieser Arbeit wurden auch Methoden zur Schätzung der Parameter des parametrischen Bruchmodells auf der Grundlage historischer (verfügbarer) Deichbruchdaten entwickelt. Insbesondere wurde eine Regressionsanpassung für die finale Durchbruchsbreite mittels multipler linearer Regression, multipler nichtlinearer Regression und künstlicher neuronaler Netze durchgeführt. Darüber hinaus wird ein Ansatz entwickelt, um eine mögliche Bruchstelle auf der Grundlage von Hochwassereigenschaften (Wasserstand und Hochwasserdauer), geometrischen und geologischen Eigenschaften des betroffenen Deichs und seines Fundaments, der Ursache des Bruchs und Informationen aus historischen Deichbrüchen über deren Bruchstelle zu schätzen.

Durch die Nachbildung physikalischer Laborexperimente, in denen ein Deichbruch simuliert wurde, konnte in dieser Arbeit gezeigt werden, dass das hydrodynamische numerische Modell Telemac-2D ein geeignetes Modell für die Modellierung von Überflutungen infolge von Deichbrüchen ist. Die durch den Deichbruch am Awash River in Wonji, Äthiopien, im August 1996 verursachte Überschwemmung konnte mit dem vorgeschlagenen integrierten Ansatz reproduziert werden. Darüber hinaus wurde mit dem in dieser Arbeit vorgeschlagenen Ansatz zur Bestimmung der Bruchstelle die tatsächliche Bruchstelle am Awash River bestimmt, was die allgemeine Anwendbarkeit des Ansatzes untermauert.

Die mit den verwendeten Modellen verbundenen Unsicherheiten werden ebenfalls diskutiert. Um die Unsicherheiten des Durchbruchmodells zu demonstrieren, wird die Sensitivität der Deichdurchbruchparameter auf die Berechnung der Überflutungstiefe und des Durchbruchabflusses anhand des Hochwasserereignisses vom August 1996 am Awash River in Wonji, Äthiopien, systematisch analysiert.

Table of Contents

1 Introduction

1.1 Background and motivation

Historically, floodplains along rivers have been reclaimed by humans because they provide the resources necessary for life: water and fertile soil. Over time, many floodplains have been transformed into agricultural fields, residential villages, towns and cities, manufacturing and industrial areas, valuable historical heritage sites, etc. In most cases, such reclaimed floodplains are protected from flooding by levees (CIRIA 2013).

Levees (also known as dikes or flood defence embankments) are earthen embankments, often constructed from locally available soil material, used to contain flood flows in rivers or other water bodies to protect people and their property in the hinterland from flooding (CIRIA 2013). They are linear structures built along riverbanks and are often very long. Figure 1 shows part of Awash River and its levees near Wonji, Ethiopia. Levees are widely used to protect floodplains along rivers. The protection provided by a levee is as good as the protection provided at the weakest point along its length (CIRIA 2013).

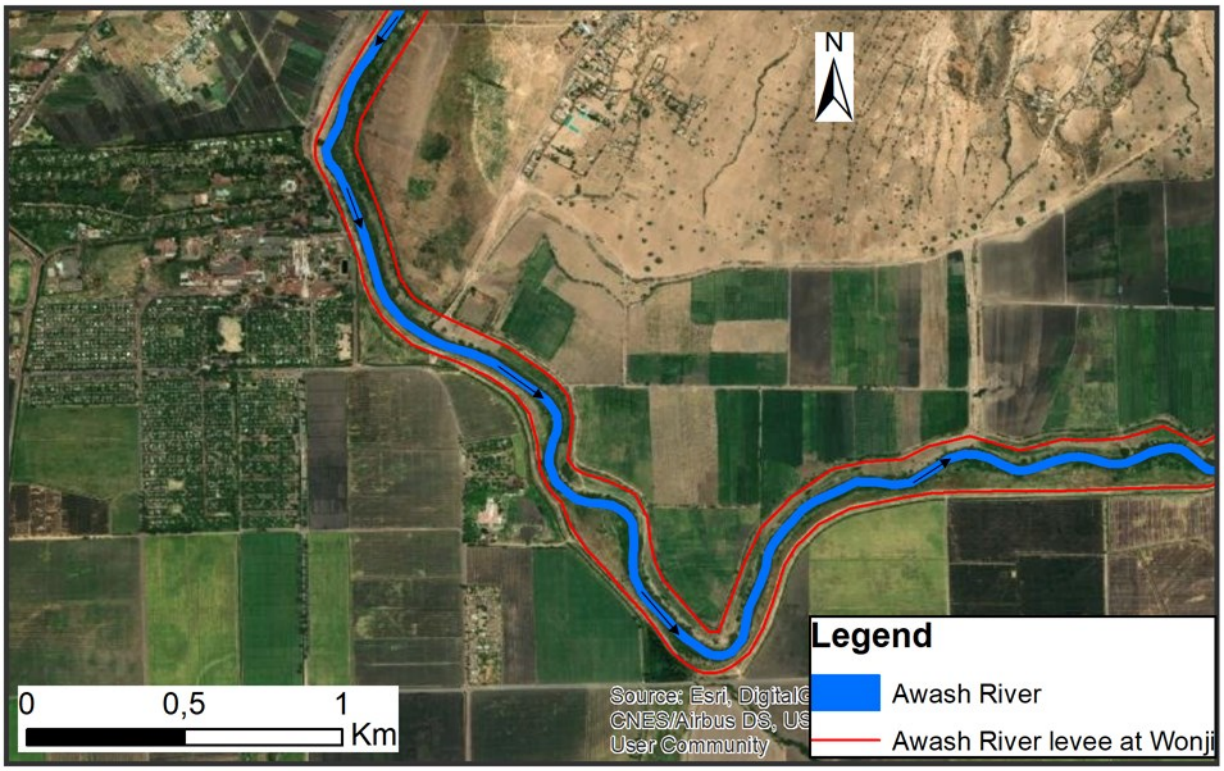

Figure 1: Part of the Awash River and its levees near Wonji, Ethiopia; arrows show direction of river flow (own image, background map courtesy of ESRI®, ArcGIS online service).

Levee design standards have improved over time, contributing to their reliability in providing flood protection. However, levees can never provide absolute flood protection (Merz et al. 2014). A number of recent flood disasters due to breaches of levees designed and constructed to the highest standards, such as the Elbe River levee breaches in 2002 and 2013, are good examples of the fact that levees do not provide absolute flood protection. Levees are designed to contain specified design flows, which are often determined based on extreme value analysis of past flood events. And these design flows can be exceeded at any time in the future. In addition, the probability of extreme flood events is projected to increase due to climate change (IPCC 2023). Furthermore, the levees themselves deteriorate over time (ASCE/EWRI 2011).

Flood disasters associated with levee breaches are therefore not uncommon, if not frequent. Levee breach floods often result in unprecedented economic losses and loss of life. Some historical levee breach flood disasters reported in the literature include the 1996 Wonji levee breach flood in Ethiopia (Ahrens (1996), Tadesse & Fröhle (2015)), the 2005 New Orleans flood in the USA (Sills et al. (2008), van Emelen et al. (2012)), the 2002 and 2013 levee breaches of the Elbe River and its tributaries in Germany (Merz et al. 2014), the Yangtze River levee breaches in China (Li et al. 2003), and others. To give just one example of the scale of losses, the flooding caused by the Elbe River levee breaches in 2013 resulted in the loss of 8 lives, economic damage of 12 billion euros, the evacuation of 52,000 people, the interruption of industrial production and traffic disruptions (Merz et al. 2014).

Public authorities are often required to prepare flood hazard maps and flood emergency plans for communities, businesses, and other stakeholders living in flood prone areas, including leveed areas (e.g., EU Floods Directive (EU 2007)). The task of flood zone mapping behind levees is challenging. If the floodplains are protected by levees, floodwater will not enter the area during most flood events. However, if the levees are breached, the floodplains will be inundated. In this case, the propagation of the floodwater and the consequences of the flood inundation depend on the nature of the levee breaches (such as the number of breaches, the locations of the breaches, the breaching processes, and the final breach dimensions of the breaches), the topography of the floodplain, the magnitude of the flood, and others. The modelling of flood inundation due to a levee breach must therefore include the modelling of (i) the levee breaching process and (ii) the propagation of the floodwater through the breach into the floodplain.

The modelling of the two processes can be done in a decoupled or coupled (integrated) manner (Coleman et al. 2002). In the first approach, the modelling of the levee breaching is decoupled from the modelling of flood inundation. First, the discharge hydrograph through the levee breach is determined using 1D overflow formulae and levee breach models, or an empirical relationship between the flow through the breach and the flow in the river channel (Wahl 1998). This discharge hydrograph is then used in a second step as a boundary condition for flood inundation mapping. For the flood mapping itself, a simple GIS-based approach of filling the floodplain with the volume of water from the discharge hydrograph or a more complex approach using a 2D hydrodynamic numerical model with the breach discharge hydrograph as a boundary condition is used. The second approach

is the integrated modelling of the levee breaching processes and the flood inundation (Roger et al. 2010). The flood inundation is modelled with a 2D hydrodynamic numerical model that has an integrated levee breach model that simultaneously models the levee breaching process.

The flow through a levee breach is at an angle to the main flow direction in the river (Roger et al. 2010). This makes it difficult to establish a universal equation to determine the flow through the breach from the flow in the main river. As a result, the decoupled approach can lead to inaccurate results. In addition, backwater flow from the floodplain into the river cannot be accounted for in the decoupled approach (Roger et al. 2010). On the other hand, in the integrated approach, the flow from the main river into the floodplain is calculated by the hydrodynamic numerical model used, based on the prevailing conditions, including possible backwater flow (Dazzi et al. 2019; Roger et al. 2010).

Therefore, modelling of flood inundation due to levee breach is better performed using a 2D hydrodynamic numerical model with an integrated levee breach model (Dazzi et al. (2019), Apel et al. (2009)). Although 2D hydrodynamic numerical flood modelling is a well-established discipline, its applicability to levee breach type flows, which could be supercritical flows, needs systematic verification. Currently available hydrodynamic numerical models are well tested for subcritical flows. While 2D hydrodynamic numerical flood modelling is a well-established subject (at least for subcritical flows and to some extent beyond that), levee breach modelling is still a research subject (Dazzi et al. (2019), ASCE/EWRI (2011)). There is no established approach for modelling levee breaching.

Nevertheless, we find a variety of breach models in the literature, which can be grouped into three main types: empirical, parametric and physically-based breach models (ASCE/EWRI 2011). Empirical breach models are a group of breach models derived from statistical best fit to historical breach data to estimate breach parameters such as breach peak discharge, breach width or depth. Parametric breach models describe the levee breaching process using parameters by making simplifying assumptions about the location, initiation, evolution, number, and shape of the levee breaches based on experience and past levee breaches. Breach parameters often include number of breaches, breach location, final breach width, final breach level, initial breach width, breach duration, and breach mechanism (Tadesse & Fröhle (2015), Dazzi et al. (2019)). Physically-based breach models use morphodynamic equations to model the levee breaching process (Dazzi et al. (2019)). They are typically integrated into a 2D hydrodynamic numerical model, i.e., these models couple 2D shallow water equations with sediment transport equations (such as the Meyer-Peter and Müller formula) and bed evolution equations (such as the Exner equations) (Canelas et al. 2013; Murillo & García-Navarro 2010; Li & Duffy 2011).

Although physically-based breach models are the correct approach from a physical point of view, their applicability to real cases is limited. Sediment transport and bed evolution equations have not been developed for levee breach flow conditions (Coleman et al. 2002). Furthermore, attempts to develop sediment transport and bed evolution equations (erosion laws) for levee breach conditions are limited to levee breaches due to overtopping flows (ASCE/EWRI 2011); they often require the use of parameters (e.g. erodibility parameter

(Dazzi et al. 2019)); and they are mainly tested with laboratory test cases. Therefore, parametric breach models, which are the next best approach from a physical point of view, are the appropriate breach models for modelling of real levee breaches.

1.2 Objectives

As highlighted above, and as will be discussed in more detail in Chapter 2, currently available methods for modelling levee breaching are often applied and tested for laboratory scale studies. They are inaccurate and have high uncertainties (see e.g. Mohamed et al. (2002)) for real levee breaches. As a result, the modelling of flood inundation due to levee breaches, and hence the estimation of the associated flood risk, would be inaccurate.

It is, thus, the objective of this research to develop and test an approach for modelling flood inundation due to real-world riverine levee breaches. For this purpose, it is necessary to develop a parametric levee breach model based on the results of physical experiments on levee breaching processes and real levee breaches in the literature, and to integrate the developed parametric levee breach model into a hydrodynamic numerical model. The latter enables an integrated modelling of levee breaching and flood inundation. Since the range of values for the parameters of a parametric levee breach model is large (Danka & Zhang 2015) and some breach parameters (e.g., breach location) are difficult to estimate, this research also aims to develop methods and guidelines for the estimation of breach parameters. The applicability of the approaches will be demonstrated using a laboratory levee breach test case and a real-world levee breach case.

Specifically, the research aims to:

- develop a parametric levee breach model based on results from physical experiments on levee breaching processes and real levee breaches in the literature,
- integrate the developed parametric breach model into a hydrodynamic numerical model to enable an integrated modelling of levee breaching and flood inundation,
- develop methods and guidelines for the estimation of breach parameters, and
- demonstrate the applicability of the approach using a laboratory levee breach test case as well as a real-world levee breach case.

1.3 Organisation of the thesis

The thesis is organised according to the research framework shown in Figure 2.

Chapter 2 reviews and analyses the literature on the causes of levee breaching, levee breaching processes and modelling of levee breaching. The governing mathematical equations for flood inundation modelling are presented in Chapter 3. The derivation of the shallow water equations, which are the governing mathematical equations for flood inundation modelling, from the Navier-Stokes equations is briefly discussed. Furthermore, the hydrodynamic numerical model Telemac-2D, which is used in this work, is described.

Chapter 4 presents a parametric levee breach model developed based on the results of the literature review in Chapter 2. The implementation of the breach model in Telemac-2D is also discussed.

Chapter 5 discusses methods for estimating levee breach parameters based on past levee breaches. Both regression fitting as well as artificial neural networks are used to estimate the final breach width. Chapter 6 presents an approach for estimating the location of a levee breach.

In Chapter 7, Telemac-2D is used to model a levee-breach type physical laboratory experiment to demonstrate the capacity of Telemac-2D to model levee-breach-type flows.

In Chapter 8, the approaches developed in this work for modelling flood inundation due to levee breaching are applied to the 1996 Awash River levee breach flood at Wonji, Ethiopia.

In Chapter 9, the uncertainties of the integrated approach are discussed, and the sensitivity of the levee breach model parameters are analysed.

Chapter 10 gives the conclusions of this work and areas for further research. The summary of the thesis is given in Chapter 11.

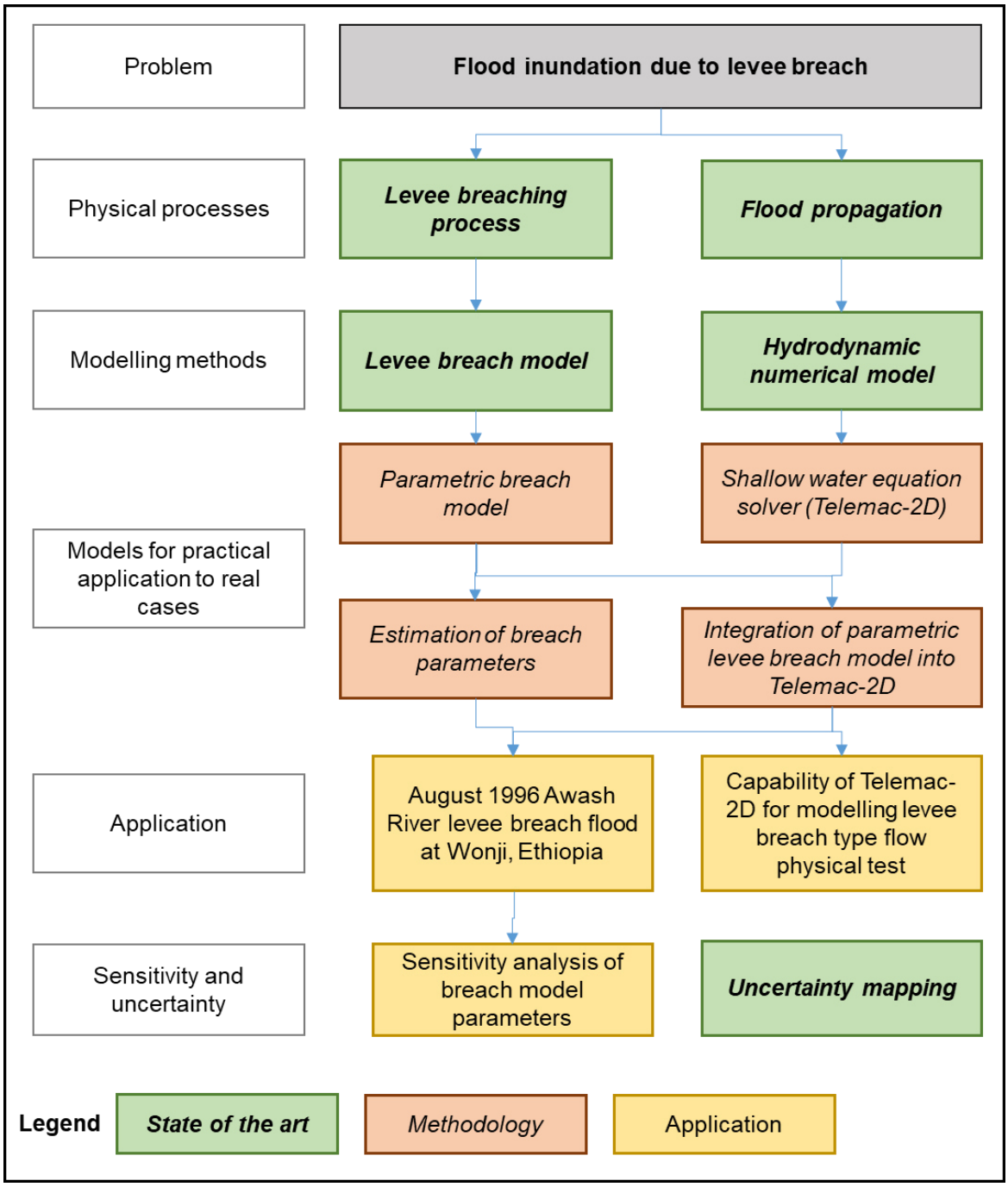

Figure 2: Framework of the research.

2 Levee breaching processes and modelling approaches

In this chapter, the state of the art on levee beaching processes and modelling approaches is given. Before that, the design of levees followed by the major causes of levee failures is discussed.

2.1 Design of levees

The design of levees plays an important role in the process of levee breaching. A common assumption in the design of levees is that these structures are under flood load only for few days in a year during flood events. If this is not the case, that is, if elongated loading period of river flow per year is expected, for example at downstream parts of large rivers where flood loading periods of several weeks can occur, other design standards such as those used for embankment reservoirs need to be considered (DWA 2011).

Designing of levees include determination of the properties of the available soil, dividing the levee into reaches of similar sections, and designing of the sections for each reach, and analysis of each section for seepage, slope stability, settlement, etc as required. Based on the results of the analysis of each section, revision in the design of the sections might be necessary (USACE 2000).

Many factors affect well-functioning of levees and need to be considered in the designing of levees. The factors differ from place to place and on the type and value of the items the levees protect from flooding. The main factors taken into consideration for design of the levee sections for each reach are design discharge and water level, embankment material, seepage through levee, seepage through foundation, slope stability, settlement, method of construction, etc (USACE 2000). Based on these and other factors, the engineer need to design the levee sections such as levee height, side slopes, and slope protection.

The design discharge and water level are fixed for each representative reach along the river length. They are usually fixed from statistical analysis of historical floods at the reach in question. From statistical analysis annual probability of occurrence of floods, also known as return period, is established. Then, based on the type and value of the property to be protected, the design discharge and water level are fixed. Standards adopted vary from region to region, as well as according to the type and value of property in the area to be protected.

Here are some examples used to fix the design discharge. In British Columbia, Canada, the standard design flood for levees is a 200-year return period flood (a flood with annual occurrence probability of 0.5%) at the river reach where the levee is to be built. A lower design flood flow of 50-year return period flood is used for the design of levees protecting agricultural land (GA & AE 2003).

The current recommendation in Germany is also to fix the design flood level based on mean statistical return period, which will depend on damage potential in case of flooding. It varies from design flood level corresponding 5 years return period for protection of agricultural area up to 500 years return period for protecting areas with exceptionally high damages in an event of flood (DWA 2011). The guideline prepared by NBI-ENTRO (2010) for Ethiopia outlines first the determination of the design discharge corresponding to return periods 25, 50, 100 years or higher depending on the type of area to be protected. Once the design flood discharge is fixed, the design flood level is estimated from the uniform flow equation (Manning's equation) using the design discharge, river cross- and longitudinal sections of the river reach in question.

Levee crest elevation at a given section of a levee reach is often fixed by adding a freeboard on the design flood level. The freeboard serves to account for water level increase due to wind surge, ice jam, and wave run-up. It also accounts for elevation changes due to future settlement. Like design flood level, freeboard is also fixed in different ways in different countries. U.S. Army Corps of Engineers recommends the use of risk based design in order to fix the height of levee and the use of free board is not necessary (USACE 2000). The German standard specifies the freeboard as the maximum of minimum free board and freeboard calculated as the sum of the components. The minimum freeboard is a function of levee class and levee height. In British Colombia, Canada, the freeboard is fixed depending on the type of design flood level. A freeboard of 0.3 m in combination with a design flood level based on instantaneous flood level or a freeboard of 0.6 m in combination with a design flood level based on maximum daily flow level have to be used (GA & AE 2003). The guideline in Ethiopia recommends a freeboard for wave run up calculated for a design wind speed of 30 m/s. For river widths in the range of 200 – 400 m, a minimum freeboard of 0.32 m is required (NBI-ENTRO 2010).

After fixing the levee height for a given reach of the levee, the cross-section of levee (levee profile) for the reach is determined. First the type of cross-section is fixed. One can choose between homogeneous (see Figure 3) and zoned (structured) (see Figure 4) levee cross-sections. Depending on the chosen type of cross-section, the cross-section of a levee is determined by levee crest, side slopes, and the arrangement of berms. The main components of a levee are shown in Figure 5.

The cross-sectional design depends primarily on the exerting loads, the levee construction material, and the subsoil conditions. A levee is designed in such a way that it is stable on the subsoil and in the cross-section for all load cases under consideration (DWA 2011). Levee crest width is designed based on the following factors: need to use it as a road, emergency needs such as flood emergency works and levee maintenance, future need for levee heightening, duration of flood flows to be protected by the levee, etc. U.S. Army Corps of Engineers (USACE 2000) recommends a minimum crest width of about 3.05 - 3.66 m for emergency needs and as determined by the road authorities if the levee crests is to be used as a road. DWA (2011) recommends a minimum levee crest width of 3 m. in addition, the levee crest should gently incline to the river direction (2% slope).

The other important design aspect is the design of the levee side slopes. Levee side slopes depend on the levee material, construction requirements, maintenance requirements, seepage, slope protection, and landscape design. Levee sides should in general have gentle slope, often gentler than 2:1 (horizontal (H):vertical(V)) to avoid sliding and sloughing by forces acting on the levee such as rain and seepage. A side slope of 3H:1V or flatter is generally sufficient (DWA 2011; GA & AE 2003). Seepage control requirements might require very gentle slopes. For example, for sand levees a side slope of 5H:1V is the steepest to prevent seepage through the levee (DWVK,1986).

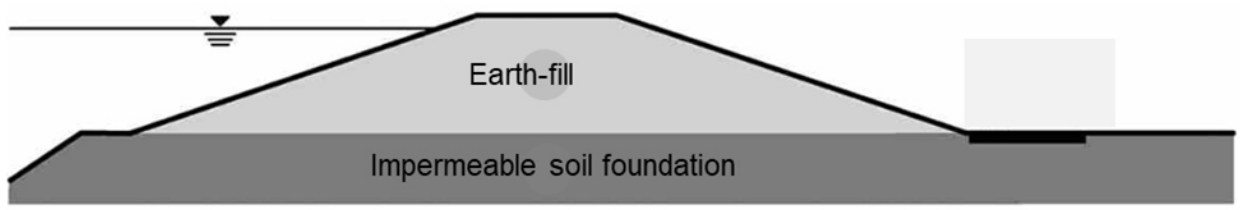

Figure 3: Cross-section of a homogeneous levee (Figure taken from DWA (2011, p. 18).

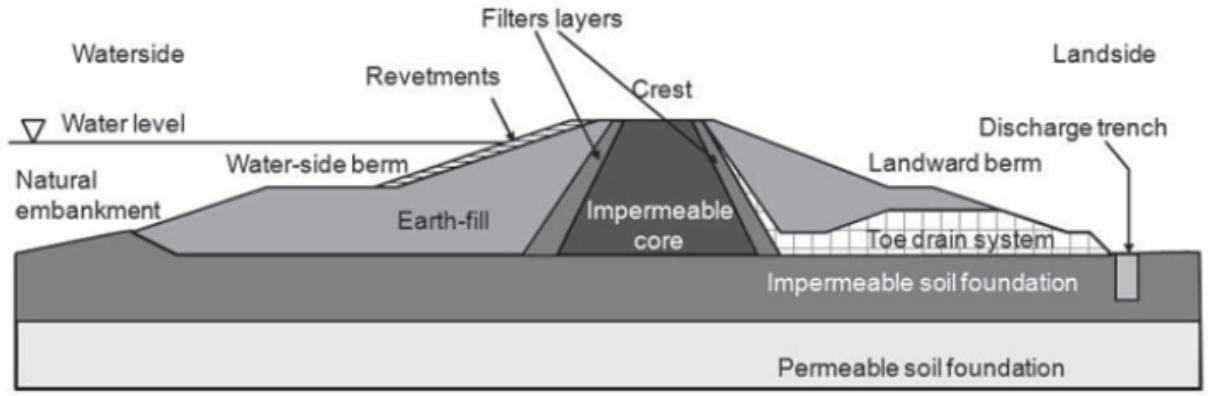

Figure 4: Main components of levee taken from CIRIA (2013, p. 86).

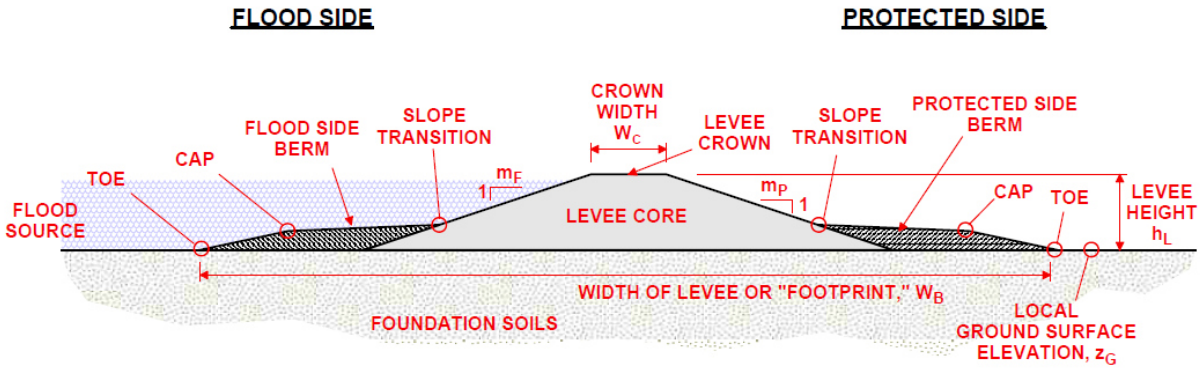

Figure 5: Definition of terms associated with levees (taken from Howard et al. (2009, p. 11)).

2.2 Causes of levee breach

In the context of flood risk reduction function of a levee, levee failure can be defined as the inability of the levee to confine flood water away from the protected area. This could be due to hydraulic (non-structural) or structural failure (CIRIA 2013, p. 156). Hydraulic failure includes through flow, overflow and overtopping of the levee without prior damage of the levee and before the design protection level. Structural failure is failure due to damage to the levee. However, failure types can be interdependent, i.e., hydraulic failure can induce structural failure and vice versa. A levee breach is a structural as well as a hydraulic failure.

Levee breach is damage to the structure that results in significant lowering of the crest or the creation of a significant opening through the levee body that would cause uncontrolled flow of water into the leveed area. This could be the failure of the levee body itself or the subsoil.

The most probable cause of a levee breach case can be identified using detailed fault trees available in the literature. Kortenhaus et al. (2002) developed a fault tree to point down the exact cause of an estuary and sea levee failure. Horlacher et al. (2007) developed a theoretic model to map the cause of river levee failure based on the fault tree of Kortenhaus et al. (2002) as shown in Figure 6. Further fault trees are presented by Vorogushyn et al. (2009) and Özer et al. (2020).

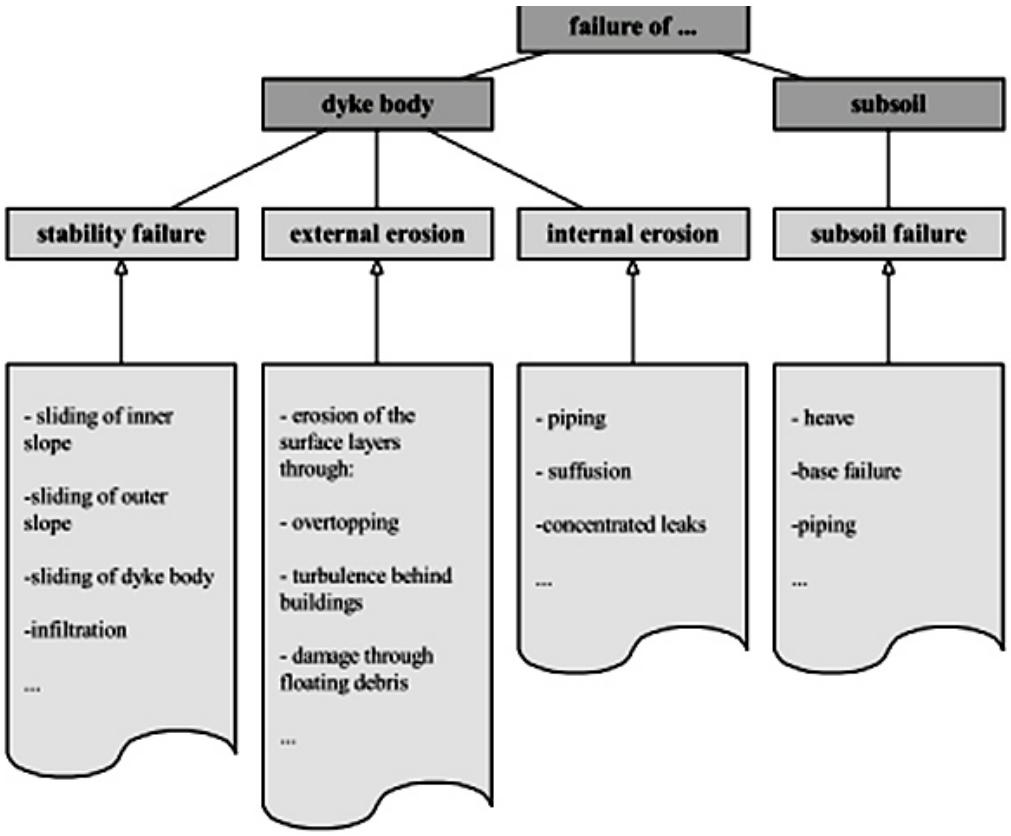

Figure 6: Theoretic model to map the cause of levee failure (adapted from Horlacher et al. (2007, p. 65)).

Statistics based on historical levee breaches show that the major causes of levee breach are external (surface) erosion (caused by flow overtopping the levee), internal erosion

(initiated by hydrodynamic forces acting on the soil particles of the levee body or foundation) and instability (when loading on the levee causes sliding of part of the levee or levee foundation along a shear surface) (USACE 2000) (CIRIA 2013). In some cases, burrowing animals such as beaver and rodents could burrow the levee material and create tunnels in the levee, which might lead to levee breach due to concentrated leak erosion during flood flows (Bonelli et al. 2012; CIRIA 2013; GA & AE 2003). The analysis of Orlandini et al. (2015) on the causes of the 2014 levee breaches on Secchia and Panaro Rivers in Italy pointed out burrowing animals as the main causes.

Statistics from August 2002 levee breaches in Saxony, Germany showed that 70% of the breaches are attributed to external erosion (overtopping), 17% of the breach are due to instability, 9.5% due to subsoil failure and 3.6% due to internal erosion (CIRIA (2013, p. 175), Horlacher et al. (2007)). It is, however, noted that one mechanism can often trigger other mechanisms. For example, overtopping can trigger other mechanisms such as erosion of inner slope and seepage leakage (Heyer et al. 2010).

The analysis of 120 levee breach records in France also showed internal erosion and external erosion due to overtopping as causes for 16% and 84% of the breaches respectively (Bonelli et al. 2012). Based on analysis of levee breaches in Japan, Fujita and Tamura (1987) identified seepage-leakage and overtopping as the most dominant causes of levee breaches. In their analysis of highway embankment failures, Chen and Anderson (1987) noted that external erosion due to flood overtopping is the major cause of levee failures in which flood loading of the embankments last only few days in a year. For long duration floods that have considerable time for the saturation of the embankment soil, they identified internal erosion due to seepage leakage as the most probable cause of levee breach.

Danka & Zhang (2015) analysed historical levee breach data from several countries. From the 503 breach cases for which the breach cause is identified, they determined that external erosion and internal erosion accounted for 68.6% and 14.3% of levee breaches respectively. Other studies have also shown that the major causes of levee breaches in the past are external erosion due to overtopping and internal erosion (Tóth & Nagy 2006; Nagy 2006a; van Baars & van Kempen 2009).

Thus, it can be concluded that the major causes of levee breaches are external erosion due to overtopping and internal erosion. In the following sections, levee breaching processes caused by external erosion due to overtopping and internal erosion are discussed.

2.3 Levee breaching process caused by external erosion due to overtopping

As indicated in section 2.2, the major cause of river levee breach is external erosion due to overtopping flow. Flow overtopping occurs when the water level in the river exceeds the levee crest level. The levee crest level can be exceeded by the flood level in the river in one of the following cases:

- A very high river flow due to excessive rainfall or upstream dam release that could result in water level above the design level of the levee.
- High settlement of levee crest that could lead to overtopping even by a water level under the design water level.
- Furthermore, inadequate design, construction and maintenance of the levee might lead to a situation of lower levee level than it should be, causing the levee to be overtopped by a flood level lower than the design level.

If flood level in the river exceeds the levee crest level, the water starts to flow laterally over the levee. The overflowing water starts to erode first the levee cover followed by the levee material if the force exerted by the flow is greater than the resistance force of the cover or the levee material. If the force exerted by the flow remains high for longer period, the erosion continues and eventually leads to the breach of the levee. The eroding force of an overflowing water is usually high since levee side slope are generally steep.

The erosion and breaching process of levees and other embankments caused by external erosion due to overtopping flow are studied by many laboratory- and field-scale physical experiments found in the literature. The experiments are carried out to understand the erosion and breaching processes and develop mathematical and numerical models. They can also serve as validation cases for numerical models.

The configuration of the experiments in the literature can be grouped into plane (2D) or spatial (3D) and frontal (embankment perpendicular to flow direction like in dams or sea dikes) or side (embankment parallel to flow direction like in riverine levees) as demonstrated in Figure 7. In plane (2D) tests, the process of erosion of the embankment is investigated by overtopping it over the entire width. They are often undertaken for frontal configuration of the embankment. In spatial (3D) tests, the process of erosion of the embankment is investigated in the vertical as well as in the lateral directions. The overtopping of the embankment is initiated by digging a small channel on the embankment crest (known as pilot channel), often in the middle of the embankment. Spatial tests are available for both frontal and side configuration of the embankment.

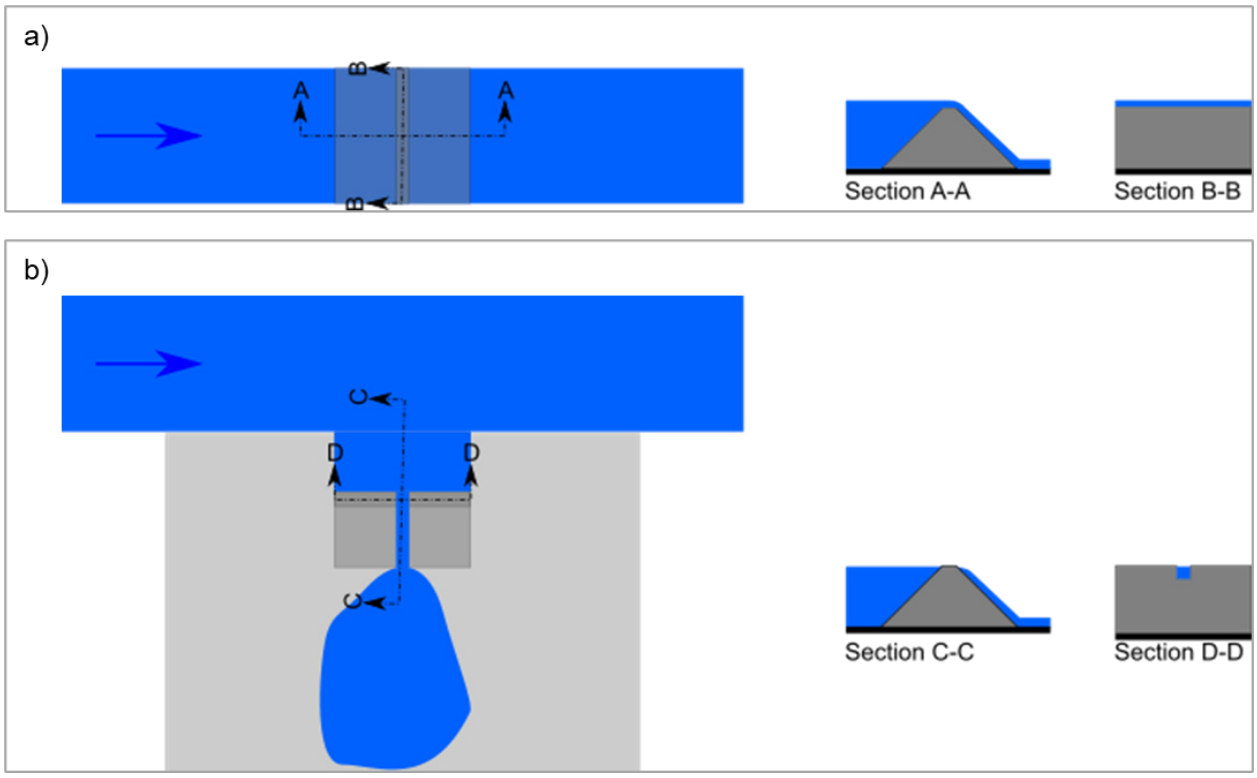

Figure 7: A sketch showing the common laboratory test configurations (not to scale): a) plane breach test with frontal embankment configuration b) spatial breach test with side embankment configuration.

Overtopping of river levees can happen only laterally as they are linear structures running parallel to the river (the main flow direction). In addition, levees are generally very long and may not be overtopped over the entire length. Thus, spatial side test configurations are relevant for levee breaching process. Laboratory and field tests in the literature with spatial side test configurations are relatively limited and are summarised in Table 1.

Table 1: Laboratory and field levee breach physical tests with spatial side test configuration in the literature.

No.	Author(s)	Country	Hydraulic boundary condition	Scale	Embankment materials	Breach initiation	Erosion process
1	Fujita & Tamura (1987)	Japan	constant inflow	flume	uniform sand	triangular pilot channel	four stages
2	Yu et al. (2013)	China	steady inflow	laboratroy tests	non-cohesive	rectangular pilot channel	four stages of breaching
3	Kakinuma & Shimizu (2014)	Japan	Constant-reservoir level	large scale laboratory (prototype)	sand levees	pilot channel at the side	four stages of breaching
4	Michelazzo (2014)	Italy, Germany	constant inflow into the main channel	laboratory experiments	non-cohesive	pilot channel at the side	four stages of breaching
5	Duo et al (2014)	China	constant inflow	laboratory experiments 180° curved channel	non homogenous sediments	rectangular pilot channel	four stages of breaching
6	Bhattarai (2015)	Japan	constant inflow into the main channel	laboratory experiments	non-cohesive	pilot channel at the center	four stages of breaching
7	Frank (2016)	Switzerland	constant inflow discharge, constant headwater level	laboratory	homogenous, non-cohesive sediments	triangular and trapezoidal pilot channels	n.a.
8	Tabrizi (2016)	USA	varying steady inflow tests	laboratroy tests	non-cohesive	rectangular pilot channel at the centre	three stages of breaching
9	Elalfy et al. (2018),	USA	varying steady inflow tests	laboratroy tests	non-cohesive	rectangular pilot channel at the centre	three stages of breaching
10	Michelazzo et al. (2018)	Italy, Germany	constant inflow into the main channel	laboratory experiments	sand	pilot channel at the center	four stages of breaching
11	Wei et al. (2016)				cohesive		three stages of breaching

The erosion process depends on the levee soil type. The erosion processes of levees constructed from non-cohesive soil is different from those constructed from cohesive soils (Hanson et al. 2005; Volz 2013). While progressive erosion is predominant in non-cohesive levees, head-cut erosion is predominant in cohesive levees (see Figure 8). While there are several physical experimental studies on the breaching process of non-cohesive levees due to overtopping, only a handful of similar studies are available for cohesive levees (see Table 1).

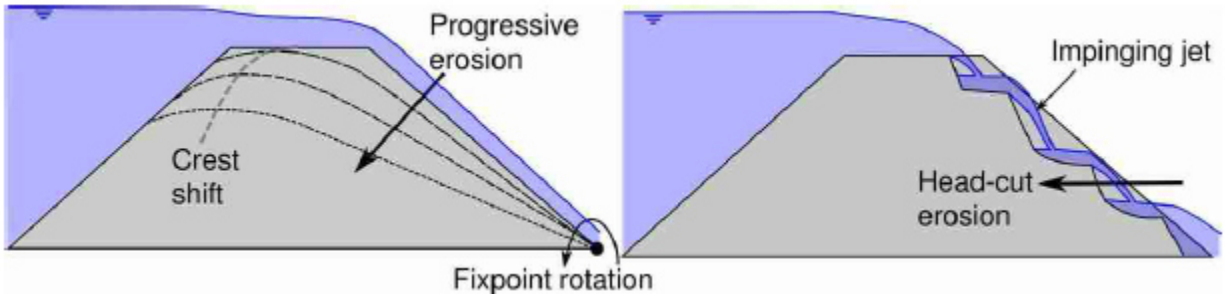

Figure 8: Sketch showing breaching process of a non-cohesive levee (left) and a cohesive levee (right) (figure taken from Volz (2013, p. 13)).

One of the first laboratory physical tests on breaching of levees constructed from non-cohesive materials is carried out by Fujita & Tamura (1987). Based on their experiments, they divided the levee breaching processes into four stages based on the variation of the breach width and breach discharge with time. At the beginning the breach width remains close to the initial width and the discharge is small. In the second stage, both breach width and discharge increase rapidly. In the third stage the changes are gradual. In the fourth stage, little changes are observed.

Comparable results are reported by Yu et al. (2013) and Dou et al. (2014). They conducted experimental investigation of overtopping breaching of a homogeneous non-cohesive levee in a 180° bend rectangular flume. The overtopping of the flow is achieved by using a small channel (often referred as pilot channel) at the crest of the model levee. They reported that the breaching progressed in four stages. First, the overtopping flow created a gully as the embankment erodes from the toe of the downstream slope to the levee towards the river side. In the second stage, breach widening and deepening due to scouring and wall shear forces dominate the breach processes. In the third stage, lateral growth of breach continues at a gradual rate as the flow at the levee toe (land side) continues to be submerged. As the downstream water level raised, the erosion capacity of the flow through the breach reduced. The final stage of the breaching process is reached when the breach discharge reaches stable conditions.

Also, Kakinuma & Shimizu (2014) presented similar results using large scale experiments on overtopping breaching of non-cohesive levee. They also used a pilot channel on the levee crest to initiate the overtopping of the model levee and divided the breaching processes into four stages based on the breach progress and hydraulic characteristics. The first stage is the erosion of the downstream levee slope at a constant overflow rate.

The second stage starts with the onset of breach widening, when the erosion of the downstream slope reached the top of the upstream slope. In this stage a gradual widening of the breach in the upstream and downstream directions and gradual increase of the overflow rate are observed. The third stage is characterized by acceleration of breach widening. Rapid widening of the breach mainly in the downstream direction is observed. This process continued until constant breach flow rate was attained. After constant breach flow rate is attained, the rate of breach widening decreased.

Also Michelazzo (2014) came to comparable phases of the overtopping breaching of non-cohesive levees based physical laboratory experiments. He divided the breaching stages into: 1) backward erosion of the landside slope of the levee, 2) erosion of the levee crest, 3) Erosion of the river side slope of the levee and 4) the widening of the breach until equilibrium state is reached.

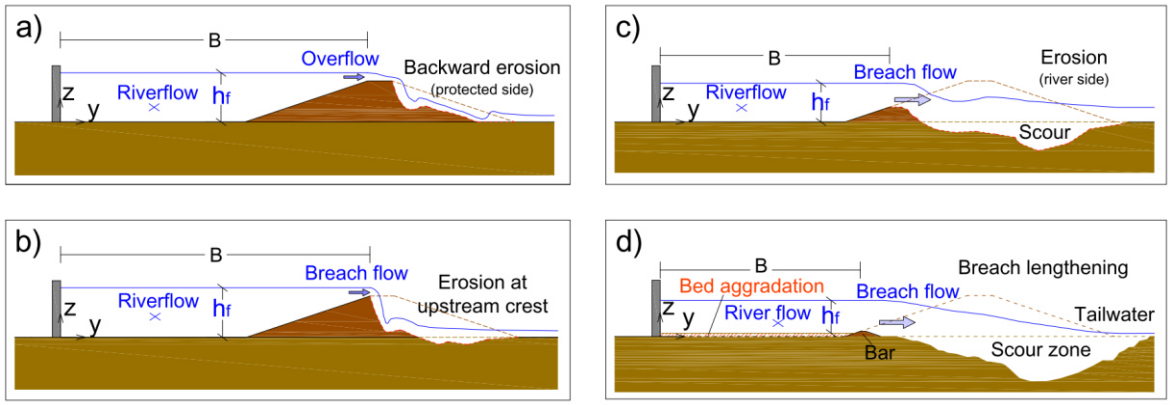

Figure 9: Schematic description of the stages of breaching of non-cohesive levees (taken from Michelazzo (2014, p. 183)).

Also, Bhattarai (2015) conducted small-scale levee breach laboratory experiments to study the breach widening behaviour and the breach discharge. He observed that, after the initiation of breach using a pilot channel at the centre of the model levee, at first, the overtopping flow eroded the pilot channel vertically to the bottom without lateral widening with vertical side slopes. Then, the breach started to widen from the toe of the land slope of the levee. Slumping of the sides of the breach opening followed as the vertical slopes got saturated. He also grouped the breaching processes into four stages: vertical undermining, start of lateral widening, acceleration of lateral widening and deceleration of the widening processes.

Frank (2016) conducted extensive laboratory physical model experiments on overtopping spatial levee breaching of non-cohesive levees with the focus on the determination of the effects of the parameters breach discharge, sediment grain size, initial breach width, levee cross-section, mobile bed, and reservoir water surface area on the breaching process. He found out the levee breaching process is strongly affected by the parameters breach discharge, levee cross-section and reservoir water surface area.

Tabrizi (2016) conducted laboratory experiments of overtopping breaching of non-cohesive levees. He divided the breaching processes into three phases: 1) start of breaching with

deepening along the pilot channel with a small and constant breach width, 2) acceleration of the widening of the breach and 3) deceleration of the breach widening. A follow up research, which strengthens these findings, is published by Elalfy et al. (2018).

Rifai et al. (2017) conducted laboratory experiments to study the erosion and breaching processes of non-cohesive levees due to flow overtopping. Following overtopping of the flow at the pilot channel, erosion of the levee downstream slope proceeded at slow rate and the eroded material deposited at the toe. The erosion process accelerated with the increase of the overtopping flow depth, which lead to breach deepening and widening. The breach widening is mainly in the direction of the flow in the channel. In the following stage, the breach widened only in the downstream direction. The last stage is characterized by slow breach development until equilibrium is attained.

Studies of the breaching process of levees constructed from cohesive soils are limited. One physical laboratory study on overtopping breaching of cohesive levees (with the configuration of the levee parallel to the main flow direction) is undertaken by Wei et al. (2016). Based on breach erosion characteristics, they divided the breaching processes into slope erosion stage, head cut retreat stage and breach widening stage (see Figure 10). The slope erosion stage is characterized by erosion of the downstream slope of the levee by the shear force of the overflowing water and creation of small scour holes at the bank toe. The head cut retreat stage is dominated by single and multi-step head cut, erosion by the shear force of the overflowing water and jet impinging erosion. The breach widening stage is characterised by erosion of side slopes and cantilever collapse of the levee part.

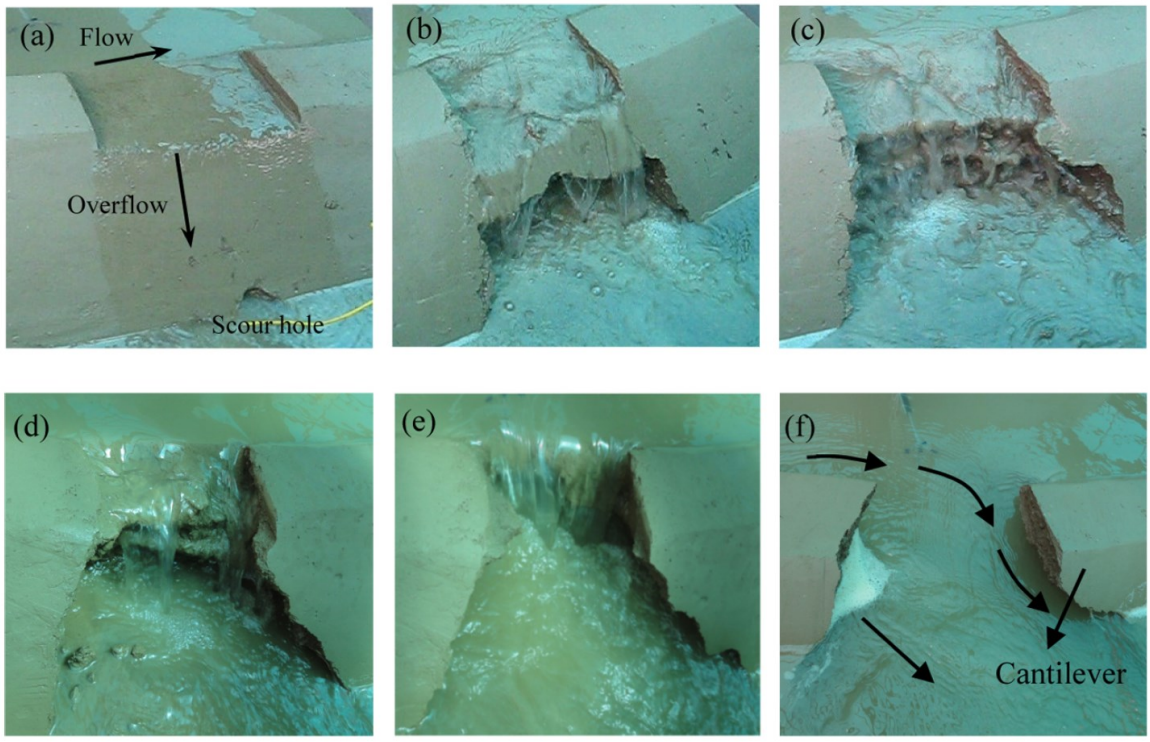

Figure 10: Processes of overtopping breaching of a cohesive levee as observed in physical experiment set up: (a) slope erosion stage; (b), (c), (d) and (e) headcut retreat stage; and (f) breach widening stage, taken from Wei et al. (2016, p. 1544).

Other studies with respect to breaching process of cohesive levee are available in the frontal test configuration. These include but are not limited to the studies by Hanson et al. (2005), Hunt et al. (2005), Morris et al. (2007), Zhu (2006), Briaud et al. (2008), Jandora & Říha (2008), Zhang et al. (2009) and Zhao (2016). The reported breaching processes are comparable to the results of the experiment in the side configuration reported by Wei et al. (2016) and discussed above.

Based on the above studies, the processes of the overtopping breaching of non-cohesive as well as cohesive levees can be generalized into the following four phases (see Figure 9 and Figure 10). The duration taken by each phase is variable and depends on different parameters:

- Phase 1: Slow to gradual erosion of the downstream slope of the levee by the shear force of the overflowing water until the erosion reaches the upstream edge of the levee crest; in the case of cohesive levees, through head cutting also plays a significant role.
- Phase 2: Vertical erosion of the levee at rapid erosion rate down to the foundation with limited lateral breach expansion.
- Phases 3: Rapid lateral erosion of the levee in combination with mass slumping due to instability of the breach side slope until peak discharge through the breach is attained.
- Phase 4: Further lateral expansion of the breach at slower rate until the maximum breach width is attained.

The overtopping breaching process of levees reported by previous studies based on laboratory scale experiments and field scale experiments show that the levee breaching processes depend on:

- the flow (discharge) in the river (Wei et al. (2016), Frank (2016), Michelazzo (2014), Kakinuma & Shimizu (2014), Yu et al. (2013), among others),
- the water level in the river (Yu et al. (2013), Wei et al. (2016), Frank (2016), Michelazzo (2014), Kakinuma & Shimizu (2014), among others),
- the levee material properties (material size (d_{50}), soil cohesion, density and tensile strength, etc) (Yu et al. (2013), Wei et al. (2016), Frank (2016), Michelazzo (2014), Kakinuma & Shimizu (2014), Bhattarai (2015), Hunt et al. (2005), Morris et al. (2007), Wei et al. (2016), among others),
- levee dimensions (Kakinuma & Shimizu (2014), Frank (2016), among others) and
- the levee conditions (compaction; compaction water content, core and outer layers, etc) (Hunt et al. (2005), Morris et al. (2007), among others).

Furthermore, the development of the breach is asymmetrical and mainly in the direction of the river flow (Rifai et al. (2017), Michelazzo (2014), Kakinuma & Shimizu (2014)). The breach discharge is proportional to the breach width (Michelazzo 2014). In his experiments, Michelazzo (2014) calculated that the ratio between the final breach discharge and the inflow discharge was on average 50%. In tests where tail water is present, it is observed that the breach discharge is a function of the head and tail water level (Dou et al. 2014).

2.4 Levee breaching process due to internal erosion

Levee breaching due to internal erosion is the second most common cause of levee breach as discussed in section 2.2. Internal erosion is the process whereby seepage or leakage flow removes fine materials of the levee body or its foundation and leads to the breach of the levee. Internal erosion is hindered by using zoning and filters (ICOLD 2017). If internal erosion process is not identified in time and measures are not taken, the erosion could lead to instability of the levee or creation of a pipe like hollow in the levee (piping) (Fell et al. 2003). This could eventually lead to the complete collapse of the levee. Downstream end of bends, junctions at tributaries and meanders can provide weak points for seepage and piping (Wu 2013).

Internal erosion of embankments can happen through four mechanisms: i) suffusion, ii) backward erosion, iii) contact erosion and iv) concentrated leak erosion (Bonelli (2013), Zhang et al. (2016a)). In all mechanisms, the path to the failure of the structure is divided into four phases based on laboratory and field tests, and analysis of historical embankment piping failure cases. These are initiation of erosion, continuation of erosion, progression of erosion to form a pipe or hollow like feature in the structure or its foundation, and the breaching of the structure (Fell et al. (2003), Zhang et al. (2016a), Fell & Fry (2007)).

Non-cohesionless soils such as silts and sands collapse when saturated under flooding. They are also relatively easily eroded and do not withstand a crack if saturated (Bonelli 2013). These make levees constructed from non-plastic soils susceptible to failure due to sustained seepage. On the other hand, cohesive soils such as clays and clayey sands are generally more resistant to erosion than non-plastic soils because high energy is required to detach soil particles from the soil. Once detached, however, the particles can easily be transported due to their small size. As a result, plastic soils are susceptible to concentrated leak and contact erosion (Bonelli 2013).

The state of the art in all the stages related to concentrated leak erosion, contact erosions and suffusion are quite poor (Bonelli 2013). Furthermore, suffusion is a common problem in embankments constructed from a poorly graded soil. This is not often the case in levees. In the following the most common internal erosion mechanisms in levee, which are backward erosion (piping), sustained seepage and concentrated leak erosion, are discussed.

2.4.1 Backward erosion (piping)

The predominant internal erosion mechanism in levees is backward erosion (piping) (ICOLD 2017). Backward erosion is a process in which soil particles from sand layer stratum under a levee (also other embankments) are removed by seepage flow as illustrated in Figure 11. The erosion starts at the downstream side of the levee, where the seepage flow exits freely. The free exit is possible if a ditch at landside is dug up to the sand layer, or the sand layer at land side has no cohesive cover layer, or the cohesive cover layer is heaved or raptured. The progression of the erosion to the water side is possible if a cohesive layer (it can be the levee itself or cohesive soil layer under the levee)

above the sand layer forms a roof. Sand boils on the land side of a levee are indications of presence of backward erosion.

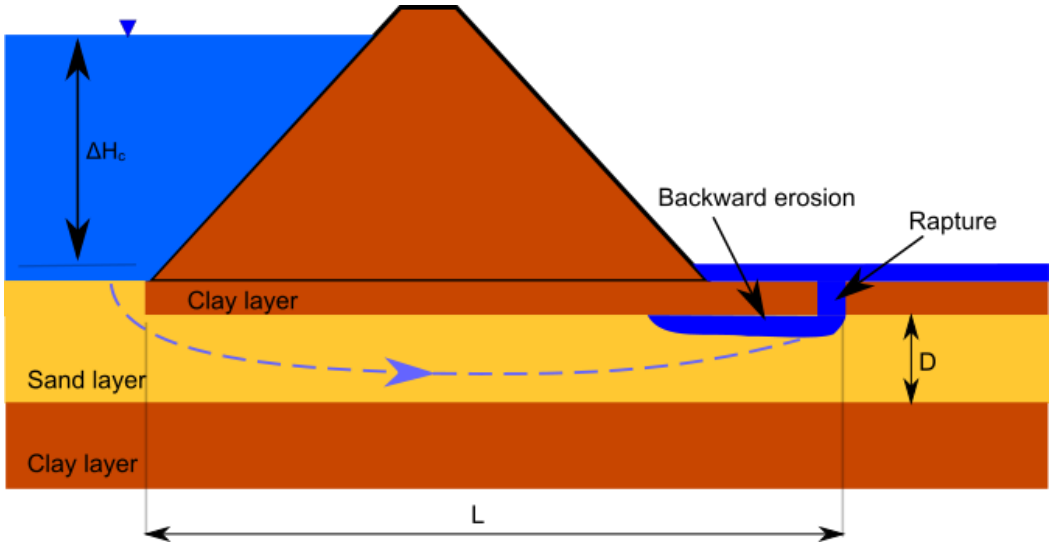

Figure 11: Schematic sketch illustrating the process of backward erosion.

The process of backward erosion and piping failure of levees and embankments is studied in the literature based on laboratory-scale experiments, field-scale experiments, and historical actual breach cases. Such investigation of backward erosion is reported by van Beek et al. (2011), Chen et al. (2015), Sellmeijer et al. (2011), Xiao et al. (2019), among others.

The process of backward erosion is studied by van Beek et al. (2010) using small-, medium- and full-scale experiments. They observed four erosion phases that ultimately lead to the failure of the structure: seepage, retrograde erosion, widening of the pipe and failure of the levee. At the beginning (seepage phase), they observed seepage underneath the levee with increasing hydraulic head without transport of sand. Then (Retrograde erosion phase), they observed sand traces at a hydraulic head below the critical. They documented that increasing of the hydraulic head lead to appearance of sand boils followed by sand craters at or near to the critical head. They could speed up the erosion process by increasing the hydraulic head. This phase ended after the backward erosion had reached the upstream side, connecting the downstream side with the upstream by a pipe-like opening. In the following phase (Channel widening phase), the pipe started to widen from the upstream side to the downstream side. They observed that the widening processes took a considerable time due to clogging of the pipe. They observed a significant amount of eroded material as the widening of the channel reached the downstream side. This is followed by the final phase (Failure phase), in which the levee either failed or deformed following the complete connection of the upstream and downstream side by an enlarged pipe. The latter clogged the pipe and extended the widening phase which ultimately resulted in significant erosion and deformation of the levee, and subsequent failure of the levee. The above mentioned four general phases are further differentiated to six phases by Bonelli (2013) as shown in Figure 12.

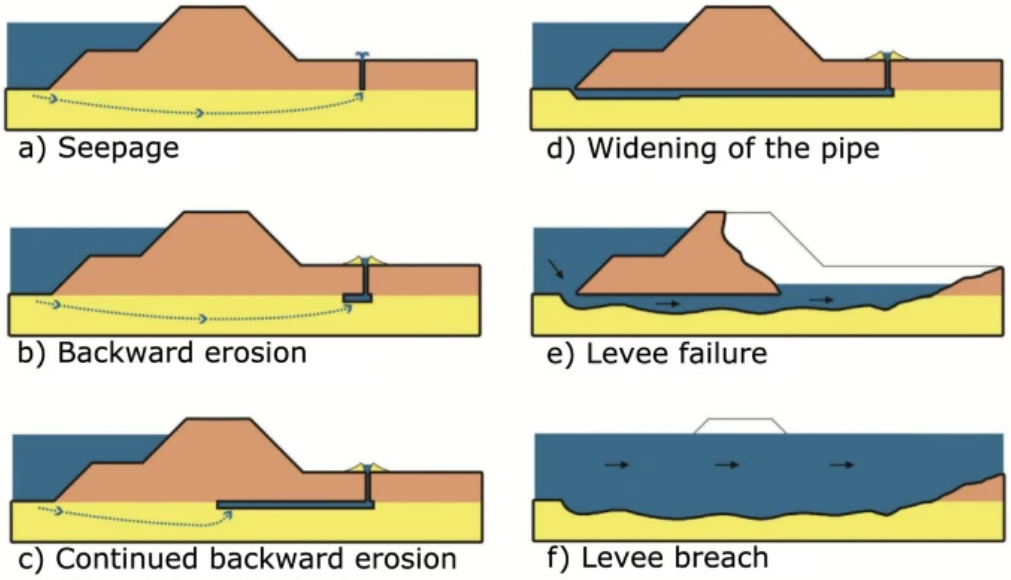

Figure 12: Phases of backward erosion (taken from Semmens & Zhou (2019, p. 2)).

Also, Chen et al. (2015) undertook experimental studies on the erosion mechanism of piping phenomenon using a laboratory-scale model. They also arrived at comparable erosion processes as described above. They observed that the erosion processes were non-uniform and intermittent, i.e., the levee material erodes in multiple events. They reported two mechanisms of erosion: erosion induced by a stress release (advancement of the pipe upstream) and erosion caused by clogging (responsible for the increase of the pipe diameter). Detailed investigation of backward erosion process at the initiation phase using laboratory experiments is under taken by Xiao et al. (2019).

The backward erosion piping failure of levees and embankments reported by previous studies based on laboratory scale experiments and field scale experiments show that the erosion processes depend on several parameters. These are listed as follows:

- **Compaction** – Sharif et al. (2015) conducted laboratory flume experimental studies on the piping erosion processes of embankments. They used embankments with a mixture of sand, silt, and clay with different compaction degrees for the tests. They observed that compaction affected the time required for erosion but not the final average erosion depth. They also observed that during the piping erosion process, the ratio of the average erosion depth to bottom width remains at about 1.
- **Soil erodibility** – According to Bonelli & Benahmed (2010), the erodibility of a soil, i.e., threshold of erosion (initiation) and rate of erosion (progression) are crucial for the piping process. They employed the Hole Erosion Test to obtain the coefficient of erosion, which they used as indicator of the remaining time until breaching.
- **Critical shear stress** – Bonelli & Benahmed (2010) established that radius of the pipe is a function of the critical shear stress of the soil and the characteristic time of the piping erosion.
- **Hydraulic gradient** – Bonelli & Benahmed (2010) related the characteristic time of piping to the initial hydraulic gradient and the coefficient of erosion. According to Zhang et al. (2016b), the likelihood of piping failure depends on the magnitude of the

seepage flow, which can be measured by the hydraulic gradient and the resistance to erosion (soil erodibility). Soil erodibility depends on the physical characteristics and mechanical conditions of the soil (compaction).

Backward erosion is a complex process to be described with a theoretical method. As a result, there are several empirical and semi-empirical approaches for the calculation of the critical hydraulic gradient (Kortenhaus & Oumeraci 2002b). The most popular one is the semi-empirical method of Sellmeijer (Sellmeijer 1988). Sellmeijer (1988) and later Sellmeijer & Koenders (1991) derived an equation for the critical hydraulic gradient for a backward erosion by employing groundwater flow in porous media, mass conservation principle, physical experiments and the prevailing boundary conditions. They showed that the critical hydraulic gradient is a function of the ratio of length of the piping channel to the length of the structure, and soil and water properties.

Sellmeijer's method is further improved using recent experiments (van Beek et al. 2011; Sellmeijer et al. 2011). Specifically, they investigated and included the effects of scale, relative density and grain size of the eroding soil using a series of experiments and updated the formula for critical hydraulic gradient for the progression of backward erosion.

The formula for the critical hydraulic gradient is given in equation (1) based on the assumption by Sellmeijer et al. (2011) and discussions by Bonelli (2013). The assumptions and simplifications are as follows:

- Sellmeijer et al. (2011) assumed an angle of repose of sand of 37° and a White's coefficient of 0.25 for their data set. This assumption may be extended for other data sets.
- Sellmeijer et al. (2011) indicated that roundness of particles and coefficient of uniformity can be ignored.

$$i_c = \frac{\Delta H_c}{L} = 0.91\eta \frac{\rho_s - \rho_w}{\rho_w} \cdot \tan\theta \cdot \boldsymbol{d_{70}} \left(\frac{\mathbf{1}}{\boldsymbol{\kappa L}}\right)^{1/3} \cdot \left(\frac{\boldsymbol{D}}{\boldsymbol{L}}\right)^{\left(\frac{0.28}{\left(\frac{D}{L}\right)^{2.8}-1}+0.04\right)} \quad (1)$$

The shortcurts in equations (1) are defined as follows: i_c is the critical hydraulic gradient [-]; ΔH_c is the critical head difference [m]; L is seepage length [m], which can be approximated to the base length of the levee; d_{70} is the grain size for which 70% (by weight) of the soil is finer [m]; ρ_s is the density of the sand [kg/m³]; ρ_w is the density of water [kg/m³]; η is White's drag coefficient [-] and is found to be 0.25 for the data sets of Sellmeijer et al. (2011); κ is the intrinsic permeability of the sand layer [m²]; θ is the angle of repose of sand [°] and is found to be 37° for the data sets of Sellmeijer et al. (2011); D is the thickness of the sand layer under the embankment or the foundation [m].

The intrinsic permeability κ is related to the hydraulic permeability k by equation (2).

$$\kappa = \frac{\nu}{g} k \tag{2}$$

Where ν is kinematic viscosity of water [m²/s] and g is acceleration due to gravity [m/s²]. The hydraulic conductivity for a given soil type can be referred from soil mechanics textbooks.

2.4.2 Seepage through the levees body

If a levee is subjected to high water level, seepage through the levee body can take place. Depending on the loading, levee material and geometric properties, the seeping water (or the phreatic line) might emerge on the landside slope. This can soften the levee at the landside toe with slope sloughing and causing internal erosion of the levee material (Camici et al. 2017; Michelazzo et al. 2018). Furthermore, this could lead to micro instability of the levee (slope failure due to seepage) (Vorogushyn et al. 2009).

The seepage flow through the levee body can be estimated using the approach used by Kortenhaus & Oumeraci (2002b). In their approach, the time required for the seepage front to reach the land side toe of the levee is determined based on Darcy Weisbach equation. Assuming a linear phreatic line, the time required for the seepage water, with a given water level in the river, to reach the landside toe of the levee can be estimated using equation (3). This corresponds to the time that leads to the point where the seepage starts to exit at the land side slope of the levee.

$$t_s = \frac{n}{k_s f_{sat}} \frac{{l_s}^2}{\Delta h} \tag{3}$$

In equation (3), t_s is seepage duration, n is air void fraction of the levee body [-], l_s is the seepage length [m] (as shown in Figure 13), Δh is the head difference between the river side and the land side toe level of the levee (as shown in Figure 13), k_s is the Darcy's filter velocity in the levee body [m/s], f_{sat} is a factor describing the influence of the already existing saturation of the levee [-]. Based on large-scale model tests the value of f_{sat} is found to be about 2 at 20% soil water content (Kortenhaus & Oumeraci 2002a).

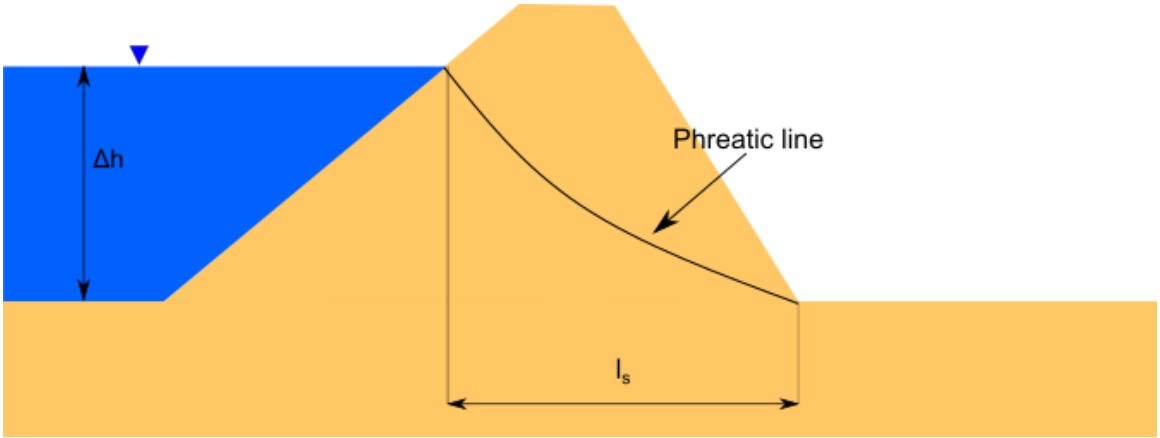

Figure 13: Sketch showing sustained seepage through a levee body exiting at the landside toe with an idealised phreatic line.

2.4.3 Concentrated leak erosion

Concentrated leak erosion in levees is removal of levee soil material by water flowing through cracks or opening or hollow in the levee body or its foundation (Fry 2012), causing the opening to increase in size (diameter) (Benahmed et al. 2012). The opening in the levee or the foundation can be caused by different reasons such as crack caused by geological reason or settlement or hydraulic fracture, animal burrows, tree roots, crack along a rigid structure running through the levee (such as pipes), crack at the contact surface between the levee and a rigid structure, opening in the foundation at the end of backward erosion, and others (Benahmed et al. 2012).

Extensive theoretical and experimental studies on concentrated leak erosion is undertaken by Benahmed et al. (2012), Benahmed & Bonelli (2012) and Bonelli (2013). Nevertheless, the phenomena remains to be still poorly understood and requires further research (Bonelli 2013).

Bonelli (2013) forwarded an equation for the estimation of the time to breaching due to concentrated leak erosion given by equation (4).

$$t = t_{er} \ln\left(\frac{R}{R_d}\right) \tag{4}$$

R [m] and R_d [m] are the radi of the opening at breach and start of concentrated leak respectively, and t_{er} [s] is the characteristic time and is given by equation (5).

$$t_{er} = \frac{2\rho_d \overline{L}}{C_e \overline{\alpha} \Delta p_T} \tag{5}$$

In equation (5), $\overline{L}$ [m], ρ_d [kg/m³], and C_e [s/m] stand for the pipe length at failure, the dry density, and the erodibility coefficient of the soil of the levee material respectively. Δp_T [N/m²] and $\overline{\alpha}$ [-] stand for the total pressure drop and the head loss factor at failure respectively and are given by equations (6) and (7).

$$\Delta p_T = \rho_w g (\Delta H_w - R) \tag{6}$$

$$\overline{\alpha} = \left(1 + \frac{0.5R}{0.02\overline{L}}\right)^{-1} \tag{7}$$

The erodibility coefficient for different soil types can be determined from in situ tests using Hole Erosion Test. It can also be estimated from other soil parameters from values in the literature. Fell et al. (2013), for example, related soil erodibility coefficient to other soil parameters. This includes the relationship of soil erodibility coefficient to soil type according to unified soil classification.

2.5 Levee breach models

Levee breach models seek to determine the levee breach morphology (i.e., the change in the morphology of the levee at the breach location), from which the breach flow (i.e., the flow through the created breach opening) are determined. The models range from simple empirical equations developed from historical levee breaches to complex physically-based models that solve coupled system of shallow water equations, bed evolution equations (such as Exner's equations) and sediment transport formula. The number of parameters determined with breach models depends on the complexity of the model employed. While the simplest approaches usually estimate the peak flow through the breach, the complex models aspire to determine the variation of the breach geometry with time, the flow hydrograph through the breach, and the inundation of the flood plain. This section reviews the breach models available in the literature.

2.5.1 Classification of breach models

In the literature, we find several ways of classifying breach models depending on the criteria employed for the classification. The major criteria for classification are model formulation and approximation of the physical processes, and the solution approach employed (ASCE/EWRI 2011). Based on model formulation and approximation of the physical processes, ASCE/EWRI (2011) grouped breach models into parametric, simplified physically-based and detailed physically-based. And based on the solution approach the models are grouped into empirical, analytical and numerical.

The classification approach which combines the physical process and solution approach seem to be the most popular among researchers (Morris et al. 2009; Broich 2003; Wahl 1998). This is because some of the physical processes can be solved only with one of the solution techniques. For example, the detailed physically-based models may only be solved with numerical methods and parametric models rely on empirical derivations. Broich (2003) groups breach models into analytical, parametric and numerical models, which is a mix of the categorization given by ASCE/EWRI (2011). Morris et al. (2009) divided breach models into empirical, semi physically-based (analytical and parametric), and physically-based models mainly based on the way the physical processes are handled. Wahl (1998) grouped breach models into physically-based, parametric, predictor equations and comparative models. Grouping breach models into empirical models, parametric models, and physically-based models generalises the classifications in the literature (Wahl 2010) and thus is used in this work. These are discussed in the following sections.

2.5.2 Empirical models

Empirical breach models are a group of breach models derived from statistical best fit to historical breach data to estimate breach parameters such as breach peak discharge, breach width or depth (Morris et al., 2009; USBR, 1988). Dozens of such models were developed (Morris et al., 2009; ASCE/EWRI, 2011; Costa, 1985; USBR, 1988) mainly for reservoir embankments.

In most of the cases, while the peak discharge is the main dependent variable, the volume of water stored above breach invert and/or height of water above breach invert at time of failure are the main predictor variables. Different models adopt different numbers and kinds of independent, and dependent variables. Depending on the model, predicted variables may include breach width, shape, side slope, peak outflow, and breach duration; and predictor variables may include initial water height, levee / dam height, levee / dam type, configuration, failure mode, and embankment erodibility. In some publications the predictor variable dam erodibility is included (Xu and Zhang, 2009; Walder and O´Connor, 1997).

Empirical breach models derived for reservoir dam breaks are in general not suitable for application to levee breach modelling (Howard et al. 2009). For application of empirical models to levee breach modelling, the empirical model itself needs to be derived from historical levee breaches or experimental levee breaches. Empirical levee breach relations in the literature are given by Danka & Zhang (2015), Nagy (2006b) among others and are given below.

Danka & Zhang (2015) used historical levee breach data around the world to derive empirical equations for estimating levee breaching parameters. They derived empirical equations for the levee breaching parameters breach width, breach depth and breach discharge as a function of levee height (h), levee bottom width (w), levee soil material, levee breach mechanism and levee type. The empirical equation for breach width, L, is given by equation (8).

$$L = 0.08 \frac{w^{3.06} e^{m}}{h^{2.11} e^{t}} \qquad (8)$$

The coefficients m and t represent the effects of levee soil material, levee type and levee breach (failure) mechanism respectively and the values are given in Table 2 and Table 3.

Table 2: Values of the coefficient m in equation (8).

Levee material	*m*
coarse-grained soils	*0.38*
fine grained soils	*0.42*
organic soils	*0.35*

Table 3: Values of the coefficient t in equation (8).

levee type	*t*
Composite	*0.94*
Earthen	0

Nagy (2006b) processed over 1000 historical levee breach data to calculate the average breach width in the levee breaches of the rivers in the Carpathian Basin (Danube, Tisza, their tributaries and other smaller rivers). He derived an empirical equation for the levee breach width as a function of head (which is approximated by the height of the levee) from the historical data as given by Eq. (9).

$$L = 5.1699e^{0.7498h} \tag{9}$$

Furthermore, empirical equations derived for earth dam breaches are sometimes adapted for estimation of levee breach parameters. Example of such empirical equation is given by U.S. Bureau of Reclamation (1988) in equation (10). The shorthand forms are as defined above.

$$L = 3h \tag{10}$$

2.5.3 Parametric models

Parametric breach models are breach models that rely on parameters to describe the levee breaching process and determine the flow through the breach analytically or numerically. Such approach is widely used to estimate outflow hydrograph from dam breaches (ASCE/EWRI 2011). According to Costa (1985), as early as 1892 Ritter used the Saint-Venant equation with the simplifying assumptions of a rectangular and horizontal channel without friction and turbulence losses to estimate the maximum flood discharge from a dam failure.

Parametric breach models are often integrated into 1D- or 2D-hydrodynamic numerical models to simultaneously simulate flood inundation of the hinterland. The parameters often include initial and final breach dimensions, breach duration, breach location and how the breach is initiated. In the literature, we observe different levels of detail regarding the breach parameters. Selected parametric levee breach models from the literature with different levels of detail are presented below.

Kamrath et al. (2006) assumed i) a levee breach along a straight river reach, ii) a rectangular breach cross-section, iii) a constant breach width, and iv) a sudden and total erosion of the levee section to derive a simple analytical formula for breach discharge. Using a 2D-hydrodynamic numerical modelling of the levee breach flow, they found that only part of river flow is influenced by the breach. They denoted the width of the river flow influenced by the breach as influence length and stated that it is dependent on the breach width. They hypothesized and proved that the breach discharge is a function of the breach width, the influence length, the flow velocity in the river, and the depth of flow at the breach.

Liu & Wu (2011) used a parametric levee breach model integrated into a flood routing model to calculate breach discharge. The levee breaching processes is described via the parameters levee breach start time, final breach width, breach duration and final breach level. They assumed that the breach width and breach level linearly increase form initial values to final values with the breach duration. They applied their approach to model the

historical levee breach in the Danshuei River system in northern Taiwan during Typhoon Talim in 2005. They obtained good agreement of the simulations results with the observations. Nevertheless, they showed that the breach flow is significantly sensitive to the levee breach parameters breach start time, final breach width, breach duration and final breach level.

The 1D flood routing model HEC-RAS also has a parametric levee breach model (Brunner & CEIWR-HEC 2020). The parametric breach model uses the breach parameters breach location, final bottom width, final bottom elevation, left and right-side slopes of the breach cross-section (assumed to be trapezoidal), breach formation time, the failure mode (piping or overtopping) and other optional parameters to be set by the modeller. The breach can be initiated by one of the three options i) at a specified time, ii) at a specified water level or iii) at a specified water level exceeded for a given duration (Bertrand et al. 2018) employed the levee breach model in HEC-RAS to simulate the 1981 historical flood event of the Garonne River between Tonneins and La Réole, France. They set up the model to initiate levee breaches due to overtopping based on water level and analysed the sensitivity of the levee breach parameters. They identified for their case that the maximum water levels in the protected areas are most sensitive to the breach parameters final breach width and final breach depth. Also, Masoero et al. (2013) used the parametric breach model in HEC-RAS to determine the breach discharge of the 1991 Po River levee breach in Italy.

Shustikova et al. (2020) implemented a parametric levee breach model into the flood model LISFLOOD-FP. The parametric breach model is dependent on the parameters breach location, final breach level (specified as breach depth relative to the levee crest level), threshold water level and duration threshold. The breach location is defined by the coordinates of the computational grid cells where the breach is expected to occur. The breach is dynamically initiated when (i) the defined threshold water level is exceeded or (ii) the defined threshold water level is exceeded longer than the defined threshold duration. Instantaneous breach is assumed if the breach initiation criteria is fulfilled. They used the approach to simulate the historic levee breach floods of January 2014 on the Secchia River and November 1951 on the Po River in North Italy. The model reproduced the maximum breach discharge well in both cases.

2.5.4 Physically-based models

Physically-based breach models are levee breach models that are based on flow hydraulics and erosion processes. A fully physically-based breach model simulates the levee breaching process using sediment transport equations (such as Meyer–Peter and Müller formula (Meyer-Peter & Müller 1948)), bed evolution equations (such as Exner equation (Paola & Voller 2005)) and slope stability conditions coupled with hydrodynamic numerical model. Some models simplify the erosion process. In the following, simplified and fully physically-based breach models from the literature are presented.

The 1D flood routing model HEC-RAS also has a simplified physically-based breach model. In this model, the lowering of the levee level and the widening of the breach are a predefined function of the overflow velocity (Brunner & CEIWR-HEC 2020).

Paquier & Béraud (2010) used a simplified physically-based breach model in their approach of levee breach flood modelling. The approach is based on coupling of four modules: i) river flow module, ii) levee breaching process module, iii) flood propagation in the vicinity of the breach module, and iv) flood propagation in the far field of the breach module. The levee breaching process module employs a simplified physically-based levee breach model based on the following simplifications. They assumed that the levee is of a trapezoidal shape and made up of a soil material with a given grain size and porosity, and the levee breaching process can be simplified into two steps (Paquier & Recking 2004). In the first stage, initial breach starts as circular pipe (piping mode of failure) or a rectangular breach (overtopping mode of failure) and the flow through the breach increases the diameter of the pipe or the depth of the breach by eroding the embankment. The process gets into the second stage if the diameter of the pipe created reaches 2/3 of the levee height or in case of overtopping if the levee is eroded to the bottom. The breach grows as a function of the volume of eroded material estimated using the Meyer-Peter and Müller sediment discharge equation (Meyer-Peter & Müller 1948).

Liu (2015) presented a simplified physically-based breach model for modelling breaching of embankments due to piping as a result of internal erosion. He employed turbulent pipe flow with erosion mechanism to determine pipe enlargement through the embankment. The model considers the upstream hydraulic head variation, the tail water head, the collapse of the pipe top and the transition to a complete breach. The internal erosion rate and thus the enlargement of the pipe diameter is dependent on the parameters erosion rate coefficient and the critical shear stress of the soil. He points out, however, that the determination of these parameters is complex.

Viero et al. (2013) used a simplified levee breach model integrated into a 2D hydrodynamic model as 1-D link to simulate levee breaching due to overtopping and piping. For the case of piping levee breach, the breach model is similar to the approach of Liu (2015). For overtopping levee breach, they adapted the five stage breaching proposed by Visser (1998) for sand dikes. They used the model to simulate the November 2010 Bacchiglione River levee breach in Italy.

Pontillo et al. (2010) also presented a simplified 1D physically-based levee breach model. They provided a formula for vertical erosion that is a power function of a parameter that accounts for shear stresses. They validated their model with a physical laboratory test result of breach erosion. The model is first calibrated for the parameters with the one physical test set and employed for modelling other tests.

Fully physically-based breach models solve the shallow water equations, the bed evolution equation, the sediment transport rate formula, and the slope instability condition for the breach side slopes to determine the levee breaching process and the breach discharge. Such models are reported by Lin et al. (2002), Mizutani et al. (2013), Cantero-Chinchilla et al. (2018), Elalfy et al. (2018), Onda et al. (2019), among others.

In their study of levee breaching processes in Yellow River, Lin et al. (2002) presented a fully physically-based numerical model for modelling levee breach. Their model solves the

equations for water flow (the shallow water equations), sediment transport rate, bed evolution and breach expansion. They validated their numerical model with experimental data from a hydraulic levee breach model. They reported qualitative agreement between the measured and modelled levee breaching processes.

Mohamed et al. (2002) presented a physically-based embankment breach model that can also be used for levee breaches. In their model, lateral breach growth is considered as a combination of continuous erosion and mass instability. They reported reasonable agreements between the model results and the observed laboratory and large-scale experimental test results. They also noted the uncertainty in the model parameters.

Faeh (2007) presented a similar approach to Mohamed et al. (2002) for modelling of river levee breaching due to overtopping flow. He reported that using the model to simulate blind laboratory tests (without calibration) resulted in poor replication. He could obtain better agreement between model results and measurements after undertaking parameter tuning. He also used his model to simulate the dike breach on a section of the River Elbe during the Elbe flood of 2002. He reported that the model reproduced the peak breach discharge and final breach width with errors of 8% and 15%, respectively. An improved version of the model, including application with other experimental results, is reported by Volz et al. (2012).

Islam (2012) and Kakinuma & Shimizu (2014) used a physically-based breach model, based on the hydrodynamic numerical model RIC-Nays (2D) (https://i-ric.org/en), to simulate laboratory levee breach tests. They reported good agreement between model results and measurements with unspecified differences. They also reported the sensitivity of the levee breaching process to the characteristics of the floodplain, riverbed level, bed material size and river slope.

Mizutani et al. (2013) developed a physically-based levee failure model to simulate the levee failure process due to overtopping flow. They considered the effect of resisting shear stress due to suction head in the erosion of levee material by overtopping flow. They validated their model using laboratory physical tests of levee breaching. They reported that the proposed model was able to reproduce the breaching process observed in the laboratory tests. A similar approach has been reported by Bhattarai (2015).

Guan et al. (2014) published a physically-based model to simulate the breaching of levees made of non-cohesive material due to overtopping flow. The levee breaching process is modelled using a morphological model integrated with a hydrodynamic numerical flow model. The lateral growth of the breach is modelled using a modified version of a slope avalanche model by Swartenbroekx et al. (2010) and Volz et al. (2012). They used results from laboratory experiments to validate their model. They reported that the model results were in good agreement with the experimental data.

One of the few physically-based breach models for modelling overtopping breaching of cohesive embankments, which can be also be used for cohesive levees, is proposed by Zhao (2016). His model consists of four modules for modelling the flow, the surface erosion

process, the head-cut erosion process, and the lateral embankment erosion process. He calibrated and validated the model using large-scale breach tests. He also used the model to simulate a laboratory-scale breach test and a prototype breach. He reported that the model gave satisfactory results compared to the measured data.

Elalfy et al. (2018) also used a physically-based breach model to simulate the breaching of non-cohesive levees due to flow overtopping. The model solves the shallow water equations and the sediment transport equation, which also accounts for slope failure. They validated their model using laboratory levee breach tests. They reported that the model successfully reproduced the breaching process and the breach discharge hydrograph. They noted that the modelled breach dimensions were sensitive to the Manning roughness coefficient and the coefficient of the Meyer-Peter and Müller formula (the sediment transport equation used).

Onda et al. (2019) used the the three-dimensional free surface flow equations extended to include flow through porous media and a non-equilibrium sediment transport equation to simulate levee breaching due to flow overtopping, unlike the above models which used the two-dimensional shallow water equations. They used their model to simulate laboratory levee breaching tests and showed that the model reasonably reproduced the levee breaching process. They also identified limitations of their model in reproducing sediment standstill and slope slumping.

Unlike the physically-based breach models listed above, Cantero-Chinchilla et al. (2018) presented a physically-based breach model for modelling of levee breaching due to flow overtopping based on the two-dimensional Reynolds-averaged Navier-Stokes equations for a fluid-sediment mixture. They compared simulation results with experimental data and reported that the model satisfactorily reproduced the levee breaching process. They pointed out that the erosion at the toe of the levee was overestimated by the model.

From a theoretical point of view, the physically-based breach models listed above are the appropriate approaches for modelling of levee breaching. However, the simplifying assumptions in the reported models limit their applicability for use in practice for modelling real levee breaches. The main limitations of these models are listed below:

- Physically-based breach models are mainly tested for modelling the breaching of levees constructed of non-cohesive homogeneous material due to flow overtopping as mentioned above.
- They are also mainly tested using laboratory levee breaches. The models that have been tested on real breaches (e.g. Faeh (2007)) have used extensive simplifying assumptions.
- The models require the breach location and the initiation of the breach in the form of a notch at the breach location to be defined a priori.
- The breaching process modelled by these models is sensitive to the values of the parameters of the sediment transport formula used, such as the coefficient of the Meyer-Peter and Müller formula (Elalfy et al. 2018) or the coefficient of erodibility (Bonelli 2013).

- It is also questionable whether the sediment transport equation derived for normal flow conditions, such as the Meyer-Peter and Müller formulae, is valid for levee overtopping flow conditions (ASCE/EWRI 2011). The equation is often corrected with an erodibility coefficient (Dazzi et al. 2019).
- In addition, the models use highly simplified approaches to model the lateral erosion of the levee due to slope slumping, which plays an important role in the widening of the breach, as can be seen from the references cited above.

Thus, although physically-based breach models are the appropriate approach for modelling of levee breaching from the theoretical point of view of, their applicability to real cases is limited.

2.5.5 Summary

It can be seen from the literature that a wide range of models with different assumptions and complexity are available for modelling levee breaching. The literature also shows that the choice of model type depends to some extent on the purpose of the study. Empirical models are used to estimate breach dimensions and breach discharge. Parametric and simplified physically-based models are used to model real levee breaching. And fully physically-based are often used to model laboratory levee breaching tests.

The literature has shown that parametric breach models are the best existing models for modelling of real levee breaches. As highlighted above, the state-of-the-art physically-based levee breach models have shortcomings for modelling of real levee breaches. Furthermore, a physically-based levee breach model can be seen as a special case of a parametric levee breach model, where the breach parameters are determined by the mathematical equations describing water flow, sediment transport, bed evolution and slope slumping. Since the objective of this research is to develop a methodology for the modelling of flood inundation due to real levee breaches, a parametric levee breach model is considered appropriate.

3 Flood inundation modelling

This chapter presents the physical basis and current methods of modelling flood inundation. A flood is the flow of a large volume of water over otherwise dry land when the water level in a water body, such as a river, rises above the level of the bank of the water body or the flood protection structure, or when the flood protection structure fails. The physical laws governing floods are therefore conservation of mass and conservation of momentum. Simplification of the mathematical equations derived from these laws is necessary to solve them numerically with reasonable resources. The hydrodynamic numerical model used in this research, Telemac-2D, is also described in this chapter.

3.1 Governing mathematical equations

Flooding is governed by the laws of conservation of mass and momentum like any other fluid flow such as water flow in rivers, estuaries, and pipes. In fluid flow problems, the law of the conservation of mass can be applied by considering a given control volume of the flow section. The law of the conservation of mass states that the mass of the fluid entering the control volume must be equal to the mass leaving the control volume plus the increase or decrease in the mass of the fluid in the control volume. When this law is applied to a transient incompressible fluid flow, it is possible to derive what is commonly known as the continuity equation. Similarly, when the law of conservation of momentum is applied to a transient incompressible fluid flow, it is possible to derive the equations for the conservation of momentum in fluid flows, also known as the Navier-Stokes (NS) equations. The derivation of the continuity equation and the NS equations is the subject of many books on fluid mechanics, see for example Schobeiri (2010) or (Hervouet 2007), and is therefore not repeated in this dissertation.

The continuity equation and the NS equations in a three-dimensional Cartesian coordinate system form a closed set of partial differential equations. The method of solving these equations without further simplification by numerical methods is known as direct numerical solution (DNS). Most flows of practical importance, such as pipe flows, open channel flows, floods, etc., are turbulent flows. Turbulent flow is a fluid flow that exhibits a chaotic flow nature in which fluid layers mix randomly. Laminar flow, on the other hand, is an ordered flow in which the fluid layers do not mix randomly. DNS for turbulent flows requires the flow domain to be described at a very high spatial and temporal resolution, high enough to capture the chaotic nature of turbulent flows. This is computationally expensive and impractical for modelling of environmental flows that span over large spatial and temporal dimensions.

To solve turbulent flows numerically with acceptable resources, the continuity and the NS equations are modified to account for turbulence fluctuations by decomposing the turbulent quantities into a mean and a fluctuating component (Schobeiri 2010). The resulting equations are known as the Reynolds Averaged Navier-Stokes (RANS) equations. The RANS equations have a closure problem because the modification leads to the introduction of new terms. These new terms are turbulent stresses (losses) known as Reynolds stresses. They are analogous to other surface stresses such as friction. The turbulent stress terms are a function of the fluctuating components and the average quantities, which leads to more number of unknown variables than the RANS equations (Rodi 1993). To obtain a solution to the RANS equations, it is therefore necessary to reduce the number of variables to the number of equations. This can be achieved by relating the turbulent stress terms to the average quantities. For this reason, several turbulence models have been developed. These models are discussed in section 3.1.2.

For most open channel flows, such as floods, the vertical momentum equation plays an insignificant role. In addition, the length scale of the vertical dimension in such hydraulic flows is much smaller than that of the horizontal dimensions. Therefore, the RANS equations can be averaged over the depth by assuming that the vertical momentum is negligible. This reduces the vertical momentum equation to a hydrostatic pressure distribution over the depth of the flow. This assumption is often referred to as the hydrostatic approximation. The resulting equations are known as the shallow water equations.

The shallow water equations, i.e., the depth averaged continuity and momentum equations, in Cartesian coordinates are given by equation (11) (continuity equation), equation (12) (momentum equation in the x-direction), and equation (13) (momentum equation in the y-direction).

$$\frac{\partial h}{\partial t}+\frac{\partial (hu)}{\partial x}+\frac{\partial (hv)}{\partial y}=S_h \tag{11}$$

$$\frac{\partial u}{\partial t}+u\frac{\partial u}{\partial x}+v\frac{\partial u}{\partial y}=-g\frac{\partial Z}{\partial x}+\frac{1}{h}\frac{\partial}{\partial x}\left(h\upsilon_t\frac{\partial u}{\partial x}\right)+\frac{1}{h}\frac{\partial}{\partial y}\left(h\upsilon_t\frac{\partial u}{\partial y}\right)+S_x \tag{12}$$

$$\frac{\partial u}{\partial t}+u\frac{\partial v}{\partial x}+v\frac{\partial v}{\partial y}=-g\frac{\partial Z}{\partial y}+\frac{1}{h}\frac{\partial}{\partial x}\left(h\upsilon_t\frac{\partial v}{\partial x}\right)+\frac{1}{h}\frac{\partial}{\partial y}\left(h\upsilon_t\frac{\partial v}{\partial y}\right)+S_y \tag{13}$$

The symbols in the equations (11) - (13) are defined as follows:

- x, y – the horizontal Cartesian coordinates in [m],
- t – time in [s],
- h – water depth in [m],
- Z – free surface elevation in [m],
- u – velocity components in the x-direction in [m/s],
- v – velocity components in the y-direction in [m/s],
- g – acceleration due to gravity in [m/s²],
- υ_t – momentum diffusion coefficient (also known as eddy viscosity) in [m²/s],

- S_h – fluid source or sink given in [m/s],
- S_x – a source or a sink of momentum within the domain in the x-direction in [m/s²], and
- S_y – a source or a sink of momentum within the domain in the y-direction in [m/s²].

The terms in the continuity equation are the variation of depth with time $\frac{\partial h}{\partial t}$, the variation of the flux in the x-direction ($\frac{\partial (hu)}{\partial x}$), the variation of the flux in the y-direction $\frac{\partial (hv)}{\partial y}$, and the sources and / or sinks of water in the domain (S_h), such as precipitation (source) or evaporation (sink).

The terms in the momentum equations are the depth-averaged velocity variation with time ($\frac{\partial u}{\partial t}$), the convective momentum transport ($u\frac{\partial u}{\partial x} + v\frac{\partial u}{\partial y}$), gravitational force ($-g\frac{\partial Z}{\partial x}$), diffusive momentum transport ($\frac{1}{h}\frac{\partial}{\partial x}\left(hv_t\frac{\partial u}{\partial x}\right) + \frac{1}{h}\frac{\partial}{\partial y}\left(hv_t\frac{\partial u}{\partial y}\right)$), and momentum sources or sinks including body forces (S_x). The terms are described using the momentum equation in the x-component as an example. The terms have the same meaning in the momentum equation in the y-direction. Sources or sinks of momentum and body forces are driving or dissipative forces such as bed friction (shear stress at the bed), wind drag (shear stress at the free surface due to wind), atmospheric pressure, etc.

Like the turbulent stress terms, the source terms and body forces in the shallow water equations should either be constant or must be related to the mean flow variables h, u and v to have a closed set of equations. For this reason, several empirical relationships have been developed in the past to relate the body forces to the mean flow variables. For flows in rivers and open channels, most of the body forces can be neglected except for bed friction. The bed shear stress can be evaluated using one of the various friction laws discussed in section 3.1.1.

3.1.1 Bottom friction

An important body force in environmental flows is the flow resistance loss at the bed. It is used to calibrate numerical models. It is a quadratic function of the flow velocity and is given by equation (14), in the form it would appear in equations (12) and (13).

$$S_{fi} = -\frac{1}{2h}C_f u_i\sqrt{u^2 + v^2} \qquad (14)$$

Where C_f is a dimensionless friction coefficient, i stands for the x- and y- directions, and the other variables are as defined above. In practice, the dimensionless friction coefficient C_f is replaced by the Chezy coefficient or another friction coefficient. The dimensionless friction coefficient can be related to coefficients of the common empirical friction laws as given by equations (15) – (18) (Hervouet 2007).

$$\text{Chezy's law, } C_f = \frac{2g}{C^2} \qquad (15)$$

$$\text{Strickler's law, } C_f = \frac{2g}{(Kh^{1/6})^2} \quad (16)$$

$$\text{Manning's coefficient, } C_f = \frac{2gn^2}{\left(h^{1/6}\right)^2} \quad (17)$$

$$\text{Nikuradtse's law, } C_f = \frac{2g}{\left(7.83 \ln 12\frac{h}{k_s}\right)^2} \quad (18)$$

The variables in equations (15) to (18) are as follows: g is the acceleration due to gravity [m²/s]; c is Chezy's friction coefficient [$m^{1/2}/s$]; K is Strickler's friction coefficient [$m^{1/3}/s$]; h is the depth of flow [m]; n is Manning's friction coefficient [$s/m^{1/3}$]; and k_s is the roughness height in Nikuradtse's friction formulation [m].

3.1.2 Turbulence modelling

The RANS equations or the shallow water equations are the mathematical basis for the modelling of environmental flows. However, as discussed in section 3.1, these equations are an unclosed set of equations due to the turbulent stress terms. Turbulence models have been developed in the past to close the set of equations. Rodi (1993, p. 2) defines a turbulence model as "a set of equations (algebraic or differential) which determine the turbulence transport terms in mean-flow equations and thus close the system of equations".

The approach of many turbulence models is based on the Boussinesq hypothesis, which is based on the eddy viscosity principle. In analogy to the viscous stresses in laminar flow, Boussinesq proposed that turbulent stresses are proportional to mean velocity gradients with eddy viscosity (υ_t) as the constant of proportionality. Unlike the molecular viscosity, eddy viscosity is not a physical property of the flowing fluid. It depends on the turbulence state of the flow and is difficult to estimate. It can vary in both time and space. Therefore, most turbulence models are based on determining the value of the eddy viscosity from the mean flow velocities. The turbulence models commonly used in hydraulic engineering and also implemented in Telemac-2D are the constant eddy viscosity model, the Elder model, mixing length models (e.g. Smagorinski model) and the κ-ε model.

The constant eddy viscosity model is one of the most widely used turbulence models. It assumes that the eddy viscosity in the Boussinesq equation is constant in space and time, although this is theoretically incorrect. The difficulty with the constant eddy viscosity model is the choice of the value of the eddy viscosity. Studies show that the value of the eddy viscosity can vary from as low as 0.12 m²/s up to as high as 1500 m²/s in river flow modelling applications alone (Hervouet 2007). The common methods used to determine the value of eddy viscosity are dye experiments, existing empirical relationships, and trial and error simulations (Rodi 1993). Rodi (1993) states that the turbulent stress terms in the RANS equations are less important for flow in large water bodies and can be neglected. He further states that the use of eddy viscosity is often necessary to increase numerical stability. In shallow water equations, the value of the constant eddy viscosity is the sum of the turbulent viscosity, the molecular viscosity and the dispersion resulting from depth averaging (Hervouet 2007).

The Elder turbulence model is proposed for the shallow water equations. It accounts for dispersion effects due to the depth averaging. The model proposes the use of two different coefficients: K_l in the longitudinal flow direction [m²/s] and K_t in the transverse flow direction [m²/s]. Based on observations and calculations, Edler determined the values of these coefficients to be as given by equations (19) and (20) (Hervouet 2007).

$$K_l = 6u^* h \tag{19}$$

$$K_t = 0.6u^* h \tag{20}$$

Where h is the depth of flow [m] *and* u^* is the shear velocity [m/s] given by equation (21). The variables in equation (21) are as defined above.

$$u^* = \sqrt{\frac{C_f}{2}(u^2 + v^2)} \tag{21}$$

The so-called mixing length turbulence models are turbulence models based on Prandtl's hypothesis. Prandtl proposed in 1925 the hypothesis that Boussinesq's eddy viscosity is proportional to a mean fluctuating velocity *V'* and a length dimension l_m, often referred to as the mixing length. He further postulated that the mean fluctuating velocity is given by $V' = l_m \left|\frac{\partial V}{\partial y}\right|$. Thus, the eddy viscosity, assuming proportionality constant of 1, is given by equation (22) (Hervouet 2007).

$$v_t = {l_m}^2 \left|\frac{\partial V}{\partial y}\right| \tag{22}$$

The mixing length l_m [m] is determined from empirical formulae. For free layers it is assumed to be proportional to the laminar layer width. The most popular empirical equation is that proposed by von Karman, who gave the mixing length as $l_m = \kappa z$, where $\kappa = 0.41$ (von Karman constant) and z [m] is the distance from the wall in the region of the wall's influence and is otherwise constant.

The Smagorinski turbulence model is a sub-grid type of turbulence model based on the mixing length concept. The formula for the eddy viscosity in two-dimensions is given by equation (23) (Hervouet 2007). It is analogous to equation (22).

$$v_t = {C_s}^2 \Delta^2 \sqrt{\left(\frac{\partial u}{\partial x}\right)^2 + \left(\frac{\partial v}{\partial y}\right)^2 + \left(\frac{\partial u}{\partial y} + \frac{\partial v}{\partial x}\right)^2} \tag{23}$$

Where C_s is a dimensionless coefficient and Δ [m] is the mesh size. C_s ranges from 0.1 (channel flow) to 0.2 (isotropic turbulence) and needs to be calibrated. According to Hervouet (2007), this model is best understood in 3D and dispersion is not included in 2D.

Finally, we have the k-ε turbulence model. It is based on the concept of accounting for the effect of turbulence by calculating physical quantities that represent turbulence in the flow:

turbulence kinetic energy and its dissipation. The letters k and ε are often used to denote turbulent kinetic energy and its dissipation respectively. The eddy viscosity is related to κ and ε by equation (24) (Hervouet 2007).

$$v_t = C_\mu \frac{k^2}{\varepsilon} \tag{24}$$

The two-dimensional forms of the k and ε equations are given by equations (25) and (26) (Hervouet 2007).

$$\frac{\partial k}{\partial t} + u\frac{\partial k}{\partial x} + v\frac{\partial k}{\partial y} = \frac{1}{h}\frac{\partial}{\partial x}\left(h\frac{\nu_t}{\sigma_k}\frac{\partial k}{\partial x}\right) + \frac{1}{h}\frac{\partial}{\partial y}\left(h\frac{\nu_t}{\sigma_k}\frac{\partial k}{\partial y}\right) + P - \varepsilon + P_{kv} \tag{25}$$

$$\frac{\partial \varepsilon}{\partial t} + u\frac{\partial \varepsilon}{\partial x} + v\frac{\partial \varepsilon}{\partial y} = \frac{1}{h}\frac{\partial}{\partial x}\left(h\frac{\nu_t}{\sigma_k}\frac{\partial \varepsilon}{\partial x}\right) + \frac{1}{h}\frac{\partial}{\partial y}\left(h\frac{\nu_t}{\sigma_k}\frac{\partial \varepsilon}{\partial y}\right) + \frac{\varepsilon}{k}[C_{1\varepsilon}P - C_{2\varepsilon}\varepsilon] + P_{\varepsilon v} \tag{26}$$

The production terms in equations (25) and (26) are always positive and can be determined with the following equations.

$$P = \nu_t\left[2\left(\frac{\partial u}{\partial x}\right)^2 + 2\left(\frac{\partial v}{\partial y}\right)^2 + \left(\frac{\partial u}{\partial y} + \frac{\partial v}{\partial x}\right)^2\right] \tag{27}$$

$$P_{kv} = C_k\frac{u_*^3}{h} \tag{28}$$

$$P_{\epsilon v} = C_\epsilon\frac{u_*^4}{h^2} \tag{29}$$

In equations (28) and (29), u_* [m/s] is the friction velocity on the bottom, which can be determined from the employed bottom friction law as given by equation (21). Likewise, the coefficients C_k [-] and C_ε [-] are related to the employed friction law as given by the equations (30) and (31).

$$C_k = \frac{1}{\sqrt{C_f}} \tag{30}$$

$$C_\epsilon = 3.6\frac{C_{2\varepsilon}\sqrt{C_\mu}}{C_f^{3/4}} \tag{31}$$

where C_f is a dimensionless friction coefficient that can be calculated from the bed friction law. The other constants used in equations (24) to (31) have been determined experimentally and are given in Table 4 as reported by Hervouet (2007, p. 72)

Table 4: Constants of the k-ε model (taken from Hervouet (2007, p. 72)).

C_μ	$C_{1\varepsilon}$	$C_{2\varepsilon}$	σ_κ	σ_ε
0.09	1.44	1.92	1.0	1.3

In this work, the constant eddy viscosity model is chosen to model turbulence. The more complex models, such as the k-e model, require calibration of the model constants for the particular flow situation and are often required to study flow patterns, velocity fields and turbulence intensity in rivers with complex geometries or near obstacles such as bridges, weirs and groynes. For flood inundation modelling, it is sufficient to apply the constant turbulence viscosity model (Hervouet 2007).

3.1.3 Hydraulic jump

Hydraulic jump is a phenomenon observed in open channel flows when a supercritical flow discharges into a subcritical flow region. The high velocity in the supercritical flow region is slowed down with a corresponding increase in flow depth in the subcritical flow region. Hydraulic jumps represent discontinuities in the solution of the shallow water equations (Hervouet 2007).

Hydraulic jumps might occur after flow through a levee breach depending on the breach characteristics. Thus, it is important to use a hydrodynamic numerical model which is capable of handling hydraulic jumps. Hervouet (2007) showed, using flow over a weir with a hydraulic jump, that Telemac-2D gives a good approximation to the discontinuous solution due to a hydraulic jump.

3.2 Hydrodynamic numerical model - Telemac-2D

This research uses the hydrodynamic numerical model Telemac-2D. Telemac-2D is part of the open Telemac-Mascaret suite of solvers, which are in the public domain. The source codes can be downloaded from Telemac-Mascaret GitLab repository (https://gitlab.pam-retd.fr/otm/telemac-mascaret) and compiled for use. The software suites are developed and maintained by a consortium of organisations, of which Electricité de France Research and Development (EDF R&D) is the main developer and maintainer of Telemac-2D (TELEMAC 2019a). Telemac-Mascaret version v7p3r1 is used in this work.

Telemac-2D numerically solves the shallow water equations discussed in section 3.1. Both the finite element and finite volume methods are implemented in Telemac-2D. In this work, the finite element method is used with a semi-implicit time stepping scheme, as this combination provides the optimal computational time without compromising accuracy (Hervouet 2007).

In addition, the method of characteristics is chosen for the simulations in this work. In this case, the fractional step method is used to solve the equations in two steps: advection and propagation steps. In the advection step, the advection terms of the physical quantities are solved. In the second step, the propagation step, the remaining terms such as propagation, diffusion and source terms are solved. If the method of characteristics is not preferred, the entire system of equations is solved in one step together with the advection terms.

The time and space discretisation of the equations transforms them into algebraic equations with unknown h, u, and v at the mesh nodes. The resulting algebraic equations are then solved using the conjugate gradient method. For further details on the numerical

approach used by Telemac-2D, the reader is referred to the user manual (Ata 2018) and the book by the main developer of Telemac-2D (Hervouet 2007).

3.3 Summary

Flooding, like any other fluid flow, is governed by the laws of conservation of mass and momentum. Applying these laws to fluid flow gives the continuity equation and the NS equations. Averaging the continuity equation and the NS equations to account for turbulence fluctuations gives the RANS equations. The vertical averaging of the RANS equations gives the shallow water equations, which are the mathematical equations for the modelling of flood propagation.

The shallow water equations are non-linear partial differential equations for which analytical solutions exist only for few simple cases. In the majority of cases, the equations must be solved numerically. Telemac-2D is a publicly available code for the numerical solution of the shallow water equations. In this work, Telemac-2D is used with the options finite element method, the method of characteristics and semi-implicit time stepping scheme.

4 Development and implementation of a parametric levee breach model

As discussed in Chapter 2, parametric levee breach models are the best existing models for modelling of real levee breaches. Since the objective of this research is to develop a methodology for the modelling of flood inundation due to real levee breaches, a parametric levee breach model is considered appropriate. Therefore, a parametric levee breach model is developed based on the levee breaching processes discussed in the literature (Chapter 2). This chapter describes the development and implementation of this parametric levee breach model.

4.1 Simplified levee breaching processes

As discussed in section 2.2, the main cause of levee failure is hydraulic failure (high flood levels, prolonged high flows). The main causes of levee breaching are external erosion of the levee due to flow overtopping, internal erosion of the levee or levee foundation material (seepage), slope failure or a combination of these. The high river flow itself may be the result of extremely high precipitation, snowmelt, or water releases from upstream reservoirs, or a combination of these.

The processes of breaching of both non-cohesive and cohesive levees due to overtopping can be generalised into four phases as given in Section 2.3. The initiation of levee breaching due to internal erosion can be generalised into four phases as described in Section 2.4. The last phase is comparable to the end of the first phase of overtopping breaching. The breaching of the levee then follows the phases 2 – 4 of levee breaching due to overtopping. The duration of each phase is variable and depends on the flow (discharge) in the river, the water level in the river, the properties of levee material (material size, soil cohesion, density, tensile strength, etc), the levee dimensions and the levee conditions (compaction, compaction water content, core and outer layers, etc.). These levee breaching phases can be further simplified into 3 stages: 1) initiation of the breach, 2) formation of the initial breach channel and the vertical erosion of the levee, and 3) the lateral widening of the breach channel, as shown schematically in Figure 14.

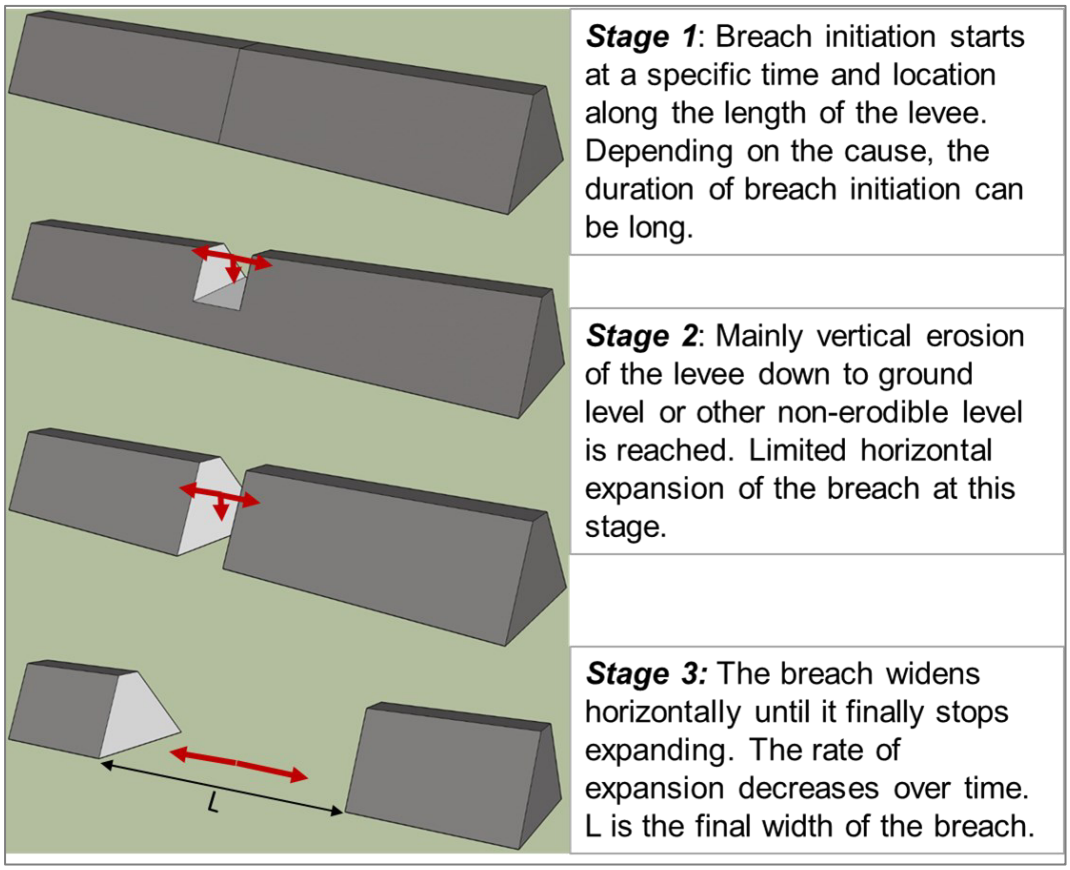

Stage 1: Breach initiation starts at a specific time and location along the length of the levee. Depending on the cause, the duration of breach initiation can be long.

Stage 2: Mainly vertical erosion of the levee down to ground level or other non-erodible level is reached. Limited horizontal expansion of the breach at this stage.

Stage 3: The breach widens horizontally until it finally stops expanding. The rate of expansion decreases over time. L is the final width of the breach.

Figure 14: Schematic diagram showing the three main stages of levee breaching.

4.2 Parametric levee breach model

A parametric levee breach model is developed based on the simplified levee breaching processes described above. In the model, the stages of the breaching processes are defined by parameters that need to be defined a priori. They could be estimated from historical values or using empirical equations. The breach model creates the breach opening by lowering the elevation of the levee based on the defined parameters. Erosion and deposition processes are not considered. The effect of the erosion and deposition processes on the flood inundation is insignificant and therefore the simplification is reasonable.

The first stage of breaching (stage 1), i.e., the initiation of the levee breach, is defined by the breach location and the method of breach initiation. Depending on the method of breach initiation, additional parameters might be required. The second and third stages of the levee breaching process are defined by the breach duration, the initial breach width, the final breach width and the final level of the breach.

The vertical erosion stage (stage 2) is assumed to be significantly faster than the horizontal expansion stage (stage 3). It takes place in fraction of the total breach duration. In this model, the duration of the vertical erosion stage is taken as tenth of the total breach duration, but it can be adapted to suite other needs. The lateral breach expansion continues for the duration of the breach until the final breach width is attained.

4.2.1 Breach initiation

The initiation of levee breaching is a complex phenomenon and the most difficult to predict. The breach model uses the water level in the river to initiate levee breaching at pre-defined breach location(s). Depending on the expected cause of the breach, three breach initiation options are provided. These are at a specified time (option 1), when the water level on the levee is greater than a specified level (when the levee is overtopped) (option 2), or when the water level in the river is greater than a specified critical value (option 3).

Option 1 is of particular interest when investigating historical levee breach floods where the time of breach is known. It can also be used in other cases where the start time of the breach can be predicted by the modeller, or where the other options are known to be unsuitable, for example in laboratory monitored breaches.

Option 2 can be used for levee breach studies where there is an established relationship between levee stability and water level. Such information may be available for well designed and maintained levees. This option is suitable for levee breaches due to overtopping, as overtopping occurs when the water level in the river channel is higher than the levee crest level. The critical water level should be chosen carefully when using this option. Many numerical models use drying and wetting algorithms to deal with model areas that are partially flooded. These algorithms typically add a fictitious water depth to nodes that are not flooded.

Option 3, on the other hand, is suitable for levees that have sufficient free board but are known to fail when the water level in the river reaches a known critical value, which is lower than the levee crest level. Levee breaching due to internal erosion (piping) can occur at water levels below the levee crest. Option 3 is therefore suitable for initiating levee breaches due to internal erosion.

4.2.2 Breach duration

The time taken by the breaching processes from the start to the end of levee erosion, both laterally and vertically, is given by the breach duration. Breach duration depends on the characteristics of the levee material, the flow in the river, the geometric characteristics of the levee, the breach flow, etc, as discussed in Sections 2.3 and 2.4. As a result, there is a high degree of uncertainty in estimating the breach duration. It can be estimated on the basis of historical breaches, the duration of breaches of other levees with similar characteristics in terms of both levee material properties and river flow characteristics, and empirical equations.

4.2.3 Breach location

Levees can be many kilometres long and they can breach at any point along their length during extreme river floods. This makes determining the location of a potential levee breach a challenging task. Failure of engineering structures such as levees generally occur when the loads acting on the structure exceed the resisting forces (Apel et al. 2006). The loads to be considered vary depending on the cause of the breach. A methodology for the determining the location of a potential levee breach is discussed in Chapter 6.

4.2.4 Final breach width

The final breach width is the final width of the bottom of the resulting breach along the axis of the levee. Like the breach duration, the final breach width also depends on the characteristics of the levee material, the flow in the river, the geometric characteristics of the levee, the breach flow, and so on. Like the breach duration, there is a high degree of uncertainty in estimating the final breach width and it can be estimated from historical breaches, the final breach widths of other levees with similar characteristics in terms of both levee material properties and river flow characteristics, and empirical equations.

4.2.5 Final breach level

The final breach level is the final elevation of the breached levee. It can be assumed to be the elevation of the water-side floodplain or berm in the case of a complete breach, as this is a relevant factor for the flow through the breach and thus the inundation of the leveed area.

4.3 Implementation of the levee breach model in Telemac-2D

The breach model is integrated into the hydrodynamic numerical model Telemac-2D. This enables the integrated modelling of the levee breach and the subsequent flood inundation. As highlighted in Chapter 1, the integrated modelling of levee breach and flood inundation is a recommended approach for the modelling of flood inundation due to levee breach (Dazzi et al. (2019), Apel et al. (2009)), as this way the flow from the river to the floodplain (or back from the floodplain to the river) can be calculated by the flow model based on the prevailing conditions without further simplifications.

The levee breach model presented in Section 4.2 is implemented in Telemac-2D by programming it in the subroutine ‘breach.f’, which can be obtained from the Telemac-Mascaret GitLab repository (https://gitlab.pam-retd.fr/otm/telemac-mascaret). The new implementation extends an existing breach implementation. In the existing breach implementation, the levee breach is created by lowering the levee height along the entire length of the breach.

The modelling of levee breaches in Telemac-2D is activated by setting the keyword ‘BREACH’ = YES and providing the file containing the breach parameters with the keyword ‘BREACHES DATA FILE’ in the steering file of Telemac-2D. When a levee breach is intended, Telemac-2D reads the breach parameters from the BREACHES DATA FILE. By default, Telemac-2D does not assume a breach. Furthermore, at each time step of the flow simulation, Telemac-2D checks whether a breach should be initiated or not, based on the breach initiation criteria provided in the breaches file.

The breaches data file specifies the number of breaches and the breach parameters for each breach. Table 5 gives the list of the breach parameters of the parametric breach model and their description. An example of a breaches file is given in Appendix 1.

Table 5: Parameters in the breaches file and their description.

No.	Parameter	Description
1	Number of breaches	This gives the number of independent levee breaches in the current model. The following parameters should be provided for each breach.
2	Width of polyline defining breach	This parameter corresponds to the bottom width of the levee. It is used to create a breach zone. The heights of the mesh nodes within the breach zone are lowered to the breach level calculated for the time at questions based on the other parameters.
3	Option for the breach initiation	This parameter specifies the method of initiating the levee breach, which can be: - 1: at a given time - 2: when the water level above the levee crest reaches a specified value - 3: when the water level in the river reaches a specified value
4	Breach duration	The duration of the levee breach in seconds. An instantaneous breach would have a breach duration of 0 seconds.
5	Option of levee lowering	This parameter specifies how the levee is lowered. Two options are available: - 1: vertical lowering (old method in Telemac-2D) - 2: vertical lowering and horizontal widening (developed in this work).
6	Final level of breach	This parameter specifies the final level of the breach area (see Section 4.2.5).
7	Number of nodes	This parameter gives the number of nodes on the levee crest that are affected by the breach.
8	Coordinates of the nodes	This gives the coordinates of the points along the levee axis affected by the breach. The sum of the distances between adjacent points is the final breach width (see Section 4.2.4).
9	Start time of breach	This parameter specifies the breach start time in seconds from the simulation start time of the flow model when the option for the breach initiation is 1, i.e., at a given time.
10	Global mesh node number controlling the breach	This specifies the global mesh node number of a point in the river when the option for the breach initiation is 3, i.e., when the water level in the river reaches a specified value.

No.	Parameter	Description
11	Control level of breach	This parameter gives the value of the limit water level value when the option for the breach initiation is 2 or 3 (see the parameter "option for breach initiation").

The number of breaches specifies the number of independent levee breaches to be simulated. The levee bottom width is the bottom width of the levee cross-section at the given breach location. Together with the breach width, it defines the levee breach area for which the height of the mesh nodes is lowered during the simulation.

If the breach is initiated at a specific time, this time is given as a parameter in the breaches data file. If the initiation of the breach is based on a water level above the levee crest level, then the corresponding critical water level is given in the breaches data file. If the initiation of the breach is based on a water level at a point in the river, then the global node number of the point and the corresponding critical water level are given in the breaches data file.

For the case of the option of levee breaching developed in this work (vertical and horizontal breaching), if the conditions for initiating a breach are met, the breach starts at the centre of the levee length affected by the breach. The initial breach width is set to one tenth of the final breach width or the distance between the mesh nodes at the centre of the levee affected by the breach, whichever is greater (see Section 4.2).

The levee breaching process then takes place in two stages. The first stage occurs in one tenth of the specified breach duration and the breach grows both vertically and laterally. The heights of the nodes in the affected area are calculated using a vertical lowering rate. The vertical lowering rate of the first stage is calculated as the maximum difference between the heights of the nodes in the affected area and the final breach level divided by the duration of the first stage. The active breach area at time t from the start of the breach is determined from the width of the polyline defining the breach and the active breach width at time t. The active breach width at time t from the start of the breach is calculated from a linear relationship between the breach duration and the final breach width. At each simulation time step after the start of breach and for the duration of the breach, a new breach level is calculated for the nodes lying in the breach area and, if the height of a given node in the breach area is greater than the calculated breach level, it is lowered to the breach level. The heights of the nodes that are less than the breach level remain unaffected.

In the second stage, the breach grows laterally. At each simulation time step after the start of the breach and for the duration of the breach, the active breach width is calculated using a similar linear relationship as in the first stage, and the area affected by the breach is also determined in the same way as in the first stage. The heights of all nodes in the breach area that are greater than the final breach level are then lowered to the final breach level.

4.4 Summary

This chapter discussed the development of a parametric breach model and its implementation in Telemac-2D. The breach model is based on the simplification of levee

breaching processes observed in physical experiments and field tests in the literature. In the presented parametric breach model, levee breaching is described by parameters and takes place in three stages: i) initiation of the breach, ii) mainly vertical lowering of the levee and iii) mainly lateral widening of the breach. These stages are defined in the breach model by the parameters breach initiation, breach location, breach duration, final breach level, and final breach width. Breach location and final breach width are defined by the coordinates of the mesh nodes affected by the breach.

5 Estimation of levee breach parameters from historical levee breaches

In this chapter, historical levee breaches are presented and analysed to derive empirical equations for levee breach parameters (mainly final breach width, due to the limited information available) using regression fitting and artificial neural networks.

5.1 General

As discussed in Chapter 2, we have a limited understanding of levee breaching processes and therefore modelling levee breaches is associated with high uncertainty. One way to reduce uncertainty is to use full-scale levee breach experiments. However, full-scale experiments are not only very expensive, but also cannot represent the complex hydraulic and geotechnical characteristics of real levee breaches (Özer et al. 2020).

Historical levee breaches can play an important role in this regard. Historical breach data can be used to derive empirical equations for breach parameters, given the relatively large number of historical levee breaches. Such empirical equations help modellers to estimate breach parameters, which otherwise may have to be estimated from past comparable breach events and the modeller's engineering judgement. Unfortunately, limited breach data are often collected during levee breach events, as saving lives and property is the first priority during such disasters. This limitation makes it difficult to derive empirical equations with high coefficients of determination.

There are some freely accessible levees breach databases that can be used for the analysis of historical levee breaches, including the derivation of empirical equations for breach parameters. Recently, a freely accessible levee breach and performance database called International Levee Performance Database (ILPD) has been created at TU Delft, The Netherlands (Özer et al. 2020). The database is available online at https://leveefailures.tudelft.nl/. It is compiled from information available in publications and other regional, national, and international databases.

5.2 Database of historical levee breaches

The list of levee breaches used in this research is primarily compiled from the ILPD. This data is supplemented and cross-checked with other existing compilations and the literature. This section describes the data from the ILPD and the additional compilation of breach data from the literature not yet included in the ILPD.

5.2.1 International Levee Performance Database (ILPD)

The ILPD is a freely accessible database on levee breach and performance, developed and maintained by TU Delft. The data are collected from various literatures and databases, which can be found in Özer et al. (2020). The database is event-based, where levee breaches are grouped according to a hydrological event. For example, all levee breaches on the River Elbe during the August 2002 floods are listed under one event. For each levee breach case, the following data, if available, are included in the database:

- Data on the levee
- Embankment type
- Embankment soil type
- Levee geometry (cross-sectional elements)
- Date of failure
- Breach mechanism
- Location of levee breach (country, address, geo-coordinates, etc.)
- Breach data
- Final breach width
- Final breach level
- Duration of loading
- Time of peak discharge
- Peak discharge
- River flow data
- Maximum water level
- Design flow
- Source of information (references)

The ILPD used consistent terminology for definitions and levee breach parameters for the database. The main elements of a levee cross-section included in the ILPD are given in Figure 15.

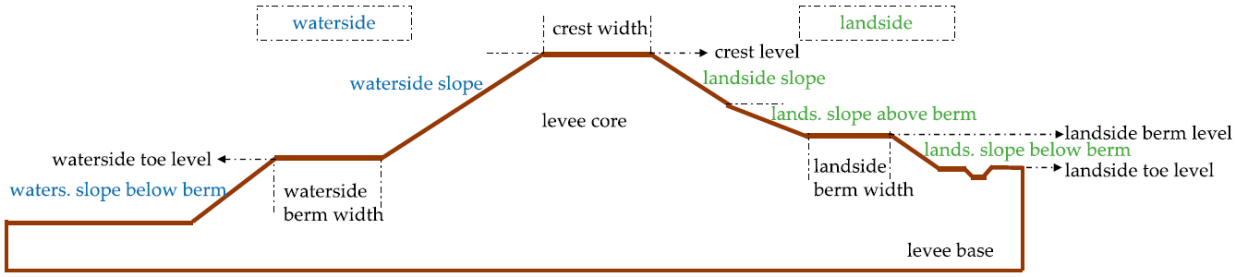

Figure 15: Cross-section of a levee showing the main geometric elements included in the ILPD (taken from Özer et al. (2020, p. 6)).

The general statistics of the ILPD can be found in Özer et al. (2020). For the analysis here, the datasets from the year 1900 to 2020 (downloaded from the database as of February 2021) are used. The database contains limited information for the levee breaches before 1900, which are not relevant for the regression analysis of the levee breach parameters. For the period 1900 - 2020, the database contains 882 number of breach records, of which 103 are dam breaches, 762 are levee breaches, 13 are levee-structure combination

breaches, one is a dune breach and 14 are cases where the type of flood defence structure is not specified (see Figure 16). Most cases are reported from the USA, Hungary, Germany, the Netherlands, the Czech Republic, the UK and China, as shown in Figure 17.

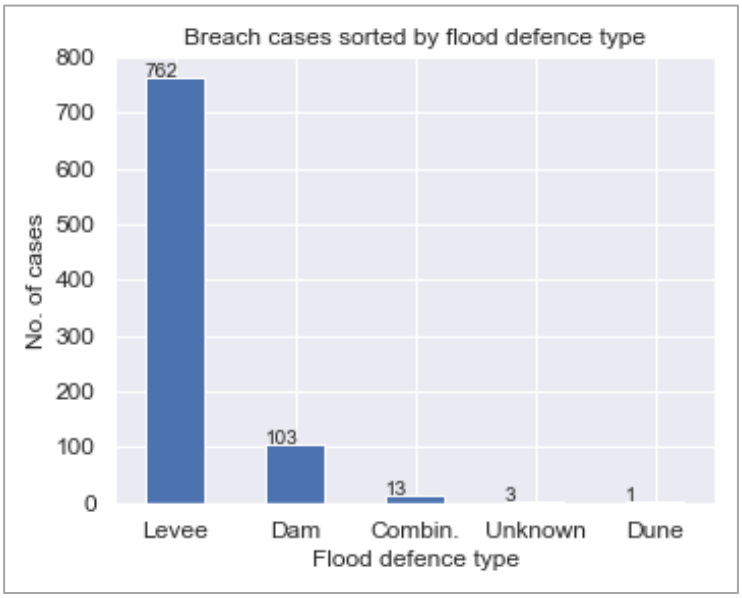

Figure 16: Number of flood defence failure cases from the ILPD grouped by flood defence type.

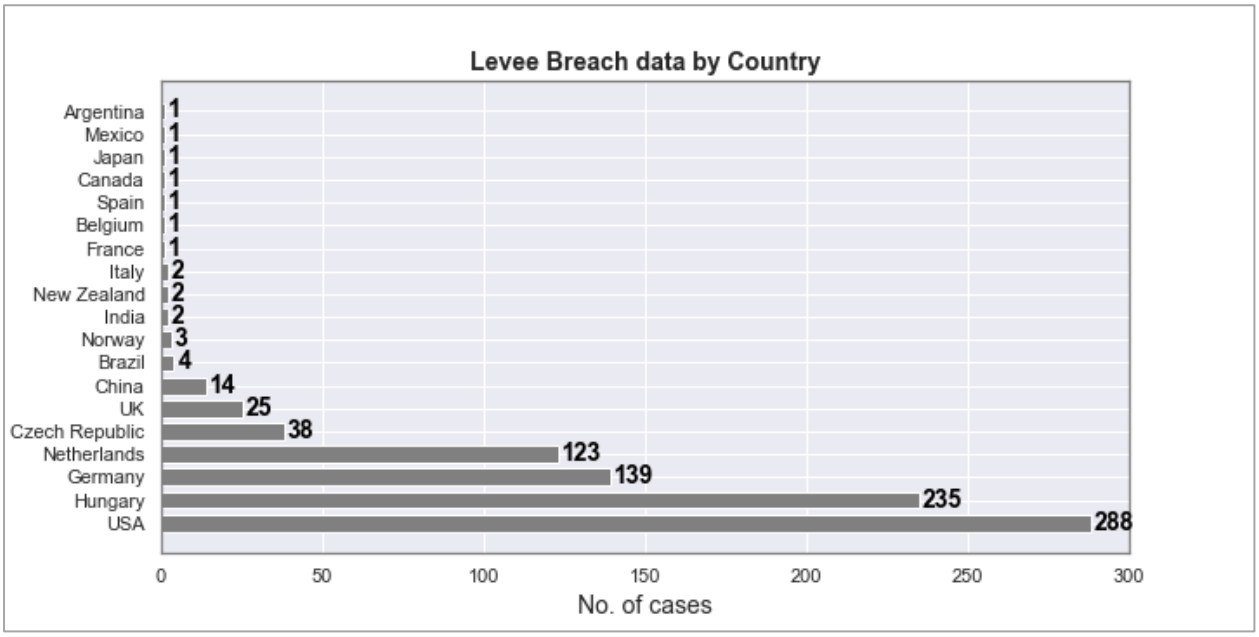

Figure 17: Number of levee breach cases in the ILPD grouped by country where the failure occurred.

Since the aim of this analysis is to establish empirical equations for the estimation of breach parameters, only datasets in the ILPD that meet the following criteria are considered:

- Flood defence type: only levees and levee-structure combinations are considered.
- Breach parameters: Only cases with at least data on the final breach width are included. There are 510 breach cases that meet this criterion. These consist of 495 real failure cases, 5 full scale experiments and 10 small scale experiments as shown in Figure 18.

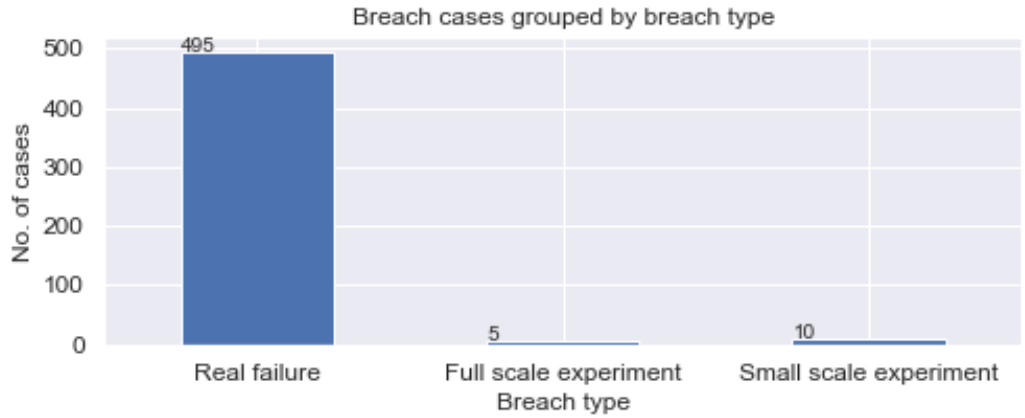

Figure 18: Number of levee and levee-structure breach cases in sthe ILPD grouped by breach type.

- Real levee breaches: In line with the objective, only real levee breaches are considered. Incidents that did not result in a breach, such as incidents that resulted in overtopping but no breach, and breaches deliberately created to relieve flooded areas are excluded from the dataset. There are 15 man-made breaches, 2 incidents that did not result in a breach and 3 duplicate entries in the dataset. This reduces the number of breaches to 474.
- River levee breaches: Some of the levee breaches in the database correspond to sea levees. As the focus of this analysis is on riverine levees and there are important differences between breaching of sea and riverine levee breaches, such as the direction of loading, flood duration, design approach, etc., only riverine levee breaches are retained for analysis. There are 409 riverine levee breaches in the dataset filtered above.
- Final breach width: the examination of the final breach width in the dataset shows that the minimum and maximum final breach widths are 2 m and 2086 m respectively, which are quite small and large respectively. These datasets are therefore examined further. It can be seen from the information in the ILPD that breaches with quite small final breach widths are associated with too many other breaches during the same event, breaches initiated by failure of a structure crossing the levee, and poor design, construction and maintenance of the levee. Therefore, all breach cases with a final breach width of less than 10 m are excluded from the dataset for this analysis. Levee breaches with a final breach width greater than 400 m are summarised in Table 6. Some of the cases with unjustifiably large final breach widths, i.e., greater than 600 m, are removed from the dataset for this analysis. This leaves a total of 388 levee breaches that could be extracted from the ILPD for this analysis.

Table 6: Actual riverine levee breaches in the ILPD with final breach widths greater than 400 m.

Nr.	Case name (ILPD)	Date	Final breach width [m]	Contributing factors	Country	Comments
1	Zhaoyan County Farm dike	14.08.1998	480	-	China	The final breach width is within a plausible range and the case is therefore included in this analysis.
2	Paizhou dike	01.08.1998	760	Locally smaller cross-section of the levee	China	The case was excluded from this analysis as it was reported that the levee was too low at the point of the breach.
3	Levee failure in water body called Feather River, 1909	01.01.1909	2086	-	USA	The case was excluded from this analysis as the final breach width is unusually large (outlier).
4	Levee failure in water body called Feather River, 1911	01.01.1911	2086	-	USA	Same comment as 3.
5	Levee failure in water body called Feather River, 1955	01.01.1955	2086	-	USA	Same comment as 3.
6	Levee failure in water body called Feather River, 1955	01.01.1955	1529	-	USA	Same comment as 3.
7	Levee failure in water body called Feather River, 1997	01.01.1997	418	-	USA	Same comment as 1.

Nr.	Case name (ILPD)	Date	Final breach width [m]	Contributing factors	Country	Comments
8	Levee failure in water body called Sacramento River, 1907	01.01.1907	488	-	USA	Same comment as 1.
9	Levee failure in water body called Feather River, 1955	01.01.1955	418	-	USA	Same comment as 1.
10	Levee failure in water body called Georgiana Slough, 1992	01.03.1992	434	-	USA	Same comment as 1.
11	Czech Republic, Ostravice, 1997	01.07.1997	500	bad maintenance	Czech Republic	Same comment as 1.
12	Levee failure in water body called San Joaquin River, 1997	01.01.1997	530	-	USA	Same comment as 1.
13	Levee failure in water body called San Joaquin River, 1997	01.01.1997	457	-	USA	Same comment as 1.

5.2.2 Additional levee breach cases

Levee breach cases in the literature that are not yet included in the ILPD are compiled to complement the data from the ILPD. Most of these breach cases are from Japan, which occurred during Typhoon Hagibis in 2019 and are reported by Enomoto et al. (2021). In addition, levee breaches in Italy reported in the literature but not yet included in the ILPD are compiled. These are the levee breaches on the Secchia and Panaro rivers in January 2014 reported by Orlandini et al. (2015), Vacondio et al. (2016) and Shustikova et al. (2020) and the levee breaches on the Po River in November 1951 reported by Shustikova et al. (2020) and Masoero et al. (2013), and in June 1979 reported by Di Baldassarre et al. (2009).

Two levee breaches from Romania (Chendeș et al. 2015; Popescu et al. 2010), one from Ethiopia (Tadesse & Fröhle 2020) and one from the USA (Risher & Gibson 2016) are other additional cases found in the literature that are not yet included in the ILPD. The complete list of these additional breach cases and their corresponding levee, flow and breach parameters is given in Table 7.

Table 7: Levee breach cases in the literature not included in the ILPD yet.

No.	Description	Date	Final breach width [m]	Crest width [m]	Levee height [m]	Levee mater-ial	Breach mechanism	Country	Reference
1	Sacramento River Levee failure near Sutter Bypass 1997	04.01. 1997	260	-	14	Silt	internal erosion	USA	Risher & Gibson (2016)
2	Oppegawa River left side levee breach at river kilometer 7.6	13.10. 2019	40	-	5.2	Gravel	External erosion	Japan	Enomoto et al. (2021)
3	Oppegawa River right side levee breach at river kilometer 0	13.10. 2019	70	-	4.7	Silt	External erosion	Japan	Enomoto et al. (2021)
4	Tokigawa River left side levee at river kilometer 6.5	13.10. 2019	30	-	2.8	Clay	External erosion	Japan	Enomoto et al. (2021)
5	Tokigawa River left side levee breach at river kilometer 0.4	13.10. 2019	90	-	4.3	Sand	External erosion	Japan	Enomoto et al. (2021)
6	Tokigawa River right side levee breach at river kilometer 5.9	13.10. 2019	20	-	3	Gravel	External erosion	Japan	Enomoto et al. (2021)

No.	Description	Date	Final breach width [m]	Crest width [m]	Levee height [m]	Levee mater-ial	Breach mechanism	Country	Reference
7	Naka River left side levee breach at river kilometer 40	13.10. 2019	200	3	3.2	Gravel	External erosion	Japan	Enomoto et al. (2021)
8	Naka River left side levee breach at river kilometer 28.6	13.10. 2019	250	-	3.2	Sand	External erosion	Japan	Enomoto et al. (2021)
9	Naka River right side levee breach at river kilometer 41.2	13.10. 2019	250	3.7	2.7	Sand	External erosion	Japan	Enomoto et al. (2021)
10	Kuji River left side levee breach at river kilometer 25.5	13.10. 2019	100	-	3.1	Gravel	External erosion	Japan	Enomoto et al. (2021)
11	Kuji River left side levee breach at river kilometer 27	13.10. 2019	64	-	2.7	Silt	External erosion	Japan	Enomoto et al. (2021)
12	Kuji River left side levee breach at river kilometer 34	13.10. 2019	60		3-5	-	External erosion	Japan	Enomoto et al. (2021)
13	Kuji River right side levee breach at river kilometer 25.5	13.10. 2019	40	-	2.5	Sand	External erosion	Japan	Enomoto et al. (2021)

No.	Description	Date	Final breach width [m]	Crest width [m]	Levee height [m]	Levee mater-ial	Breach mechanism	Country	Reference
14	First of the four levee breaches along Omoigawa River Kanuma City	13.10. 2019	450	-	-	-	External erosion	Japan	Enomoto et al. (2021)
15	Second of the four levee breaches along Omoigawa River Kanuma City	13.10. 2019	450	-	-	-	External erosion	Japan	Enomoto et al. (2021)
16	Third of the four levee breaches along Omoigawa River Kanuma City	13.10. 2019	450	-	-	-	External erosion	Japan	Enomoto et al. (2021)
17	levee breach along Sabigawa River near Otawara City	13.10. 2019	150	-	-	Sand	External erosion	Japan	Enomoto et al. (2021)
18	Secchia River levee breach	19.01. 2014	80	-	-	-	Internal erosion	Italy	Orlandini et al. (2015); Vacondio et al. (2016)
19	Po River breach at Paviole	14.11. 1951	220	-	6.35	-	External erosion	Italy	Shustikova et al. (2020);

No.	Description	Date	Final breach width [m]	Crest width [m]	Levee height [m]	Levee mater-ial	Breach mechanism	Country	Reference
									Masoero et al. (2013)
20	Po River breach at Bosco	14.11. 1951	312	-	6.35	-	External erosion	Italy	Shustikova et al. (2020); Masoero et al. (2013)
21	Po River breach at Malcantone	14.11. 1951	204	-	6.35	-	External erosion	Italy	Shustikova et al. (2020); Masoero et al. (2013)
22	Timis River levee breach on the right bank at 6.25 km.	20.04. 2005	180	1	4	-	-	Romania	Popescu et al. (2010) and Chendeș et al. (2015)
23	Timis River levee breach on the right bank at 6.8 km.	20.04. 2005	250	1	4	-	-	Romania	Popescu et al. (2010) and Chendeș et al. (2015)
24	Awash River levee breach at Wonji	24.08. 1996	100	1.5	3	Silt	External erosion	Ethiopia	Tadesse & Fröhle (2020)

5.3 Data analysis

The total number of cases from ILPD and own compilation (see Table 7) that could be compiled for this analysis is 412. The information contained in the dataset that are relevant for this analysis are levee information (geometry, material, type, age), flow boundary conditions in the river (maximum water level, return period, duration of loading) and breach information (duration of breach, final breach width, final breach level, peak breach discharge, breach mechanism, intervention activities). Unfortunately, these parameters are not available for all the breach cases. The statistics of the parameters available for a relatively high number of breach cases are summarised in Table 8.

Information on the flow boundary conditions in the river available in the dataset are the maximum water level, the return period of the flood event and the loading duration. These are only available for a few cases. Therefore, the flow parameters could not be included for this analysis. The levee breach and levee parameters are discussed further in sections 5.3.1 and 5.3.2 respectively.

Table 8: Summary of the statistics of the parameters of the dataset used.

Statistics	Final breach width	Final breach depth	Levee height	Levee bottom width	Soil type	Breach mechanism	Levee type
Number of cases	412	163	341	290	212	315	186
Mean	86.8	5.8	2.9	17.3	n.a.	n.a.	n.a.
Std	88.9	4.5	1.5	8.0	n.a.	n.a.	n.a.
Min.	10.0	1.0	0.6	5.6	n.a.	n.a.	n.a.
Max.	530.4	22.0	14.0	59.4	n.a.	n.a.	n.a.

5.3.1 Levee breach parameters

The relevant breach-related parameters available in the dataset are final breach width, final breach depth, breach mechanism, peak breach discharge, breach duration and intervention activities. The number of available cases in the dataset corresponding to these parameters is given in Table 9.

Table 9: Number of cases for each breach parameter in the dataset.

Parameter	Final breach width	Final breach depth	Breach mechanism	Peak breach discharge	Breach duration	Intervention activities
No. of cases	412	163	315	73	7	1

Information on final breach width, final breach depth and breach mechanism is available for a significant number of cases in the compiled dataset. Final breach width is available for all the cases, as this is one of the criteria for including a breach case in the dataset. The final breach width in the compiled breach dataset varies between 10 m and 530 m. The final breach depth is available for 163 breach cases. The value varies between 1 m and 22 m. The distribution of the number of cases with respect to the values of final breach width and depth is shown in Figure 19.

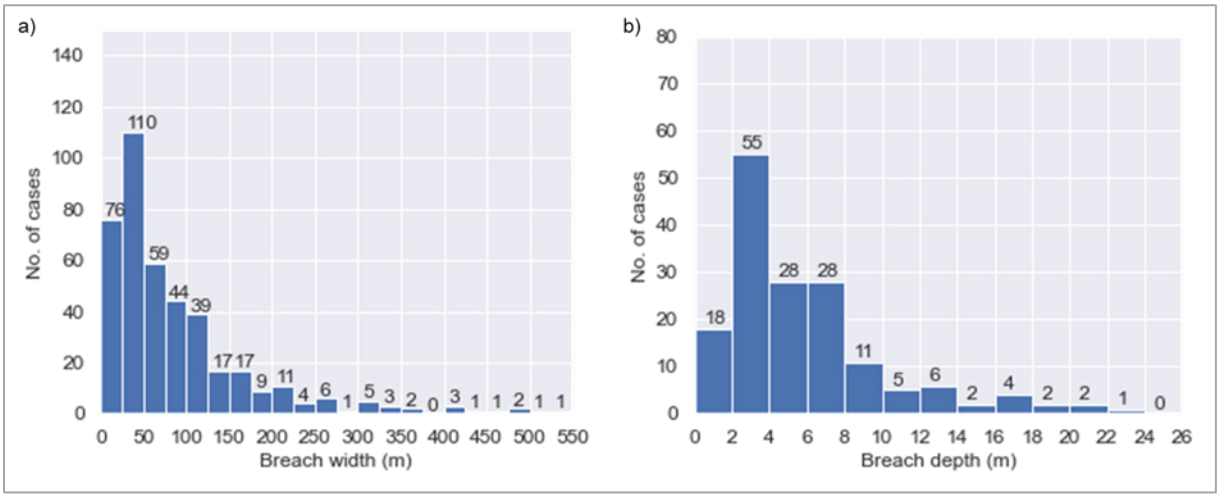

Figure 19: Number of breach cases in the dataset sorted by a) final breach width (412 cases) and b) final breach depth (163 cases).

Information on the breach mechanism is available for 315 cases. The breach mechanisms in the ILPD are given as primary and secondary mechanisms. The mechanisms include instability, internal erosion, external erosion, overtopping and overflow. For the purpose of this analysis, the breach mechanisms are grouped into three main mechanisms: external erosion, instability and internal erosion, as shown in Table 10. The dataset contains information on the breach mechanism for 315 cases. The number of levee breach cases corresponding to the main mechanisms is given in Table 10.

Table 10: Classification of breach mechanism.

Given primary mechanism in the ILPD	Overtopping, overflow, external erosion	Instability	Internal erosion
Main mechanism	External erosion	Instability	Internal erosion
No. of cases	216	22	77

The other breach related information, namely: breach discharge, duration of breach and breach intervention activities, are available for a limited number of cases, as shown in Table 9. Therefore, these parameters cannot be used in the following regression analysis (see Section 5.4.2).

Breach depth is also excluded from the following regression analysis as it is not a relevant parameter for hinterland inundation. The value of the breach depth in the dataset is based on the final breach invert, which is the deepest point in the breach cross-section. The deepest point in the breach cross-section is not the critical parameter for hinterland inundation. It is the average breach level along the breach section on the river side that is relevant for hinterland inundation. However, this information is not available in the dataset. This leaves the final breach width and breach mechanism as the only important breach parameters in the dataset available for regression analysis (see Section 5.4.2).

5.3.2 Levee parameters

The relevant levee related information available in the dataset are levee geometry parameters, soil type and levee type. The different geometric parameters of a levee are as shown in Figure 15. The most relevant levee geometric parameters for breach analysis are levee height and levee bottom width and are often determined from the other geometric parameters. The statistics of levee height and bottom width are given in Table 8. The number of breach cases in the dataset with information on the parameters levee soil type and levee type are also given in Table 8.

The dataset contains information on levee height and levee bottom width for 341 and 290 breach cases, respectively. The levee height varies between 0.6 m and 14.0 m and the levee bottom width varies between 5.6 m and 59.4 m. The distribution of the number of cases with respect to the values of levee height and levee bottom width and the scatter plot of levee height versus levee bottom width are shown in Figure 20.

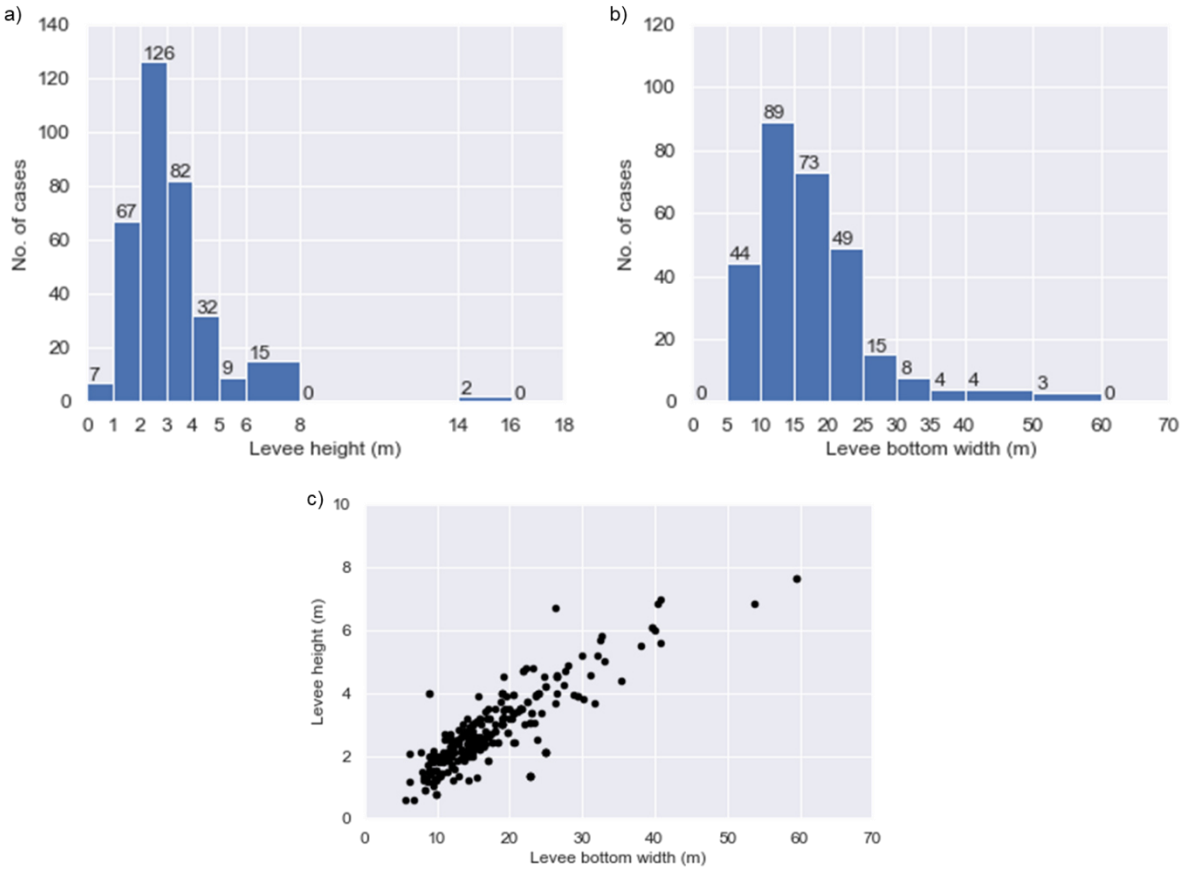

Figure 20: Histogram of the number of cases in the dataset versus a) levee height and b) levee bottom width; and c) scatterplot of levee height against levee bottom width (correlation coefficient = 0.85).

The soil types of the levees in the ILPD are approximately 20, ranging from clay to gravel as, shown in Table 11. For this analysis, these detailed soil types are aggregated into five soil types: clay, silt, sand, peat and gravel, using the unified soil classification system (USCS) (Carter & Bentley 2016), as shown in Table 11. The soil types are further aggregated into fine (clay, silt and peat) and course (sand and gravel) soils (see Table 12).

Table 11: Aggregating the levee soil type based on the unified soil classification system.

No.	Given Soil type	Soil type (USCS)
1	Clay	Clay
2	Sandy clay	Clay
3	Gravelly clay	Clay
4	Medium sand	Sand
5	Medium gravel	Gravel
6	Clayey sand	Sand
7	Sand	Sand
8	Sandy silt	Silt

No.	Given Soil type	Soil type (USCS)
9	Silty sand	Sand
10	Silt	Silt
11	Fine gravel	Gravel
12	Silty clay	Clay
13	Gravel; Silt	Gravel
14	Gravelly sand	Sand
15	Clayey silt	Silt
16	Clay-Sand-Silt mixture	Sand
17	Silty gravel	Gravel
18	Gravel	Gravel
19	Peat	Peat
20	Organic	Peat

The dataset contains information on the levee soil type for 212 breach cases, of which 79 levees were constructed of fine soil and 134 of course soil. The distribution of breach cases by levee soil type is shown in Table 12.

Table 12: Number of levee breach cases sorted by levee soil type.

Levee soil type	Clay	Silt	Peat	Sand	Gravel
Levee soil type	**Fine**			**Course**	
Number of cases	63	15	1	127	6

The dataset also includes information on the type of levee, i.e., whether the levee is constructed from mainly the same material (homogeneous levee) or from a combination of materials (e.g., different core material) (inhomogeneous levee). The dataset contains 186 breach cases with information on the levee type. Of these, 125 are homogeneous and 61 are inhomogeneous levee types.

5.4 Derivation of an empirical equation for the final breach width

The sensitivity analysis in Section 9.2 shows that the most important breach parameters leading to maximum flood inundation for non-flash floods are final breach width, final breach depth and breach location (see also Tadesse & Fröhle (2020)). Breach duration and breach evolution, i.e., the rate of breach growth, are only important for levee breaches caused by flash floods. Furthermore, as discussed in Section 5.3, enough levee breach data are available in the compiled dataset only for the breach parameter final breach width. Therefore, an empirical equation for final breach width is derived here.

5.4.1 Factors affecting levee breaching processes (control variables)

Previous studies show that the process of levee breaching (and thus the final breach width) depends on several factors. Based on field and laboratory test data, Morris et al. (2007) observed that the process of levee breaching is strongly related to the material properties and condition of the levee. They recommend including these variables in predictive breach models. Based on the analysis of two breach cases, Risher & Gibson (2016) showed that the final breach dimensions are strongly related to the flow parameters tail water level and loading duration. Based on the Changkai levee breach in 2010, Peng & Zhang (2015) showed that the levee breaching process depends on the river flood level, the levee type and the characteristics of the levee and foundation soil. These studies show that the final levee breach width is a function of:

i. Flow boundary conditions in the river (river discharge, head above levee foot (river side))
ii. Levee geometry (crest width, side slopes, height)
iii. Cause of the failure (mode of failure)
iv. Type of levee (homogeneous / zoned levee with core)
v. Soil type of the levee (cohesive / non-cohesive)
vi. Condition of the levee (age, state of maintainance, etc.)

The variables for which data are available for more than 100 breach cases in the dataset are levee height, levee bottom width, soil type, levee type, and breach mechanism (see Section 5.2). These data are used to establish an empirical equation for the final breach width using both a regression model (Section 5.4.2) and an artificial neural network (ANN) model (Section 5.4.3).

5.4.2 Fitting regression model for final breach width

An empirical equation for the final breach width can be derived using a regression fit by taking the variables that influence it. Different types of regression fits can be considered. For example, Ashraf et al. (2018) used multiple non-linear regression to derive empirical equations for different breach parameters. Danka & Zhang (2015) used multiple linear and non-linear regression to derive empirical equations for breach width, breach depth and peak discharge. The multiple linear and non-linear regression fits have the form shown in equations (32) and (33), respectively.

$$Y = \beta_0 + \sum_{j=1}^{n} \beta_j X_j + \varepsilon \tag{32}$$

$$Y = \beta_0 \prod_{j=1}^{n} X_j^{\beta_j} + \varepsilon \tag{33}$$

Where Y is the dependent variable (in this case, final breach width), β_0 is the value of the intercept, β_j is the regression coefficient of the independent variable X_j, j is the number of independent variables, and ε is the error of the fit.

The plots of final breach width against levee height and levee bottom width grouped by the variables soil type, levee type and breach mechanism are shown in Figure 21, Figure 22 and Figure 23, respectively. The linear fits to the data set, including the 95% confidence interval, are also shown in the figures. The plots show that the final breach width is positively related to both levee height and levee bottom width, except in the case of the breach mechanism “instability”. A strong correlation between the final breach width and the variables is not evident from these plots.

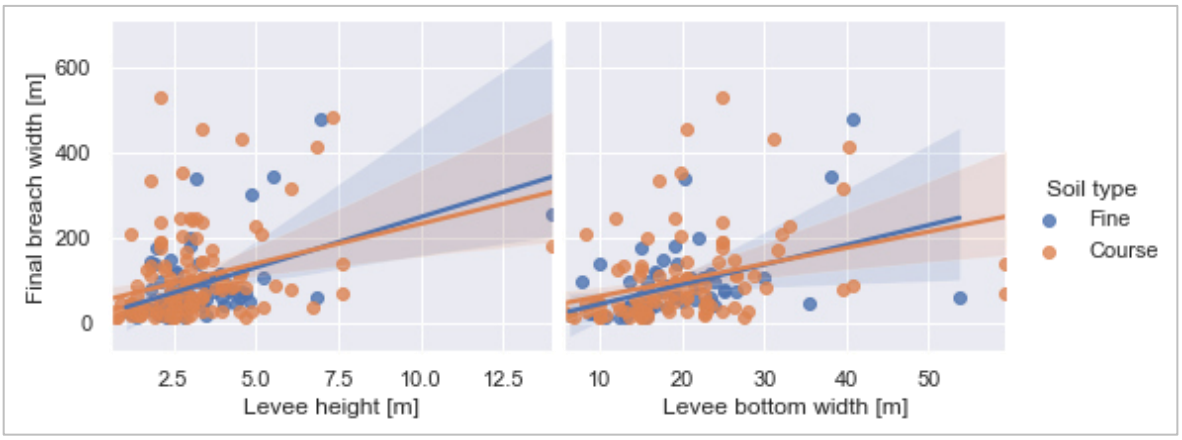

Figure 21: Plots of final breach width versus levee height and levee bottom width differentiated by soil type. See Table 13 variable combination h, s for correlation coefficient and other statistics.

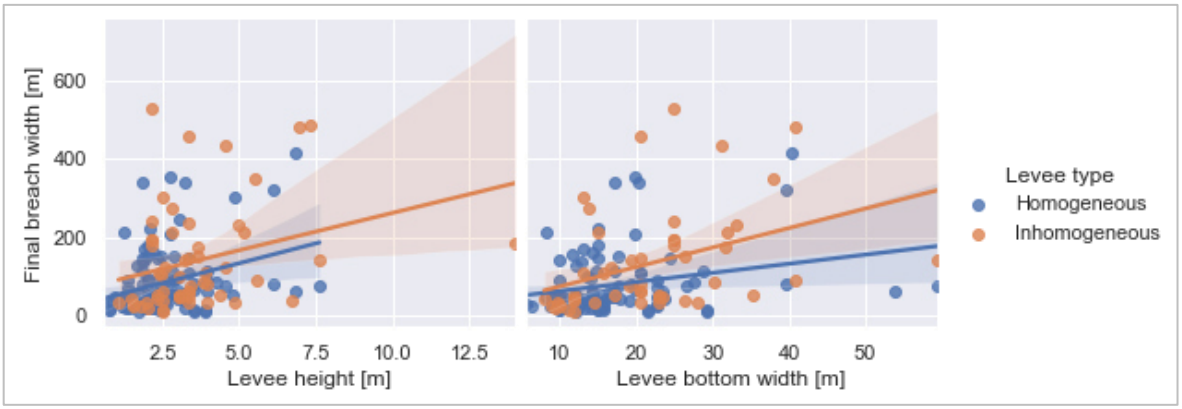

Figure 22: Plots of final breach width versus levee height and levee bottom width differentiated by levee type. See Table 13 variable combination h, t for correlation coefficient and other statistics.

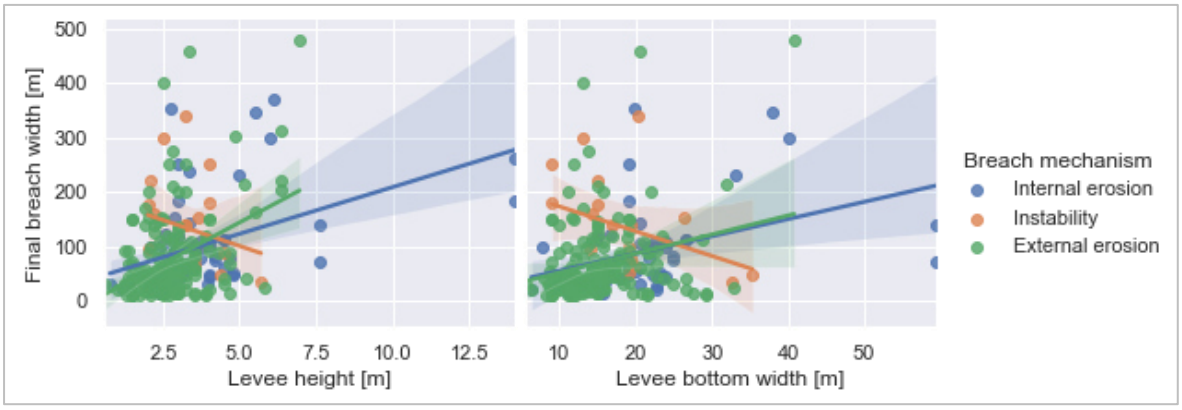

Figure 23: Plots of final breach width versus levee height and levee bottom width differentiated by breach mechanism. See Table 13 variable combination h, m for correlation coefficient and other statistics.

To check the suitability of the non-linear (logarithmic) fit, the plots of the natural logarithm of the final breach width versus the natural logarithm of the levee height and the levee bottom width grouped by the variables soil type, levee type and failure mechanism are shown in Figure 24, Figure 25 and Figure 26 respectively. The non-linear fits to the data set, including the 95% confidence interval, are also shown in the figures. As in the linear plots, the final breach width is positively related to both levee height and levee bottom width, except in the case of the breach mechanism “instability”. Also in these plots, there is no strong correlation between the final breach width and the variables.

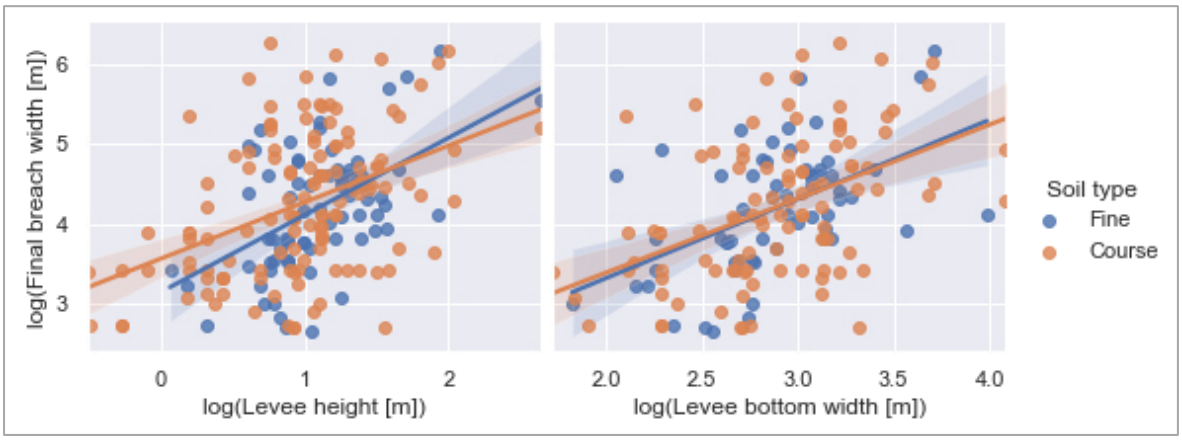

Figure 24: Plots of the natural logarithm of final breach width versus the natural logarithm of levee height and levee bottom width differentiated by soil type. See Table 14 variable combination h, s for correlation coefficient and other statistics.

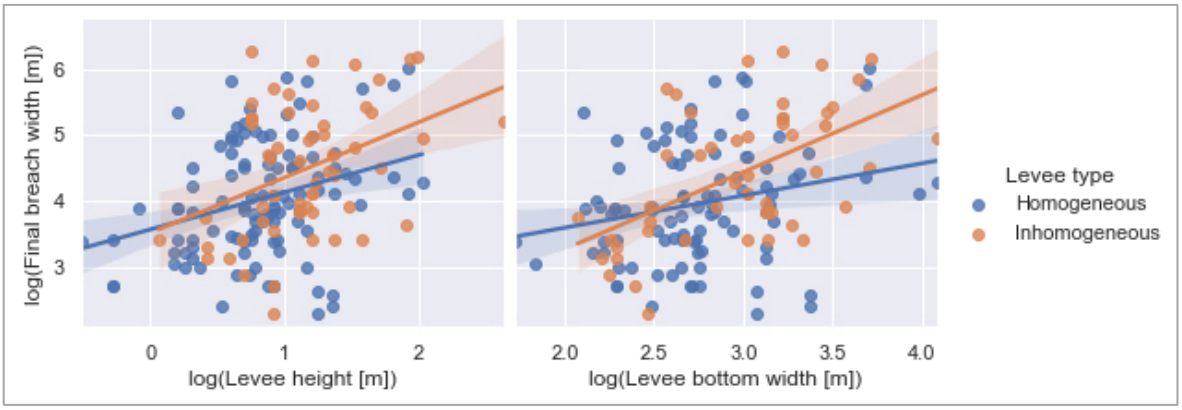

Figure 25: Plots of the natural logarithm of final breach width versus the natural logarithm of levee height and levee bottom width differentiated by levee type. See Table 14 variable combination h, t for correlation coefficient and other statistics.

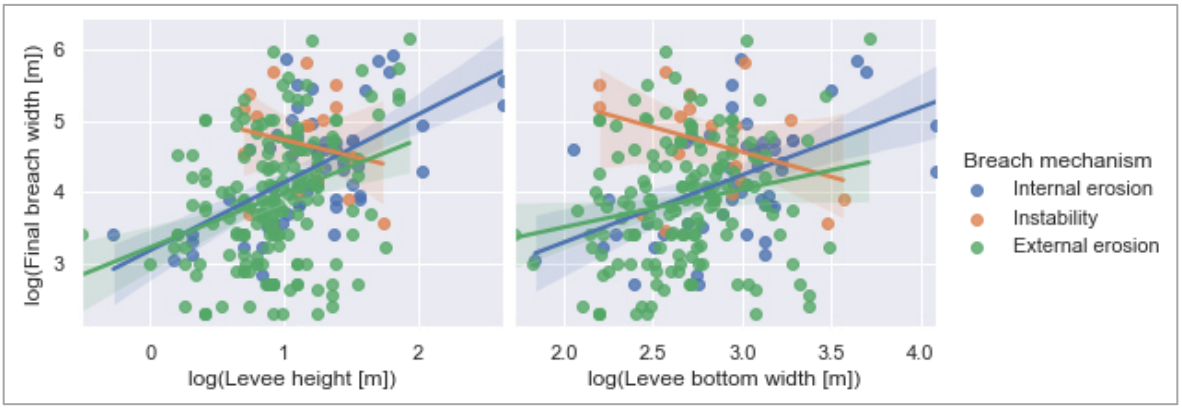

Figure 26: Plots of the natural logarithm of final breach width versus the natural logarithm of levee height and levee bottom width differentiated by breach mechanism. See Table 14 variable combination h, m for correlation coefficient and other statistics.

Regression fitting using both multiple linear and non-linear regression methods is performed using the Python module statsmodels (Seabold & Perktold 2010) (www.statsmodels.org). Final breach width is the dependent variable and levee height, levee bottom width, soil type, levee type, and breach mechanism are the independent variables. Soil type, levee type and breach mechanism are used as categorical variables in the regression fitting.

Different combinations of the independent variables (levee height, levee bottom width, soil type, failure mechanism and levee type) are considered in the regression fitting. As levee height and width are strongly correlated (see Figure 20 c), the two variables are not combined simultaneously in the regression. Levee bottom width is a function of levee height, crest width and side slopes.

The goodness of fit of the regression equations is assessed by the coefficient of determination (adjusted R^2), mean absolute error (MAE) and root mean square error (RMSE). These criteria are used by Ashraf et al. (2018), among others. To select the best fit, the fits are first filtered based on the adjusted R^2. The selection is then further narrowed down based on MAE and RMSE. The best model is the one with the highest adjusted R^2 and the lowest MAE and RMSE.

The results of the regression analysis for the different combinations of the control variables are given in Table 13 and Table 14. Combinations of variables that result in a number of breach cases below 100 are excluded from the analysis and from the tables. The logarithmic (multiplicative) regression models are better in terms of coefficient of determination (adjusted R^2) and MAE than the linear regression counterparts. The (multiple) linear regression models are better in terms of RMSE. Comparable results are reported by Danka & Zhang (2015).

Table 13: Results of (multiple) linear regression analysis for the dependent variable, final breach width (L), for different combinations of the independent variables. The following abbreviations are used in the table: n – number of cases (-), h – levee height (m), w – levee bottom width (m), s - levee material (-), classified as either coarse (C) or fine (F) material, m – levee breach mechanism (-), which is classified as external erosion (Ext.), instability (Ins.), and internal erosion (Int.), and t – embankment type (-), which is divided into homogeneous (Hom.) and inhomogeneous (Inh.) categories. The regression coefficients of the variables are expressed in dimensionless units.

No.	Variables	n (-)	Regression coefficients										MAE	RMSE	Adj.
			Interc-ept (m)	h (-)	w (-)	s (-)		m (-)			t (-)				
						C	F	Ext.	Ins.	Int.	Hom.	Inh.			
1	h	338	13.76	26.99	-	-	-	-	-	-	-	-	59.9	87.1	0.14
2	h, s	199	-	26.32	-	26.82	6.89	-	-	-	-	-	62.6	90.2	0.13
3	h, m	258	-	26.41	-	-	-	4.05	50.09	8.02	-	-	51.2	74.5	0.17
4	h, t	166	-	25.35	-	-	-	-	-	-	18.28	52.03	69.6	96.9	0.15
5	h, s, m	132	-	28.05	-	4.26	6.30	-	49.15	-2.20	-	-	51.9	78.3	0.15
6	h, s, t	119	-	25.92	-	25.34	22.49	-	-	-	-	32.84	75.0	105.1	0.16
7	h, t, m	113	-	27.66	-	-	-	-	72.46	-0.50	-3.56	28.66	55.9	81.8	0.23
8	w	289	28.24	-	3.40	-	-	-	-	-	-	-	58.4	85.9	0.09
9	w, s	163	-	-	4.03	22.35	11.81	-	-	-	-	-	61.0	90.2	0.13
10	w, m	229	-	-	2.66	-	-	30.11	89.64	34.55	-	-	50.8	74.8	0.10
11	w, t	146	-	-	3.40	-	-	-	-	-	19.81	57.92	68.1	96.8	0.14
12	w, s, m	114	-	-	3.76	12.04	27.26	-	41.28	-8.51	-	-	51.1	80.2	0.12
13	w, s, t	100	-	-	3.57	21.17	24.99	-	-	-	-	34.79	75.1	107.1	0.13
14	w, t, m	103	-	-	2.72	-	-	-	76.32	-6.79	14.93	65.52	55.8	84.0	0.20

Table 14: Results of (multiple) logarithmic regression analysis for the dependent variable, final breach width (L), for different combinations of the independent variables. The following abbreviations are used in the table: n – number of cases (-), h – levee height (m), w – levee bottom width (m), s - levee material (-), classified as either coarse (C) or fine (F) material, m – levee breach mechanism (-), which is classified as external erosion (Ext.), instability (Ins.), and internal erosion (Int.), and t – embankment type (-), which is divided into homogeneous (Hom.) and inhomogeneous (Inh.) categories. The regression coefficients of the variables are expressed in dimensionless units.

No.	Variables	n (-)	Regression coefficients										MAE (m)	RMSE (m)	Adj. R^2 (-)
			Intercept (-)	h (-)	w (-)	s (-)		m (-)			t (-)				
						C	F	Ext.	Ins.	Int.	Hom.	Inh.			
1	h	338	3.36	0.78	-	-	-	-	-	-	-	-	54.8	91.9	0.15
2	h, s	199	-	0.78	-	3.50	3.35	-	-	-	-	-	56.6	93.9	0.18
3	h, m	258	-	0.78	-	-	-	3.20	3.80	3.38	-	-	48.9	78.8	0.18
4	h, t	166	-	0.67	-	-	-	-	-	-	3.48	3.72	63.6	102.3	0.14
5	h, s, m	132	-	0.86	-	3.23	3.24	-	0.56	0.10	-	-	48.6	80.7	0.20
6	h, s, t	119	-	0.73	-	3.55	3.52	-	-	-	-	0.21	70.1	109.0	0.20
7	h, t, m	113	-	0.64	-	-	-	-	0.91	0.16	3.24	3.54	52.0	87.0	0.22
8	w	289	1.96	-	0.76	-	-	-	-	-	-	-	53.0	89.7	0.12
9	w, s	163	-	-	0.95	1.46	1.45	-	-	-	-	-	55.8	92.9	0.22
10	w, m	229	-	-	0.56	-	-	2.36	3.10	2.53	-	-	48.0	78.4	0.12
11	w, t	146	-	-	0.75	-	-	-	-	-	1.91	2.19	61.6	100.7	0.16
12	w, s, m	114	-	-	0.90	1.45	1.66	-	0.47	0.00	-	-	48.1	81.3	0.19
13	w, s, t	100	-	-	0.90	1.54	1.62	-	-	-	-	0.19	68.9	109.5	0.23
14	w, t, m	103	-	-	0.53	-	-	-	0.94	0.01	2.28	2.73	51.3	88.5	0.22

It can be seen from Table 13 and Table 14 that the maximum adjusted R^2 is in the range of 0.20. This means that the variables levee height, levee bottom width, levee type, soil type and breach mechanism explain about 20% of the variance of the final breach width. This is a low adjusted R^2 and indicates that important variables influencing the final breach width are not included in the regression analysis. Important variables influencing levee breaching such as river flow, design flow, levee condition, etc. are not included due to limited data availability (see Section 5.4.1).

The highest adjusted R^2 in both the linear and the logarithmic regression models is obtained with the combination of the variables levee height, levee type and breach mechanism as shown in Table 13 and Table 14. The adjusted R^2 and the RMSE of the linear regression fit for this combination of variables are 0.23 and 81.8 m respectively (see Table 13). The regression coefficients are also given in Table 13. The corresponding regression equation for the final breach width (L) can be written as equation (34). The logarithmic model of this combination of variables has an adjusted R^2 of 0.22 and an RMSE of 87.0 m (see Table 14). The regression coefficients are also given in Table 14. The corresponding regression equation for the final breach width (L) can be written as in equation (35).

$$L = m + t + 27.66h \tag{34}$$

$$L = e^{t} e^{m} h^{0.63} \tag{35}$$

For the linear regression equation (equation (34)), the values of t (the coefficient for levee type) are -3.56 and 28.66 for homogeneous and inhomogeneous levees, respectively, and the values of m (the coefficient for breach mechanism) are 0, -0.50 and 72.46 for external erosion, internal erosion and instability, respectively.

For the logarithmic regression equation (equation (35)), the values of t (the coefficient for levee type) are 3.25 and 3.55 for homogeneous and inhomogeneous levees respectively, and the values of m (the coefficient for breach mechanism) are 0, 0.16 and 0.91 for external erosion, internal erosion and instability respectively.

5.4.3 Artificial neural network (ANN) model for final breach width

5.4.3.1 General

An artificial neural network (ANN) is composed of interconnected nodes called neurons that mimic the structure of the human brain in a simplified way. ANN is used in machine learning algorithms to solve complex problems. ANN uses training data to learn and extract patterns and features (Yalçin 2021, p. 38).

The general structure of an ANN is shown in Figure 27. It has three layers of neurons: input, hidden and output layers. The number of hidden layers and the number of neurons in each hidden layer need to be optimized through a process of trial and error for a given problem (Nourani et al. 2012). Nevertheless, studies suggest that one hidden layer may be sufficient to approximate a complex non-linear function. Also, the number of neurons in a given hidden layer can be approximated by 2n + 1, where n is the number of neurons in the input layer (i.e. the number of independent variables) (Sammen et al. 2017).

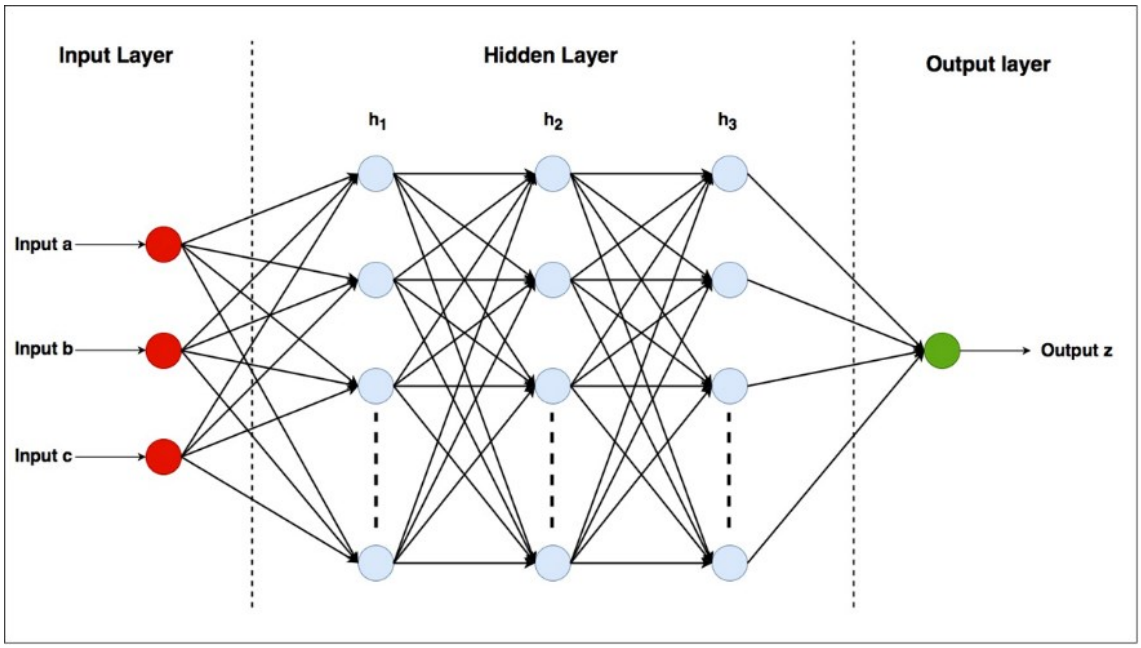

Figure 27: Structure of an ANN model with an input layer with three neurons, three hidden layers with an unspecified number of neurons each, and an output layer with one neuron (taken from Kumar et al. (2020)).

ANN are often classified based on the connection pattern or the number of hidden layers. Based on the connection pattern, ANN are often classified as feedforward or recurrent. Based on the number of hidden layers, ANN are classified as single-layer and multi-layer. Single or multi-layer feedforward ANN are used for regression type problems, such as the case here (Gill 2021).

Using the compiled levee breach dataset, an ANN model for final breach width can be built. The built model can be used to predict the final breach width using the predictor variables. Some studies show that the ANN model can perform better than a regression model (Mahmoud et al. 2017). There are some studies that have used ANN to estimate dam break parameters. Sammen et al. (2017) used generalised regression artificial neural network (GRNN) model to predict dam break outflow. Mahmoud et al. (2017) used multilayer perceptrons (MLP) ANN model to predict dam break peak outflow and failure time. Nourani et al. (2012) employed three-layer feedforward ANN model to predict dam break outflow.

5.4.3.2 Model building

In this work, a MLP ANN model is built for the levee breach dataset using Keras sequential Python API (https://keras.io/) in jupyter notebook. The building of the ANN model with Keras follows the following steps: data preparation, model creation, compilation, training, evaluation and prediction step (using the model).

Data preparation: The data set is first prepared for the building of the ANN model. This basically includes normalising the independent variables, encoding categorical variables and dividing the data set into training, validation and test data sets. Normalising the independent variables helps to increase the accuracy of the ANN model and reduces the model training time. Dividing the dataset helps to have dataset for training, validation and testing the model.

The non-categorical independent variables (levee height and levee bottom width) are standardized using equation (40).

$$x' = \frac{x - x_{mean}}{\sigma} \tag{36}$$

In equation (40), x' is the standardised independent variable, x is the value of the independent variable, x_{mean} is the mean value of x and σ is the standard deviation of x.

The independent categorical variables (soil type, levee type and breach mechanism) are used as dummy variables, encoded as 0 or 1 to indicate their presence or absence. To avoid the problem of multicollinearity, one of the categories of each categorical variable is omitted (Yalçin 2021). Here, the category 'Fine' of the variable soil types, the category ‘Inhomogeneous’ of the variable levee type and the category ‘Instability’ of the variable breach mechanism are omitted. Thus, the categorical variables are encoded as follows:

i. Soil type[‘course’] → {‘Course’: 1, ‘Fine’: 0},
ii. Levee type[‘Homogeneous’] → {‘Homogeneous’: 1, ‘Inhomogeneous’: 0},
iii. Breach mechanism [‘External erosion’] → {‘External erosion’: 1, ‘Internal erosion’: 0, ‘Instability’: 0}, and
iv. Breach mechanism [‘Internal erosion’] → {‘External erosion’: 0, ‘Internal erosion’: 1, ‘Instability’: 0}.

For a given combination of independent variables, the data set is divided into a training (80%) and a test (20%) data set. During model training, the training data set is further divided into training (80%) and validation (20%) data sets.

Creating the ANN model: Creating the ANN model involves specifying the input layer, the hidden layers and the output layer (i.e., specifying the number of layers and the number of neurons in each layer). The activation function for each hidden layer is also defined in this step. For our variable here, the final breach width, an ANN mode is created with an output layer of one neuron (final breach width), an input layer and one or more hidden layers. The number of neurons in the input layer is equal to the number of the independent variables considered, including the dummy variables. The number of hidden layers and the number of neurons in each hidden layer are determined by trial and error (Benardos & Vosniakos 2007). Here, 1 to 3 hidden layers with up to 32 neurons each are tested.

Hidden layers require an activation function to learn patterns from the training data. The most commonly used activation functions for activating single neurons are Tanh, ReLU (Rectified Linear Unit) and sigmoid functions. These functions are given in Figure 28. In this work, the ReLU activation function is used for the hidden layers. The ReLU activation function is recommended for hidden layers and converges quickly.

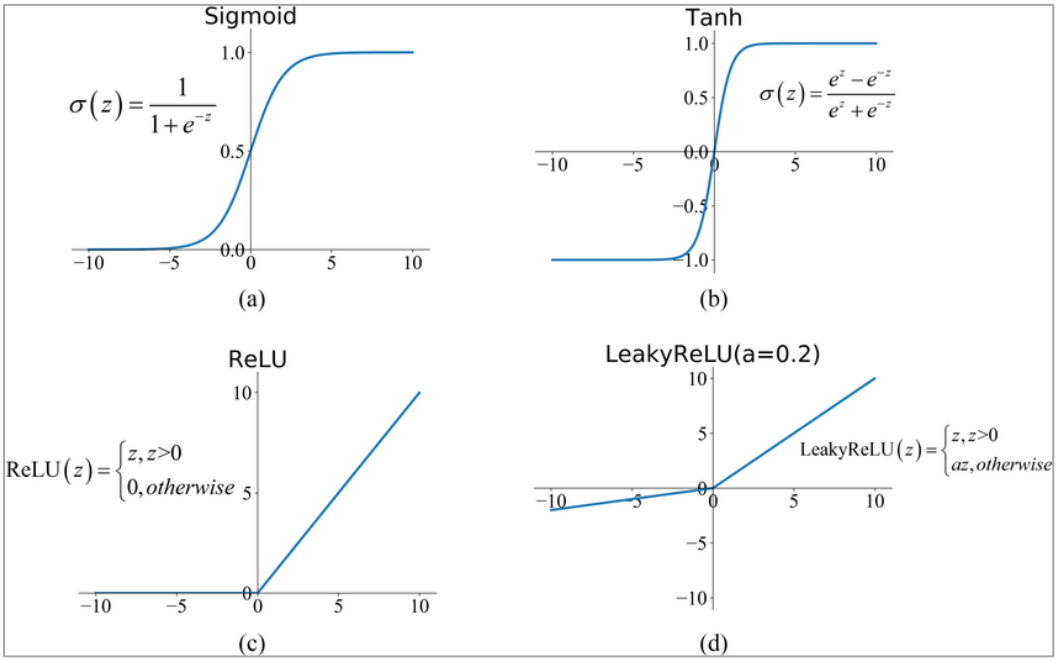

Figure 28: Activation functions commonly used in ANN a) sigmoid b) Tanh c) ReLU and d) Leaky ReLU functions (taken from Feng et al. (2019)).

Compiling the model: Compiling is the step of the ANN model building where important parameters for model training are defined. These include the definition of the loss function, the optimisation algorithm (optimiser), performance metrics and call-backs, etc. The loss function is a function used to measure model performance, i.e. the deviation of the predicted values from the measured (input) data. Root mean squared error (RMSE), mean squared error (MSE), and mean absolute error (MAE) are appropriate loss functions for regression type problems (Yalçin 2021). The MSE is used as the loss function for this analysis.

An optimisation algorithm (or optimiser) is an algorithm used to improve the performance of the model by minimising the loss. Commonly used optimisers include Adam, Stochastic gradient descent (SGD), Adamax and others. In this work, Adam is used because it is available in the Keras sequential Python API used for the ANN model. Local minima, saddle points and vanishing gradients can cause problems for optimisation algorithms. Early stop configurations are used in the model compilation step to deal with optimisation challenges. Here we define what to monitor (the call-backs for early stopping are defined in the training step) and how long to wait (patience). For the present investigation early stopping is set to monitor validation loss with a patience of 100.

Training: In the training step, the compiled ANN model is fed with the training data so that it learns from the data. Additional parameters such as epoch, validation split, and call-backs are defined for the training. The epoch parameter sets the maximum number of adjustments of the ANN using the training data. With validation split, we split the training data into training and validation sets so that the model is evaluated during the training phase. We use the parameter call-backs to provide information for model evaluation and plotting. Call-backs are also used to stop model training early, before reaching the defined epochs, if no performance improvement is observed.

Evaluation and prediction steps: In the evaluation step, the trained model is used to evaluate the performance of the ANN model using a test dataset that the model has not seen before. If the model performs well on the test dataset, it can be used directly for prediction and saved for future use.

5.4.3.3 ANN models for final breach width

Analogous to the regression model fitting discussed in section 5.4.2, different ANN models for the final breach width are built using the breach dataset and different combinations of the variables. First, the sensitivity of the ANN model to the ANN architecture and the dataset splitting (data sampling for training, validation, and testing) is analysed.

There is no general recommendation for the choice of an ANN architecture. Therefore, it is helpful to investigate the sensitivity of the model output to the ANN architecture. For this purpose, different architectures are tested for the case of the independent variable levee height (h). The results for different architectures are shown in Table 15 and Figure 29. It can be observed from Table 15 that the performance of the models is relatively insensitive to the choice of ANN architecture. However, some effect of the model architecture can be seen from Figure 29.

Table 15: Sensitivity of the ANN model with levee height as the independent variable and data splitting resample value = 1 to the choice of ANN architecture.

Nr.	Variables	Architecture	Epoch no.	Training		Validation		Test	
				MAE (m)	RMSE (m)	MAE (m)	RMSE (m)	MAE (m)	RMSE (m)
1	h	(1,3,1)	786	68.33	91.92	70.90	97.83	53.87	62.06
2	h	(1,32,1)	349	69.55	97.59	73.14	98.44	54.79	62.46
3	h	(1,3,3,1)	439	69.45	94.79	72.91	98.49	53.97	61.54
4	h	(1, 16,8,4,1)	329	69.56	96.88	72.69	98.27	54.29	61.62

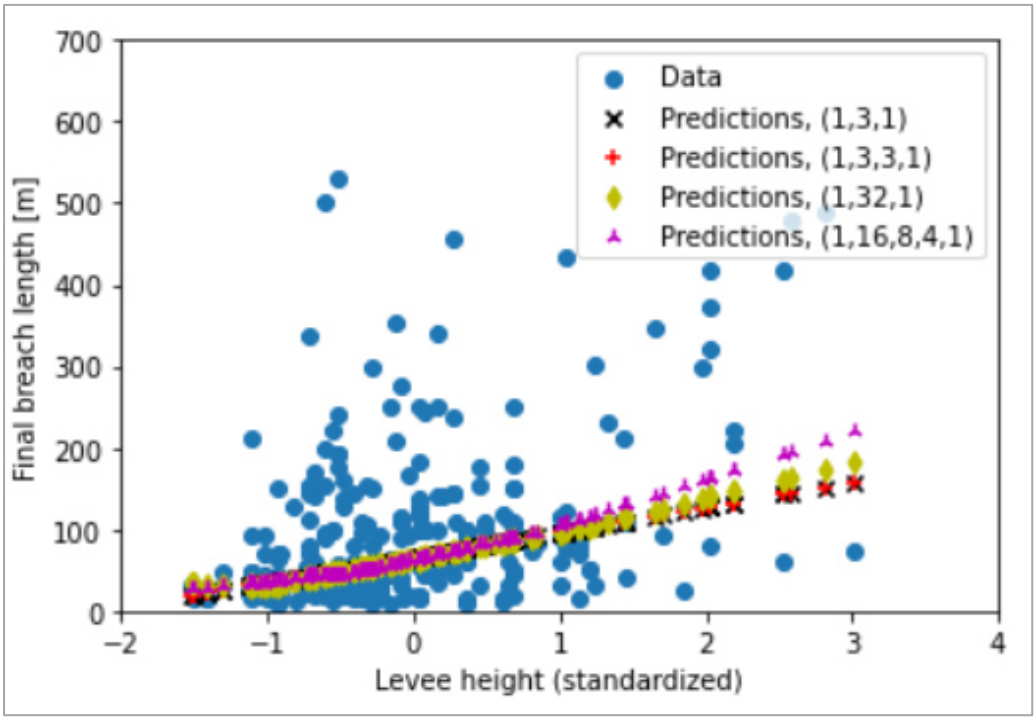

Figure 29: Sensitivity of the ANN model to ANN architecture.

Random data splitting method is recommended in order to have statistically comparable training, validation, and test datasets. However, this can significantly affect the outcome of the model training (May et al. 2010) and it is recommended to check the sensitivity of data splitting on the model outcome for a given case. Four different data splittings are tested for the case of the independent variable levee height (h) and the architecture (1,3,1). The results are shown in Table 17 and Figure 30. The results show that the performance of the ANN model is sensitive to the data splitting.

Table 16: Sensitivity of the ANN model with levee height as the independent variable and the architecture (1,3,1) to data splitting (resample value when training data is split into training and validation).

Nr.	Variables	resample	Epoch no.	Training		Validation		Test	
				MAE (m)	RMSE (m)	MAE (m)	RMSE (m)	MAE (m)	RMSE (m)
1	h	0	1216	59.78	82.13	75.12	113.62	49.98	73.32
2	h	1	786	68.33	91.92	70.90	97.83	53.87	62.06
3	h	2	2713	56.77	78.93	67.1	89.46	63.15	72.90
4	h	3	772	67.59	97.86	58.09	76.22	65.99	102.73

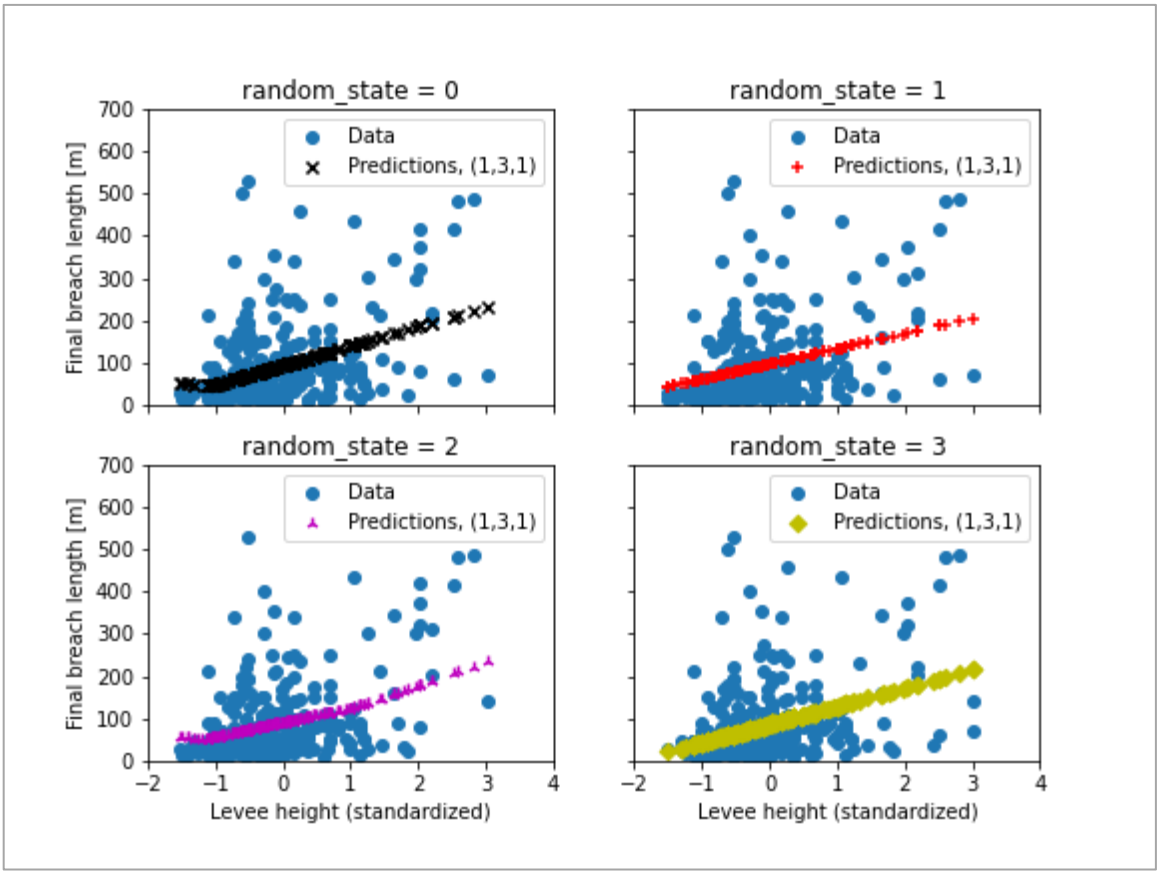

Figure 30: Sensitivity of the ANN model to data splitting.

ANN models for the final breach width are built for the different combinations of the independent variables with the architecture (n, 2n + 1, 1), where n is the number of variables. The sensitivity of each ANN model to data splitting is checked and the results with good performance are given in Table 17.

The results in Table 17 showed that the performance of the ANN models was comparable to that of the regression models in terms of MAE and RMSE. The regression models performed better in terms of Adj. R^2. In both cases, the best prediction of the final breach width is obtained with the combination of the independent variables levee height, levee type and breach mechanism.

Table 17: ANN models for the final breach width for the different combinations of variables and architecture (input layer, hidden layer(s), output layer) that gave better performance.

Nr.	Variables	No. of cases	MAE (m)	RMSE (m)	Adj. R^2 (-)
1	h	338	59.72	86.85	0.14
2	h, s	199	61.23	89.65	0.13
3	h, m	260	52.31	76.90	0.10
4	h, t	167	71.49	96.43	0.15
5	h, s, m	134	51.57	80.54	0.06
6	h, s, t	120	75.90	106.13	0.11
7	h, t, m	114	54.73	84.26	0.15
8	w	289	57.68	85.70	0.09
9	w, s	163	60.94	89.49	0.13
10	w, m	229	50.97	73.67	0.11
11	w, t	146	67.74	96.64	0.12
12	w, s, m	114	52.07	81.79	0.04
13	w, s, t	100	75.11	110.26	0.04
14	w, t, m	103	63.03	89.18	0.05

5.5 Summary

Many levee breaches have occurred in the past. The compilation of historical breaches can be found in various databases and in the literature. The ILPD is the most comprehensive freely available levee breach database and is used in this research. It is augmented in this research by additional levee breach cases found in the literature. A total of 412 breach cases were compiled. However, only few breach parameters are documented in the breach cases. Only the final breach width is documented for all 412 cases. The independent variables for which information is available for more than 100 breach cases in the dataset are levee height, levee bottom width, soil type, levee type, and breach mechanism. These data are used to establish an empirical relationship for the final breach width as a function of various combinations of the independent variables levee height, levee bottom width, levee soil material type, embankment type and breach mechanism using both regression and ANN models. The results showed that the performance of the ANN models was comparable to that of the regression models in terms of MAE and RMSE. The regression models performed better in terms of Adj. R^2. In both cases, the best prediction of the final breach width is obtained with the combination of the independent variables levee height, levee type and breach mechanism. The maximum Adj. R^2 is in the range of 0.20, which

means that the variables levee height, levee type and breach mechanism explain about 20% of the variance of the final breach width. The low Adj. R^2 is explained by the absence of important explanatory variables influencing levee breaching, such as river flow, design flow, levee condition, etc., which are not included in this analysis due to limited data availability.

6 Estimation of breach location

6.1 General

Levees are linear structures built along river banks to protect a specific area from flooding during river floods. They can be hundreds of kilometres long, depending on the topography of the area to be protected. Levees in the upper reaches of rivers are generally shorter than those in the lower reaches (near river mouths) because of the frequent topographic variations in the upper reaches of rivers and the flat topography near river mouths.

Historical levee breaches show that the number of breaches of a levee protecting a given area is limited to about one. Nevertheless, the exact location of the breach affects the consequences of the resulting flooding. Therefore, the location of a levee breach is important for flood inundation due to a levee breach.

Due to the long length of levees and the complex causes of breach initiation, estimating the location of a levee breach is challenging. In fact, the location of a levee breach is often assumed in levee breach scenario studies. In the case of embankment dam breaches, the breach location is often assumed or taken to be at the historical record of seepage or foundation problems, if any, or simply at the centre of the embankment (Gee 2008). This may be sufficient given that embankment dams are relatively short compared to levees. While historical records of seepage and foundation problems are also very important in estimating the location of levee breach, in the absence of such records, other methods need to be used. The breach cannot simply be assumed to be at the centre of the levee, as this would lead to an underestimation of the consequences of the flood.

An approach for estimating a possible breach location is presented below. The approach makes use of the flood characteristics (water level and duration), geometric and geological characteristics of the levee in question and its foundation, and the information from historical levee breaches on their breach location.

6.2 Location of historical levee breaches

Before developing an approach for estimating a potential levee breach location, historical breaches from the breach database (see Section 5.2) with information on the cause or sign of breach initiation at a given location are analysed. The breach database contains information on the indication of breach location for approximately 160 breach cases. These are grouped into 17 indications, as given in Table 18 with an associated example from the breach database.

Table 18: Information in the ILPD indicating the location of the breach.

Nr.	Indications of breach location	Examples of historical levee breach
1	Levee section with historical records of seepage, sand boils and foundation problem or levee section with signs showing that internal erosion is taking place (e.g. sand boils)	Changkai River levee breach in Jiangxi Province, China in 2010; Tarna River levee breach near Tarnaörs, Hungary in 1963
2	Levee section with significantly lower crest level compared to design water level and other sections of the levee	Douglas River levee breach in the UK in 2015
3	Levee section with known defects or damages to the levee such as sign of cracking (slip circles)	Tisza River levee breach near Tarpa, Hungary during the 2001 flood event; levee failure near Breitenhagen at Saale-Elbe confluence in Saxony-Anhalt, Germany during the 2013 flood event
4	Levee sections at river confluences	Levee failure near Breitenhagen at Saale-Elbe confluence in Saxony-Anhalt, Germany during the 2013 flood event
5	Levee section without maintenance and surveillance for long period of time (levee age)	Olza River levee failure in Czech Republic in 1997
6	Levee section with signs of erosion or scour on the waterside toe of the levee that could create access to permeable foundation layer	Missouri River levee breach near the city of Hamburg, Iowa, during the 2011 flood event
7	Levee section where tree roots infiltrate horizontally into the levee, along which water could flow into the levee	Mulde river levee failure near Niesau, Germany during the August 2002 flood; White Elster River levee failure near Bornitz, Germany during the June 2013 flood
8	Levee sections with clay or pit soils in association with extreme drought or dehydration, which could lead to low specific weight of the soil material	Breach of secondary peat dike in Wilnis, The Netherlands in 2003
9	Levee section with known bad design, bad material and construction	Oder River levee breach near Petrvald, Czech Republic in 1997
10	Levee section where other infrastructure is passing through the levee body (e.g. seepage along a pipe line)	Mulde river levee failure near Roesa, Germany during the August 2002 flood; Zijkanaal levee breach in Northern Amsterdam in 1960

Nr.	Indications of breach location	Examples of historical levee breach
12	Levee section where wave erosion taking place	Ostravice river Levee breach case of 2003 in Czech Republic
13	Levee sections with bad cover (bad grass quality)	Douglas River levee breach 2015 in the UK
15	Levee sections where animal burrows are known (squirrel holes in the levee)	White Elster River levee failure near Bornitz, Germany during the June 2013 flood; levee failure in water body called Paradise Cut, USA, March 1938; levee failure in water body called Berenda Slough, 1969, USA
16	Levee section along a river meander	Awash River levee breach at Wonji, Ethiopia in 1996
17	Levee section at which flow blockage due to debris, fallen trees (e.g., due to wind), or washed bridge may be possible	Mulde River levee failure near Retzau, Germany during the June 2013 flood; Fehér-Körös river levee breach near Gyula, Hungary in 1995

6.3 Approach for estimating the location of a levee breach

Identifying the potential breach location of a levee is a critical step in modelling flood inundation of floodplains due to levee breach, and therefore in assessing flood risk and planning mitigation strategies. In this work, an approach is developed to identify a potential levee breach location. The approach is inspired by the approach used by Apel et al. (2009) to determine breach locations in their study of the effect of levee breaches on downstream flood frequency. To determine breach locations, they assumed levee breaches every kilometre of a river reach. They identified a possible breach location based on the resulting flood inundation similarities.

The developed approach for estimating the potential breach location of a given levee protecting a given area corresponding to a given flood scenario is based on the following steps and is illustrated schematically in Figure 31 or Figure 32.

1) The first step in determining the potential levee breach location is to identify the leveed river reach for which the levee breach flood study is to be conducted and to locate the critical points in the protected area. The critical points are those points in the floodplain where the maximum flood damage would occur. Depending on the situation, these could be the lowest points in the area or the location of critical infrastructure such as hospitals, nursing homes for the elderly, schools, etc.
2) The second step is to build a hydrodynamic numerical model for the identified stretch of river.

3) Thirdly, the numerical model of the river reach is used to simulate the flood event or scenario selected for the levee breach analysis. This will help to determine the water level at any given levee reach.
4) The next step is to divide the levee into representative levee reaches and determine representative hydraulic (water level), geometric and soil characteristics for each levee reach. Guidance on dividing the levee into representative reaches is given in Section 6.4.
5) For each levee reach, the possibility of levee breach due to one of the four main causes, namely, overtopping (and hence external erosion), backward erosion (piping), failure due to sustained seepage through the levee body (micro instability) and concentrated leak erosion, shall then be checked. For this purpose, deterministic methods are discussed in Section 6.5.
6) If levee breaching is possible in one or more levee reaches, the breach parameters, such as the final breach width, are determined using the empirical approaches developed in Chapter 5.
7) Finally, depending on the resources available, either a simplified or a more detailed approach can be used to select the breach location with the highest likely damage.
    a. Simplified approach (see Figure 31): For each levee reach where a breach is possible, calculate the distance from the critical point identified in Step 1 to the centre of the levee reach. The levee reach with the minimum distance from the critical point in the protected area and with the maximum breach width (Step 6) is taken as the breach location.
    b. Detailed approach (see Figure 32): For each levee reach where a breach is possible, a 2D hydrodynamic numerical model of the river and the leveed area with an integrated levee breach modelling as discussed in this thesis is set up. The levee breach parameters are determined in step 6. The levee reach that gives the maximum inundation depth at the critical location and the maximum inundation area is selected as the breach location.

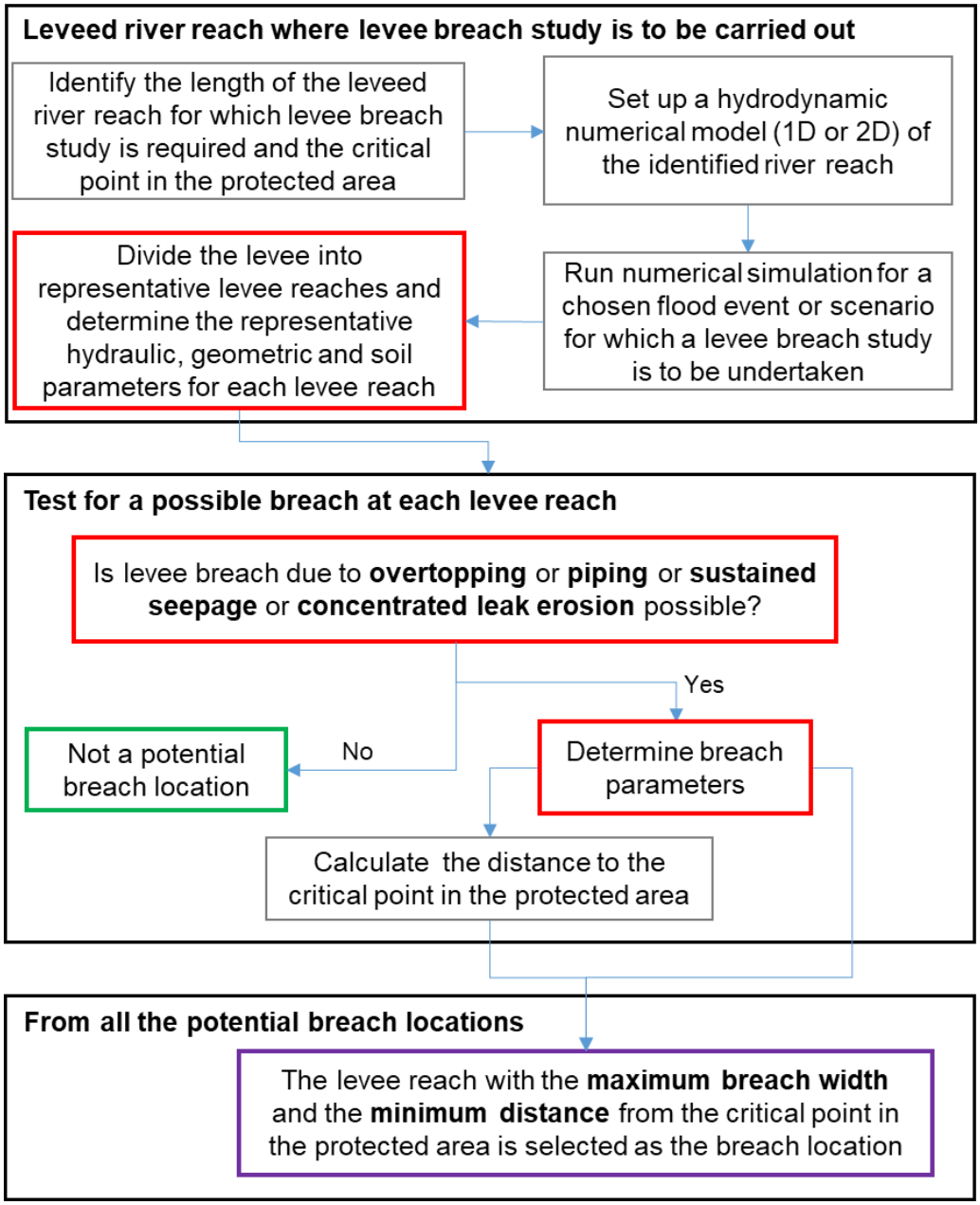

Figure 31: Steps to identify a potential levee breach location with the highest damage potential (simplified approach).

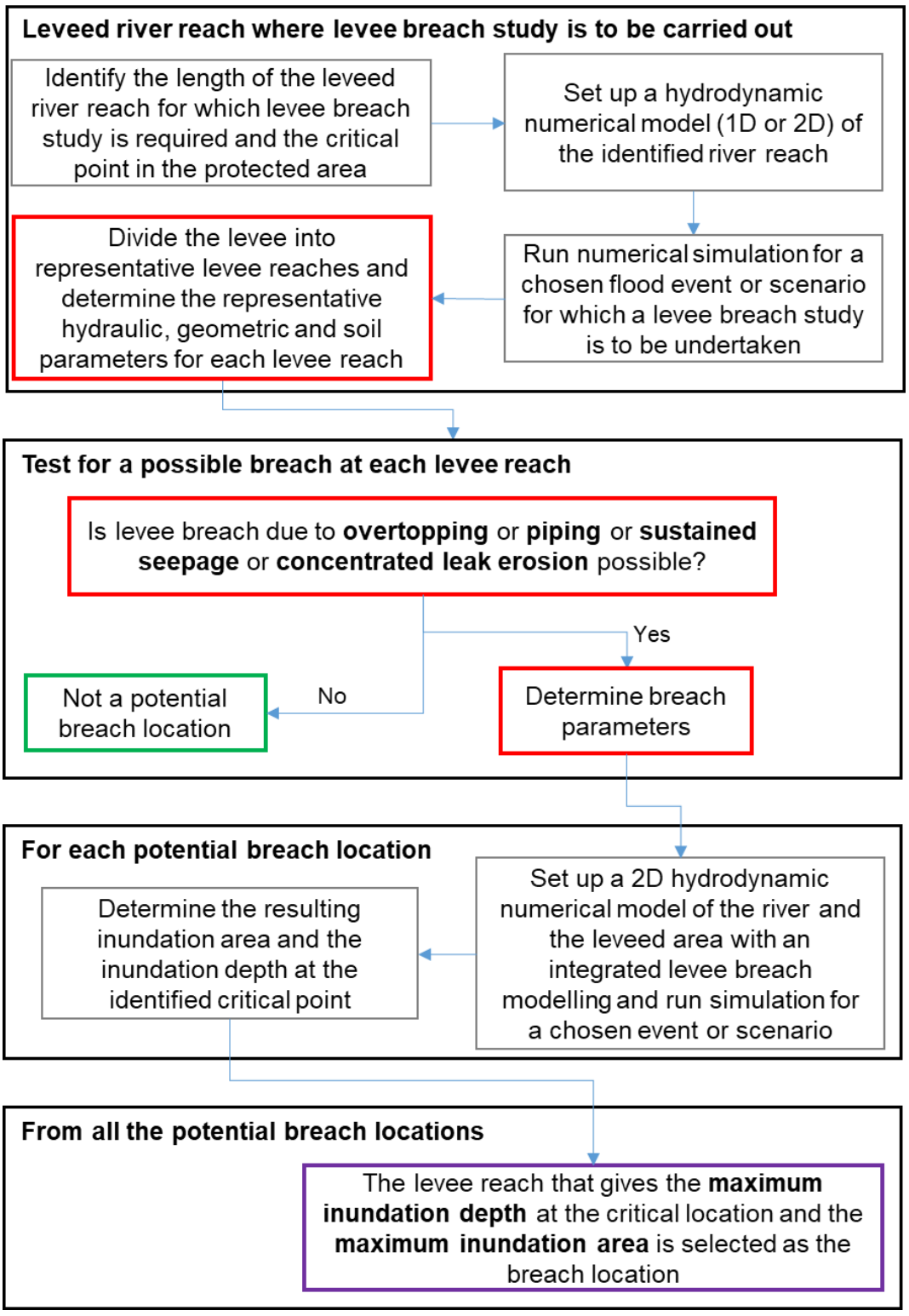

Figure 32: Steps to identify a potential levee breach location with the highest damage potential (detailed approach).

6.4 Dividing the levee into representative reaches

Both the simplified and the detailed approaches to identifying a potential levee breach location require the levee to be divided into representative levee reaches. The following steps can be used to divide the levee into representative levee reaches.

First, the minimum levee reach length should be fixed. The levee reach length should be at least equal to the maximum expected breach width. The maximum breach widths of historical breaches are in the range of 500 m. In this sense, the levee reach length should be at least 500 m. Apel et al. (2009) used levee reach length of 1 km.

Once the minimum length of a levee reach has been determined, the levee is divided into reaches of at least the same length as the minimum length, considering the following aspects.

i. Geometry of the levee (dimensions)
ii. Levee type (homogeneous vs. composite)
iii. Type of levee soil (cohesive vs. non-cohesive)
iv. Design, construction, and maintenance condition of the levee
v. Confluence of tributaries
vi. Longitudinal variation of the levee (meanders)
vii. Longitudinal profile of the river (meanders)
viii. Presence of defects or damage to the levee

Therefore, a levee reach should, as far as possible, have the same geometric characteristics (levee width, crest level, crest width, side slopes, riverside and land-side toe levels), levee type (homogeneous vs. composite), material type (cohesive vs. non-cohesive), construction and maintenance conditions.

The longitudinal profile of the river and the longitudinal profile of the levee (meander) should also be considered. A meandering levee reach should be considered as a single reach. Leakage and seepage along the concave side of a river meander is usually higher than along the straight part of the river. Visible and known defects or damage to the levee or other factors listed in Table 18 give an indication of possible weak points along the levee. Such weak points along the levee should be considered when dividing the levee into reaches so that they are located approximately in the centre of a levee reach.

6.5 Possibility of levee breach in a levee reach

Apel et al. (2009) used a limit state equation to estimate the possibility of levee breach due to external erosion (overtopping). Similarly, limit state equations are formulated for each of the main levee breach mechanisms to determine whether levee breach is possible at a given levee reach. References to limit state equations for various breach mechanisms of sea and estuarine levees are given in Kortenhaus et al. (2002). These are adapted for the main riverine levee breach mechanisms. The main levee breach mechanisms are external erosion due to overtopping, backward erosion of the levee body or the foundation due to seepage (piping), sustained seepage through the levee body, and concentrated leak erosion of the levee body or the foundation (see Chapter 2).

6.5.1 Possibility of levee breach due to external erosion (overtopping)

External erosion due to overtopping flow can lead to breaching of the levee if the erosive force of the flow on the levee surface exceeds the erosion resisting forces. The erosive force of the flow on the levee is a function of the discharge per width overtopping the levee,

which can be calculated using the Poleni overflow formula given by equation (37) (Bollrich 2000).

$$q = \frac{2}{3}\mu\sqrt{2g}\Delta h^{3/2} \tag{37}$$

In equation (37), μ is the dimensionless discharge coefficient, which is a function of the shape of the levee crest (width, roundness), the river- and landside slopes of the levee, flow constriction, etc.; g is the acceleration due to gravity, which is equal to 9.81 m/s²; and Δh [m] is the energy head above the levee crest. For a wide, sharp-edged and horizontal levee crest, μ can be approximated by 0.5 (Bollrich 2000). Δh can be approximated by the water depth above the levee crest.

The levee resists the erosion by the overflow up to a critical discharge. This critical discharge can be calculated using the equation given by Apel et al. (2009) (equation (38)).

$$q_c = \frac{v_c^{5/2} k^{1/4}}{125 \tan \alpha_i^{3/4}} \tag{38}$$

In equation (38), v_c [m/s] is the critical flow velocity and can be calculated using equation (39), α_i [°] is the slope angle, k [m] is the surface roughness.

$$v_c = \frac{3.9117 + 1.5(f_g - 1)}{1 + \left(0.8575 - 0.45\left(f_g - 1\right)\right)\log_{10}(t_e)} \tag{39}$$

In equation (39), f_g [-] is a parameter for the quality of the levee cover and t_e [hours] is the duration of the overtopping. According to Hewlett et al. (1987), the value of f_g varies between 0.5 for poor cover conditions and 1.5 for good cover conditions.

Therefore, the possibility of a levee breach due to overtopping at a given levee reach can be estimated using the following steps:

i) Determine the water level time series at the centre of this reach.
ii) Check whether the maximum water level exceeds the levee crest level.
iii) If so, calculate a) the overtopping duration (t_e) from the water level time series, b) the overtopping discharge (q_a) using equation (37) and c) the critical discharge using equation (38).
iv) If the overtopping discharge is greater than the critical discharge, levee breach at this levee reach is possible.

6.5.2 Possibility of levee breach due to backward erosion (piping)

If the conditions for the occurrence of backward erosion are fulfilled (see section 2.4.1), the limit state equation for estimating the possibility of levee breach along a given levee reach

due to backward erosion is to compare the prevailing hydraulic gradient with the critical hydraulic gradient that would cause and sustain backward erosion. The critical hydraulic gradient that would cause and sustain backward erosion and eventually piping can be determined using the empirical formula given by Sellmeijer et al. (2011) in equation (1).

The prevailing hydraulic gradient (i) is equal to the difference in total head between the river and the land side (Δh) divided by the length of the seepage path (L) as given by equation (40). L can be approximated by the horizontal distance between the contact point on the river side and the exit point on the land side (see Figure 11).

$$i = \frac{\Delta h}{L} \tag{40}$$

The possibility of levee breach due to backward erosion along a given levee reach can be estimated by the following steps:

i) The first step is to check the conditions for backward erosion. To do this, the vertical soil profile of the levee and its foundation should be examined. Backward erosion is possible if the vertical soil profile has a (relatively thin) layer of clay soil over a thick layer of sand. In addition, free flow from the sand layer should be possible on the landside. If a vertical soil profile is not available, sand boils from past flood events can be used as an indication that backward erosion is possible in such levee reaches.
ii) If the necessary conditions for backward erosion are met, determine the water level time series in the river along the centre of the levee reach in question.
iii) Then, for the levee reach in question, calculate a) the hydraulic gradient corresponding to the maximum water level using equation (40) and b) the critical hydraulic gradient using equation (1).
iv) If the hydraulic gradient corresponding to the maximum water level is greater than the critical hydraulic gradient, levee breach at this levee reach is possible.

6.5.3 Possibility of levee breach due to sustained seepage

The conditions for seepage through the levee body are a) the levee is homogeneous and constructed of non-cohesive material, b) the levee has no impermeable layer on the river-side slope or the impermeable layer on the river-side slope is damaged, and c) the levee has no drainage filter at the landside toe. Under such conditions, water seeping through the levee body may exit on the landside slope of the levee and, if the seepage continues for a sufficient period, may lead to the eventual breaching of the levee due to instability.

The possibility of breach due to sustained seepage can therefore be determined by comparing the duration of the water level above a given critical level with the time required for the water column to seep through the levee to the landside toe, which can be calculated using equation (3). If the duration of the water level above a given critical level is longer than the time required for the water column to seep through the levee to the landside toe, levee breach due to sustained seepage at this levee reach is possible.

6.5.4 Possibility of levee breach due to concentrated leak erosion

Some historical levee breaches are known to have been initiated by concentrated leak erosion through cracks and fissures, animal burrows, pipes penetrating the levee, etc. As discussed in Section 2.4.3, little is known about the process of concentrated leak erosion. Nevertheless, the works of Benahmed et al. (2012) and Bonelli (2012), both at the theoretical and experimental level, have improved our understanding of the process.

For levees, the time required for concentrated leak erosion from the start of erosion to breaching of the levee is given by equation (4). Using this time, it is possible to estimate the possibility of levee breach due to concentrated leak erosion. The steps are as follows:

i) Check the conditions for concentrated leak erosion. This is the presence of a continuous opening in the levee body or foundation below the water level in the river, connecting the water side to the land side.
ii) Calculate the duration of the flood level sufficiently above the identified continuous opening (flood level near the top of the levee).
iii) Calculate the time required for a concentrated leak erosion to cause a levee breach (equation (4)).
iv) If the duration of the flood level calculated in step ii) is greater than the duration required for a concentrated leak erosion to cause a levee breach calculated in step iii), then a levee breach is possible at the levee reach in question.

6.6 Summary

In this chapter, an approach is proposed for estimating a possible breach location. The approach makes use of the flood characteristics (water level and duration), the geometric and geological characteristics of the levee in question and its foundation, the cause of the breach and the information from historical levee breaches on their breach location. Depending on the cause of the breach, limit state equations are applied to estimate the possibility of a levee breach at a given levee reach.

7 Numerical modelling of the flow propagation of a levee breach type physical test[3]

Assessing the performance of hydrodynamic numerical models through calibration and validation with real levee breach flows is often not possible since detailed flow data during a levee breach are often not collected. The main priority during a levee breach flood is to save lives and property. As an alternative, laboratory physical tests that mimic levee breach flows can be used to evaluate the performance of the hydrodynamic numerical models for modelling levee breach type flows. This chapter examines the performance of Telemac-2D for modelling levee-breach-type flows using the laboratory physical tests carried out by Briechle and colleagues at RWTH Aachen University, Institute of Hydraulic Engineering and Water Resources Management.

7.1 River levee breach type flow physical experiment

For the sake of completeness, the laboratory test is discussed in this section. As highlighted above, the physical test used here was carried out at RWTH Aachen University, Institute of Hydraulic Engineering and Water Resources Management and is published by Briechle et al. (2004) and Briechle (2006). Furthermore, Roger et al. (2007), Roger et al. (2009), Roger et al. (2010) and Roger (2011) have further discussed the experiments and compared the physical test results with numerical simulation results, modelled by two 2D hydrodynamic numerical models (DGFlow (Roger et al. 2009) and WOLF 2D (Archambeau et al. 2002)) and the 3D model Star-CD.

7.1.1 Set-up of the laboratory physical test

The experiment has been designed to mimic the conditions of flood propagation due to a river levee breach. As such, the physical model consists of a channel and an adjacent propagation area separated by a gate that can be suddenly opened by a pneumatically operated system. The channel, the sudden opening of the gate, and the propagation area attached to the gate serve as the representation of the river, the levee breach phenomena, and the floodplain protected by the levee respectively. A 3D schematic diagram of the experiment is shown in Figure 33.

The channel is 1 m wide, 8.50 m long, horizontal (no slope) and has an adjustable sharp-crested weir at the outlet. The flow into the channel is regulated by an ultrasonic flow measuring device. The weir at the outlet is used to regulate the water depth in the channel prior to the opening of the gate (breaching). The weir height is calibrated based on the inflow discharge and the desired constant water depth in the channel before the gate is opened. The gate is installed on the side of the channel connected to the propagation area. It can be adjusted to three different widths: 30 cm, 50 cm and 70 cm. The centre of the gate is located 3.97 m from the channel inlet.

[3] The manuscript of Chapter 7 is partly taken from the author's publication (Tadesse & Fröhle 2017) , and only editorial changes for the sake of readability are made here.

The propagation area measures 3.5 m by 4.0 m and is made of glass. The use of glass for the propagation area serves two purposes. Firstly, it minimises the frictional losses; and secondly, it allows the depth of flow to be measured by a laser from below. It has no slope and water can flow freely over its three edges (Briechle et al. 2004; Briechle 2006).

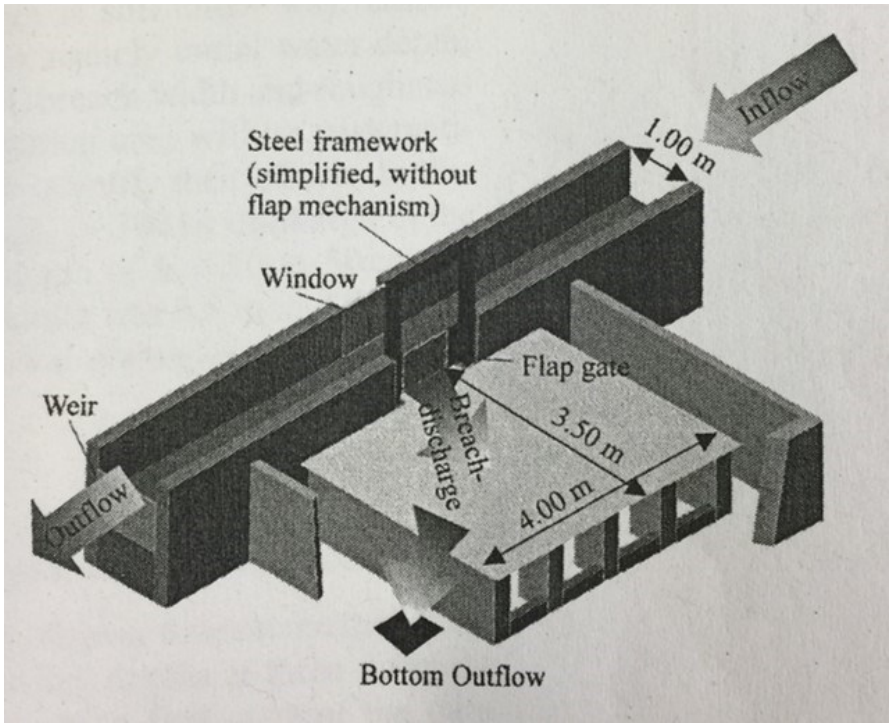

Figure 33: 3D schematic diagram of the physical model setup, taken from Briechle et al. (2004).

The breach flow is calculated from the difference between the inflow and the outflow at the weir. Ultrasonic sensors with a frequency of 25 Hz were employed to measure the water depth in the propagation area at grid points of 0.2 x 0.2 m and at refined grid points of 0.1 x 0.1 m near the gate (Roger et al. 2009).

Table 19: Measurement techniques employed to measure flow characteristics.

Quantity measured	Measuring techniques employed
Inflow	Ultrasonic flow-measuring device
Outflow	Weir
Breach discharge	Difference of inflow and outflow
Water depth in propagation area	25Hz ultrasonic sensors
Velocity profiles *u(z), v(z)*	1D Laser-Doppler Anemometer

Water depth measurements in the channel were undertaken at a resolution of 0.5 x 0.5 m grid points. 1D Laser-Doppler Anemometer (LDA) was used to measure the depth averaged velocity components. High resolution measurements of average velocity profiles were taken at three cross-sections – y = 0.25 m, 0.30 m and 0.35 m – with higher grid

density of $\Delta x = 0.05\ \mathrm{m}$ and $\Delta z = 0.01\ \mathrm{m}$ (Roger et al. 2009; Briechle et al. 2004; Briechle 2006).

7.1.2 Test configurations

Briechle et al. (2004) and Briechle (2006) carried out many breach experiments with different test configurations. This thesis uses 12 well-documented test configurations listed in Table 20. These are sufficient for the purpose here, which is to demonstrate the capability of Telemac-2D for modelling levee breach type flows.

The test configurations differ in the inflow discharge (Q_{in}), the initial steady water depth in the channel before gate opening (h_{init}) and the width of the gate opening (b_{br}). The initial steady-state water depth in the channel prior to gate opening (h_{init}) depends on Q_{ini} and the weir height at the channel outlet (h_w).

Table 20: Test configurations used for this analysis with the corresponding values of b_{br}, Q_{in}, h_{init} and h_w.

Nr.	Configuration name	b_{br} [cm]	Q_{in} [l/s]	h_{init} [cm]	h_w [m]
1	b50_Q300_h50	50	300	50	0.241
2	b50_Q300_h40	50	300	40	0.152
3	b50_Q200_h50	50	200	50	0.297
4	b50_Q200_h40	50	200	40	0.202
5	b50_Q200_h30	50	200	30	0.113
6	b50_Q100_h30	50	100	30	0.175
7	b70_Q300_h50	70	300	50	0.241
8	b70_Q300_h40	70	300	40	0.152
9	b70_Q200_h50	70	200	50	0.297
10	b70_Q200_h40	70	200	40	0.202
11	B70_Q200_h30	70	200	30	0.113
12	b70_Q100_h30	70	100	30	0.175

The configurations are named in the same way as in Roger (2011), where the name indicates the breach width in cm, the inflow discharge in l/s and the initial depth in the channel before gate opening in cm. For example, the test configuration name ‘b50_Q300_h50’ corresponds to a configuration with gate opening of 50 cm, inflow discharge of 300 l/s and initial water depth in the channel before gate opening of 50 cm.

7.2 Telemac-2D numerical model setup for the physical experiment

Telemac-2D models are set up for the different configurations of the physical test described above. The models are set up to replicate the conditions of the physical test as closely as possible. The important aspects of the model setup are discussed in the following sections.

Setting up a 2D hydrodynamic numerical model is usually carried out in three steps. In the first step, often referred to as pre-processing, the inputs to the numerical model are prepared. This includes preparing the computational mesh, boundaries, boundary and initial conditions and settings in the required formats. The second step is the calculation or simulation step, where the calculations are performed according to the settings in the first step. The last step is the processing of the results, where the simulation results from the second step are evaluated and presented.

7.2.1 Computational mesh

The computational mesh provides the spatial discretisation of the continuous physical phenomena and must be good enough to represent the geometry and the physical phenomena. The computational mesh for the physical test is generated using the triangulation code Triangle.exe (Shewchuk 1996), which is used within the free software Kalypso1D2D. Kalypso1D2D is a pre- and post-processing module of Kalypso for hydrodynamic numerical models (2D, 3D). Kalypso is an open source software developed by Björnsen Consulting Engineers (BCE) and the Institute of River and Coastal Engineering, Hamburg University of Technology (TUHH) (TUHH) (BCE 2022).

The inputs required for the generation of the computational mesh include the model boundary (as a polygon feature class), break lines (as polyline feature classes), maximum triangle area restrictions (as polygon feature classes). These inputs can be created within Kalypso1D2D, but the fastest way is to create them in a GIS software such as ArcGIS™ and import them into Kalypso1D2D. The vertical dimension of the mesh, i.e., the elevation, is taken from the elevation model created for the area. The resolution of a computational mesh affects the results of a numerical model; the higher the mesh resolution, the better are the results, at least until grid convergence is achieved. The resolution of the computational mesh can be optimised by reducing the maximum triangle size during mesh generation.

For this reason, a high-resolution mesh is generated and used for the current work. It has approximately 46,500 elements and 23,700 nodes. The edge length of the mesh elements varies between 0.01 m and 0.03 m in the gate area and between 0.03 m and 0.05 m in the other parts of the model. This mesh resolution is chosen based on the sensitivity analysis of Roger (2011), who analysed the sensitivity of mesh resolution for another finite element based hydrodynamic numerical model used to model this physical test. A part of the computational mesh used in this work is shown in Figure 34.

The flap gate is represented in the mesh with a sill of elevation 0.65 m. The gate opening is simulated by an instantaneous levee breach. This means that the sill is immediately lowered to the level of the channel at the time of the sudden opening of the flap gate. The

parametric levee breach model integrated in Telemac-2D (Chapter 4) is used to define the necessary parameters.

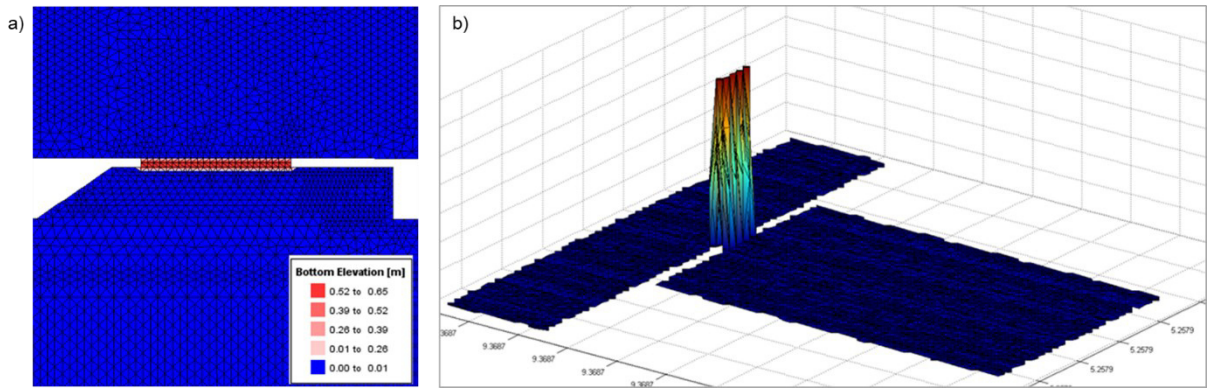

Figure 34: Computational mesh of the physical test setup: a) part of the mesh near the gate area (not to scale), the gate is represented in the model with an elevation of 0.65 m above the bottom of the channel and the propagation area (0 m) and b) 3D view of the mesh (not to scale) (own image).

7.2.2 Initial and boundary conditions

The numerical solution of partial differential equations, such as the shallow water equations (see Chapter 3), requires the solutions of the variables at the beginning (initial conditions) and at the model boundaries (boundary conditions). For the 2D numerical model of the physical tests simulated here, the initial conditions are set to a dry condition, i.e., the initial water level is set to 0 m (the bottom elevation of the channel and the propagation area is 0 m), except at the inflow boundary, where the elevations of the nodes are set to -0.1 m to have some water depth at the beginning for numerical stability reasons.

The boundary conditions should represent the physical reality as accurately as possible. For the numerical model of the physical test, the boundary conditions at the various boundaries are taken from the physical test configuration. The boundary conditions are discharge at the channel inlet, water level – discharge relationship (h-Q) at the channel outlet, free flow at the sides of the propagation area and no flow across the solid boundaries. The types of the boundary conditions for the physical test are shown schematically in Figure 35.

The boundary condition at the channel inlet is prescribed using the measured inflow, which is constant for a given test configuration (see Table 20 for the test configurations). Two inflow discharge configurations, which are 300 l/s and 200 l/s, are considered in the present analysis. The boundary condition at the three edges of the propagation area is set to free flow and is determined automatically by the numerical model.

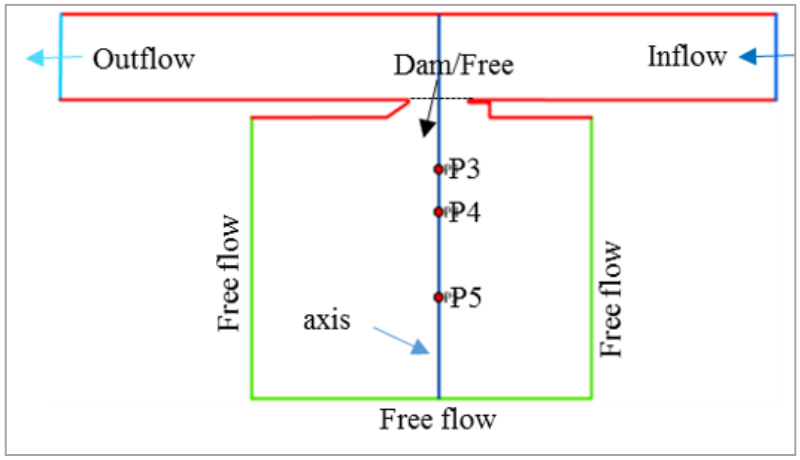

Figure 35: Schematic diagram showing the boundary conditions of the numerical model of the physical test, three points in the propagation area at which point results were evaluated, and an axis along which the water level profiles of the results were analysed (own image).

The boundary condition at the channel outlet is prescribed using a water level – discharge relationship (h-Q) condition. The h-Q relationship at the weir for the test configurations can be derived from equation (37) using an appropriate discharge coefficient. Roger et al. (2009; 354) determined experimentally variable discharge coefficients for the different test configurations. The discharge coefficient is a cubic polynomial function of the overflow depth as given by equation (41).

$$\mu = a_3 {h_0}^3 + a_2 {h_0}^2 + a_1 h_0 + a_0 \quad \textbf{(41)}$$

The symbols are: h_0 is the overflow depth (m) and is equal to h - h_w, h is the upstream water depth (m), h_w is the weir crest height (m), and a_0, a_1, a_2 and a_3 are polynomial coefficients (-) determined experimentally for different test configurations and are given in Table 21.

Table 21: Coefficients of the cubic polynomial approximation for the discharge coefficient given by Equation (41) (taken from Roger et al. (2009, p. 354)).

Configuration	a_3	a_2	a_1	a_0	Range of validity (m³/s)
Q300-h50	-7.291	4.561	-0.554	0.752	0.05 < Q < 0.3
Q300-h40	-10.84	6.009	-0.359	0.738	0.05 < Q < 0.3
Q200-h50	-62.63	26.61	-3.508	0.887	0.03 < Q < 0.2
Q200-h40	-65.62	29.01	-3.665	0.877	0.03 < Q < 0.2

Equation (37) is used to calculate an h-Q relationship in tabular form for each test configuration. These data are used as the boundary conditions at the channel outlet for the respective test configurations. An example of an h-Q relationship for different discharge coefficient values for the configuration Q300-h50 is shown in Figure 36. The final h-Q relationships used at the weir are determined by comparing different discharge coefficients. The h-Q relationships that reproduce the initial water level in the channel prior to gate opening are selected. This is presented in Section 7.3.

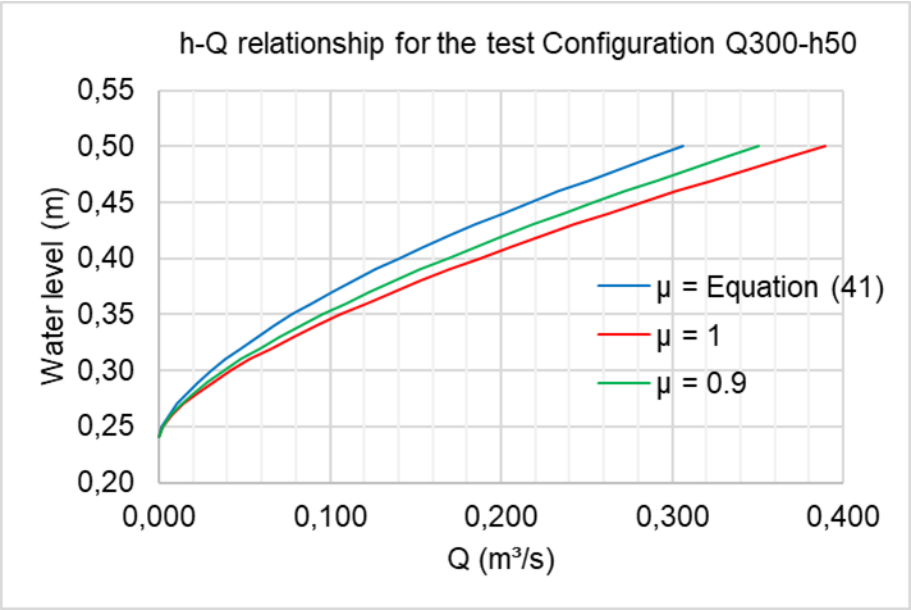

Figure 36: h-Q relationships for the test configuration Q300-h50 calculated with equation (37) for three different discharge coefficient values.

7.2.3 Physical and numeric model settings

In addition to the computational mesh, initial and boundary conditions, a number of physical and numerical settings need to be specified.

The most important physical parameters are the water density, the bed friction and the turbulence model. A water density of 1000 kg/m³ is used for all the simulations. The bed friction formulation of Nikuradse (Nikuradse 1933) and a constant viscosity turbulence model are used. The friction coefficient and the turbulent (eddy) viscosity are calibration parameters. The expected value of the friction coefficient (Nikuradse's roughness height, ks) is 0 because the surfaces used in the experiment are frictionless (made of glass).

In this work, the finite element method implementation of Telemac-2D with the wave equation and the method of characteristics advection scheme are used. This scheme does not have to satisfy the Courant-Friedrichs-Lewy (CFL) condition and uses a semi-implicit time-stepping. Hence, the correct choice of the simulation time step is important. The simulation time step defines the discretisation in the time. It can significantly affect the simulation results if not chosen carefully. The accuracy of the results increases with decreasing time step, but the simulation time and numerical diffusion increase with decreasing time step. After several sensitivity runs, a time step of 1 millisecond gave optimal results and this is used for all simulations.

Other numerical parameters are set on the basis of the recommended values given in the Telemac-2D user manual (Ata 2018) for levee breach type flows. These include the choice of option for treatment of tidal flats, solver, solver accuracy and implicitation options for the different variables.

7.3 Calibration and validation of the numerical model

7.3.1 Model calibration for the initial steady flow in the channel prior to gate opening

The numerical model is calibrated using the physical test configuration b70_Q300_h50. Firstly, the initial steady flow in the channel prior to gate opening is calibrated by varying the discharge coefficient of the weir at the channel outlet (i.e. the h-Q relationship at the weir). The modelled water level in the channel prior to gate opening is compared with the measurement. A comparison of the results is given in Table 22. It can be seen from Table 22 that a steady flow depth in the channel equal to 0.50 m, the same as the value in the physical test configuration, could be achieved by using an h-Q relationship at the weir calculated with a discharge coefficient μ = 0.98. Using the h-Q relationship at the outlet weir calculated with the discharge coefficient determined experimentally by Roger et al. (2009), i.e. equation (41), a steady flow depth in the channel prior to gate opening of 0.53 m is obtained for this configuration, which is higher than 0.5 m. Hence, the h-Q relationship at the weir calculated with a discharge coefficient μ = 0.98 is used for this and the other test configurations.

Table 22: Effect of the boundary condition at the channel outlet on the simulated steady water depth in the channel prior to gate opening (h_{ini}). The boundary condition at the channel outlet is an h-Q relationship determined by equation (37). For these simulations, ks-value = 0.01 m, eddy viscosity $\nu = 10^{-5}$ m²/s, and free surface gradient compatibility = 0 are used.

No	h-Q relationship at channel outflow	Simulated h_{ini} [m]	Measured h_{ini} [m]	% Difference to measurement
1	obtained with μ given by equation [22]	0.5298	0.4991	6.14%
2	obtained with μ = 0.8	0.5248	0.4991	5.16%
3	obtained with μ = 0.85	0.5172	0.4991	3.62%
4	obtained with μ = 0.9	0.5101	0.4991	2.21%
5	obtained with μ = 0.95	0.5040	0.4991	0.98%
6	obtained with μ = 0.98	0.5004	0.4991	0.27%
7	obtained with μ = 1.0	0.4983	0.4991	-0.16%

Furthermore, the effects of the friction coefficient (ks-value), eddy viscosity (ν) and free surface gradient compatibility (TETAZCOMP) on the simulated initial water depth are checked and given in Table 23. The channel bed is smooth paintwork. As such, different relatively low ks-values between 0.10 m and 0 m (no friction) were tested in order to check the effect of friction on the simulated steady water depth prior to gate opening. As can be seen from Table 23, the influence of the friction coefficient on the steady water depth in the channel prior to gate opening is insignificant. A ks-value of 0 m resulted in the simulated h_{ini} closest to the measurement (0.13% difference) and is adopted for further use.

The flow is also calibrated for eddy viscosity (ν). As can be seen from Table 23, model runs with different eddy viscosity values showed that the steady water depth in the channel prior to gate opening tended to decrease with increasing eddy viscosity value. This is contrary to the expectation that the water level should increase with increasing eddy viscosity. The reason for this was found to be a leakage of flow into the propagation area in the model with increasing eddy viscosity. This can be seen from the comparison of the water level area plots shown in Figure 37. An eddy viscosity value between 10^{-6} m²/s and 10^{-3} m²/s gave the simulated h_{ini} closest to the measurement (0.13% difference). The eddy viscosity value of 10^{-5} m²/s is adopted for further use.

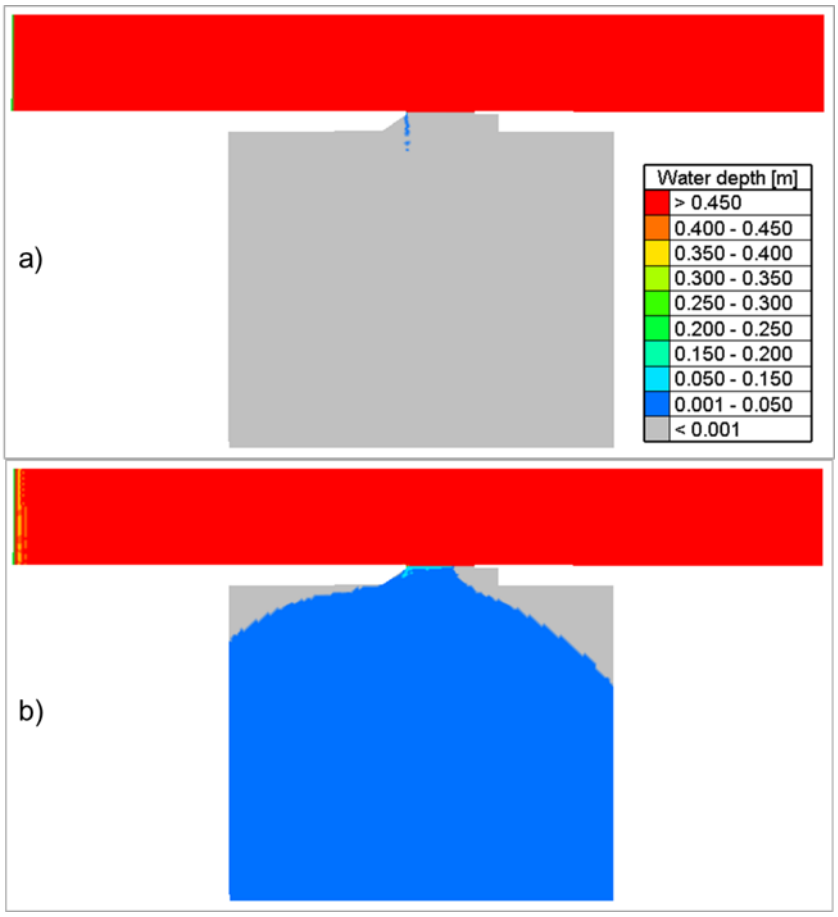

Figure 37: Simulated water depth in the model just before gate opening for a) v = 10^{-5} m²/s b) v = 10^{-1} m²/s. The model with v = 10^{-1} m²/s shows leakage of water into the propagation area.

Reducing the "free surface gradient compatibility", a numerical parameter used by Telemac-2D to reduce the appearance of wiggles, to 0 (value range 0-1) also improved the steady water depth in the channel prior to the gate opening. Low values of free surface gradient compatibility help to smooth numerically generated free surface wiggles (Ata 2018).

Table 23: Calibration of the flow in the channel prior to gate opening: simulated steady water depth in the channel for the test configuration b70_Q300_h50 for various combinations of Nikuradtse's coefficient of friction (ks-value), eddy viscosity (ν) and free surface gradient compatibility (TETAZCOMP). The boundary condition at the channel outlet for these simulations is an h-Q relationship determined by equation (37) and μ = 0.98.

No.	ks-value [m]	ν [m²/s]	TETAZCOMP [-]	Simulated h_{ini} [m]	Measured h_{ini} [m]	Difference (%)
1	0.10	10^{-5}	0.00	0.5015	0.4991	0.48%
2	0.01	10^{-5}	0.00	0.5004	0.4991	0.27%
3	10^{-3}	10^{-5}	0.00	0.5001	0.4991	0.21%
4	10^{-4}	10^{-5}	0.00	0.5000	0.4991	0.18%
5	0.00	10^{-5}	0.00	0.4997	0.4991	0.13%
6	0.00	10^{-6}	0.00	0.4998	0.4991	0.13%
7	0.00	10^{-4}	0.00	0.4997	0.4991	0.13%
8	0.00	10^{-3}	0.00	0.4997	0.4991	0.13%
9	0.00	10^{-2}	0.00	0.4978	0.4991	-0.27%
10	0.00	10^{-1}	0.00	0.4798	0.4991	-3.87%
11	0.00	10^{-5}	0.50	0.5020	0.4991	0.59%
12	0.00	10^{-5}	0.90	0.5068	0.4991	1.55%
13	0.00	10^{-5}	1.00	0.5287	0.4991	5.94%

7.3.2 Model calibration for the flow in the propagation area

After calibrating of the steady-state flow in the channel prior to the gate opening, the model is further calibrated for the flow in the propagation area. The propagation area is made of glass and hence no friction is expected. A ks-value of 0 m is used for the propagation area.

Thus, the flow in the propagation area is calibrated with the eddy viscosity. Model runs are carried out for eddy viscosity values between 10^{-6} m²/s and 10^{-1} m²/s and the simulated steady state water levels at three locations in the propagation area are compared with the measured water levels as shown in Table 24. As can be seen from Table 24, the eddy viscosity values between 10^{-6} m²/s and 10^{-4} m²/s reproduce the measured water level at three locations with better accuracy (less than 10% differnce, see Table 25). The model also reproduces the water level over time at three locations very well, as can be seen from Figure 38. The water surface profile along the centre of the propagation area is also reproduced very well by the model, as can be seen from Figure 39.The eddy viscosity value of 10^{-5} m²/s is adopted for further use.

Table 24: Comparison of simulated steady state water levels [m] at three locations in the propagation area for different eddy viscosity (ν) values [m²/s] with the measured water level at these locations (see Figure 35 for the location of the points) for the configuration b70_Q300_h50.

Location	$\nu = 10^{-6}$ [m]	$\nu = 10^{-5}$ [m]	$\nu = 10^{-4}$ [m]	$\nu = 10^{-3}$ [m]	$\nu = 10^{-2}$ [m]	$\nu = 10^{-1}$ [m]	Measured [m]
P3	0.078	0.078	0.078	0.078	0.076	0.082	0.085
P4	0.045	0.045	0.045	0.045	0.044	0.050	0.045
P5	0.024	0.024	0.024	0.024	0.024	0.028	0.025

Table 25: Steady water level [m] at three points in the propagation area (see Figure 35 for the location of the points) for the configuration b70_Q300_h50; measured values compared to Telemac-2D ($\nu = 10^{-5}$) results and simulated values by Roger et al. (2009).

Location	Measured [m]	Telemac-2D [m]	Difference (%)	Simulated by Roger et al. (2009) [m]	Difference (%)
P3	0.085	0.078	-8%	0.075	-12%
P4	0.045	0.045	0%	0.044	-2%
P5	0.025	0.024	-5%	0.023	-8%

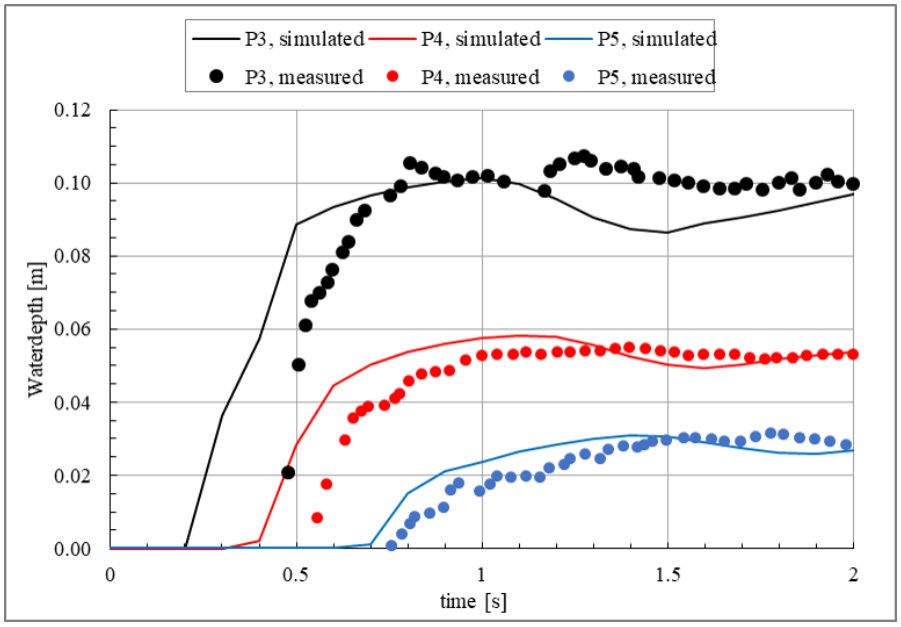

Figure 38: Measured (values reported by Roger et al. (2009)) and simulated (corresponding to eddy voscosity $\nu = 10^{-5}$ m²/s) water levels in the first 2 s after gate opening at three points in the propagation area (see Figure 35 for the location of the points) for the configuration b70_Q300_h50.

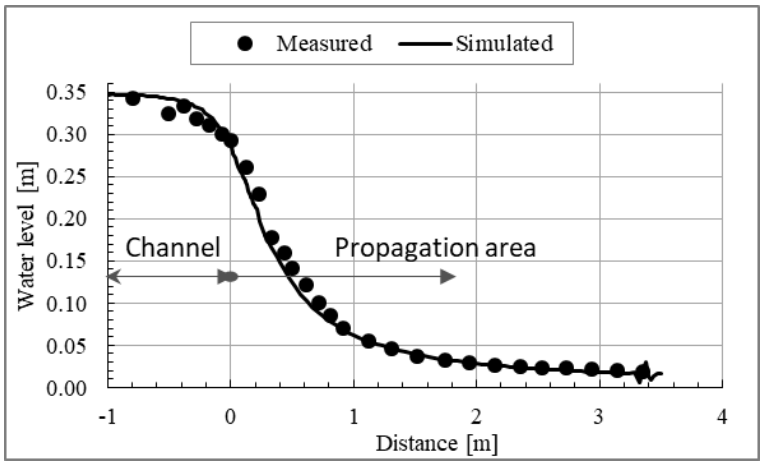

Figure 39: Measured and simulated steady state (1 minute after gate opening) water surface profile along the centre line of the propagation area (see Figure 35) for the test configuration b70_Q300_h50.

7.3.3 Model validation

After obtaining the physical and numerical calibration parameters with the configuration b70_Q300_h50, the numerical model is validated with the test configuration b70_Q200_h40. This is to show that the numerical model with the adapted values of the calibration parameters also performs well for an independent configuration.

As can be seen from Table 26, the model reproduced the measured initial steady-state water depth in the channel prior to gate opening very well (only 0.18% overestimation). Furthermore, the model reproduced the measured steady water depths in the propagation area after gate opening with a maximum deviation of only about 5%, which is within the limits of the measurement accuracy for such relatively shallow flow depths.

Table 26: Comparison of measured values reported by Roger et al. (2009) and simulated water depths: initial steady-state water depth before gate opening (h_{ini}), water depths at three locations in the propagation area (P1, P2, and P3) (see Figure 35 for the location of the points) 1 minute after gate opening.

Location	measured (m)	Telemac-2D (m)	Difference (%)
h_{ini}	0.3993	0.4000	0.18%
P3	0.0657	0.0630	-4.17%
P4	0.0385	0.0365	-5.22%
P5	0.0200	0.0193	-3.32%

Further validation of the model is provided by the comparison of the measured and simulated longitudinal water surface profile along the centre of the propagation area as shown in Figure 40. The model reproduced the steady state water surface profile quite well.

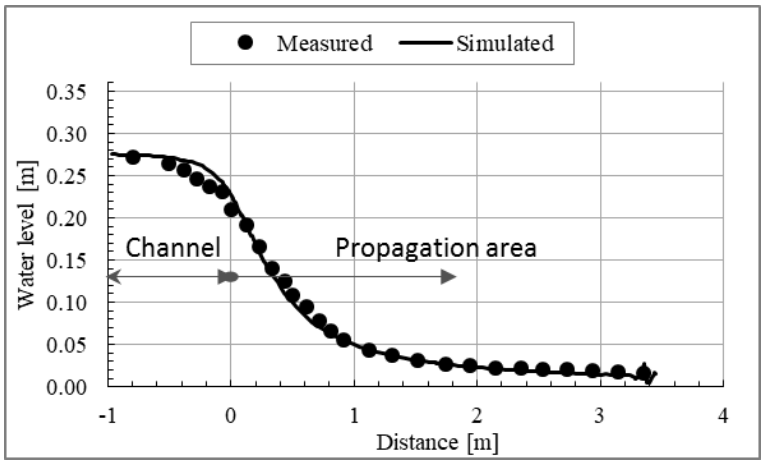

Figure 40: Measured and simulated water surface profile along the centre line of the propagation area for the test configuration b70_Q200_h40 at steady state (1 minute after gate opening).

The above model validation results show that the values of the calibration parameters determined during model calibration are also valid for an independent configuration. Hence, these settings are used to simulate the remaining configurations. The main results are presented in Section 7.4.

7.4 Comparison of Telemac-2D results with the physical tests

The wavefront in the propagation area at various times immediately after gate opening, the breach discharge, the water level at selected points in the propagation area and the water surface profile along the centre line of the propagation area are used to compare the Telemac-2D results with the measured values and other numerical model results.

7.4.1 Wavefront in the propagation area after gate opening

The wavefront immediately after the sudden opening of the gate was documented using Charge-Coupled Device (CCD) camera. For some of the test configurations, data is available at known time intervals. At similar time intervals, the wavefront of the propagation simulated with Telemac-2D was extracted and compared with the measurements. The comparison of the recorded and simulated wavefronts for the test configuration b50_Q300_h50 is shown in Figure 41.

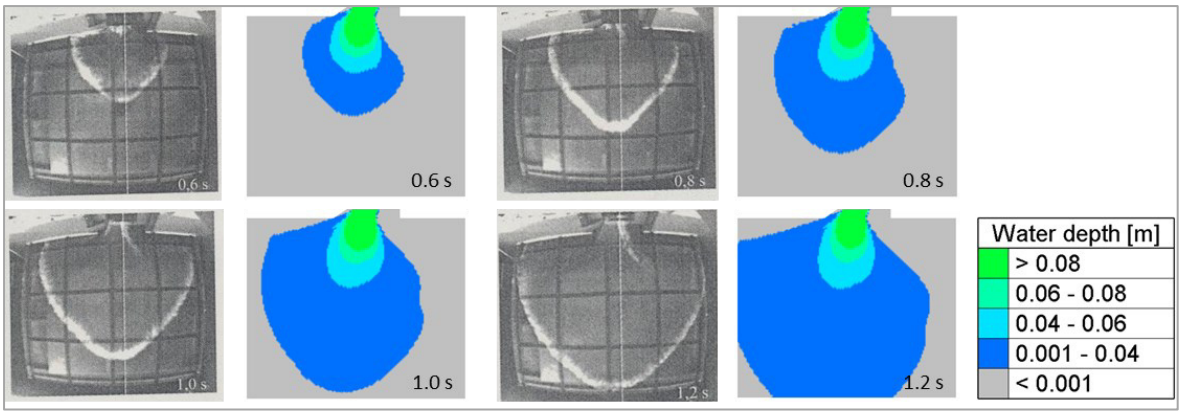

Figure 41: Wavefronts for the configuration b50_Q300_h50 at 0.6, 0.8, 1.0 and 1.2 seconds after gate opening as recorded by a CCD camera (grey images adapted from Briechle et al. (2004)) and as modelled by Telemac-2D.

Figure 41 shows that Telemac-2D reproduced the recorded wavefront very well. In both the measurements and the simulations, the wavefront is deflected towards the flow direction in the channel. The deflection of the wavefront is more pronounced in the numerical model results compared to the measurements. This could be due to the different gate opening mechanisms in the physical model and the numerical model. In the numerical model, the gate is opened by suddenly lowering of the bottom elevation of the nodes representing the gate (the sill), whereas in the physical test the gate is opened with lateral and vertical movements using sophisticated mechanisms to avoid affecting the water column in the channel (Briechle et al. 2004). Roger et al. (2009) and Roger (2011) also obtained similar results using other numerical models. This further supports the argument that the difference is related to the gate opening mechanism.

7.4.2 Water level at selected points in the propagation area

During the physical test, water level measurements are taken at fixed points in the propagation area over an extended period. Figure 42 shows the measured and simulated (with Telemac-2D) water level hydrographs at three points in the propagation area (see Figure 35 for the location of the points) during the first 2 seconds after gate opening for the configuration b70_Q300_h40. The corresponding results from the experiment and as modelled by Roger et al. (2007) are shown in Figure 43.

It can be seen from Figure 42 that the measured and simulated water levels at the three points are quite comparable. However, the flow arrives earlier at points P3 and P4 in the Telemac-2D results compared to the measurements. The arrival time at point P5 is comparable between the Telemac-2D result and the measurement. A similar behaviour of the flood arrival time at the three points can be observed in the numerical results of Roger et al. (2007) as shown in Figure 43. The cause of this slight deviation between the measurements and the model results is likely related to the difference in the gate opening mechanism in the physical test and the numerical model, as highlighted in Section 7.4.1.

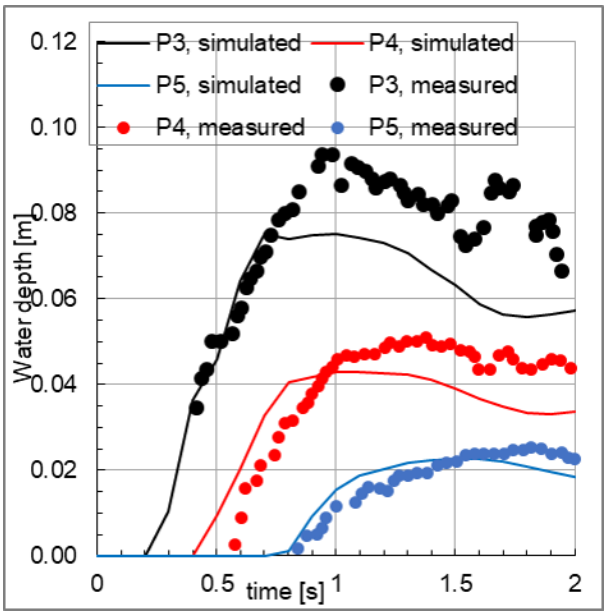

Figure 42: Water level at three points in the propagation area (see Figure 35 for the location of the points) over time for the configuration b70_Q300_h40 (unsteady phase), measured values compared to values simulated with Telemac-2D.

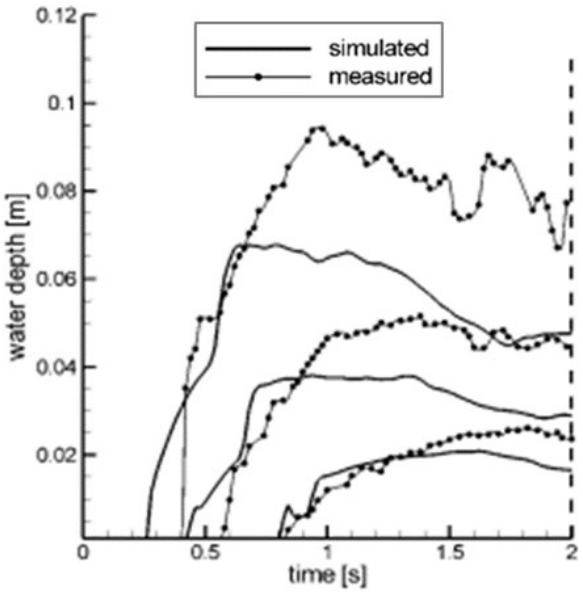

Figure 43: Water level at three points in the propagation area (see Figure 35 for the location of the points) over time for the configuration b70_Q300_h40 (unsteady phase), measured values compared to simulated values by Roger et al. (2007).

The comparison of the steady water level between the measurements and the Telemac-2D results at the three points in the propagation area mentioned above is shown in Table 27 for four test configurations. As can be observed from Table 27, the final steady water levels calculated by Telemac-2D are generally comparable to the measured values. Telemac-2D also performed better than the numerical model results of Roger et al. (2007).

Table 27: Steady-state water levels at three points in the propagation area (see Figure 35 for the location of the points) for four configurations; measured values compared to Telemac-2D results.

Configuration	Location	measured [m]	Telemac-2D [m]	Difference (%)
b50_Q300_h50	P3	0.059	0.062	4.34%
	P4	0.033	0.035	5.24%
	P5	0.017	0.019	7.73%
b50_Q200_h30	P3	0.037	0.034	-8.17%
	P4	0.019	0.019	-0.19%
	P5	0.010	0.010	-0.08%
b70_Q300_h40	P3	0.074	0.055	-25.34%
	P4	0.036	0.032	-10.65%
	P5	0.017	0.017	0.46%
b70_Q200_h50	P3	0.079	0.076	-2.72%
	P4	0.040	0.045	10.55%
	P5	0.022	0.024	9.32%

7.4.3 Breach discharge

In the physical tests, the breach discharge, i.e., the discharge through the gate opening, is determined from the difference between the inflow at the channel inlet and the outflow at the channel outlet. In the same way, the breach discharge is determined for the Telemac-2D simulation results. The comparison of the measured and simulated steady-state breach discharges is given in Table 28. The steady-state breach discharges determined by the numerical models DGFlow (2D model) and STAR-CD (3D model) by Roger (2011) are also given in Table 28.

The steady-state breach discharges computed by Telemac-2D for the different test configurations agree very well with the measurements. The numerical results generally underestimate the breach discharge. The maximum underestimation of the breach discharge is obtained for the test configuration b50_Q200_h40 and is 8.4% (see Table 28). Telemac-2D overestimated the breach discharge by 1.8% for the test configuration b50_Q200_h30 (see Table 28). Furthermore, as can be seen from Table 28, Telemac-2D performed better than the 2D model DGFlow in terms of breach discharge. However, the 3D model STAR-CD performed slightly better than Telemac-2D in terms of breach discharge. This is due to the use of non-hydrostatic pressure by the 3D model, as also pointed out by Roger (2011).

It can be observed from Table 28 that the breach discharge is positively related to the breach width, the inflow discharge, and the water depth in the channel prior to the gate

opening. The breach discharge for the breach width of 70 cm is greater than that for the breach width of 50 cm if the inflow discharge and the water level in the channel prior to the gate opening are kept constant. The breach discharge increases with increasing inflow discharge, and a deeper water depth in the channel prior to the gate opening results in higher breach discharge if the other parameters are held constant.

Table 28: Measured and simulated steady-state (1 minute after gate opening) breach discharges in l/s for the different test configurations.

Configuration	Measured (l/s)	Telemac-2D		Numerical results of Roger (2011)	
		Simulated (l/s)	Difference (%)	DGFlow (l/s)	STAR-CD(l/s)
b50_Q300_h50	182	167	8.1%	164	174
b50_Q300_h40	127	123	3.5%	114	130
b50_Q200_h50	171	157	8.0%	156	163
b50_Q200_h40	130	119	8.4%	118	122
b50_Q200_h30	79	80	-1.8%	74	81
b50_Q100_h30	81	75	7.5%	74	72
b70_Q300_h50	218	201	7.6%	200	211
b70_Q300_h40	159	148	7.0%	141	153
b70_Q200_h50	194	185	4.9%	183	190
b70_Q200_h40	154	143	7.2%	143	148
b70_Q200_h30	98	97	1.1%	92	99
b70_Q100_h30	91	88	3.1%	87	90

7.4.4 Water level profile along the axis of the propagation area

The comparison of the measured and simulated water level profiles along the axis of the propagation area for four test configurations is shown in Figure 44. As can be seen from Figure 44, the comparison of the water level profiles shows that Teleamc-2D reproduced the water surface profiles very well. The slight deviation of the model results from the measurements is related to the difference in the flow direction between the physical tests and the model runs as highlighted in Section 7.4.1, which might be related to the difference in the gate opening mechanism in the physical test and the numerical model.

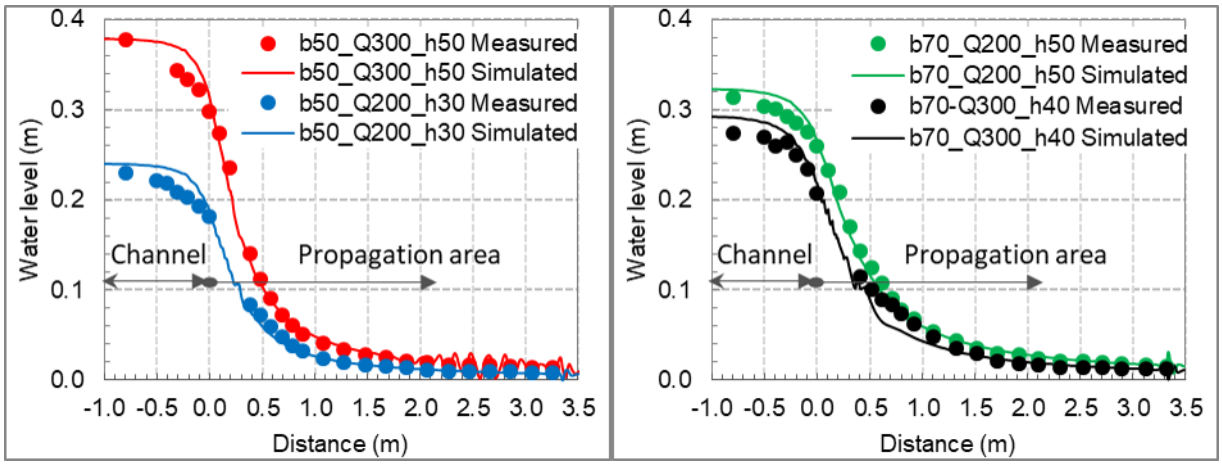

Figure 44: Measured and simulated steady-state (1 minute after gate opening) water level profiles along the axis of the propagation area (see Figure 35) for four test configurations. The measured water level profiles are adapted from Roger (2011, p. 90) and Roger et al. (2009, p. 355).

7.5 Summary

In this chapter, Telemac-2D models are set up for laboratory physical tests simulating levee breaches. The model is calibrated and validated using two independent test configurations. With the optimal settings, Telemac-2D simulations are performed for different test configurations and the results are compared with the measurements. The parameters breach discharge, wave front after breach, water level at selected points in the propagation area, and water level profile along the axis of the propagation area are compared between the measurements and the Telemac-2D results. Telemac-2D reproduced these parameters very well. It is worth noting that Telemac-2D reproduced the breach discharge very well. As the breach discharge is the most important factor in hinterland flooding due to levee breach, it can therefore be concluded that Telemac-2D is a suitable tool for modelling flood inundation due to levee breach.

8 Modelling of the August 1996 Awash River levee breach flooding at Wonji, Ethiopia

8.1 Description of the area

The Awash River is one of the major rivers of Ethiopia. It is an endorheic river that originates in the highlands west of the Ethiopian capital Addis Ababa near the town of Ginchi and terminates in Lake Abbe on the Ethio-Djibouti border (see Figure 45). The catchment area of the Awash River Basin is approximately 110,000 square kilometres and is home to over 11 million people (Emiru et al. 2022). The Awash River is also the most exploited river in Ethiopia compared to other rivers in the country. It hosts a number of hydropower and irrigation schemes (Tola & Shetty 2021).

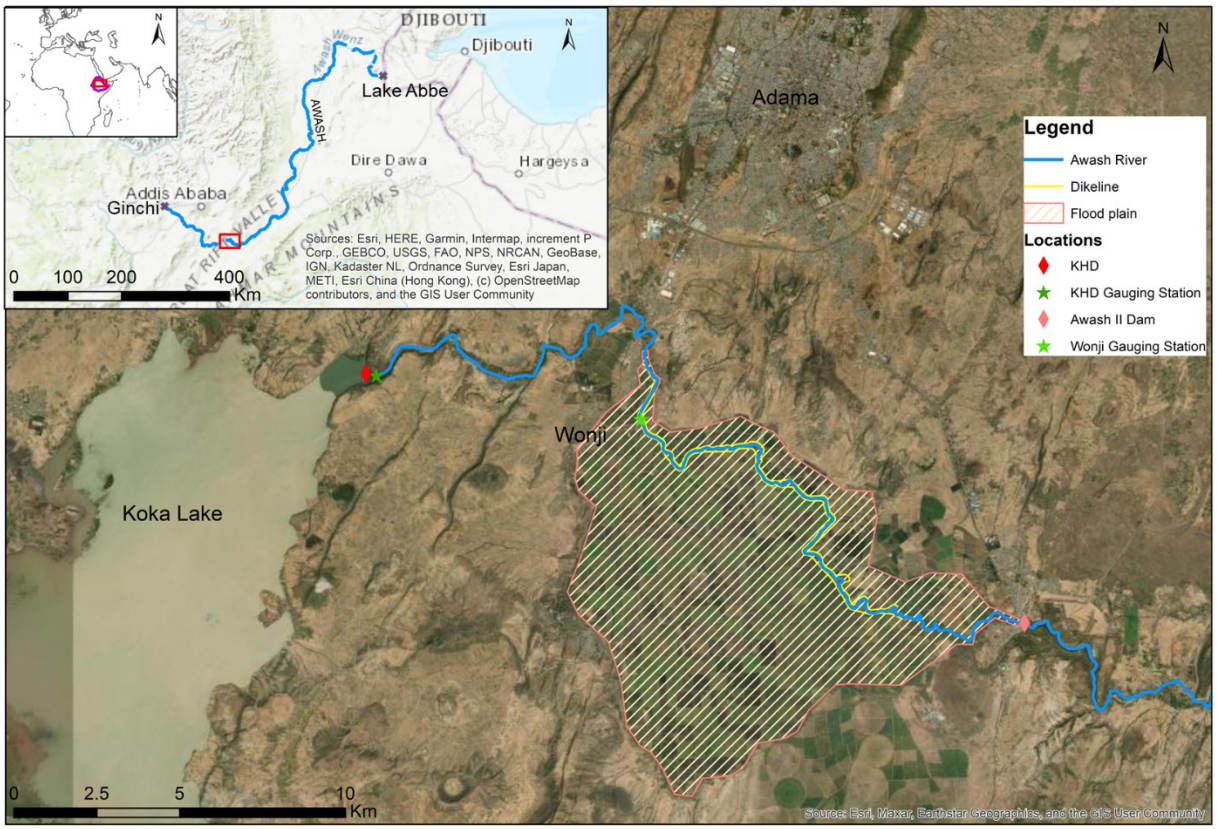

Figure 45: Location and details of the Wonji floodplains along the Awash River protected by levees. The flow direction of part of the Awash River shown on the map is from northwest to southeast (background map courtesy of ESRI®, ArcGIS online service).

The climate condition of the Awash River Basin varies with altitude. It becomes hotter and drier as altitude decreases. The average annual rainfall in the high-altitude regions (above 2500 m a.m.s.l) is between 1400 – 1800 mm, the middle altitude regions (600 – 2500 m a.m.s.l) receive annual rainfall between 1000 – 1400 mm and the low altitude regions (below 600 m a.m.s.l) receive less than 200 mm.

The rainfall pattern is bimodal in the highlands, with the main rainy season between June and September and a short rainy season in March and April. The average temperature varies between 20 °C in the highlands and 33°C in the lowlands (Hailemariam 1999).

Following days of heavy rainfall in the Awash River basin upstream of the Koka hydropower dam (KHD) in August 1996, the water level in the KHD reservoir reached a critical level, forcing the opening of the spillways to avert a potentially catastrophic failure of the dam. The released water caused high flows in the Awash River downstream of KHD and breached the levee protecting the Wonji floodplains. The levee breach resulted in widespread flooding, affecting sugar cane plantation of the Wonji Shoa Sugar Factory (WSSF), buildings of WSSF, the residential houses of the WSSF's employees and private farms. The WSSF and its sugar cane plantation are located in the upper Awash River basin near the town of Adama, downstream of the KHD, approximately 100 km south of the capital Addis Ababa, Ethiopia (see Figure 45).

As Wonji is located only about 20 km downstream of the KHD, the flow of the Awash River at Wonji is directly related to the release of water from the KHD reservoir. During normal operation, the KHD regulates the flow of the Awash River downstream. However, in exceptional cases of high inflow into the KHD reservoir, the water level in the reservoir can exceed the design water level and the spillways of the dam have to be opened to avoid the rather catastrophic phenomena of dam failure. High water levels in the reservoir usually occur following several days of heavy rainfall in the upstream catchment. The KHD reservoir has lost considerable volume due to sedimentation (Abebe H. 2001; Shahin 1993). This leads to higher water levels in the reservoir, even if the inflow to the reservoir and outflow from the reservoir remain unchanged.

8.2 Data

Geographic and river flow data are essential for flood modelling. A digital elevation model (DEM) is required to describe the topography of the area under investigation. The land use of the area is important to estimate the roughness in the flow calculation. Flow data are required not only to prescribe boundary conditions and estimate initial conditions, but also to calibrate and validate the numerical model. Historical flood inundation maps, if available, can also be used to calibrate and validate the numerical model.

8.2.1 Levee data

As highlighted above, the opening of the spillway during high-water levels in the KHD reservoir results in flood flows in the Awash River downstream of the KHD. This often results in a high probability of flooding at Wonji. To protect Wonji from flooding, an approximately 15 km long stretch of the Awash River at Wonji is protected by levees on both banks of the river (see Figure 45).

The levees are constructed from soil material available in the area. The soils in the area are of alluvial-colluvial origin and range mainly from sandy loam to clay loam soils (Dinka & Ndambuki 2014). The levees are constructed with approximately 1:2 (vertical : horizontal) side slopes, an average bottom width of 15 m, a height of 3 m and a top width of 3 m

(Halcrow et al. 2005). According to Halcrow et al. (2005) , the following criteria are used in the design and construction of the levees:

- The design flow is a 20-year return period flood.
- A minimum free board of 0.5 m is used.
- The topsoil under the levee is stripped to a depth of 15 cm for stability and to prevent seepage.
- The levee is compacted to 95% proctor density during construction.
- A minimum distance of 200 m is left between the levee and the river to prevent erosion of the inner slope and to leave room to the river.

8.2.2 Levee breach data

Data on the August 1996 Wonji levee breach are compiled from personal communications with the WSSF levee foreman (Mr. Desta), government and disaster relief organisation reports, and news reports. The breach occurred on 24 August 1996 (Associated Press 1996). According to Mr. Desta, an eyewitness to the flood and WSSF levee foreman, the levee breach occurred upstream of the office area (see Figure 45), was approximately 100 m wide, and the levee was eroded to ground level.

The time taken for the breach to develop to its final state is not documented. Breach durations ranging from instantaneous breach to several hours are considered in the literature (Vorogushyn et al. 2009; Di Baldassarre et al. 2009; Vorogushyn et al. 2010). Previous studies have shown that, for non-flash floods, the duration of the levee breach does not significantly influence the resulting flooding (Di Baldassarre et al. 2009; Chatterjee et al. 2008). Thus, in consultation with the levee foreman, a breach duration of about one hour is considered realistic for the 1996 Wonji levee breach case.

Extensive flooding of the WSSF and its sugar cane plantation is reported (Ahrens 1996; Associated Press 1996). It is documented that the flood mark in the WSSF office buildings reached window beam levels (see Figure 45 for the location of the office building) (Mr. Desta, pers. comm.), which is about 0.90 m above the ground level. In addition, Ahrens (1996) reported widespread flooding with rising water levels on 27 August 1996.

8.2.3 Digital elevation model (DEM)

To model flood propagation, a digital elevation model (DEM) of the area of interest, including the river bathymetry, is required. The DEM of the Wonji area is created from two sources. For the floodplains, georeferenced topographic maps from the Ethiopian Mapping Agency are used. According to this topographic map, the floodplains in Wonji are approximately 1538 m a.m.s.l. The floodplains are very flat with a slope of 0.05% (Dinka & Ndambuki 2014).

The bathymetry of the Awash River and the height of its levees in the Wonji area are generated from the cross-sectional data measured by WSSF in 2007. The cross-sectional data of the Awash River and the levees are available at 200 m intervals for about 15 km length of the Awash River (for the length of the levee at Wonji). For the part of the river without cross-sectional data, the DEM is created by extrapolation of the cross-sectional

data. The DEM of the floodplains and the river, created as described above, is shown in Figure 46.

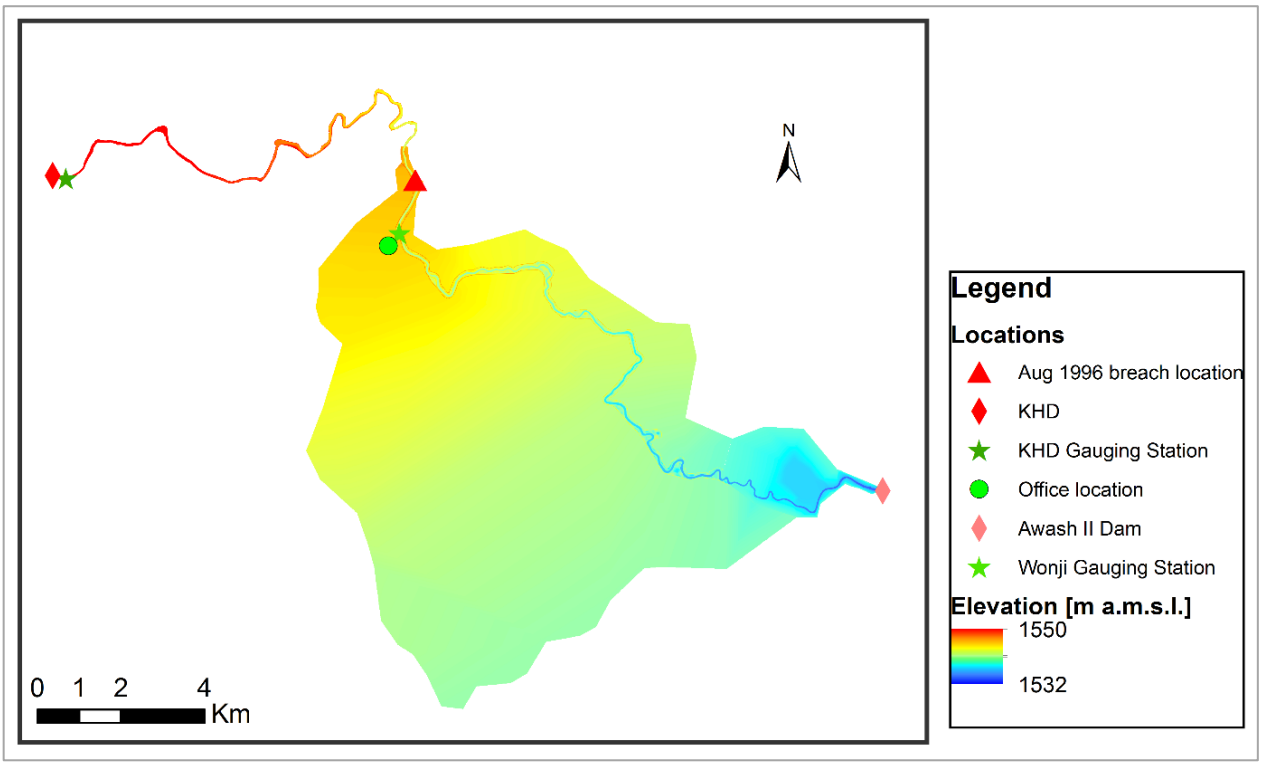

Figure 46: DEM of the Wonji floodplains and the bathymetry of the Awash River between KHD and Awash II Dam.

8.2.4 Land use

Flood propagation is strongly influenced by the roughness of the surface over which the water flows. Land use or land cover is an important aspect in flood inundation modelling. For the Wonji floodplains, the land use is determined from satellite images obtained from ESRI™ World Imagery. The land use of the area is classified into river channel, riverbank, levee, bare land, buildings, and sugar cane plantation. The areal extent of each land use is shown in Figure 47.

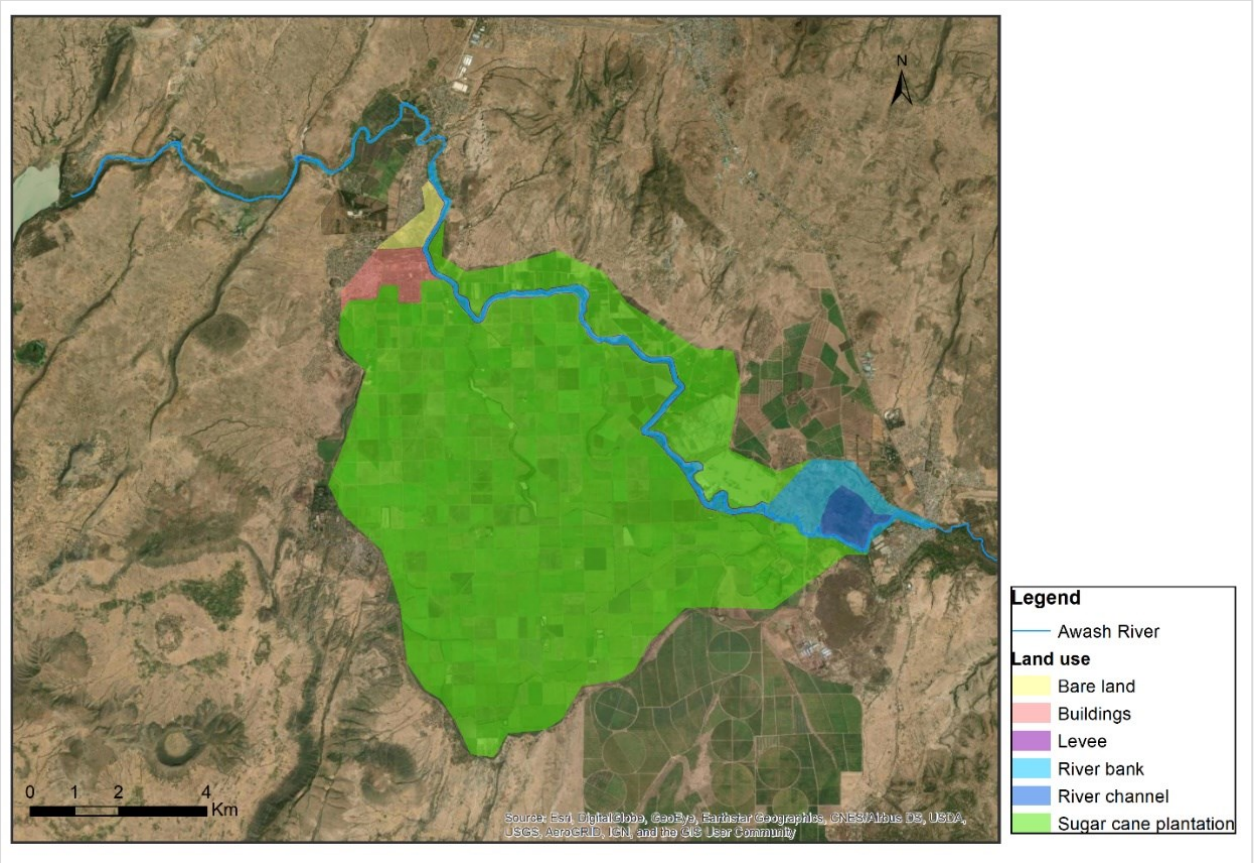

Figure 47: Land use of the study area. Background map is from ESRI ™ online services.

8.2.5 Awash River flow data

The Awash River gauging stations relevant to the model area are the gauge immediately downstream of the KHD and the gauge at Wonji (see Figure 45). Measurement of the Awash River flow at these stations began in 1969, and flow data are available for the period since then, with several data gaps in between.

Water levels are measured twice a day at both stations. The water level measurements are then converted into discharge using a rating curve established for each station by the Ethiopian Ministry of Water and Energy (MWE, personal communication). The average of the two snapshot measurements is recorded as the daily river discharge at each station, which may be significantly less than the instantaneous flood peak of the day. Some past flood hydrographs at KHD and Wonji gauging stations are shown in Figure 48.

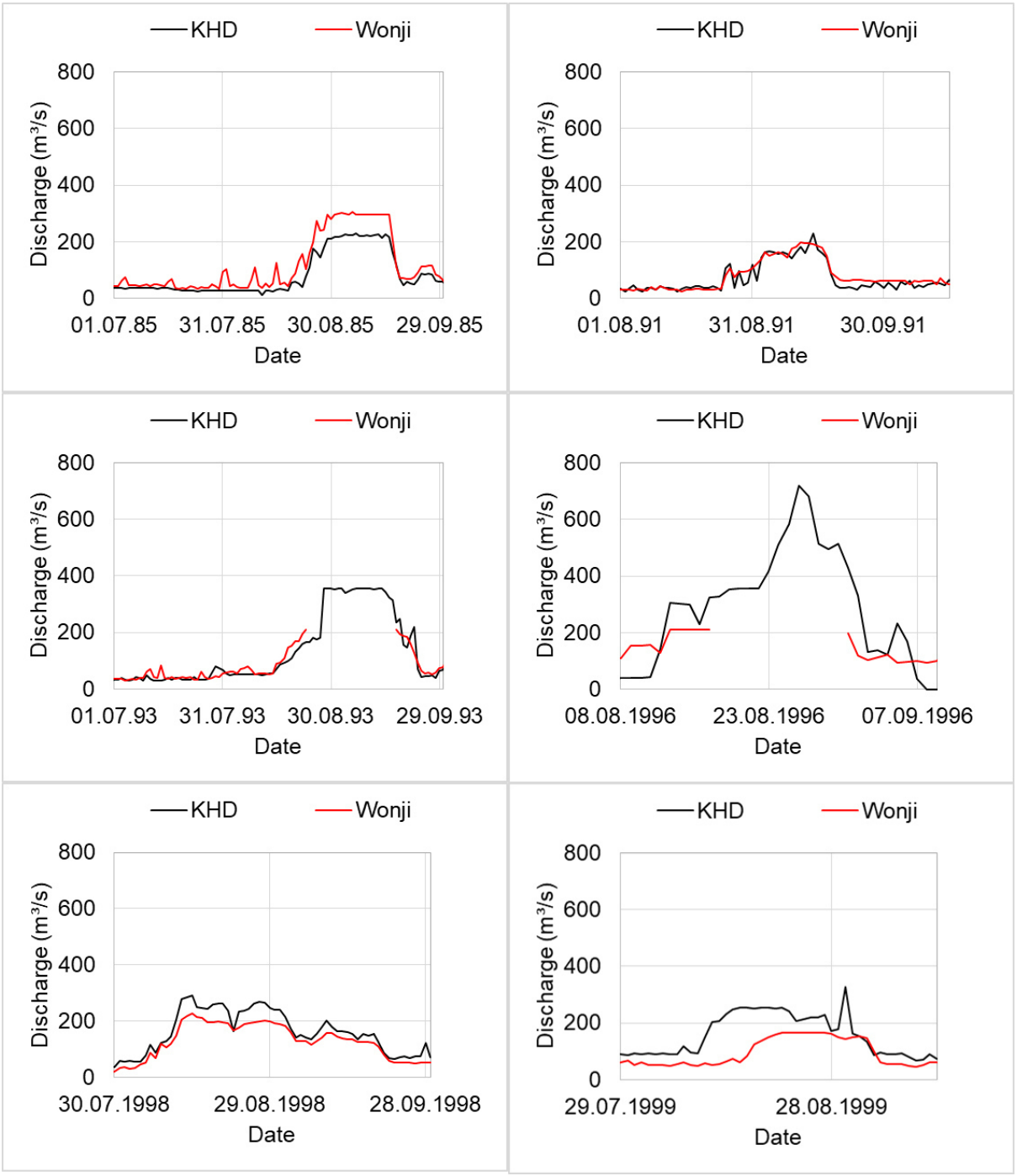

Figure 48: Some past flood hydrographs of the Awash River at KHD and Wonji gauging stations.

The flow of the Awash River immediately downstream of the KHD is more dependent on the operation of the dam than on the natural flow generation from rainfall (Halcrow et al. 2005). This is evident from the hydrographs shown in Figure 48. The hydrographs at KHD and Wonji, both downstream of the KHD, are analogous and have comparable values with a slight time lag.

8.3 Telemac-2D numerical model setup

This section discusses the setup of the 2D hydrodynamic numerical model based on Telemac-2D is discussed. This encompasses the definition of the model domain, the discretisation of the model domain, the selection of the physical and numerical parameters,

the definition of the boundary and initial conditions and the calibration and validation of the numerical model.

8.3.1 Model domain

The boundaries of the model should be set to include areas that can potentially be inundated by flood flows, including the possibility of levee breaches. The focus here is on the leveed Wonji floodplains. Thus, the model domain is set to begin at the KHD, sufficiently upstream of the Wonji floodplains, and to end at the Awash II dam at Awash Melkasa town, downstream of the Wonji floodplains. The lateral boundary of the model domain is set based on the DEM and background map of the area. The model domain contains the Awash River between the KHD and the Awash II dam, the Wonji floodplains on both sides of the river and the levees on both banks of the river as shown in Figure 49.

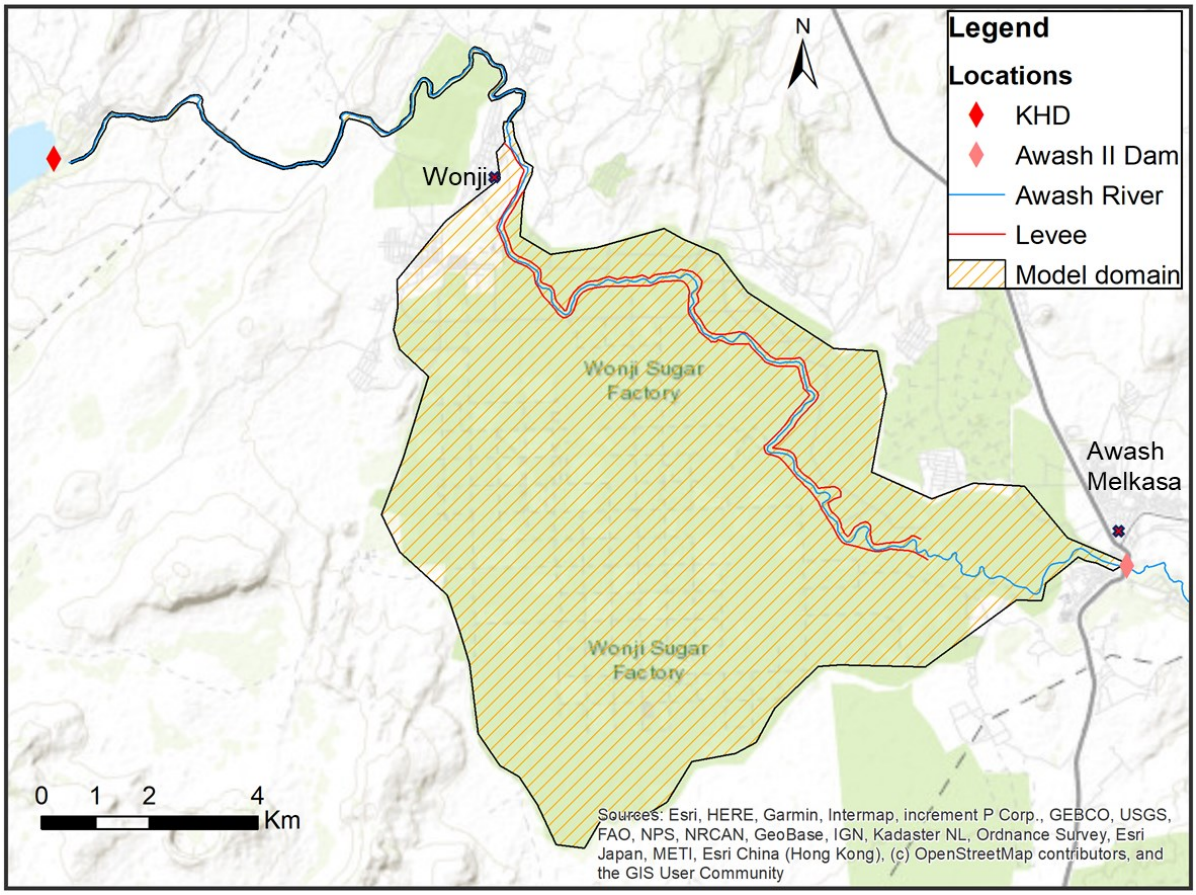

Figure 49: Model domain (Background map is from ESRI ™ online services).

8.3.2 Discretisation of the model domain

As mentioned in chapter 3, the shallow water equations can only be solved using numerical methods. This requires the partial differential equations describing the continuous flow to be evaluated at discrete points in space and time. The discrete locations are determined by dividing the flow domain of interest into small areas. The process of dividing the domain into small areas (often triangular or rectangular or mixed) is known as discretisation and the resulting grid of triangles / rectangles is known as the mesh.

The accuracy of the numerical solution depends on the quality of the computational mesh. The finite element method option in Telemac-2D is used for the simulations. The finite element method generally uses unstructured triangular meshes. The following characteristics determine the quality of finite element meshes:

- The quality of the input geographic data used to generate the mesh.
- Fulfilment of the Delaunay criterion, which requires that no triangle lies within the circumcircle of another mesh triangle, and that the internal angle of the mesh triangles is maximised.
- A good quality mesh has an aspect ratio close to 1. Aspect ratio is the ratio of the areas of adjacent triangles. A good quality mesh has therefore smooth transitions from triangles with small areas to mesh triangles with large areas.
- A good quality mesh is one that is well refined so that it captures the elevation of the area well. This is particularly important in areas with steep slopes and when capturing the elevation of linear structures such as levees.

The mesh for the model domain is generated using BlueKenue™. BlueKenue is a pre- and post-processing software developed by the National Research Council Canada (NRCC 2019). It can generate good quality triangular meshes from a combination of inputs representing points, break lines, and polygons as required. It accepts ESRI™ shape files as input. The mesh inputs here are polyline shape files representing the levee, the riverbed, the riverbank and a polygon shape file representing the model boundary. Additional polyline shape files in the river channel, along the levee and in some areas of the model domain are used to increase the mesh refinement.

The model area is discretised into triangular mesh elements of varying spatial resolution. The levee is discretised by at least three mesh nodes between the levee foot and crest, and the size of the triangles is on average 1.5 m². This detailed discretisation of the levee ensures that it is accurately represented in the model. The river channel is discretised with more than ten mesh nodes over the cross-section and triangles with long edge sizes in the flow direction. The average element size in the river channel is 21 m². The floodplain is discretised with mesh element sizes of approximately 1.2 ha. In total, the computational mesh contains about 725,000 triangular mesh elements. Excerpts of the mesh are shown in Figure 50.

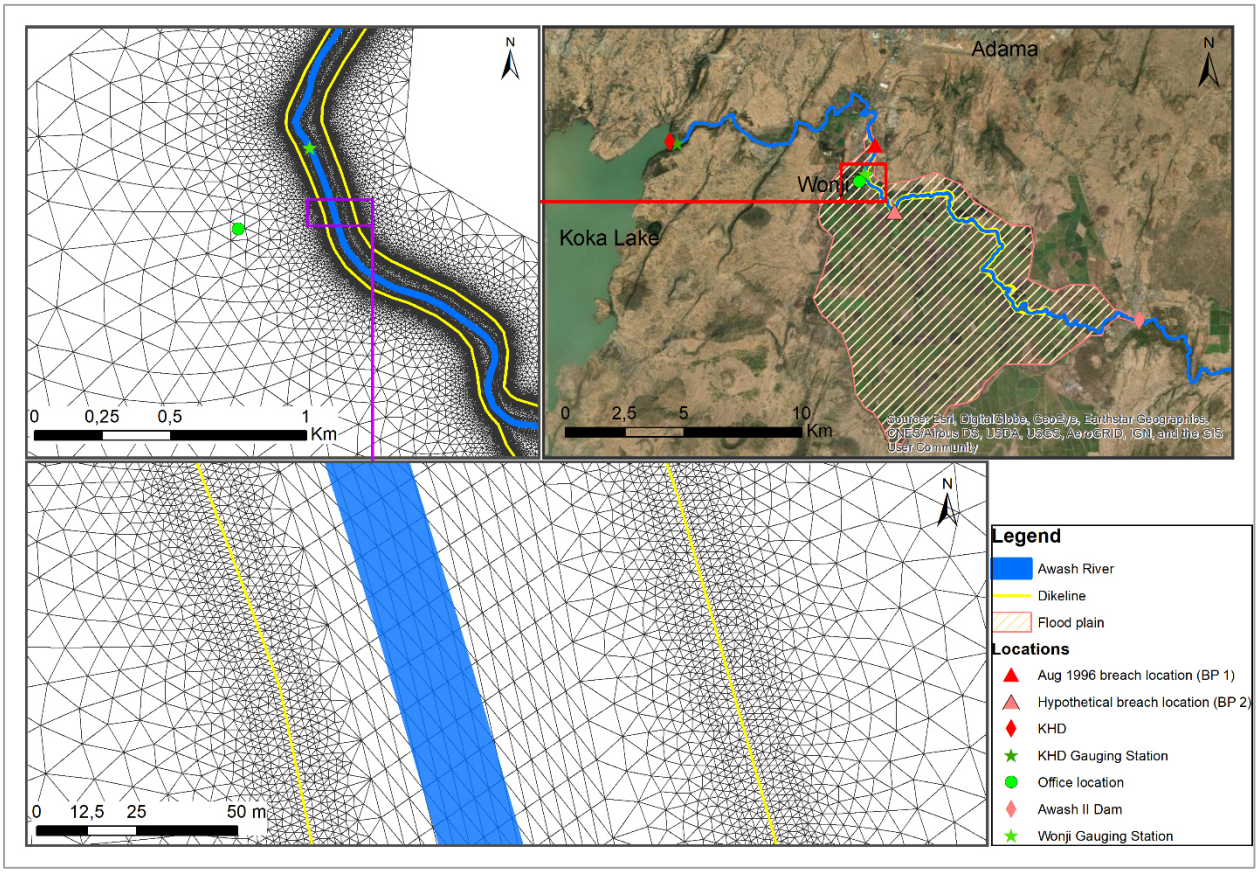

Figure 50: Excerpts of the computational mesh, showing high mesh resolution for levee and discretisation of the river with more than 10 mesh nodes across the cross-section and longer mesh elements in the flow direction (Background map is from ESRI ™ online services).

8.3.3 Boundary conditions

In flood inundation studies, only a selected stretch of the river is included in the numerical model to obtain realistic simulation times. The flow conditions at the discontinuities must be specified as boundary conditions as accurately as possible. As stated in Section 8.3.1 and shown in Figure 49, the model starts at KHD and ends at Awash Dam II. The discharge measurement at the KHD gauging station is used as the upstream boundary condition. Some discharge hydrographs at KHD are shown in Figure 48.

The downstream end of the model is the Awash II Dam. The Awash II Dam is a concrete gravity dam, 16 m high and 88 m long, with a storage capacity of 6×10^6 m³ (International Bank for Reconstruction and Development 1964). The water level at maximum capacity is 1539.04 m a.m.s.l. The flow overflows the dam when the water level exceeds the maximum level. The downstream boundary condition of the model is therefore a stage-discharge relationship. The stage-discharge relationship is derived using an overflow formula for broad-crested weirs given by Equation (37). Experiments show that the discharge coefficient for a broad-crested weir can be very low (Jiang et al. 2020). An average discharge coefficient value of 0.55 is adopted. The upstream total head h_0 is approximated by the upstream water depth over the crest level. The width of the dam is 88 m. Therefore, the stage–discharge relationship at Awash II Dam is established by calculating the values

of stage (depth over crest plus the crest level of the dam) for various Q values and is shown in Figure 51.

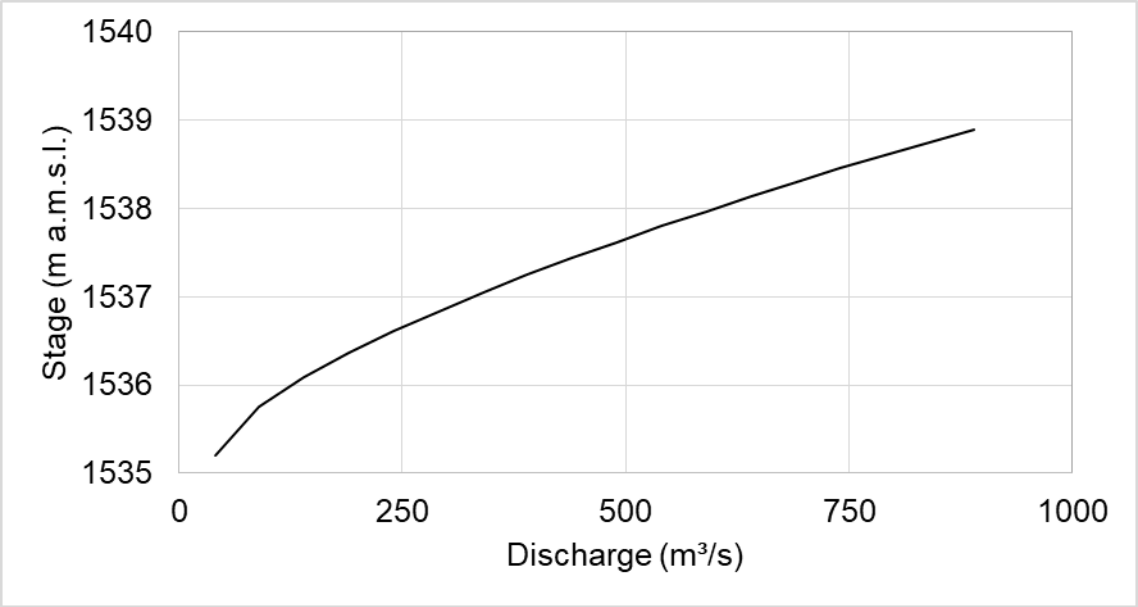

Figure 51: Stage-discharge relationship of the Awash River at the Awash II dam, derived using an overflow equation for a broad-crested weir.

8.3.4 Initial conditions

In addition to boundary conditions, numerical models require initial conditions, which specify the values of the variables (depth and velocity of flow) at the start of the simulation. Whereas boundary conditions specify model conditions at spatial boundaries of the model, initial conditions specify conditions initially in the model domain.

Initial conditions of a 4 m water depth in the river channel, 0 m water depth for the rest of the model domain and a velocity of 0 m/s for the whole domain are used. To eliminate the effect of the initial conditions on the model results, all simulations are run with a sufficient warm-up period of several days, which is much longer than the time required for the water in the model domain to flow out of the domain.

8.3.5 Friction and turbulence losses

Bottom friction is one of the external forces acting against the flow. The bottom resistance force is taken into account in the flow equations by relating it to the flow velocity and the type of bottom roughness. The resistance is high on rough bottoms and low on smooth bottoms. Various friction equations are given in 3.1.1. In Telemac-2D, the friction equations of Chezy, Manning, Cool-Brook and White, and Nikuradse are implemented. In this model, the Nikuradse's friction equation is used.

The model area is divided into six roughness zones according to the different land uses in the model area (see Section 8.2.4 and Figure 47). The corresponding roughness ks-values are taken from hydraulic textbooks (Chow 2009) and are given in Table 29.

Table 29: The values of the Nikuradse's roughness heights (ks-values) corresponding to the land use type in the model area.

Land use	Levee	Plantation	Riverba-nks	Buildings	Bare land	River and pond
Ks-value (m)	0.3	0.4	0.2	0.2	0.25	0.10

Turbulent losses are modelled here using a constant eddy viscosity model. A constant eddy viscosity value of 2.0 m²/s is used for the whole model domain. Such an approach is widely used in the literature and gives acceptable results, especially in river flow modelling (Hervouet 2007).

8.3.6 Numerical parameters

Numerous numerical parameters should be optimised to obtain good model results in a reasonable time for a given problem. The choice of the numerical parameters is made based on the recommendations given in the Telemac-2D user manual or by undertaking sensitivity analysis of the parameter in question. The list of the numerical parameters modified from the default values is given in the steering file in Appendix 2.

8.3.7 Calibration of the numerical model

The model is calibrated using the August 1998 flood event. The model calibration parameters are friction coefficient (ks-values) and eddy viscosity. In the calibration process, several simulations with different ks-values and eddy viscosity coefficients (ν) are performed and the simulation results are compared with measurements as shown in Figure 52. The comparison of the simulated and measured discharges at the Wonji gauging station for different ks-values is shown in Figure 52a. A similar comparison for different eddy viscosity coefficients is shown in Figure 52b. The model reproduces the measured discharge with an average deviation of 8% for this flood event. A ks-value of 0.10 m and an eddy viscosity value of 2.0 m²/s are adopted for further use.

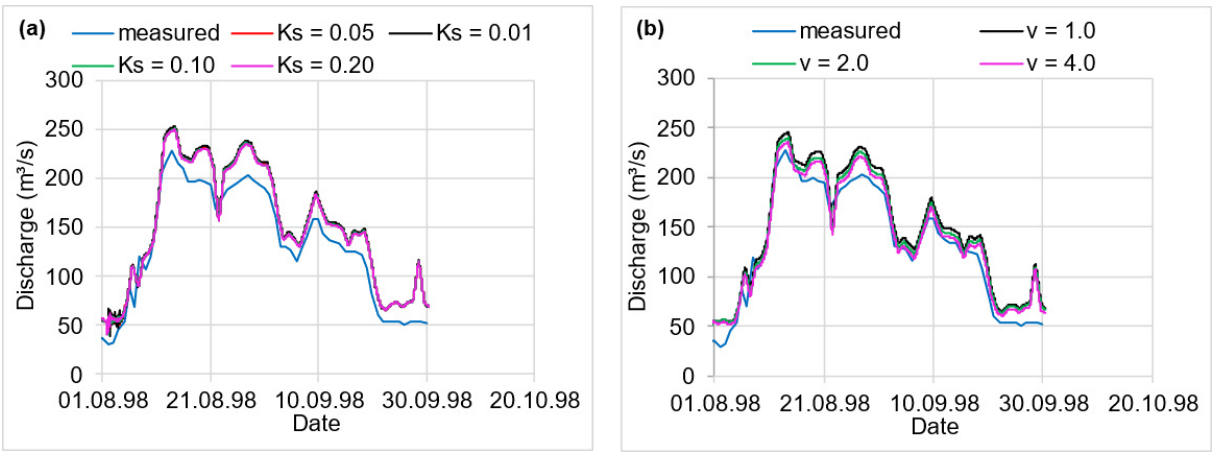

Figure 52: Measured discharge hydrograph for the summer of 1998 at the Wonji gauging station: (a) compared with modelled discharge hydrographs for different Nikuradse's roughness ks-values [m] and (b) compared with modelled discharge hydrographs for different eddy viscosity coefficients (ν) [m²/s].

8.4 Modelling of the Wonji levee breach and the subsequent flooding in August 1996

The model set up in Section 8.3 is used to simulate the Wonji levee breach and the subsequent flooding in August 1996. The physical and numerical model parameters for the river channel are taken from the calibration results and for the floodplain from literature recommendations and based on sensitivity analysis.

The levee breaching is modelled using the parametric breach model presented in Chapter 4. The levee breach parameters are given in Section 8.2.2. The input file for the breach model is given in Appendix 2. The sensitivity of the breach parameters is analysed in Section 9.2.

Figure 53 shows the modelled water depth at the office location (see Figure 54 for the location of the point). The modelled maximum water depth at the office location is 0.87 m. This is in good agreement with the eyewitness information that the water level at the office location reached window beam levels during the flood event. The window beam levels are at 0.90 m above the ground level. In addition, the modelled water depth is increasing on 27 August 1996, in agreement with the report of Ahrens (1996).

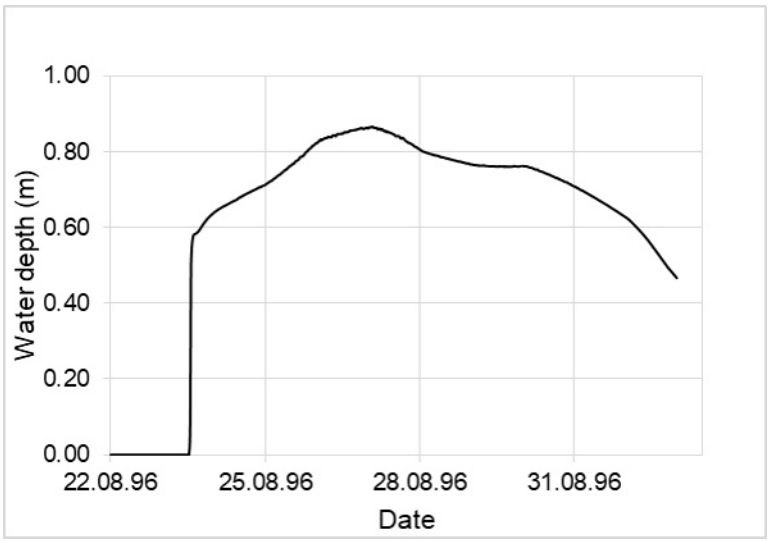

Figure 53: Modelled water depth at the office location corresponding to the breach information.

8.5 Estimation of the breach location

The approach proposed in Chapter 6 is used to determine the location of the August 1996 levee breach at Wonji and compare it with the actual levee breach.

8.5.1 Identification of the leveed river reach and the critical point in the protected area

The location of the Awash River levees at Wonji and the protected area are shown in Figure 45. As can be seen from Figure 45, the flood plains on the right side of the Awash River make up the majority of the floodplains. For this reason, the breach of the levee on the right bank of the river is considered.

The floodplain is mainly covered by sugar cane plantation, except for the upper part of the floodplain on the right side of the river, where the sugar factory, the factory offices and

residential houses are located. The point labelled 'Office location' in Figure 54 is identified as the first critical point of the area. This location is the centre of the critical infrastructure, i.e., the residential housings, offices, and the sugar factory.

A breach anywhere along the levee would cause damage to at least to the sugar cane plantation. For this reason, the entire right bank levee is considered as a critical levee reach and the centre of the plantation is also considered as a second critical point (see Figure 54). In this particular case, a levee breach in an upstream reach is expected to cause the most damage.

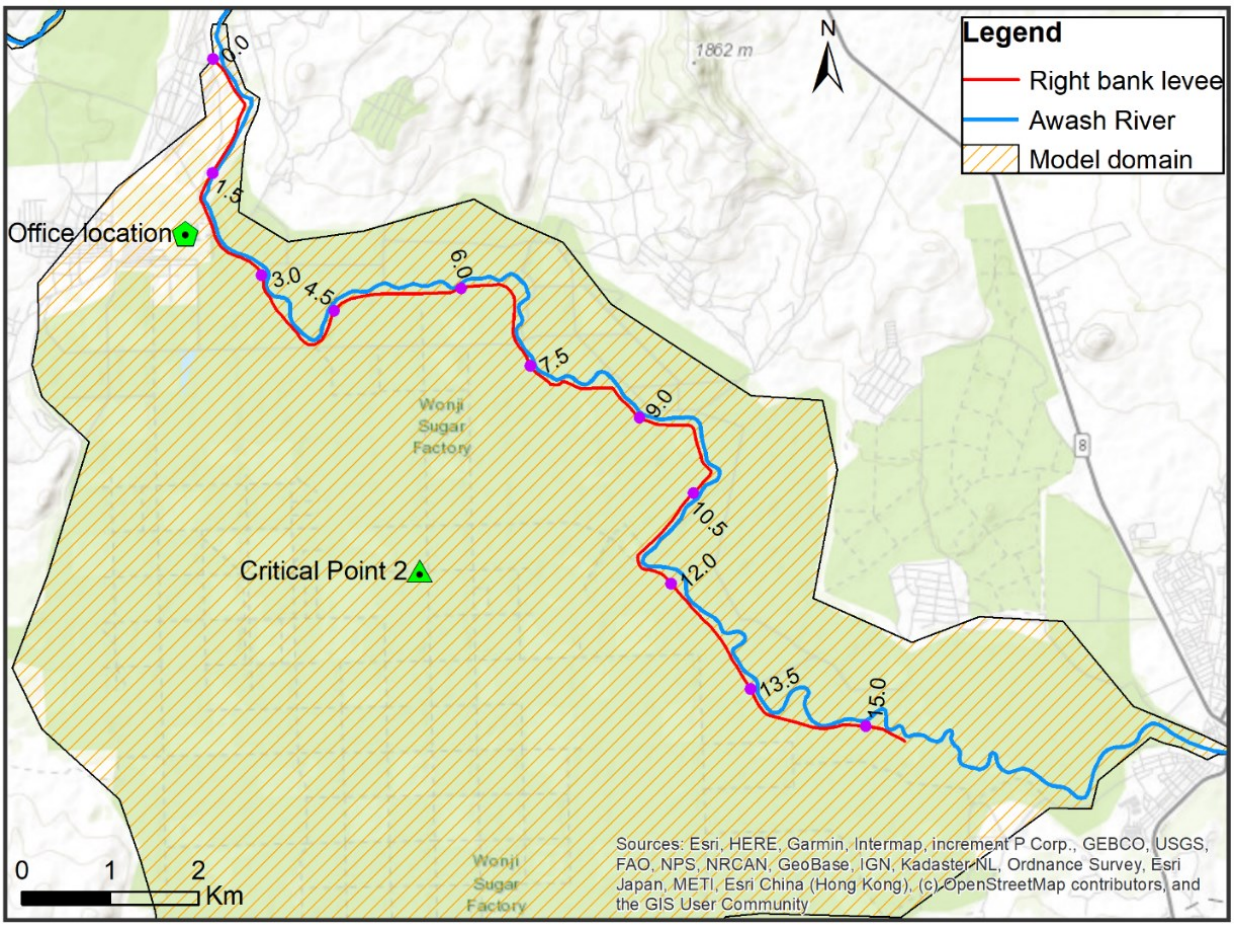

Figure 54: Awash River levee at Wonji: Critical points in the floodplain, critical levee reach with levee kilometers and division of the critical levee reach into representative reaches (Background map is from ESRI ™ online services).

8.5.2 Determination of the water level in the river channel

To estimate the possibility of breaching at a particular levee reach, the water level in the river at that levee reach is required. For this purpose, a 2D hydrodynamic numerical simulation of the Awash River without the flood plains is carried out for the August 1996 flood event. From the simulation results, the flood levels along the longitudinal sections of the river are extracted and compared with the levee crest level as shown in Figure 55. As can be seen in Figure 55, approximately 3 km of the upstream reach of the levee was overtopped by the August 1996 flood event.

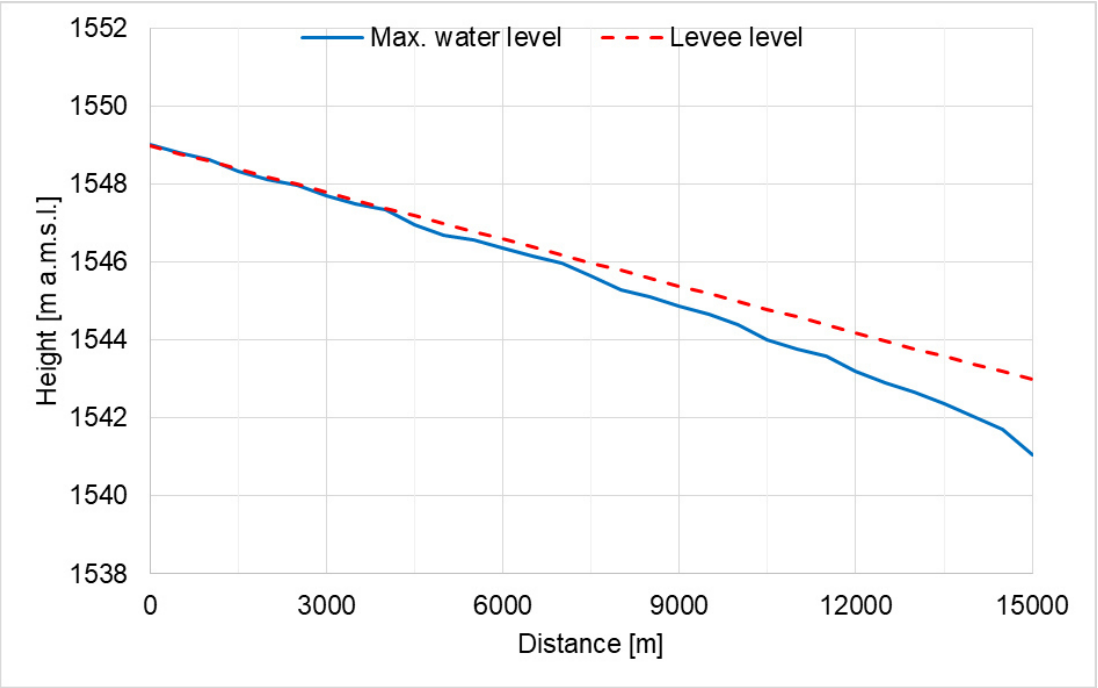

Figure 55: Crest level of the Awash River right bank levee and and the simulated maximum water level along a longitudinal section parallel to the levee corresponding to the August 1996 flood event.

8.5.3 Determining representative levee reaches

As discussed in Section 6.4, the representative levee reaches are identified as follows.

Step 1: The minimum levee reach length is fixed at 1 km. The rationale for this can be referred in Section 6.4.

Step 2: The final representative levee reach length is further adjusted based on the aspects listed in Section 6.4. The Awash River levee is constructed from homogeneous soil material found in the vicinity. The cross-section of the levee is similar throughout its length (see Section 8.2.1). No tributaries join the Awash River along this reach and there are no known defects or damage to the levee. Construction and maintenance conditions are also similar along the entire length. Thus, further adjustment of the representative levee reach is considered based on a change in the longitudinal direction of the Awash River and / or the levee (meandering). Based on these criteria, the levee is divided into a representative levee reach length of 1.5 km as shown in Figure 54.

8.5.4 Testing for a possible breach at each levee reach

The potential for levee breach due to external erosion (overtopping), backward erosion (internal erosion), sustained seepage (internal erosion) and concentrated leak erosion (internal erosion) in each levee reach is analysed below.

8.5.4.1 Levee breach due to external erosion (overtopping)

The upstream part of the levee is overtopped (see Figure 55) and therefore levee breach due to external erosion is possible along this reach. The detailed analysis based on the limit state equation presented in Section 6.5.1 is carried out below.

The first step is to check for each levee reach whether or not the flow in the river is overtopping the levee. For this, the time series of the water level in the river at the centre of each levee reach is extracted and compared with the levee crest level as shown in Figure 56. The maximum water levels at each reach and the corresponding levee crest levels are also given in Table 30. From Figure 56 and Table 30 it can be seen that the water level in the river exceeds the levee crest level only in the uppermost levee reach. Along the other levee reaches, the water level is below the levee crests.

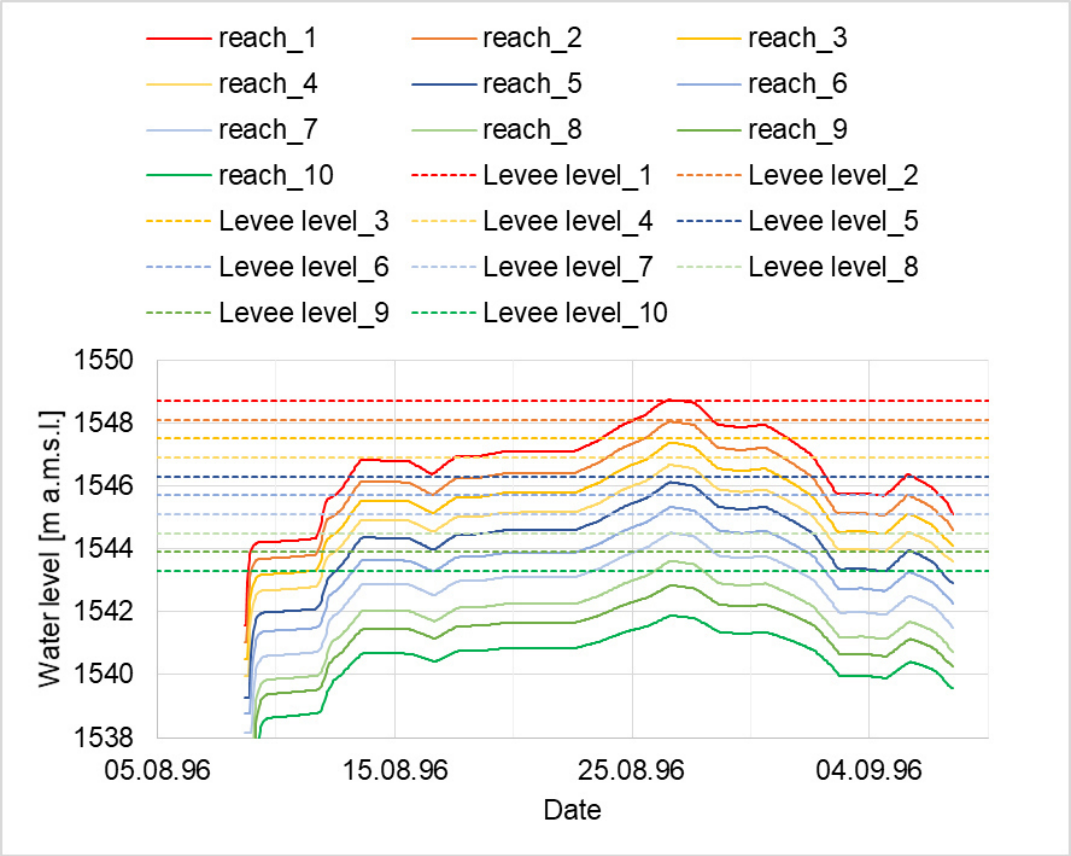

Figure 56: Plot of the simulated water level in the Awash River at a cross section corresponding to the centre of each levee reach (solid lines) and the levee crest level of each levee reach (dashed lines).

To apply the limit state equation, the calculation of the actual and critical overflow discharge is carried out using equations (37) to (39) for the uppermost reach. Poor levee cover is assumed for the calculation of the critical velocity. Data on the levee cover during the August 1996 flood event are not available. The assumption of poor levee cover condition is on the conservative side. For the other levee reaches, only the simulated maximum water level and the levee crest level are given in Table 30, as there is no flow overtopping along these levee reaches. It can be seen from Table 30 that the calculated overtopping discharge for the uppermost levee reach is below the calculated critical discharge. This means that the resistance of the levee to external erosion is greater than the erosion force. And since the levee is not overtopped along the other levee reaches, a levee breach due to external erosion (overtopping) is unlikely to occur at any of these levee reaches.

Table 30: Assessment of the possibility of levee breach due to external erosion (overtopping) for the August 1996 Awash River flood event. CL and WL stand for levee crest level and water level respectively. The other abbreviations are as defined in equations (37) to (39).

From (km)	To (km)	CL	WL	t_e [hr]	q_a	v_c	q_c	Comment
0.0	1.5	1548.70	1548.71	13	0.0030	1.4333	0.0186	Breach unlikely
1.5	3.0	1548.10	1548.04	0	0	-	-	No overtopping
3.0	4.5	1547.49	1547.37	0	0	-	-	No overtopping
4.5	6.0	1546.90	1546.66	0	0	-	-	No overtopping
6.0	7.5	1546.30	1546.11	0	0	-	-	No overtopping
7.5	9.0	1545.70	1545.33	0	0	-	-	No overtopping
9.0	10.5	1545.10	1544.51	0	0	-	-	No overtopping
10.5	12.0	1544.50	1543.62	0	0	-	-	No overtopping
12.0	13.5	1543.90	1542.83	0	0	-	-	No overtopping
13.5	15.0	1543.29	1541.94	0	0	-	-	No overtopping

8.5.4.2 Levee breach due to backward erosion (piping)

As discussed in Section 6.5.2, the possibility of levee breach due to backward erosion can be checked by comparing the prevailing hydraulic gradient with the critical hydraulic gradient that would result in internal levee erosion if the conditions for backward erosion were met. The prevailing hydraulic gradient is determined from the model results and the critical hydraulic gradient is calculated using equation (1). As the soil profile below the levee is not available, it is assumed here that the levee lies over a sand layer of 1 m thickness for the calculation of the critical hydraulic gradient. The other parameters are taken from the literature recommendations (see Appendix 3). The calculation results are shown in Table 31 for each levee reach.

It can be seen from Table 31 that the prevailing hydraulic gradient exceeds the critical hydraulic gradient in the seven upstream levee reaches. Therefore, given the assumptions, i.e., that the conditions for backward erosion are met and that the levee is over a sand layer of more than 1 m thickness, a levee breach due to backward erosion is possible in one of these reaches.

Table 31: Estimation of the possibility of breaching of the Wonji levee due to backward erosion for the August 1996 flood, assuming that the conditions for backward erosion are met and that the levee is above a sand layer of 1 m thickness.

From (km)	To (km)	Head above levee toe, Δh (m)	Hydraulic gradient, I	Critical hydraulic gradient, i_c	Comment
0.0	**1.5**	3.02	0.2011	0.1685	breach possible
1.5	**3.0**	2.95	0.1962	0.1685	breach possible
3.0	**4.5**	2.88	0.1921	0.1685	breach possible
4.5	**6.0**	2.76	0.1838	0.1685	breach possible
6.0	**7.5**	2.81	0.1875	0.1685	breach possible
7.5	**9.0**	2.63	0.1752	0.1685	breach possible
9.0	**10.5**	2.41	0.1605	0.1685	breach unlikely
10.5	**12.0**	2.13	0.1418	0.1685	breach unlikely
12.0	**13.5**	1.94	0.1290	0.1685	breach unlikely
13.5	**15.0**	1.64	0.1098	0.1685	breach unlikely

8.5.4.3 Levee breach due to sustained seepage

As discussed in Section 6.5.3, levee breach due to sustained seepage can be assessed by comparing the duration of the flood level above a specified critical level with the duration required for the water to seep through the levee to the landside toe.

The water level time series at each levee reach for the 1996 Wonji flood event are shown in Figure 56. From these, the exceedance durations for different depths above the levee toe are calculated. The corresponding seepage durations for the different depths above the levee toe level are calculated using equation (3). A sandy loam levee soil type, which is the soil type in the area, is considered for the calculation of the seepage durations. Since the cross section and soil type of the levee are similar for the whole levee, the seepage duration is similar for all the levee reaches.

The plots of the exceedance and seepage durations against the depth above the levee toe are shown in Figure 57. It can be seen from Figure 57 that for levee reaches 1 to 7 the exceedance duration is greater than the theoretical seepage duration required for a potential levee breach, at least for some depths above the toe. For levee reaches 8 to 10, the exceedance duration is less than the theoretical seepage duration required for a potential levee breach.

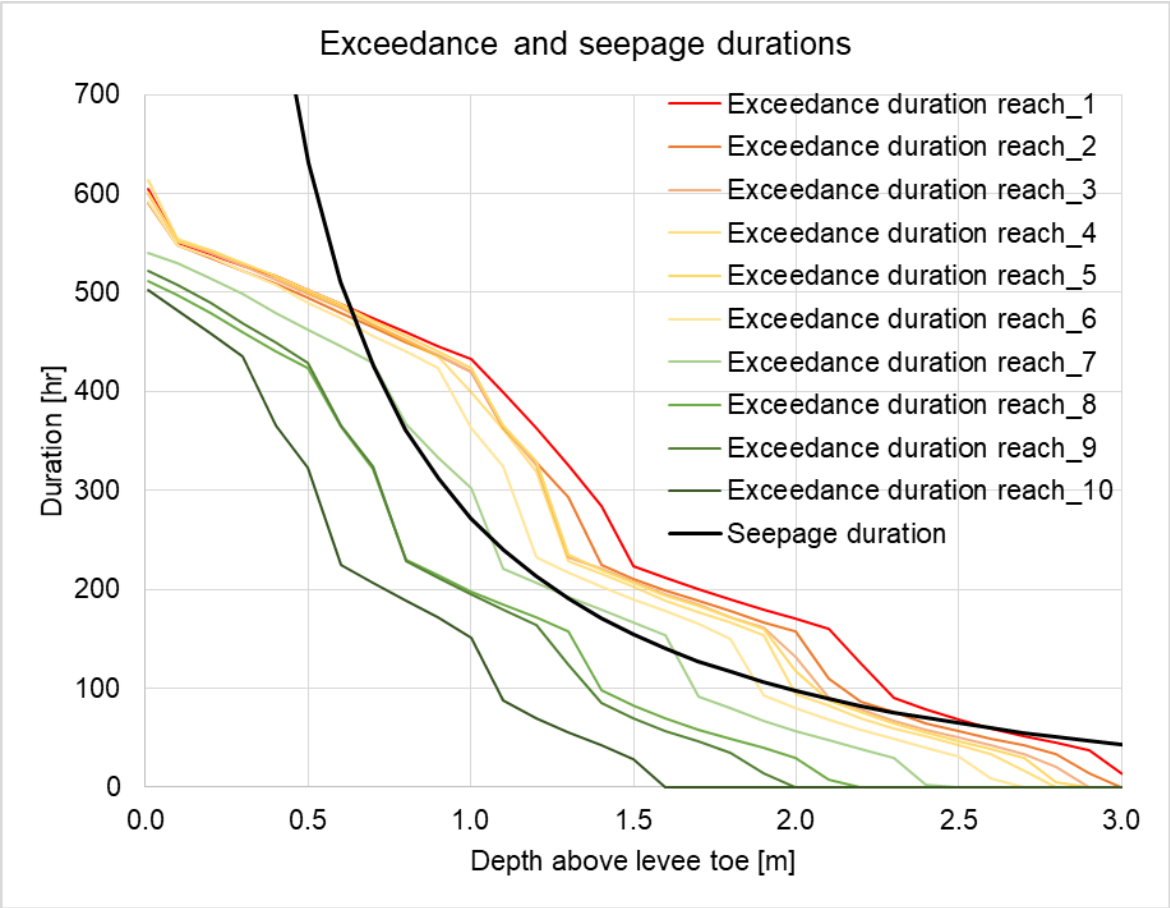

Figure 57: Exceedance durations of the simulated water level in the river above the levee toe (Exceedance duration) for the different levee reaches and the theoretical seepage duration (Seepage duration) required for the water to seep through the levee to the landside toe, as calculated by equation (3) for hydraulic conductivity of 3.45E^{-5} m/s (sandy loam soil).

For each levee reach, the maximum difference between the exceedance duration and the seepage duration is extracted and summarised in Table 32. The maximum differences correspond to a depth above the levee toe of 1.0 m for all reaches except for reach 6 where the maximum difference corresponds to a depth above the levee toe of 0.9 m.

The highest maximum difference between exceedance and seepage durations corresponds to levee reach 1. It is followed by reach 5, reach 3, reach 2, reach 4, reach 6 and reach 7 in decreasing order of the maximum difference. The higher the difference, the higher the possibility of levee breach. Thus, reach 1 is the likely breach reach due to sustained seepage for this flood event.

Table 32: Depth above toe (h_w), seepage duration (t_s) and exceedance duration (t_{exc}) corresponding to the maximum difference between exceedance and seepage durations for each levee reach.

Reach	From (km)	To (km)	h_w (m)	t_{exc} (h)	t_s (h)	t_{exc} - t_s (h)	Comment
Reach_1	0.0	1.5	1.00	433	272	161	breach possible
Reach_2	1.5	3.0	1.00	420	273	147	breach possible
Reach_3	3.0	4.5	1.00	420	272	148	breach possible
Reach_4	4.5	6.0	1.00	399	272	127	breach possible
Reach_5	6.0	7.5	1.00	423	272	151	breach possible
Reach_6	7.5	9.0	0.90	423	312	111	breach possible
Reach_7	9.0	10.5	1.00	302	272	30	breach possible
Reach_8	10.5	12.0	1,30	158	191	-	breach unlikely
Reach_9	12.0	13.5	1,20	164	214	-	breach unlikely
Reach_10	13.5	15.0	1,00	151	270	-	breach unlikely

8.5.4.4 Levee breach due to concentrated leak erosion

The possibility of levee breach due to concentrated leak erosion can be determined using the method described in Section 6.5.4. A prerequisite for concentrated leak erosion is the presence of a continuous opening in the levee body or foundation connecting the water side to the land side that lies below the water level in the river. If this prerequisite is met, the possibility of levee breach due to concentrated leak erosion can be estimated by comparing the duration of water level above the opening and the duration required by a concentrated leak erosion to cause breach, as given by equation (4).

The water level time series at each levee reach for the 1996 Wonji flood event are shown in Figure 56. These can be used to calculate the exceedance duration for different depths above an opening location in the levee. The exceedance duration will be highest if the location of the opening is at the lowest level possible, i.e., at the levee toe. In this case, the exceedance durations are a function of depth as shown in Figure 57.

The erodibility coefficient (Ce) of the soil is an important factor for the erosion rate in concentrated leak erosion. For the levee at Wonji, which are made up of sandy loam soils, Ce is approximated to be 5.0×10^{-4} from the values given by Fell et al. (2013, p. 359). For the 1996 Wonji flood event, using the standard assumption in the literature that complete breaching occurs when the pipe diameter reaches 2/3 of the levee height (Bonelli 2013), the duration to breach due to concentrated leak erosion as a function of water depth above the levee toe is determined using equation (4) and is shown in Figure 58.

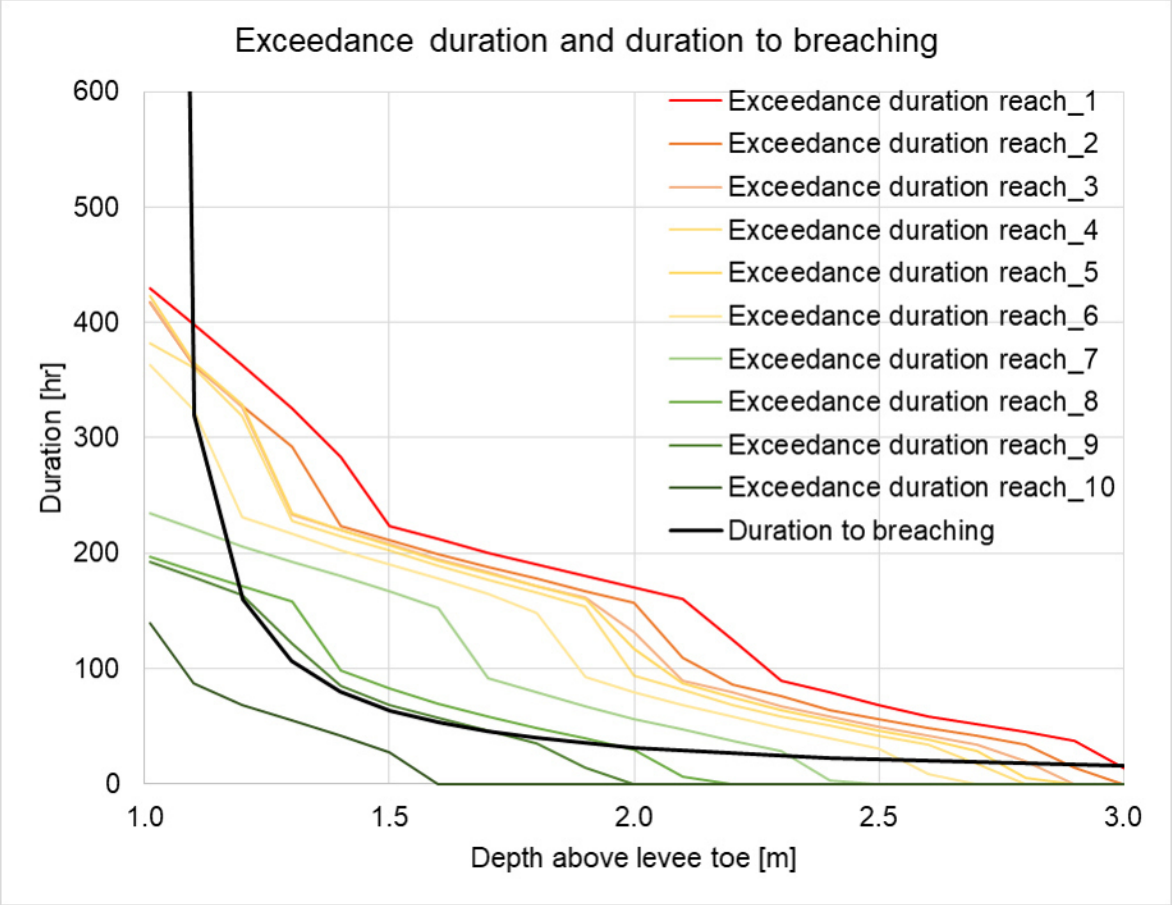

Figure 58: Exceedance durations of the simulated water levels in the river above the levee toe (Exceedance duration) for the different levee reaches and the theoretical duration until breaching due to concentrated leak erosion (duration to breaching), calculated from equation (4) for C_e = 5.0x10^{-4} s/m, opening radius at breaching R = H_{levee}/3 = 1.0 m, and opening radius at erosion initiation R_d = 0.02 m.

It is important to note that the duration until breaching from the onset of concentrated leak erosion, calculated by equation (4) , is strongly dependent on the soil erodibility coefficient Ce and the opening radius at breaching R. Therefore, the duration to breaching in Figure 58 is only valid for the specified values of Ce and R. For these adopted values, it can be seen from Figure 58 that for levee reaches 1 to 9, the exceedance duration is longer than the duration to breaching required by concentrated leak erosion to cause a levee breach during the August 1996 Wonji flood event.

For each levee reach, the maximum difference between the exceedance duration and the duration to breaching is calculated and summarised in Table 33. The maximum differences correspond to the depths above the levee toe of between 1.2 m and 1.5 m. The highest maximum difference is calculated for levee reach 1, followed by levee reaches 2, 5, 3, 4, 7, 8 and 9 in decreasing order of the maximum difference. Again, the higher the difference, the higher the possibility of levee breach. Thus, reach 1 is the likely breach reach for this flood event if the conditions for concentrated leak erosion are met.

Table 33: Depth above toe (h_w), the duration to breaching (t_b) from onset of concentrated leak erosion and the exceedance duration (t_{exc}) corresponding to the maximum difference between exceedance duration and duration to breaching for each levee reach.

Reach	From (km)	To (km)	h_w (m)	t_{exc} (h)	t_d (h)	t_{exc} - t_d (h)	Comment
Reach_1	0.0	1.5	1,30	325	106	219	breach possible
Reach_2	1.5	3.0	1,30	292	106	186	breach possible
Reach_3	3.0	4.5	1,20	326	159	167	breach possible
Reach_4	4.5	6.0	1,20	319	159	160	breach possible
Reach_5	6.0	7.5	1,20	329	160	169	breach possible
Reach_6	7.5	9.0	1,50	190	64	126	breach possible
Reach_7	9.0	10.5	1,50	167	64	103	breach possible
Reach_8	10.5	12.0	1,30	158	106	52	breach possible
Reach_9	12.0	13.5	1,30	122	106	16	breach possible
Reach_10	13.5	15.0	1,50	28	64	-	breach unlikely

8.5.5 Discussion: estimation of levee breach location

In sections 8.5.1 to 8.5.4, the approach for determining levee breach location, developed and discussed in Chapter 6, is applied to the August 1996 Awash River flood event at Wonji. The analysis shows that the possibility of levee breach for this event is high. The flood event would have resulted in a breach at the upstream levee reach due to overtopping. Seepage (backward erosion, sustained seepage, or concentrated leak erosion) would have caused levee breaching at almost all levee reaches except for the downstream levee stretch. It should be noted that the analysis is partly based on assumptions due to data limitations. These assumptions are indicated in the individual sections above.

Nevertheless, the analysis estimated the upstream levee reach as the most likely breach location for the August 1996 flood event, which corresponds to the actual levee breach location of the flood event. This confirms the applicability of the developed approach for estimation of breach location.

8.6 Summary

In this chapter, the proposed approach of integrated flood inundation modelling due to levee breach is applied to a real levee breach event at Wonji, Ethiopia. The data required for the modelling are discussed and prepared for use in the hydrodynamic numerical model of the area. A 2D hydrodynamic numerical model based on Telemac-2D is built, calibrated, and validated for a part of the Awash River reach and the adjacent floodplains at Wonji. The validated 2D hydrodynamic model is used to model the flood inundation of the August 1996

levee breach at Wonji. The model results are in good agreement with the information documented during and after the disaster. Furthermore, the applicability of the approach proposed in Chapter 6 for determining levee breach location is demonstrated in this chapter using the Wonji flood of August 1996.

9 Uncertainty mapping and sensitivity analysis of breach parameters

This chapter discusses the uncertainties associated with modelling flood inundation due to levee breach. First, the sources of the uncertainty in the approach are mapped and the methods available in the literature for estimating the uncertainties are discussed. A sensitivity analysis of the levee breach parameters is then carried out to show how uncertainty can affect the model results.

9.1 Uncertainty mapping

The integrated approach to modelling of flood inundation due to levee breach uses a 2D hydrodynamic numerical model and a parametric levee breach model, which rely on input data and parameters. Each of these has an associated uncertainty. The uncertainties can be mapped to individual sources of uncertainty as shown in Figure 59.

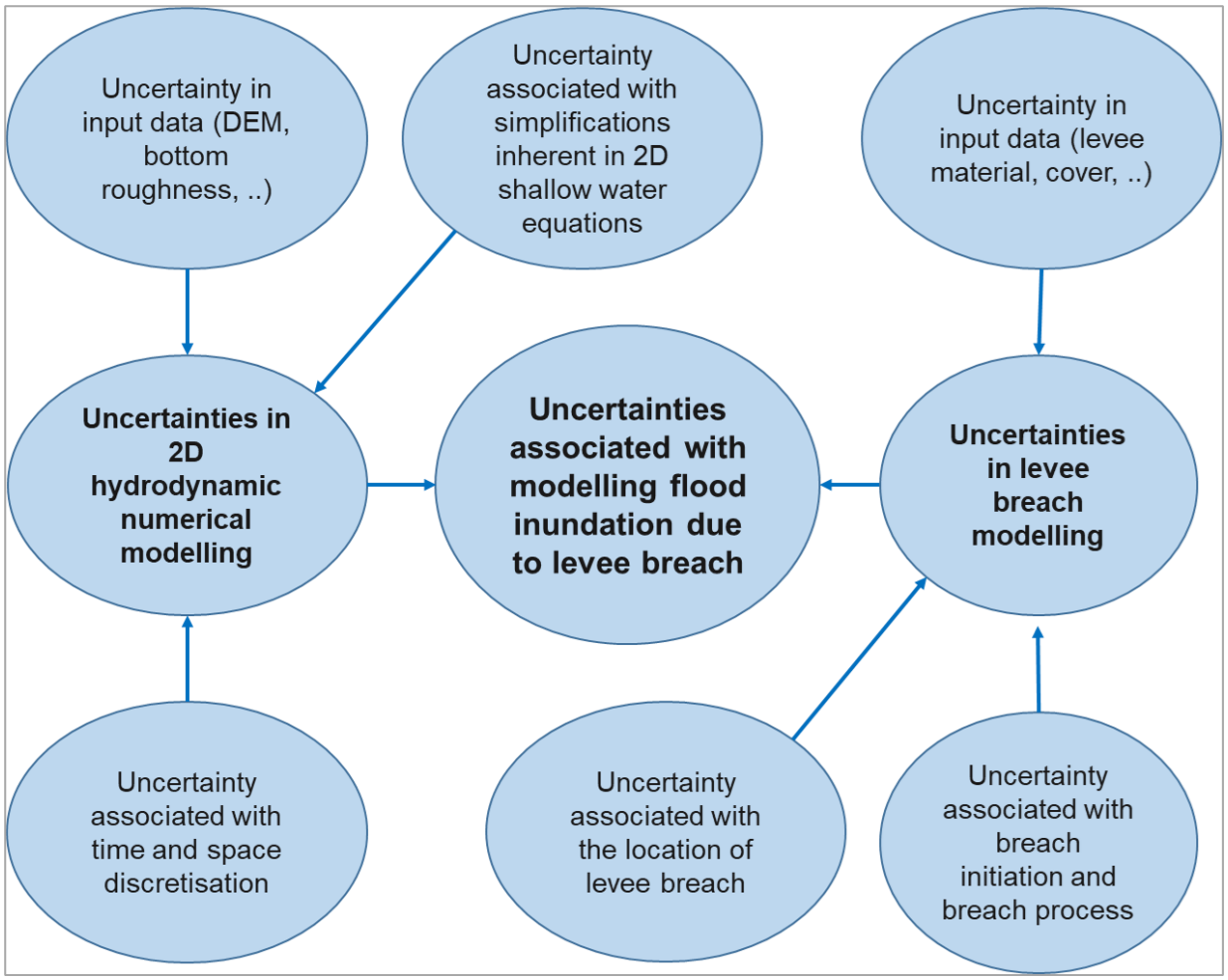

Figure 59: Mapping of uncertainties associated with modelling of flood inundation due to levee breach.

9.1.1 Uncertainties in 2D hydrodynamic numerical modelling

As discussed in Chapter 3, 2D hydrodynamic numerical models, such as Telemac-2D, solve the shallow water equations numerically. The shallow water equations are derived from the simplification of the NS equations, which in turn are derived from the conservation of mass and momentum. In the process of simplifying the NS equations to the shallow water equations, parameterisations and assumptions are introduced. These introduce uncertainty in the model results. Although the data requirements and number of parameters are modest, the underlying physical equations are non-linear. Furthermore, the input data may have spatially and temporally varying errors (Bates et al. 2014).

Thus, it is imperative to look at the uncertainties in the model outputs. The uncertainty in the model outputs of 2D hydrodynamic numerical models can be attributed to (see Altarejos-García et al. (2012), Bates et al. (2014), Thompson et al. (2008) and Willis et al. (2019)):

- The error associated with the approximation of the physical process by a simplified mathematical equation,
- The uncertainty associated with the error in the numerical resolution of the mathematical model (numerical approximation in space and time discretisation of the physical equations, the accuracy chosen for the numerical solvers (convergence tolerance and truncation error), and
- The uncertainty in the input data (DEM, initial and boundary conditions, hydraulic structures, calibration / validation data, model parameters (roughness, turbulence), etc.).

Neither the NS equations nor the shallow water equations for environmental flows have analytical solutions. As a result, it is generally difficult to quantify the error, and therefore the uncertainty, due to the simplification of the NS equations to the shallow water equations. For the same reason, the error in the numerical resolution of the shallow water equations cannot be determined. Thus, the uncertainty of 2D hydrodynamic model results due to the simplification of the physical equations and numerical resolution can only be analysed by comparing model results with measured data.

The hydrodynamic numerical model used in this work, Telemac-2D, has been validated for a wide range of flow regimes, as can be seen from the validation documentation of the software (TELEMAC 2019b). The validation documentation shows that Telemac-2D can be used for a wide range of flow conditions. This indicates that the uncertainty associated with the model itself should be low.

Model results are also subject to uncertainty in the input data and model parameterisation. The input data for a 2D hydrodynamic numerical model are mainly initial and boundary conditions, DEM including river channel bathymetry, hydraulic structures, roughness coefficients, turbulence model coefficients and data for model calibration and validation.

As discussed in Section 8.3.4, 2D hydrodynamic models require at least the values of the water depth and the velocity at each computational node at the start of the simulation. The values of these variables at each computational node are generally unknown at the start of

the simulation. Thus, in practice, the initial conditions are estimated based on existing point data in the model domain (gauging stations) or a rainfall-runoff model. To minimise the discrepancy, the start of the simulation is often chosen to be well before a flood event (spin-up period) and in a near steady-state situation. The uncertainty of the data used to estimate the initial conditions should be taken into account.

2D hydrodynamic numerical models require the conditions at the model boundaries, i.e., boundary conditions. The boundary conditions, often discharges at the upstream boundaries and water levels or depths at the downstream boundaries, are often taken from gauging stations. Discharges are often estimated using rating curves from water level measurements. This can introduce not only measurement error but also possible error in the calculation of the discharge from the rating curve. These are generally low, but can be high in some cases. Errors of up to 50% in discharge calculations using rating curves are reported by Bates et al. (2014).

The accuracy of the DEM can significantly affect the uncertainty of 2D hydrodynamic numerical model results. DEM data are obtained by field measurements, laser scanning (LiDAR) and radar interferometry mounted on satellites, probably in increasing order of uncertainty in the DEM. The increased availability of airborne DEM data, especially in the developed countries, has significantly improved the uncertainty of 2D hydrodynamic numerical model results due to DEM and landuse uncertainty (Bates et al. 2014).

There are often many hydraulic structures in and around many rivers. These include weirs, gates, bridges and locks. The representation of hydraulic structures strongly influences the results of 2D hydrodynamic numerical models (see Bates et al. 2014, Pappenberger et al. 2006). The analysis of Pappenberger et al. (2006) shows that model outputs are sensitive to how hydraulic structures (in their case bridges) are represented in the model, indicating a high uncertainty in the results of 2D hydrodynamic numerical models associated with the representation of hydraulic structures.

The common parameters in 2D hydrodynamic models are the bottom friction coefficient and the turbulence viscosity. The bottom friction coefficient accounts for the effects of skin friction losses, form drag, losses and losses due to flow acceleration and deceleration. Commonly used bottom friction coefficients are derived from uniform flow formulas and include Nikuradse’s ks-value, Manning’s n or Chezy’s C. The friction coefficient and eddy viscosity are used for model calibration and validation. Thus, the values often compensate for energy losses due to unaccounted processes and the grid resolution. This indicates that an analysis of the uncertainty of 2D hydrodynamic numerical model results due to friction coefficient and eddy viscosity is necessary if the model is intended to be used for predictive purposes.

In addition, the data used for calibration, validation and uncertainty analysis have their own uncertainty. Calibration and validation of a model use data from gauging stations (often water level), from field measurements (water level, velocity or discharge measurements) or from remote sensing (often flood extent and depth). The errors in such data also contribute to the uncertainty in the results of 2D hydrodynamic numerical models.

Several authors have attempted to analyse the uncertainty of 2D hydrodynamic model results associated with model input data or parameters using different methods, which can be divided into analytical and approximate approaches (Thompson et al. 2008; Bessar et al. 2020). Due to the non-linear nature of the shallow water equations, approximate methods are mainly used for uncertainty analysis of 2D hydrodynamic models (Bessar et al. 2020). Commonly used uncertainty analysis methods for 2D hydrodynamic models include Monte Carlo (Thompson et al. 2008; Kalyanapu et al. 2012) and quasi-Monte Carlo methods (Goeury et al. 2015), point estimate method (PEM) (Altarejos-García et al. 2012; Oubennaceur et al. 2018), first order second moment (FOSM) method (Thompson et al. 2008), among others.

Thompson et al. (2008) used a fist order second moment (FOSM) and Monte Carlo analysis to estimate the uncertainty of water levels and velocities simulated by a 2D hydrodynamic numerical model of the Upper St. Lawrence River, Canada. They found out that the bottom friction coefficient (Manning's n) contributed more to the model uncertainty than other parameters they considered. They found out that FOSM provided a conservative estimate of the uncertainty for the application case compared to Monte Carlo analysis. They reported that FOSM was easy to use and required less information and fewer model runs. They also reported that FOSM provided an immediate indication of the main contributors to the uncertainty and that additional effort is required to obtain the same information in the case of Monte Carlo analysis.

Goeury et al. (2015) used Monte Carlo and quasi-Monte Carlo approaches to analyse the uncertainty in the modelled water depth associated with the friction coefficient and upstream discharge boundary condition. In the quasi-Monte Carlo approach, the approximate sampling technique of the uncertain parameter is constrained as compared to the pure Monte Carlo approach, where the sampling of the uncertain variable is random. They reported that the quasi-Monte Carlo approach converged much faster than the pure Monte Carlo method.

Oubennaceur et al. (2018) used PEM to assess the uncertainty of water depths in the Richelieu River (Canada), simulated with a 2D hydrodynamic numerical model. In its application to uncertainty analysis in 2D hydrodynamic numerical modelling, PEM evaluates the statistical moments (mean and standard deviation) of the model results with respect to the variation of the model inputs (Altarejos-García et al. 2012; Oubennaceur et al. 2018). Oubennaceur et al. (2018) analysed the uncertainties associated with the inflow rate at the upstream boundary, Manning's coefficient and DEM. They found that the standard deviation of the simulated water depth varied spatially and was up to 27 cm.

9.1.2 Uncertainities in levee breach modelling

As discussed in Chapter 2, levee breach models generally rely on parameters and input data depending on the type of breach model. A parametric levee breach model is used in this thesis, where the breach location, the breach initiation and the breaching process are defined by parameters. The parameters are loosely related to a physical process and therefore difficult to estimate deterministically for a specific case. This issue is discussed

in the works of Wahl (2004) and Bellos et al. (2020) for embankment dam breach parameters, and Bertrand et al. (2018) and Ranzi et al. (2012) for levee breach parameters.

There are three main sources of uncertainty in levee breach models (CIRIA 2013). These are:

- Uncertainty in breach initiation and breach process
- Uncertainty in input data used to estimate breach parameters
- Uncertainty in breach location

As already discussed in Chapter 2, there is no general mathematical model for determining the location of a breach, the initiation of a breach and the breaching process. It is thus crucial to analyse the impact of these uncertainties on the results of flood inundation modelling. In the following section, the sensitivity of the flood inundation depth and the breach discharge to the variation of the levee breach parameters is analysed.

9.2 Sensitivity analysis of the parametric breach model[4]

As described in Section 4.2, a parametric levee breach model is used in this thesis, which uses parameters to describe the levee breaching processes. For real levee breaches, the values of the parameters are associated with a high degree of uncertainty, as they depend on factors that are often not well known, such as the characteristics of the levee material, the flow in the river, the maintenance situation of the levee, the quality of construction, etc. It is therefore necessary to analyse the sensitivity of the model to these factors. This helps to identify the important parameters. In the following sections, the sensitivity of the modelled water depth in the hinterland (at office locations, see Figure 63 for the location) and the discharge through the breach (breach discharge) to each of the main breach parameters is analysed.

The August 1996 Awash River levee breach case at Wonji is used for the analysis. To analyse the sensitivity in the case of a flash flood event, a hypothetical flash flood (modified from the August 1996 flow of the Awash River) is used. The inflow hydrograph of the hypothetical flash flood is given in Figure 60.

[4] The manuscript of Section 9.2 is taken from the author's publication (Tadesse & Fröhle 2020) and only editorial changes for readability are made here.

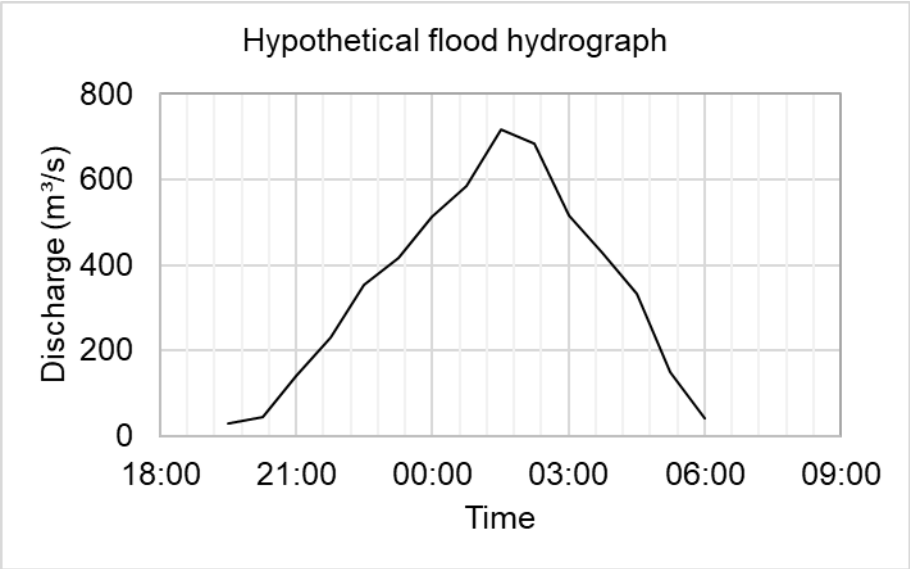

Figure 60: Hypothetical flash flood hydrograph (modified from the August 1996 flow of the Awash River) used as the inflow hydrograph for the sensitivity analysis of flood inundation due to levee breach to breach parameters during flash floods.

9.2.1 Breach duration

The sensitivity of the modelled flood depth in the floodplains and the modelled breach discharge to the breach duration is investigated by varying the breach duration within an acceptable range of the historical breach duration of 1 h. Numerical simulations were performed for breach durations of 30 min, 1 h and 2 h. The modelled flood depth in the floodplains and the breach discharge obtained for the respective breach durations (BD) are compared in Figure 61. The results show that the modelled flood inundation and breach discharge are insensitive to the breach duration. The results show oscillations, e.g., the breach discharge. This is caused by the fluctuating velocities through the breach. The flow in the breach is close to a critical condition, which causes slight variations in the solution of the velocities by the numerical model.

A similar comparison is made for the hypothetical flash flood and is shown in Figure 62. As can be observed from Figure 62, in the case of the flash flood, the modelled inundation depth and breach discharge are sensitive to the breach duration.

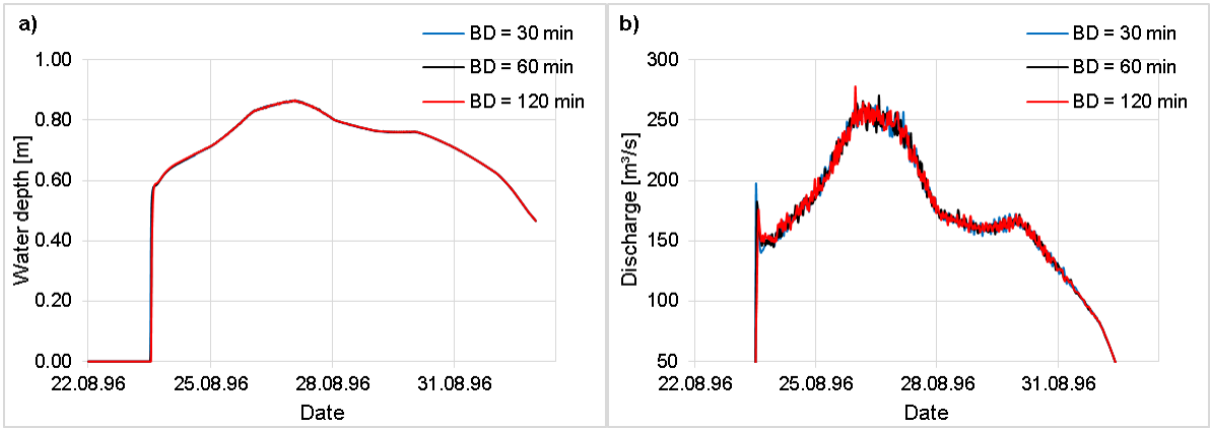

Figure 61: For the indicated levee breach durations (BD) and the historical levee breach location of the August 1996 Wonji levee breach flood event: a) modelled flood depth in the floodplains

at an office location and b) modelled breach discharge. The office location and the historical breach location are shown in Figure 63.

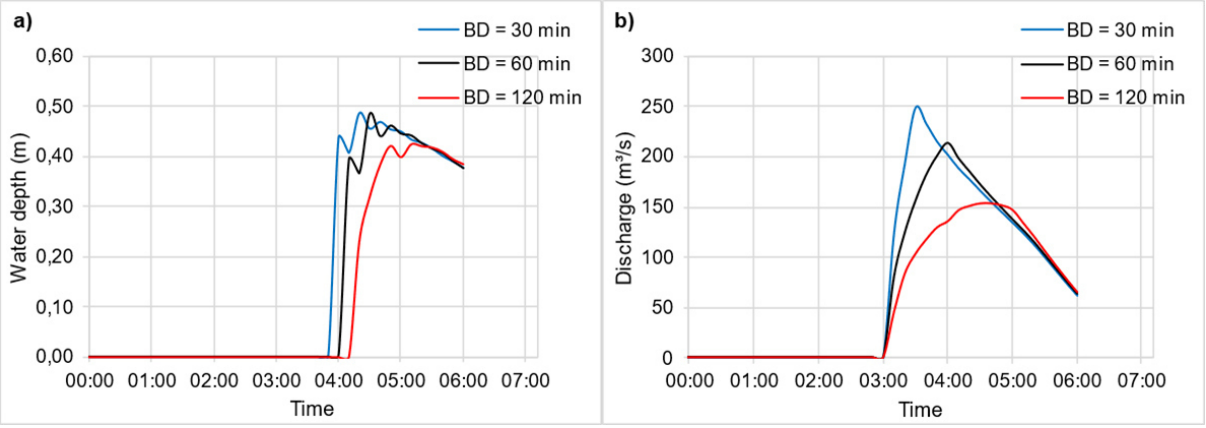

Figure 62: For a hypothetical flash flood, the indicated levee breach durations (BD) and the historical levee breach location of the August 1996 Wonji levee breach flood event: a) modelled flood depth in the floodplains at an office location and b) modelled breach discharge. The office location and the historical breach location are shown in Figure 63.

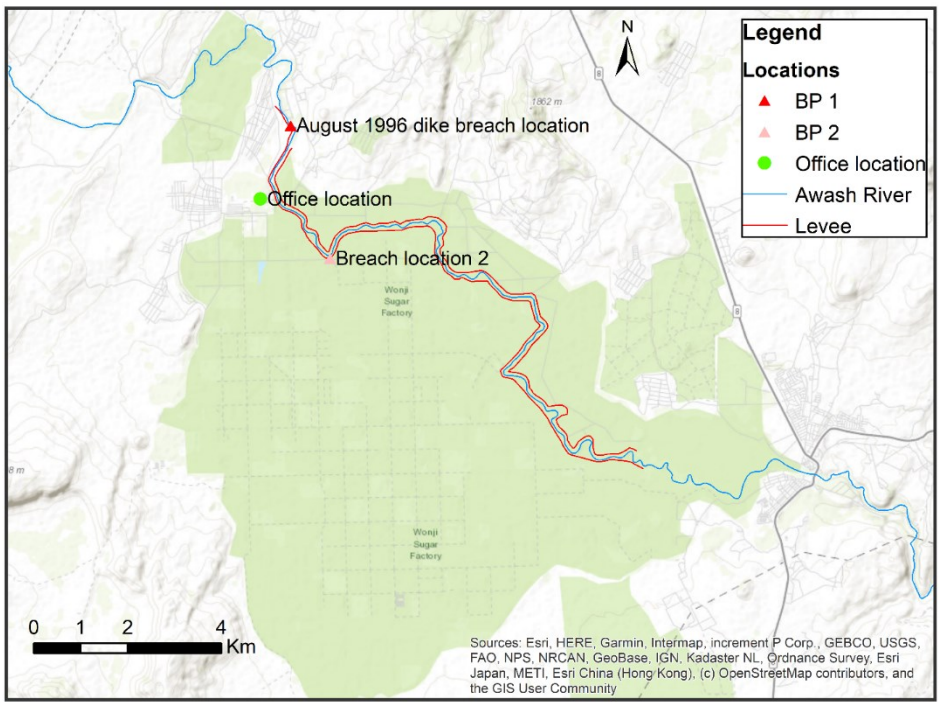

Figure 63: Map showing the location of a point in the floodplain (office location), the breach location of the August 1996 Wonji levee breach (BP 1), a hypothetical breach location (BP 2), the Awash River at Wonji and its levees. The direction of flow of the Awash River shown on the map is from northwest to southeast (background map courtesy of ESRI®, ArcGIS online service).

9.2.2 Breach start time (breach initiation)

The breach initiation options of the levee breach model are discussed in Section 4.2.1. For the sensitivity analysis, breach initiation by specifying the breach start time is used. This is to have control over the breach start time and to ensure that the breach start time is varied.

To determine the sensitivity of the modelled flood depth in the floodplains and the modelled breach discharge to the breach start time, 2D hydrodynamic numerical simulations are

performed for three breach start times (BT) at 12:00 a.m., 03:00 a.m. and 06:00 a.m. on 24 August 1996. The flood depth in the flooplain and the breach discharge obtained from the model runs for the respective breach start times are compared in Figure 64. As can be observed from Figure 64, the breach start time only affects the onset of flooding. The peak inundation depth and breach discharge are insensitive to the breach start time.

A similar comparison is made for the hypothetical flash flood and is shown in Figure 67. As can be observed from Figure 65, in the case of the flash flood, the modelled inundation depth and breach discharge are sensitive to the start time of the breach.

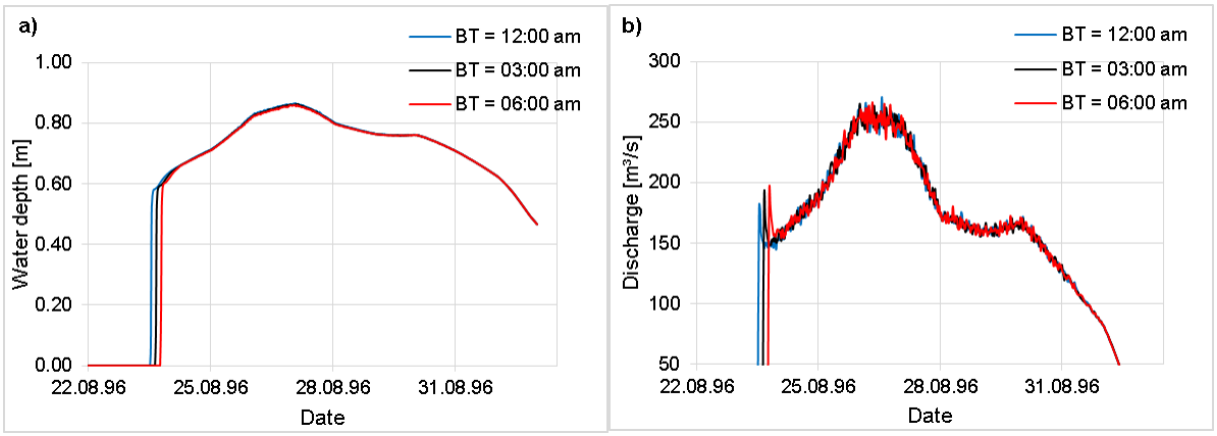

Figure 64: For the indicated levee breach start times (BT) on 24 August 1996 and the historical levee breach location of the August 1996 Wonji levee breach flood event: a) modelled flood depth in the floodplains at an office location and b) modelled breach discharge. The office location and the historical breach location are shown in Figure 63.

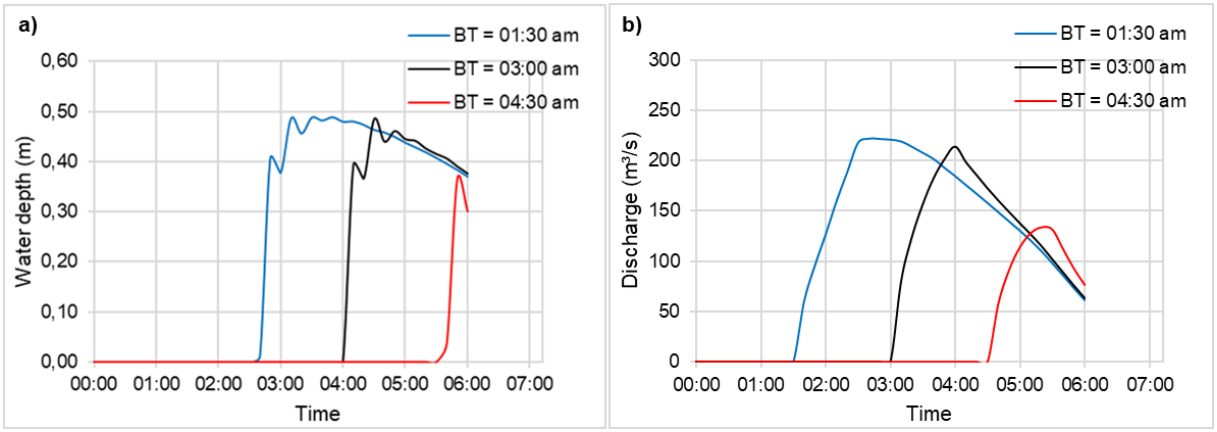

Figure 65: For a hypothetical flash flood, the indicated levee breach start times (BT) and the historical levee breach location of the August 1996 Wonji levee breach flood event: a) modelled flood depth in the floodplains at an office location and b) modelled breach discharge. The office location and the historical breach location are shown in Figure 63.

9.2.3 Final breach width

The sensitivity of the modelled water depth in the hinterland and the modelled breach discharge to the final breach width is analysed by running hydrodynamic numerical model simulations for final breach widths (BW) of 50 m, 100 m and 150 m. The modelled flood depth in the floodplains and the breach discharge obtained from the model runs for the respective final breach widths are compared in Figure 66. As can be observed from Figure

66, the modelled water depth at the office locations and the modelled breach discharge increase with increasing final breach width.

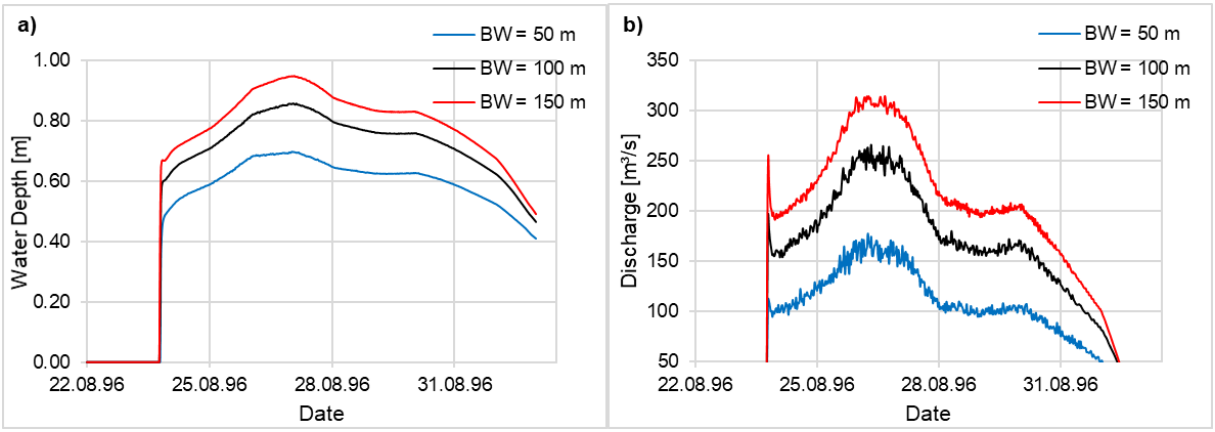

Figure 66: For the indicated final levee breach widths (BW) and the historical levee breach location of the August 1996 Wonji levee breach flood event: a) modelled flood depth in the floodplains at an office location and b) modelled breach discharge. The office location and the historical breach location are shown in Figure 63.

9.2.4 Final breach level

In the event of a levee breach, depending on the prevailing hydrodynamic and morphodynamic conditions, the levee may only erode to a certain level and not to the ground level. The sensitivity of the modelled flood depth in the floodplains and the breach discharge to the final breach level is analysed by performing hydrodynamic numerical simulations for final breach levels of BL = 0 m (levee erodes to the ground level) and BL = 1.5 m (levee erodes to half its height of 3 m). The results are shown in Figure 67. As can be seen from Figure 67, the flood depth at the office location and the breach discharge increase with increasing depth of levee breach. Simulations for additional final breach levels are avoided as the results for the two cases clearly show the sensitivity of the results.

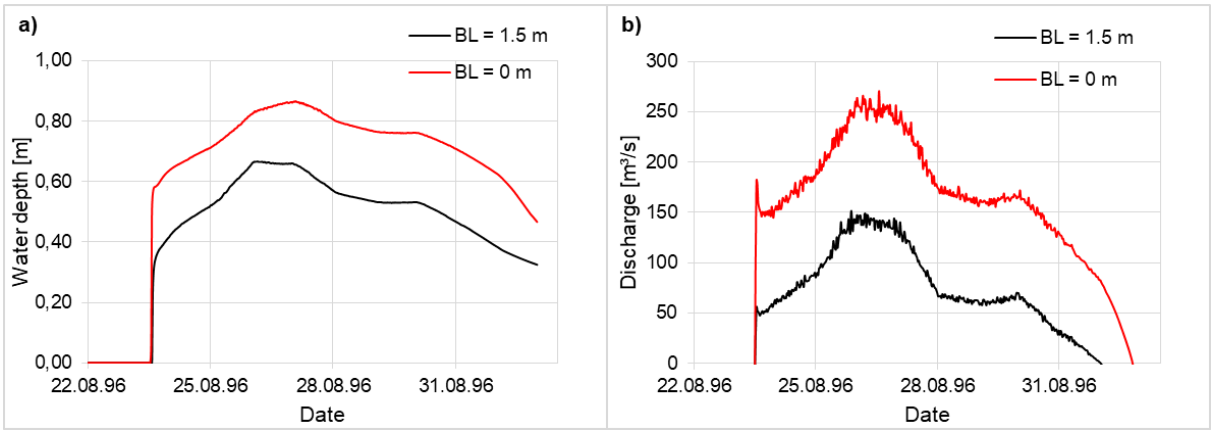

Figure 67: For the indicated final levee breach levels (BL) BL = 0 m (levee erodes to the ground level) and BL= 1.5 m (levee erodes to half its height of 3 m) and the historical levee breach location of the August 1996 Wonji levee breach flood event: a) modelled flood depth in the floodplains at an office location and b) modelled breach discharge. The office location and the historical breach location are shown in Figure 63.

9.2.5 Breach location

The sensitivity of the modelled flood depth in the floodplain and breach discharge to the breach location is analysed by performing hydrodynamic numerical simulations for two breach locations (BP 1 and BP 2) shown in Figure 63. The water depth at the office location in the floodplain and the breach discharge are extracted from the simulation results and shown in Figure 68. The results show that the water depth at the office location is sensitive to the beach location, but the breach discharge is marginally sensitive to the breach location. Simulations for additional final breach locations are avoided as the results with the two breach locations clearly show the sensitivity.

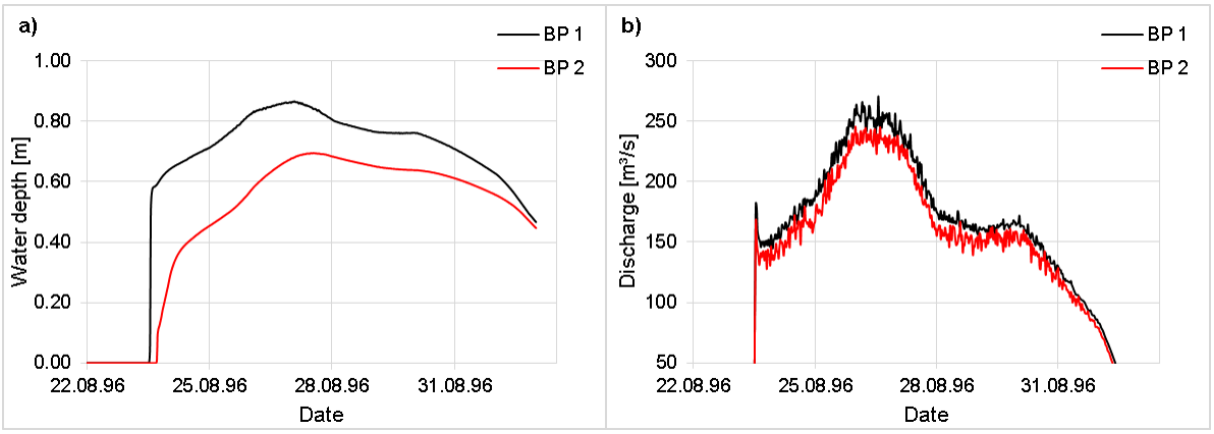

Figure 68: For two breach locations (BP 1 and BP 2) shown in Figure 50 and the August 1996 Awash River flood event at Wonji: a) modelled flood depth in the floodplains at an office location and b) modelled breach discharge. The office location is shown in Figure 63.

9.2.6 Erosion type

The levee breach model has two levee lowering options (erosion options) (see Section 4.2). The sensitivity of the modelled water depth at the office location and breach discharge to the levee erosion options is tested by performing hydrodynamic numerical simulations for each option. The water depth at office location and the breach discharge are extracted from the simulations and shown in Figure 69. The results show that the levee lowering option does not affect either the water depth at the office location or the breach discharge.

A similar comparison is made for the hypothetical flash flood and is shown in Figure 70. As can be observed from Figure 70, in the case of the flash flood, the modelled inundation depth and breach discharge are sensitive to the levee lowering option.

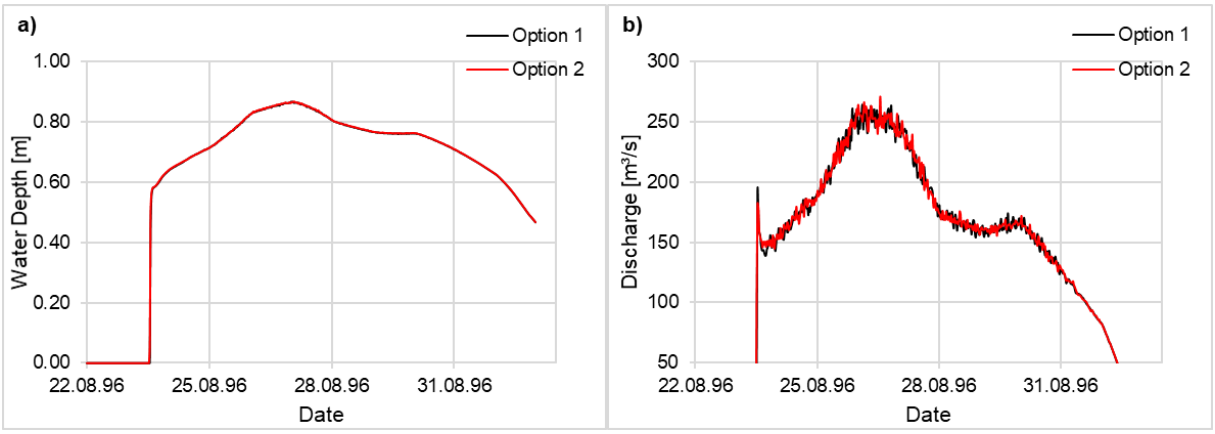

Figure 69: For the levee-lowering options (Option 1: only vertical breach growth; Option 2: vertical and lateral breach growth) and the historical levee breach location of the August 1996 Wonji levee breach flood event: a) modelled flood depth in the floodplains at an office location and b) modelled breach discharge. The office location and the historical breach locations are shown in Figure 63.

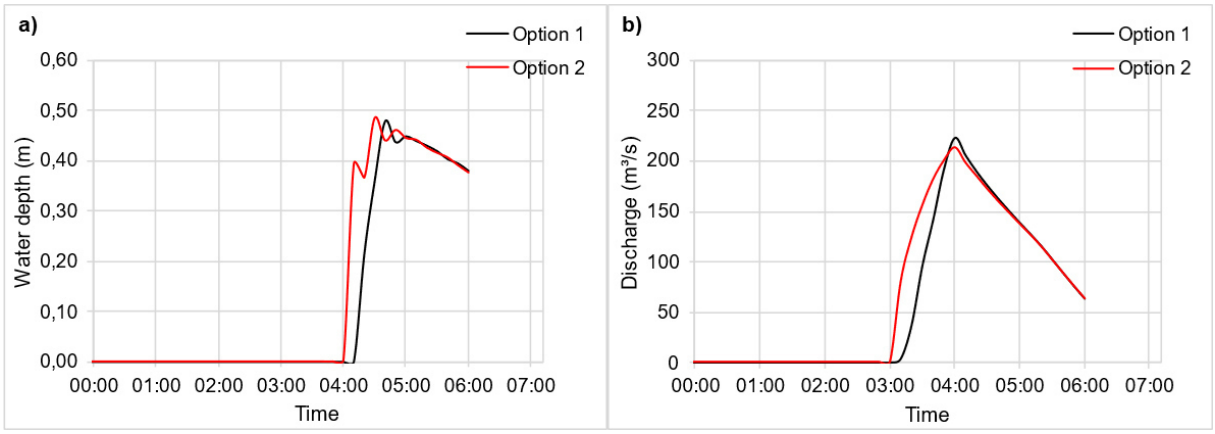

Figure 70: For a hypothetical flash flood, the levee-lowering options (Option 1: only vertical breach growth; Option 2: vertical and lateral breach growth) and the historical levee breach location of the August 1996 Wonji levee breach flood event: a) modelled flood depth in the floodplains at an office location and b) modelled breach discharge. The office location and the historical breach locations are shown in Figure 63.

9.2.7 Discussion

Some important aspects can be observed from the sensitivity analysis presented above. The model results (Figure 61 – Figure 70) show that the flood inundation due to a levee breach depends not only on the levee breach parameters but also on the type of flood (flash flood vs. non-flash flood). For flash floods, the flood inundation depends on all the parameters of the parametric levee breach model. On the other hand, for non-flash floods, i.e., floods over several days, the flood inundation (i) depends on the final breach width, final breach level and breach location and (ii) is not or only is marginally influenced by the breach start time, breach duration and levee-lowering method.

This means that for non-flash floods, the flood inundation due to the levee breach is more a function of the final breach dimensions and the location of the breach. The final dimensions of the breach strongly influence the flow through the breach (breach discharge), i.e., the volume of water entering the floodplain, and therefore proportionally influence the

depth and extent of inundation of the floodplain. For flash floods, all parameters influence the breach discharge.

The breach location affects the spatial variation of the inundation depth without significantly affecting the breach discharge, i.e., the location of the breach affects the flood consequence. To determine the maximum consequence of a levee breach, several levee breach locations should be systematically analysed. Such a systematic analysis can also be useful for prioritising the order of levee segments for maintenance and strengthening. The levee segment with the maximum consequence of breach should be maintained and strengthened first.

For non-flash floods, the levee breach parameters that describe the breaching processes (breach development), i.e. breach start time, breach duration and levee lowering method, have no or only marginal influence on the flood inundation. This means that the breach development has no significant influence on the flood inundation. In the case of flash floods, the levee breaching processes have a significant influence on the volume of water flowing into the hinterland and affect the depth and extent of inundation. Similar results are reported by Viero et al. (2013) and Dou et al. (2014).

10 Conclusions and further research

10.1 Conclusions

The following conclusions are drawn from the analysis of the literature.

- The modelling of flood inundation due to levee breaches is best performed by an integrated modelling of the levee breaching process and the flood propagation.
- The main mechanisms of levee breaching are external erosion due to flow overtopping and internal erosion. In both cases, the levee breaching process can be simplified into 3 stages: (i) initiation of the breach, (ii) formation of the initial breach channel and the vertical erosion of the levee, and (iii) the lateral widening of the breach opening. The duration of these stages is variable and depends on many factors such as the flow (discharge) in the river, the water level in the river, the levee material properties (material size, soil cohesion, density, tensile strength), the levee dimensions, the levee conditions (compaction, compaction water content, core and outer layers), maintenance condition of the levee / dike, burrow holes, etc.
- Parametric levee breach models are the appropriate breach models for an integrated modelling of flood inundation due to real-world levee breaches.

A parametric levee breach model is developed based on the levee breaching stages from the literature analysis and implemented in the hydrodynamic numerical model Telemac-2D. Furthermore, approaches for the estimation of the important parameters of the parametric levee breach model are given. The important breach parameters for non-flash floods are determined using the sensitivity of the breach discharge and flood inundation to the breach model parameters and are found to be the final breach dimensions and the breach location.

Historical levee breach data are used to establish an empirical relationship between the final breach width and the various combinations of the independent variables levee height, levee bottom width, levee soil material type, embankment type and breach mechanism using both regression and ANN models. The attained performance in terms adjusted R^2 is in the range of 0.20, which is a low value. The low adjusted R^2 is explained by the absence of important explanatory variables influencing levee breaching, such as river flow, design flow, levee condition, etc., which are not included in this analysis due to limited data availability. In addition, an approach for estimating levee breach location is developed in this research. The approach is based on limit state equations and uses flood characteristics (water level and flood duration), geometric and geological characteristics of the levee in question and its foundation, the cause of the breach, and information from historical levee breaches on their breach location. It is used to estimate the breach location for the August 1996 Awash River levee breach at Wonji, Ethiopia, and the estimate is consistent with the actual breach location.

The performance of Telemac-2D for modelling levee-breach type flows is evaluated using laboratory physical tests that mimic levee breaching. Telemac-2D reproduced the measurements in the physical test. It can be concluded that Telemac-2D is a suitable tool for modelling flood inundation resulting from levee breaches.

The integrated approach to modelling flood inundation due to levee breach is exemplarily applied to the August 1996 Awash River levee breach at Wonji, Ethiopia. The model results are in good agreement with the information documented during and after the flood event. This confirms the applicability of the approach for modelling flood inundation due to real-world levee breaches. Uncertainties in the integrated modelling of flood inundation due to levee breach and the sensitivity of the breach parameters are discussed.

10.2 Further research

The literature shows that the levee breaching processes is a complex phenomenon and therefore the estimation of breach parameters is associated with non-negligible uncertainties. The sensitivity analysis in this work showed that the flood inundation of the leveed area is strongly related to the final breach dimensions and the breach location in the case of non-flash floods. While the approach given in this work for estimating the breach location may be sufficient, the method for estimating the final breach dimensions, especially the final breach width, needs further improvement. Future research is suggested to improve the estimation of final breach width by developing empirical equations that take into account more independent variables that affect levee breaching processes, such as river flow, design flow, levee condition, etc. This will require improving the database of historical levee breaches. The database used in this research has limited data on these variables.

11 Summary

Historically, floodplains along rivers have been reclaimed by humans because they provide the resources necessary for life: water and fertile soil. Over time, many floodplains have been transformed into agricultural fields, residential villages, towns and cities, manufacturing and industrial areas, valuable historical heritage sites, etc. In most cases, these reclaimed floodplains are protected from flooding by levees, which are earthen embankments, often constructed from locally available soil material.

Levee design standards have improved over time, contributing to their reliability in providing flood protection. However, levees never provide absolute flood protection because (i) they are designed to contain floodwaters up to a specific design flow discharge or level, often statistically derived from past flood events, which may be exceeded in the future, (ii) they deteriorate over time, and (iii) there is an increase in extreme floods due to climate change. A number of recent flood disasters due to breaches of levees designed and built to the highest standards, such as the Elbe River levee breaches in 2002 and 2013, are good examples of the fact that levees do not provide absolute flood protection.

Public authorities are often required to prepare flood hazard maps and flood emergency plans for communities, businesses, and other stakeholders living in flood prone areas, including leveed areas (e.g., EU Floods Directive). Flood hazard maps can be produced using hydrodynamic numerical models that simulate flood inundation. The modelling of flood inundation due to levee breaching involves the modelling of two processes: (i) the breaching of the levee and (ii) the propagation of the flood through the resulting opening into the hinterland. The modelling of the two processes can be done in a decoupled or coupled (integrated) manner. The latter approach is superior to the former in that the flow from the main river into the floodplain is calculated by the hydrodynamic numerical model used, based on the prevailing conditions, and is more accurate than the decoupled approach, where the flow through the breach must often be estimated using a 1D overflow formula.

The modelling of flood propagation with 2D hydrodynamic numerical models is a well-established subject, although its applicability to levee-breach type flows, which could be supercritical flows, needs systematic verification. The currently available hydrodynamic numerical models are well tested for subcritical flows. However, the modelling of levee breaching is still an area of research and there is no well-established mathematical model. Nevertheless, we find a variety of breach models in the literature, which can be grouped into three main types: empirical, parametric and physically-based breach models (ASCE/EWRI 2011). The literature shows that parametric breach models are the suitable models for modelling of real-world levee breaches.

The objective of this research is to develop and test an integrated approach for modelling flood inundation due to real-world riverine levee breaches. Specifically, this work aims to:

- develop a parametric levee breach model based on the results of physical experiments on levee breaching processes and real levee breaches in the literature,
- integrate the developed parametric levee breach model into a hydrodynamic numerical model to enable an integrated modelling of levee breaching and flood inundation,
- develop methods and guidelines for estimating the breach parameters, and
- demonstrate the applicability of the approach using a laboratory levee breach test case as well as a real-world levee breach case.

Statistics based on historical levee breaches show that the main mechanisms of levee breach are external (surface) erosion (caused by the flow overtopping the levee) and internal erosion (initiated by seepage forces acting on the soil particles of the levee body or the foundation).

Experimental studies in the literature show that the process of breaching of both non-cohesive and cohesive levees due to external erosion (overtopping flow) can be generalised into the following four phases:

- Phase 1) Slow to gradual erosion of the downstream slope of the levee by the shear force of the overtopping flow (non-cohesive levees) or head cutting (cohesive levees) until the erosion reaches the upstream edge of the levee crest.
- Phase 2) Vertical erosion of the levee at a rapid erosion rate down to the foundation with limited lateral breach expansion.
- Phase 3) Rapid lateral expansion of the breach due to a combined effect of erosion and mass wasting due to instability of the breach side slope until peak discharge through the breach is reached; and
- Phase 4) Further lateral expansion of the breach at a slower rate until the maximum breach width is reached.

The duration of each phase is variable and depends on many factors such as the flow (discharge) in the river, the water level in the river, the properties of the levee material (material size (d_{50}), soil cohesion, density, tensile strength, etc), the levee dimensions and levee conditions (compaction, compaction water content, core and outer layers, etc.), etc.

The most common internal erosion mechanisms in levees are backward erosion (piping), sustained seepage and concentrated leak erosion. The predominant internal erosion mechanism in levees is backward erosion (piping). It is a process by which soil particles are removed by seepage flow from a sand layer beneath a levee or a cohesive layer. The erosion starts on the downstream side of the levee, where the seepage can flow freely to the surface. There are four stages of erosion which, if left unchecked, will eventually lead to breaching of the levee: (i) seepage and initiation of erosion, (ii) retrograde erosion until the land and river sides are connected by a pipe-like opening, (iii) widening of the pipe, and (iv) failure of the levee and breaching of the levee. The erosion process depends on the hydraulic gradient, the length of the structure, the soil properties (erodibility, critical shear

stress, degree of compaction), etc. The semi-empirical equation for the critical hydraulic gradient, such as that of Sellmeijer et al. (2011), can be used to estimate whether or not a levee breach is possible due to backward erosion.

Sustained seepage can often cause problems in non-cohesive, unfiltered levees. If such a levee is subjected to high water levels and water seeps through the levee and emerges on the landside slope, the levee may soften at the landside toe, causing slope sloughing and causing internal erosion of the levee material, which could lead to micro-instability of the levee such as slope failure. This can then lead to levee breaching. The possibility of levee breach due to sustained seepage can be estimated by comparing the duration of the flood with the time required for the seepage front to reach the landward toe of the levee, determined using the Darcy-Weisbach equation.

In the literature, a wide range of breach models with varying assumptions and complexity are currently in use. The breach models can be classified into empirical, parametric, and physically-based models. Empirical breach models are models derived from statistical best fit to historical levee breach data to estimate breach parameters such as breach peak discharge, breach width or depth. A handful of empirical equations for estimating final levee breach dimensions and breach discharge are available in the literature. Parametric breach models are breach models that rely on parameters to describe the levee breaching process and determine the flow through the breach analytically or numerically. They are often integrated into 1D or 2D numerical models to enable simultaneous simulation of the levee breaching and hinterland inundation. The number of parameters varies from model to model. Parameters often include final breach dimensions, breach duration, breach location and breach initiation. Physically-based breach models are levee breach models that are based on flow hydraulics and erosion processes. A fully physically-based breach model simulates the levee breaching process using sediment transport equation (such as the Meyer-Peter and Müller formula), bed evolution equation (such as the Exner equation) and slope stability conditions coupled with a hydrodynamic numerical model. The literature suggests that the choice of breach model depends on the purpose of the study. Fully physically-based models (2D and, to a lesser extent, 3D numerical models) are often employed to model laboratory levee breach experiments. Empirical models are used to estimate final breach dimensions and breach flow. Parametric and simplified physically-based models are used to model levee breaching when modelling flood inundation from historical levee breaches.

Flooding, like any other fluid flow, is governed by the laws of conservation of mass and momentum. Applying these laws to fluid flow gives the continuity equation and the NS equations. Averaging the continuity equation and the NS equations to account for turbulence fluctuations gives the RANS equations. Vertical averaging of the RANS equations gives the shallow water equations, which are the mathematical equations for the modelling of flood propagation. The shallow water equations for environmental flows are non-linear partial differential equations that can only be solved numerically. Telemac-2D is a publicly available code for the numerical solution of the shallow water equations. In this work, Telemac-2D is used with the options finite element method, the method of characteristics and semi-implicit time stepping scheme.

In this research, a parametric levee breach model is developed and implemented in Telemac-2D. It is based on the levee breaching processes observed in physical experiments, field tests and actual levee breaches. In the developed parametric breach model, levee breaching is described by parameters and takes place in three stages: i) initiation of the breach, ii) mainly vertical lowering of the levee and iii) mainly lateral widening of the breach. These stages are defined in the model by the parameters breach initiation, breach location, breach duration, final breach level, and final breach width. Breach location and final breach width are defined by the coordinates of the mesh nodes affected by the breach. The breach starts at the centre of the levee length affected by the breach and can be initiated in three different ways: at a given time, based on the water level on the levee, or based on the water level in the river. The second stage takes one tenth of the total time required for the entire breach and has a breach width equal to one tenth of the final breach width.

Many levee breaches have occurred in the past. The compilation of historical breaches can be found in various databases and in the literature. The ILPD is the most comprehensive freely available levee breach database and is used in this research. It is augmented in this research by additional levee breach cases found in the literature. A total of 412 breach cases were compiled. However, only few breach parameters are documented in the breach cases. Only the final breach width is documented for all 412 cases. The independent variables for which information is available for more than 100 breach cases in the dataset are levee height, levee bottom width, soil type, levee type, and breach mechanism. These data are used to establish an empirical relationship for the final breach width as a function of various combinations of the independent variables levee height, levee bottom width, levee soil material type, embankment type and breach mechanism using both regression and ANN models. The results showed that the performance of the ANN models was comparable to that of the regression models in terms of MAE and RMSE. The regression models performed better in terms of adjusted R^2. In both cases, the best prediction of the final breach width is obtained with the combination of the independent variables levee height, levee type and breach mechanism. The maximum adjusted R^2 is in the range of 0.20, which means that the variables levee height, levee type and breach mechanism explain about 20% of the variance of the final breach width. The low adjusted R^2 is explained by the absence of important explanatory variables influencing levee breaching, such as river flow, design flow, levee condition, etc., which are not included in this analysis due to limited data availability.

Another important breach parameter that can significantly affect the consequences of a levee breach is the location of the breach. Due to the long length of levees and the complex causes of breach initiation, estimating the location of a levee breach can be difficult. The ILPD has information on the indication why the levee breached at that location for about 160 breach cases. These could be grouped into 17 indications. Based on this information and the literature, an approach is developed to estimate a possible breach location. The approach uses flood characteristics (water level and flood duration), geometric and geological characteristics of the levee in question and its foundation, the cause of the breach, and information from historical levee breaches on their breach location. The steps of the approach are as follows: 1) identify the river reach and the critical points in the

protected area; 2) set up a hydrodynamic numerical model for the identified river reach and run it for a selected flood event scenario; 3) divide the levee into representative reaches; 4) for each representative reach, determine representative hydraulic (water level), geometric and soil properties; 5) for each levee reach, check the possibility of levee breach due to external erosion, backward erosion, sustained seepage through the levee and concentrated leak erosion using limit state equations; 6) if breaching is possible in one or more reaches, calculate the final breach width using the empirical approaches discussed above; and 7) select a breach location by taking the breach location closest to the critical point in the floodplain (simplified approach) or the breach location that results in the maximum inundation depth at the critical point in the floodplain (detailed approach, requires 2D hydrodynamic numerical simulation of levee breaching in each levee reach).

Calibration and validation of levee-breach type flows is often not possible because data are usually not available. In this situation, levee-breach-type laboratory physical tests can be useful to evaluate the performance of hydrodynamic numerical models for modelling levee-breach type flows. In this research, the results of levee-breach-type laboratory physical tests carried out by Briechle (2006) at the Institute of Hydraulic Engineering and Water Resources Management at the University of Aachen, Germany, were used to evaluate the performance of Telemac-2D for modelling a levee-breach type flow. In the physical tests, a levee-breach-type flow is simulated by the sudden opening of a gate on the side of a channel with an attached propagation area. For the laboratory physical test setup, a Telemac-2D model is set up and calibrated and validated with two independent test configurations. With the optimal settings, Telemac-2D simulations are performed for different test configurations and the results are compared with measurements. The parameters breach discharge, wave front after breach, water level at selected points in the propagation area, and water level profile along the axis of the propagation area in steady state are compared between the measurements and the Telemac-2D results. Telemac-2D reproduced the physical test measurements with deviations less than 10%. It can be concluded that Telemac-2D, with appropriate settings, is a suitable tool for modelling flood inundation due to levee breaching.

The proposed approach to modelling of flood inundation due to levee breaches is exemplarily applied to a real-world levee breach event at Wonji, Ethiopia. The data required for the modelling are discussed and prepared to build a hydrodynamic numerical model of the area based on Telemac-2D. The model is then calibrated and validated for a section of the Awash River and adjacent floodplains at Wonji. The validated 2D hydrodynamic numerical model is used to model the flood inundation of the August 1996 levee breach at Wonji. The model results are in good agreement with the information documented during and after the disaster. The modelled water depth at an office building is in good agreement with the water level marks left on buildings as reported by an eyewitness. The widespread flooding reported by the United Nations Development Programme's (UNDP) Emergency Unit for Ethiopia is in good agreement with the model results. Furthermore, the determination of the breach location for the August 1996 Wonji flood is carried out using the approach proposed in Chapter 6 to demonstrate the pragmatism of the approach. For this flood event, the approach estimated the most likely breach location in the upstream

section of the levee, which corresponds to the actual breach location, confirming the applicability of the proposed approach.

The presented integrated modelling of flood inundation due to levee breach uses a 2D hydrodynamic numerical model and a levee breach model. Existing studies show that these models are associated with non-negligible uncertainties. The uncertainties in the 2D hydrodynamic numerical model result from (i) the error associated with the approximation of the physical process with a simplified mathematical equation, (ii) the error in the numerical resolution of the mathematical model (numerical approximation in space and time discretisation of the shallow water equations, convergence tolerance, truncation error), and (iii) the uncertainty in the input data (DEM, initial and boundary conditions, hydraulic structures, calibration / validation data, etc.) and model parameters (roughness, turbulence).

The main sources of uncertainty in levee breach parameters are (i) uncertainty in the initiation of the breach and the breaching process, (ii) uncertainty in the input data used to estimate the breach parameters, and (iii) uncertainty in the breach location. To demonstrate the uncertainty associated with the breach model, the sensitivity of flood inundation depth and breach discharge to variation of the levee breach parameters is systematically analysed using the August 1996 Awash River levee breach flood event at Wonji, Ethiopia. The results show that the flood inundation due to the levee breach is sensitive to the final breach dimensions and the breach location. This means that the accuracy of the model results is highly dependent on the accuracy of these breach parameters.

Literature

ABEBE H., M. (2001): Sedimentation in the Koka Reservoir, Ethiopia. In: B. Honningsvag, G. H. Midttomme, K. Repp, K. Vaskinn und T. Westeren (Eds.): Hydropower in the new Millenium. Proceedings of the 4th International Conference on Hydropower Development. International Conference on Hydropower Development. Bergen, Norway, 20-22 June 2001. Lisse, Netherlands: A.A. Balkema, p. 345–350.

AHRENS, J. D. (1996): Koka Dam - River Awash Floods. Report of the Joint UN Assessment Team. UNITED NATIONS DEVELOPMENT PROGRAMME (UNDP) EMERGENCIES UNIT FOR ETHIOPIA. Addis Ababa, Ethiopia. Online available at http://www.africa.upenn.edu/eue_web/Awash29aug.htm, last updated on 08.10.2001, last checked on 19.08.2019.

ALTAREJOS-GARCÍA, L.; MARTÍNEZ-CHENOLL, M. L.; ESCUDER-BUENO, I.; SERRANO-LOMBILLO, A. (2012): Assessing the impact of uncertainty on flood risk estimates with reliability analysis using 1-D and 2-D hydraulic models. In: *Hydrol. Earth Syst. Sci.* 16 (7), p. 1895–1914. DOI: 10.5194/hess-16-1895-2012.

APEL, H.; MERZ, B.; THIEKEN, A. H. (2009): Influence of dike breaches on flood frequency estimation. In: *Computers & Geosciences* 35 (5), p. 907–923. DOI: 10.1016/j.cageo.2007.11.003.

APEL, H.; THIEKEN, A. H.; MERZ, B.; BLÖSCHL, G. (2006): A Probabilistic Modelling System for Assessing Flood Risks. In: *Nat Hazards* 38 (1-2), p. 79–100. DOI: 10.1007/s11069-005-8603-7.

ARCHAMBEAU, P.; DEWALS, B.; ERPICUM, S.; MOUZELARD, T.; PIROTTON, M. (2002): Wolf software: a fully integrated device applied to modelling gradual dam failures and assessing subsequent risks. In: M. Rahman, R. Verhoeven und C. A. Brebbia (Eds.): Advances in fluid mechanics IV. Southampton: WIT (International series on advances in fluid mechanics, 1353-808X, 32), p. 259–268.

ARTHUR, S. (Ed.) (2010): Proceedings from First IAHR European Congress: May 2010. Edinburgh, Uk, 4-6 May.

ASCE/EWRI TASK COMMITTEE ON DAM/LEVEE BREACHING (ASCE/EWRI) (2011): Earthen Embankment Breaching. In: *J. Hydraul. Eng.* 137 (12), p. 1549–1564. DOI: 10.1061/(ASCE)HY.1943-7900.0000498.

ASHRAF, M.; SOLIMAN, A. H.; EL-GHORAB, E.; ZAWAHRY, A. E. (2018): Assessment of embankment dams breaching using large scale physical modeling and statistical methods. In: *Water Science* 32 (2), p. 362–379. DOI: 10.1016/j.wsj.2018.05.002.

ASSOCIATED PRESS (1996): 20,000 Ethiopians Evacuated. Online available at https://reliefweb.int/report/ethiopia/20000-ethiopians-evacuated, last checked on 19.08.2019.

ATA, R. (2018): Telemac-2D User Manual. Version v7p3. Online available at https://gitlab.pam-retd.fr/otm/telemac-mascaret/-/blob/v7p3r1/documentation/telemac2d/user/telemac2d_user_v7p3.pdf?ref_type=tags, last checked on 07.12.2024.

ATCOLD (Ed.) (2010): Proceedings of the 8th ICOLD European Club Symposium. Dam safety: Sustainability in a changing environment. ICOLD European Club Symposium. Innsbruck, Austria, 22nd - 23rd September 2010. ÖSTERREICHISCHES NATIONALKOMITEE FÜR TALSPERREN. Graz: Verlag der Technischen Universität Graz.

BATES, P. D.; PAPPENBERGER, F.; ROMANOWICZ, R. J. (2014): Uncertainty in Flood Inundation Modelling. In: Keith Beven und Jim Hall (Eds.): Applied Uncertainty Analysis for Flood Risk Management: Imperial College Press, p. 232–269.

BELLOS, V.; TSAKIRIS, V. K.; KOPSIAFTIS, G.; TSAKIRIS, G. (2020): Propagating Dam Breach Parametric Uncertainty in a River Reach Using the HEC-RAS Software. In: *Hydrology* 7 (4), p. 72. DOI: 10.3390/hydrology7040072.

BENAHMED, N.; BONELLI, S. (2012): Investigating concentrated leak erosion behaviour of cohesive soils by performing hole erosion tests. In: *European Journal of Environmental and Civil Engineering* 16 (1), p. 43–58. DOI: 10.1080/19648189.2012.667667.

BENAHMED, N.; CHEVALIER, C.; BONELLI, S. (2012): Concentrated Leak Erosion. In: S. Bonelli (Ed.): Erosion of Geomaterials. 1st edition. s.l.: Wiley-ISTE (ISTE), p. 155–186, last checked on 16.09.2021.

BENARDOS, P. G.; VOSNIAKOS, G.-C. (2007): Optimizing feedforward artificial neural network architecture. In: *Engineering Applications of Artificial Intelligence* 20 (3), p. 365–382. DOI: 10.1016/j.engappai.2006.06.005.

BERTRAND, N.; LIQUET, M.; MOIRIAT, D.; BARDET, L.; DULUC, C.-M. (2018): Uncertainties of a 1D Hydraulic Model with Levee Breaches: The Benchmark Garonne. In: Philippe Gourbesville, Jean Cunge und Guy Caignaert (Eds.): Advances in Hydroinformatics. SimHydro 2017 - Choosing the Right Model in Applied Hydraulics. Singapore: Springer (Springer eBook Collection Earth and Environmental Science), p. 189–204.

BESSAR, M. A.; MATTE, P.; ANCTIL, F. (2020): Uncertainty Analysis of a 1D River Hydraulic Model with Adaptive Calibration. In: *Water* 12 (2), p. 561. DOI: 10.3390/w12020561.

BEVEN, KEITH; HALL, JIM (Eds.) (2014): Applied Uncertainty Analysis for Flood Risk Management: Imperial College Press.

BHATTARAI, P. K. (2015): Study on river dyke breach characteristics by overtopping flow. Doctoral thesis. KYOTO UNIVERSITY. Laboratory of Hydro-Science and Hydraulic Engineering, Department of Civil and Earth Resources Engineering. Online available at https://doi.org/10.14989/doctor.k19282, last checked on 27.08.2020.

BJÖRNSEN BERATENDE INGENIEURE GMBH (BCE) (2022): Kalypso 1D/2D. Online available at https://kalypso.bjoernsen.de/index.php?id=470&L=1, last checked on 26.04.2022.

BOLLRICH, G. (2000): Grundlagen. In collaboration withGerhard Bollrich. 5. Aufl. Berlin: Verl. für Bauwesen (Technische Hydromechanik, 1).

BONELLI, S. (Ed.) (2012): Erosion of Geomaterials. 1st edition. s.l.: Wiley-ISTE (ISTE). Online available at http://search.ebscohost.com/login.aspx?direct=true&scope=site&db=nlebk&db=nlabk&AN=531492.

BONELLI, S.; BENAHMED, N. (2010): Piping flow erosion in water retaining structures: inferring erosion rates from hole erosion tests and quantifying the failure time. In: ATCOLD (Ed.): Proceedings of the 8th ICOLD European Club Symposium. Dam safety: Sustainability in a changing environment. ICOLD European Club Symposium. Innsbruck, Austria, 22nd - 23rd September 2010. Österreichisches Nationalkomitee für Talsperren. Graz: Verlag der Technischen Universität Graz, p. 467–472.

BONELLI, S.; COURIVAUD, J.-R.; FRY, J.-J.; ROYET, P. (2012): Internal erosion on dams and dikes: lessons from experience and modelling. In: ICOLD (Ed.): Internal erosion of existing dams, levees, and dikes, and their foundations - international glossary, Vol. 1. 24th ICOLD Congress. Kyoto, Japan. ICOLD (CIGB-ICOLD Bulletin, 1), p. 366–388.

BONELLI, STÉPHANE (Ed.) (2013): Erosion in geomechanics applied to dams and levees. London, Hoboken, NJ: ISTE Ltd (Civil engineering and geomechanics series).

BOUSMAR, D. ED; ZECH, Y. ED (Eds.) (2002): River flow 2002. Proceedings of the international conference on fluvial hydraulics. Louvain-la-Neuve, Belgium, 4-6 September. Lisse, The Netherlands: Swets & Zeitlinger.

BRIAUD, J.-L.; CHEN, H.-C.; GOVINDASAMY, A. V.; STORESUND, R. (2008): Levee Erosion by Overtopping in New Orleans during the Katrina Hurricane. In: *J. Geotech. Geoenviron. Eng.* 134 (5), p. 618–632. DOI: 10.1061/(ASCE)1090-0241(2008)134:5(618).

BRIECHLE, S.; JOEPPEN, A.; KÖNGETER, J. (2004): Physical model test for dike-break induced, two-dimensional flood wave propagation. In: M. Greco, A. Carravetta und R. Della Morte (Eds.): River flow 2004. Proceedings of the Second International Conference on Fluvial Hydraulics, Vol. 2. River Flow. Napoli, Italy, 23-25 June. International Conference on Fluvial Hydraulics. Leiden, London: A.A. Balkema, p. 959–966.

BRIECHLE, S. R. (2006): Die fächenhafte Ausbreitung der Flutwelle nach Versagen von Hochwasserschutzeinrichtungen an Fließgewässern. Doctoral Thesis. RWTH AACHEN UNIVERSITY, Aachen. Institute of Hydraulic Engineering and Water Resources Management.

BROICH, K. (2003): Sediment transport in breach formation process. Institute of Water Management, Faculty of Civil Engineering and Environmental Sciences, University of the Bundeswehr Munich.

BRUNNER, G.; U.S. ARMY CORPS OF ENGINEERS INSTITUTE FOR WATER RESOURCES HYDROLOGICAL ENGINEERING CENTER (CEIWR-HEC) (2020): HEC-RAS River Analysis System User's Manual. Version 6.0 Beta. U.S. Army Corps of Engineers Institute for Water Resources Hydrological Engineering Center (USACEIWR-HEC). Davis, CA. Online available at https://www.hec.usace.army.mil/software/hec-ras/documentation/HEC-RAS_6.0_UsersManual.pdf.

BURNS, S. E.; BHATIA, S. K.; AVILA, C. M. C.; HUNT, B. E. (Eds.) (2010): Proceedings of the 5th International Conference on Scour and Erosion (ICSE-5). San Francisco, USA., November 7-10. Reston, Va.: American Society of Civil Engineers.

CAMICI, S.; BARBETTA, S.; MORAMARCO, T. (2017): Levee body vulnerability to seepage: the case study of the levee failure along the Foenna stream on 1 January 2006 (central Italy). In: *Journal of Flood Risk Management* 10 (3), p. 314–325. DOI: 10.1111/jfr3.12137.

CANELAS, R.; MURILLO, J.; FERREIRA, R. M. (2013): Two-dimensional depth-averaged modelling of dam-break flows over mobile beds. In: *Journal of Hydraulic Research* 51 (4), p. 392–407. DOI: 10.1080/00221686.2013.798891.

CANTERO-CHINCHILLA, F. N.; CASTRO-ORGAZ, O.; SCHMOCKER, L.; HAGER, W. H.; DEY, S. (2018): Depth-averaged modelling of granular dike overtopping. In: *Journal of Hydraulic Research* 56 (4), p. 537–550. DOI: 10.1080/00221686.2017.1399933.

CARTER, M.; BENTLEY, S. P. (2016): Soil Properties and their Correlations. 2. Aufl. s.l.: Wiley.

CHATTERJEE, C.; FÖRSTER, S.; BRONSTERT, A. (2008): Comparison of hydrodynamic models of different complexities to model floods with emergency storage areas. In: *Hydrol. Process.* 22 (24), p. 4695–4709. DOI: 10.1002/hyp.7079.

CHEN, J.; WANG, S.; LIANG, Y.; WANG, Y.; LUO, Y. (2015): Experimental Investigation of the Erosion Mechanisms of Piping. In: *Soil Mech Found Eng* 52 (5), p. 301–309. DOI: 10.1007/s11204-015-9345-5.

CHENDEȘ, V.; CORBUȘ, C.; PETREȘ, N. (2015): Characteristics of April 2005 flood event and affected areas in the Timiș - Bega Plain (Romania) analysed by hydrologic, hydraulic and GIS methods. In: SGEM2015 (Ed.): 15th International Multidisciplinary Scientific GeoConference, Water Resources. Forest, Marine and Ocean Ecosystems. 15th International Multidisciplinary Scientific GeoConference SGEM2015, June 18, 2015: Stef92 Technology (SGEM International Multidisciplinary Scientific GeoConference EXPO Proceedings).

CHOW, V. T. (2009): Open-channel hydraulics. International student edition. Caldwell, NJ: Blackburn Press (McGraw-Hill Civil Engineering series).

CIRIA (2013): The international levee handbook. London: CIRIA (CIRIA C, 731). Online available at https://www.ciria.org/Resources/Free_publications/I_L_H/ILH_Chapter_overviews.aspx.

COLEMAN, S. E.; ANDREWS, D. P.; WEBBY, M. G. (2002): Overtopping Breaching of Noncohesive Homogeneous Embankments. In: *J. Hydraul. Eng.* 128 (9), p. 829–838. DOI: 10.1061/(ASCE)0733-9429(2002)128:9(829).

COSTA, J. E. (1985): Floods from dam failures. Open-File Report. U.S. Department of the Interior, Geological Survey. Denver, Colorado (85-560).

DANKA, J.; ZHANG, L. M. (2015): Dike Failure Mechanisms and Breaching Parameters. In: *J. Geotech. Geoenviron. Eng.* 141 (9), p. 4015039. DOI: 10.1061/(ASCE)GT.1943-5606.0001335.

DAZZI, S.; VACONDIO, R.; MIGNOSA, P. (2019): Integration of a Levee Breach Erosion Model in a GPU-Accelerated 2D Shallow Water Equations Code. In: *Water Resour. Res.* 55 (1), p. 682–702. DOI: 10.1029/2018WR023826.

DI BALDASSARRE, G.; CASTELLARIN, A.; BRATH, A. (2009): Analysis of the effects of levee heightening on flood propagation: example of the River Po, Italy. In: *Hydrological Sciences Journal* 54 (6), p. 1007–1017. DOI: 10.1623/hysj.54.6.1007.

DINKA, M. O.; NDAMBUKI, J. M. (2014): Identifying the Potential Causes of Waterlogging in Irrigated Agriculture: The Case of the Wonji-Shoa Sugar Cane Plantation (Ethiopia). In: *Irrig. and Drain.* 63 (1), p. 80–92. DOI: 10.1002/ird.1791.

DITTRICH, ANDREAS (Ed.) (2010): River Flow 2010. Proceedings of the 5th International Conference on Fluvial Hydraulics. International Conference on Fluvial Hydraulics. Braunschweig, Germany. Karlsruhe: Bundesanst. für Wasserbau.

DORFMANN, C.; ZENZ, G. (Eds.) (2017): Proceedings of the 24th TELEMAC-MASCARET User Conference. Graz University of Technology, Austria, 17 - 20 October. GRAZ UNIVERSITY OF TECHNOLOGY. Graz, Austria: Verlag der Technischen Universität Graz. Online available at http://www.opentelemac.org/images/clubu/2017/telemac-mascaret_user_conference_2017-proceedings.pdf, last checked on 11.09.2019.

DOU, S.-T.; WANG, D.-W.; YU, M.-H.; LIANG, Y.-J. (2014): Numerical modeling of the lateral widening of levee breach by overtopping in a flume with 180° bend. In: *Nat. Hazards Earth Syst. Sci.* 14 (1), p. 11–20. DOI: 10.5194/nhess-14-11-2014.

DWA-ARBEITSGRUPPE WW-4.3 (DWA) (2011): Deiche an Fließgewässern. Teil 1: Planung, Bau und Betrieb. Dezember 2011. Hennef: DWA, Dt. Vereinigung für Wasserwirtschaft, Abwasser u. Abfall (DWA-Regelwerk : Merkblatt, DWA-M 507-1).

EASTERN NILE TECHNICAL REGIONAL OFFICE (NBI-ENTRO) (2010): Flood Embankment Design, Operation and Maintenance Manual in Ethiopia. Nile Basin Initiative, Eastern Nile Subsidiary Action Program (ENSAP).

EL NAGGAR, H.; SHAHIN, M. (Eds.) (2017): Proceedings of the 2nd World Congress on Civil, Structural, and Environmental Engineering. The 2nd World Congress on Civil, Structural, and Environmental Engineering, 4/2/2017 - 4/4/2017: Avestia Publishing (World Congress on Civil, Structural, and Environmental Engineering).

ELALFY, E.; TABRIZI, A. A.; CHAUDHRY, M. H. (2018): Numerical and Experimental Modeling of Levee Breach Including Slumping Failure of Breach Sides. In: *J. Hydraul. Eng.* 144 (2), p. 4017066. DOI: 10.1061/(ASCE)HY.1943-7900.0001406.

EMIRU, N. C.; RECHA, J. W.; THOMPSON, J. R.; BELAY, A.; AYNEKULU, E.; MANYEVERE, A. ET AL. (2022): Impact of Climate Change on the Hydrology of the Upper Awash River Basin, Ethiopia. In: *Hydrology* 9 (1), p. 3. DOI: 10.3390/hydrology9010003.

ENOMOTO, T.; HORIKOSHI, K.; ISHIKAWA, K.; MORI, H.; TAKAHASHI, A.; UNNO, T.; WATANABE, K. (2021): Levee damage and bridge scour by 2019 typhoon Hagibis in Kanto Region, Japan. In: *Soils and Foundations. DOI:* 10.1016/j.sandf.2021.01.007.

EU (2007): Directive 2007/60/Ec of The European Parliament and of The Council of 23 October 2007 on the assessment and management of flood risks. Directive 2007/60/EC. In: *Official Journal of the European Union* (288), p. 27–34, last checked on 15.10.2023.

FAEH, R. (2007): Numerical Modeling of Breach Erosion of River Embankments. In: *J. Hydraul. Eng.* 133 (9), p. 1000–1009. DOI: 10.1061/(ASCE)0733-9429(2007)133:9(1000).

FELL, R.; FRY, J. J. (Eds.) (2007): Internal erosion of dams and their foundations. London, New York: Taylor & Francis (Balkema-proceedings and monographs in engineering, water and earth sciences). Online available at https://content.taylorfrancis.com/books/download?dac=C2010-0-32542-1&isbn=9780429083051&format=googlePreviewPdf.

FELL, R.; HANSON, G. J.; HERRIER, G.; MAROT, D.; WAHL, T. L. (2013): Relationship between the Erosion Properties of Soils and Other Parameters. In: Stéphane Bonelli (Ed.): Erosion in geomechanics applied to dams and levees, Vol. 16. London, Hoboken, NJ: ISTE Ltd (Civil engineering and geomechanics series), p. 343–381.

FELL, R.; WAN, C. F.; CYGANIEWICZ, J.; FOSTER, M. (2003): Time for Development of Internal Erosion and Piping in Embankment Dams. In: *J. Geotech. Geoenviron. Eng.* 129 (4), p. 307–314. DOI: 10.1061/(ASCE)1090-0241(2003)129:4(307).

FENG, J.; HE, X.; TENG, Q.; REN, C.; CHEN, H.; LI, Y. (2019): Reconstruction of porous media from extremely limited information using conditional generative adversarial networks. In: *Physical review. E* 100 (3-1), p. 33308. DOI: 10.1103/PhysRevE.100.033308.

FRANK, P.-J. (2016): Hydraulics of Spatial Dike Breaches. Doctoral thesis. VAW ETH ZÜRICH, CH-8093 Zürich. Versuchsanstalt für Wasserbau, Hydrologie und Glaziologie (VAW), last checked on 11.06.2019.

FRY, J. (2012): Introduction to the Process of Internal Erosion in Hydraulic Structures: Embankment Dams and Dikes. In: S. Bonelli (Ed.): Erosion of Geomaterials. 1st edition. s.l.: Wiley-ISTE (ISTE), p. 1–37. Online available at https://onlinelibrary.wiley.com/doi/pdf/10.1002/9781118561737.ch1.

FUJITA, Y.; TAMURA, T. (1987): Enlargement of breaches in flood levees on alluvial plains. In: *Journal of Natural Disaster Science* 9 (1), p. 37–60.

GEE, D. M. (2008): Comparison of Dam Breach Parameter Estimators. Corps of Engineers Hydrologic Engineering Center.

GILL, N. S. (2021): Artificial Neural Networks. Applications and Algorithms. Online available at https://www.xenonstack.com/blog/artificial-neural-network-applications, last updated on 17.03.2022, last checked on 18.03.2022.

GOEURY, C.; DAVID, T.; ATA, R.; BOYAVAL, S.; AUDOUIN, Y.; GOUTAL, N. ET AL. (2015): Uncertainty Quantification on a Real Case with Telemac-2D. In: Charles Moulinec und David Emerson (Eds.): Proceedings of the XXII TELEMAC-MASCARET Technical User Conference. Unter Mitarbeit von TELEMAC-MASCARET Core Group. TELEMAC-MASCARET Technical User Conference. Warrington: STFC Daresbury Laboratory., October 15-16, p. 44–51.

GOLDER ASSOCIATES LTD. (GA); ASSOCIATED ENGINEERING LTD. (AE) (2003): Dike design and construction guide. Best management practices for British Columbia: Flood Hazard Management Section.

GOURBESVILLE, PHILIPPE; CUNGE, JEAN; CAIGNAERT, GUY (Eds.) (2018): Advances in Hydroinformatics. SimHydro 2017 - Choosing the Right Model in Applied Hydraulics. Singapore: Springer (Springer eBook Collection Earth and Environmental Science).

GOURBESVILLE, PHILIPPE; CUNGE, JEAN; GUINOT, VINCENT (Eds.) (2007): Hydroinformatics 2006: Proceedings of the 7th International Conference. International Conference on Hydroinformatics. Nice, France, 4 - 8 September, 2006. Singapore: Research Publishing.

GRECO, M.; CARRAVETTA, A.; DELLA MORTE, R. (Eds.) (2004): River flow 2004. Proceedings of the Second International Conference on Fluvial Hydraulics. River Flow. Napoli, Italy, 23-25 June. INTERNATIONAL CONFERENCE ON FLUVIAL HYDRAULICS. Leiden, London: A.A. Balkema.

GUAN, M.; WRIGHT, N. G.; SLEIGH, P. A. (2014): 2D Process-Based Morphodynamic Model for Flooding by Noncohesive Dyke Breach. In: *J. Hydraul. Eng.* 140 (7), p. 4014022. DOI: 10.1061/(ASCE)HY.1943-7900.0000861.

HADLEY, RICHARD F.; MIZUYAMA, T. (Eds.) (1993): Sediment problems: Strategies for monitoring, prediction, and control. Proceedings of an international symposium. Yokohama, Japan, 19-21 July. INTERNATIONAL ASSOCIATION OF HYDROLOGICAL SCIENCES. Wallingford: International Association of Hydrological Sciences (IAHS Publication, 217).

HAILEMARIAM, K. (1999): Impact of climate change on the water resources of Awash River Basin, Ethiopia. In: *Climate Research* 12 (2-3), last checked on 07.08.2019.

HALCROW; SOGREAH; MCE (2005): Awash River Basin Flood Control and Watershed Management Study Project. Working Paper 5. Ministry of Water Resources, Federal Democtatic Republic of Ethiopia.

HANSON, G. J.; COOK, K. R.; HUNT, S. L. (2005): Physical modeling of overtopping erosion and breach formation of cohesive embankments. In: *Transactions of the ASAE* 48 (5), p. 1783–1794. DOI: 10.13031/2013.20012.

HERVOUET, J.-M. (2007): Hydrodynamics of free surface flows. Modelling with the finite element method. Chichester: John Wiley & Sons, Ltd.

HEWLETT, H.; BOORMAN, L. A.; BRAMLEY, M. E. (1987): Design of Reinforced Grass Waterways. Report 116. CIREA.

HEYER, T.; HORLACHER, H.-B.; STAMM, J. (2010): Multicriteria stability analysis of river embankments based on past experience. In: S. Arthur (Ed.): Proceedings from First IAHR European Congress: May 2010. Edinburgh, Uk, 4-6 May.

HONNINGSVAG, B.; MIDTTOMME, G. H.; REPP, K.; VASKINN, K.; WESTEREN, T. (Eds.) (2001): Hydropower in the new Millenium. Proceedings of the 4th International Conference on Hydropower Development. International Conference on Hydropower Development. Bergen, Norway, 20-22 June 2001. Lisse, Netherlands: A.A. Balkema.

HORLACHER, H.-B.; HEYER, T.; CARSTENSEN, D.; BIELAGK, U.; BIELITZ, E.; MÜLLER, U. (2007): Analysis of dyke breaks during the 2002 flood in Saxony, Germany. Technical University Dresden, Institute for Hydraulic Engineering and Applied Hydromechanics; Dam Authority of the Free State of Saxony (Catchment and Lake Research).

HOWARD, I. L.; SAUCIER, C. L.; TOM, J. G. (2009): Levee Breach Geometries and Algorithms to Simulate Breach Closure. Civil and Environmental Engineering Department, Mississippi State University. Online available at http://www.cee.msstate.edu, last checked on 26.02.2020.

HUNT, S. L.; HANSON, G. J.; COOK, K. R.; KADAVY, K. C. (2005): BREACH WIDENING OBSERVATIONS FROM EARTHEN EMBANKMENT TESTS. In: *Transactions of the ASAE* 48 (3), p. 1115–1120. DOI: 10.13031/2013.18521.

ICOLD (Ed.) (2012): Internal erosion of existing dams, levees, and dikes, and their foundations - international glossary. 24th ICOLD Congress. Kyoto, Japan. ICOLD (CIGB-ICOLD Bulletin, 1).

IMPACT PROJECT (Ed.) (2004): Investigation of Extreme Flood Processes and Uncertainty. 4th IMPACT Project Workshop. Zaragoza, ESP, 3-5 November.

INTERGOVERNMENTAL PANEL ON CLIMATE CHANGE (IPCC) (2023): Climate Change 2023: Synthesis Report. Contribution of Working Groups I, II and III to the Sixth Assessment Report of the Intergovernmental Panel on Climate Change. In collaboration withCore Writing Team. Eds. by H. Lee und J. J. Romero. Geneva, Switzerland.

INTERNATIONAL BANK FOR RECONSTRUCTION AND DEVELOPMENT (1964): The Ethiopian Electric Light and Power Authority project. Online available at http://documents.worldbank.org/curated/en/305181468251412332/pdf/multi-page.pdf.

INTERNATIONAL COMMISSION ON LARGE DAMS (ICOLD) (2017): Internal erosion of existing dams, levees, and dikes, and their foundations. Paris, France (Bulletin 164). Online available at http://www.ussdams.org/wp-content/uploads/2016/04/B164.pdf.

ISLAM, S. (2012): Study on levee breach and successive disasters in low-land through numerical and experimental approaches. Doctoral thesis. NAGOYA UNIVERSITY, Japan. Department of Civil Engineering. Online available at http://hdl.handle.net/2237/17336, last checked on 09.09.2020.

JANDORA, J.; RÍHA, J. (2008): The failure of embankment dams due to overtopping.

JIANG, S.-H.; HUANG, Z.-F.; HUANG, J. (2020): Dike-Break Induced Flood Simulation and Consequences Assessment in Flood Detention Basin. In: Jian-Min Zhang, Limin Zhang und Rui Wang (Eds.): Dam breach modelling and risk disposal. Cham, 2020. Cham: Springer International Publishing, p. 295–310.

Joint Federal Interagency Conference on Sedimentation and Hydrologic Modeling (2010). Las Vegas, NV, June 27 - July 1.

KAKINUMA, T.; SHIMIZU, Y. (2014): Large-Scale Experiment and Numerical Modeling of a Riverine Levee Breach. In: *J. Hydraul. Eng.* 140 (9), p. 4014039. DOI: 10.1061/(ASCE)HY.1943-7900.0000902.

KALYANAPU, A. J.; JUDI, D. R.; MCPHERSON, T. N.; BURIAN, S. J. (2012): Monte Carlo-based flood modelling framework for estimating probability weighted flood risk. In: *J Flood Risk Management* 5 (1), p. 37–48. DOI: 10.1111/j.1753-318X.2011.01123.x.

KAMRATH, P.; DISSE, M.; HAMMER, M.; KÖNGETER, J. (2006): Assessment of Discharge through a Dike Breach and Simulation of Flood Wave Propagation. In: *Nat Hazards* 38 (1-2), p. 63–78. DOI: 10.1007/s11069-005-8600-x.

KORTENHAUS, A.; OUMERACI, H. (2002a): Probabilistische Bemessungsmethoden für Seedeiche (ProDeich). - Anlagenband -. Technische Universität Braunschweig, Leichtweiss - Leichtweiss Institut für Wasserbau (Bericht, 877).

KORTENHAUS, A.; OUMERACI, H. (2002b): Probabilistische Bemessungsmethoden für Seedeiche (ProDeich). Technische Universität Braunschweig, Leichtweiss - Leichtweiss Institut für Wasserbau (Bericht, 877).

KORTENHAUS, A.; OUMERACI, H.; WEISSMANN, R.; RICHWIEN, W. (2002): Failure mode and fault tree analysis for sea and estuary dikes. In: Jane McKee Smith (Ed.): Proceedings of the 28th international conference. Solving coastal conundrums. Proceedings of the 28th International Conference. Cardiff, Wales, 7 – 12 July 2002. Coastal engineering 2002 (ICCE 2002). River Edge, NJ: World Scientific, p. 2386–2398.

KUMAR, P.; LAI, S. H.; MOHD, N. S.; KAMAL, M. R.; AFAN, H. A.; AHMED, A. N. ET AL. (2020): Basic structure of ANN model. PLOS ONE. Online available at https://figshare.com/articles/figure/Basic_structure_of_ANN_model_/13014973/1, last checked on 18.03.2022.

LI, G. X.; JIE, Y. X.; LI, Q. Y. (2003): Yangtze dyke and its strengthening. In: *Lowland Technology Internationa* 5 (2), p. 39–46. Online available at http://cot.unhas.ac.id/journals/index.php/ialt_lti/article/view/317/219.

LI, S.; DUFFY, C. J. (2011): Fully coupled approach to modeling shallow water flow, sediment transport, and bed evolution in rivers. In: *Water Resour. Res.* 47 (3), p. 61. DOI: 10.1029/2010WR009751.

LIN, L.; JINREN, N. I.; BORTHWICK, A. G. L.; ROGERS, B. D. (2002): Simulation of dike-break processes in the Yellow River. In: *Science in China Series E-Technological Sciences* 45 (6), p. 606–619. DOI: 10.1360/02ye9069.

LIN, M. C.; MANOCHA, D. (Eds.) (1996): Applied computational geometry: towards geometric engineering: Springer-Verlag (Lecture Notes in Computer Science, 1148).

LIU, W.-C.; WU, C.-Y. (2011): Flash flood routing modeling for levee-breaks and overbank flows due to typhoon events in a complicated river system. In: *Nat Hazards* 58 (3), p. 1057–1076. DOI: 10.1007/s11069-010-9711-6.

LIU, Z. (2015): Hydro-mechanical analysis of breach processes due to levee failure. Doctoral thesis. UNIVERSITY OF AIX-MARSEILLE. Doctoral School Science for Engineers: Mechanics, Physics, Micro and Nanoelectronics.

MAHMOUD, M. T.; BUKHARY, A. H.; RAMADAN, A. G.; AL-ZAHRANI, M. A. (2017): Prediction of Breach Peak Outflow and Failure Time Using Artificial Neural Network Approach. In: H. El Naggar und M. Shahin (Eds.): Proceedings of the 2nd World Congress on Civil, Structural, and Environmental Engineering. The 2nd World Congress on Civil, Structural, and Environmental Engineering, 4/2/2017 - 4/4/2017: Avestia Publishing (World Congress on Civil, Structural, and Environmental Engineering).

MARSALEK, J.; STANCALIE, GHEORGHE; BALINT, GABOR (Eds.) (2006): Transboundary floods. Reducing risks through flood management. North Atlantic Treaty Organization. Public Diplomacy Division. Dordrecht: Springer (NATO science series. Series IV, Earth and environmental sciences v. 72).

MASOERO, A.; CLAPS, P.; ASSELMAN, N. E. M.; MOSSELMAN, E.; DI BALDASSARRE, G. (2013): Reconstruction and analysis of the Po River inundation of 1951. In: *Hydrol. Process.* 27 (9), p. 1341–1348. DOI: 10.1002/hyp.9558.

MAY, R. J.; MAIER, H. R.; DANDY, G. C. (2010): Data splitting for artificial neural networks using SOM-based stratified sampling. In: *Neural networks: the official journal of the International Neural Network Society* 23 (2), p. 283–294. DOI: 10.1016/j.neunet.2009.11.009.

MERZ, B.; ELMER, F.; KUNZ, M.; MÜHR, B.; SCHRÖTER, K.; UHLEMANN-ELMER, S. (2014): The extreme flood in June 2013 in Germany. In: *La Houille Blanche* 57 (1), p. 5–10. DOI: 10.1051/lhb/2014001.

MEYER-PETER, E.; MÜLLER, R. (1948): Formulas for Bed-Load transport. In: *IAHSR 2nd meeting, Stockholm, appendix 2*. Online available at https://repository.tudelft.nl/islandora/object/uuid%3A4fda9b61-be28-4703-ab06-43cdc2a21bd7/datastream/OBJ/download.

MICHELAZZO, G. (2014): Breaching of River Levees: Analytical Flow Modelling and Experimental Hydro-Morphodynamic Investigations. Doctoral thesis. UNIVERSITY OF BRAUNSCHWEIG – INSTITUTE OF TECHNOLOGY, UNIVERSITY OF FLORENCE, last checked on 27.08.2020.

MICHELAZZO, G.; PARIS, E.; SOLARI, L. (2018): On the vulnerability of river levees induced by seepage. In: *Journal of Flood Risk Management* 11, S677-S686. DOI: 10.1111/jfr3.12261.

MIZUTANI, H.; NAKAGAWA, H.; YODEN, T.; KAWAIKE, K.; ZHANG, H. (2013): Numerical modelling of river embankment failure due to overtopping flow considering infiltration effects. In: *Journal of Hydraulic Research* 51 (6), p. 681–695. DOI: 10.1080/00221686.2013.812151.

MOHAMED, M. A.; SAMUELS, P. G.; MORRIS, M. W.; GHATAORA, G. S. (2002): Improving the accuracy of prediction of breach formation through embankment dams and flood embankments. In: D. Ed Bousmar und Y. Ed Zech (Eds.): River flow 2002. Proceedings of the international conference on fluvial hydraulics, Vol. 1. Louvain-la-Neuve, Belgium, 4-6 September. Lisse, The Netherlands: Swets & Zeitlinger, p. 663–673.

MORRIS, M. W.; HASSAN, M.; VASKINN, K. A. (2007): Breach formation: Field test and laboratory experiments. In: *Journal of Hydraulic Research* 45 (sup1), p. 9–17. DOI: 10.1080/00221686.2007.9521828.

MORRIS, M. W.; KORTENHAUS, A.; VISSER, P. J. (2009): Modeling breach initiation and growth. FLOODsite Rep. T06–08-02. FLOODsite Consortium. Online available at http://www.floodsite.net/.

MOULINEC, CHARLES; EMERSON, DAVID (Eds.) (2015): Proceedings of the XXII TELEMAC-MASCARET Technical User Conference. In collaboration withTELEMAC-MASCARET Core Group. TELEMAC-MASCARET Technical User Conference. Warrington: STFC Daresbury Laboratory., October 15-16.

MURILLO, J.; GARCÍA-NAVARRO, P. (2010): An Exner-based coupled model for two-dimensional transient flow over erodible bed. In: *Journal of Computational Physics* 229 (23), p. 8704–8732. DOI: 10.1016/j.jcp.2010.08.006.

NAGY, L. (2006a): Dike breaches in the Carpathian basin. In: *Periodica Polytechnica Civil Engineering* 50 (2), p. 115–124. Online available at https://pp.bme.hu/ci/article/view/562.

NAGY, L. (2006b): Estimating Dike Breach Length from Historical Data. In: *Periodica Polytechnica Civil Engineering* 50 (2), p. 125–139. Online available at https://pp.bme.hu/ci/article/view/563.

NATIONAL RESEARCH COUNCIL CANADA (NRCC) (2019): Blue Kenue™: software tool for hydraulic modellers. NATIONAL RESEARCH COUNCIL CANADA. Online available at https://nrc.canada.ca/en/research-development/products-services/software-applications/blue-kenuetm-software-tool-hydraulic-modellers, last updated on 19.03.2019, last checked on 26.10.2021.

NIKURADSE, J. (1933): Laws of Flow in Rough Pipes (NACA-TM-1292). Online available at https://ntrs.nasa.gov/api/citations/19930093938/downloads/19930093938.pdf.

NOURANI, V.; HAKIMZADEH, H.; AMINI, A. B. (2012): Implementation of artificial neural network technique in the simulation of dam breach hydrograph. In: *Journal of Hydroinformatics* 14 (2), p. 478–496. DOI: 10.2166/hydro.2011.114.

ONDA, S.; HOSODA, T.; JAĆIMOVIĆ, N. M.; KIMURA, I. (2019): Numerical modelling of simultaneous overtopping and seepage flows with application to dike breaching. In: *Journal of Hydraulic Research* 57 (1), p. 13–25. DOI: 10.1080/00221686.2018.1442882.

OPEN TELEMAC-MASCARET (TELEMAC) (2019a): Telemac-2D - Two-dimensional hydrodynamic. Online available at http://www.opentelemac.org/index.php/presentation?id=17, last checked on 22.08.2019.

OPEN TELEMAC-MASCARET (TELEMAC) (2019b): Telemac-2D validation manual. Online available at https://gitlab.pam-retd.fr/otm/telemac-mascaret/-/blob/v8p1r1/documentation/telemac2d/validation/telemac2d_validation_v8p1.pdf, last checked on 07.12.2024.

ORLANDINI, S.; MORETTI, G.; ALBERTSON, J. D. (2015): Evidence of an emerging levee failure mechanism causing disastrous floods in Italy. In: *Water Resour. Res.* 51 (10), p. 7995–8011. DOI: 10.1002/2015WR017426.

OUBENNACEUR, K.; CHOKMANI, K.; NASTEV, M.; TANGUY, M.; RAYMOND, S. (2018): Uncertainty Analysis of a Two-Dimensional Hydraulic Model. In: *Water* 10 (3), p. 272. DOI: 10.3390/w10030272.

ÖZER, I. E.; VAN DAMME, M.; JONKMAN, S. N. (2020): Towards an International Levee Performance Database (ILPD) and Its Use for Macro-Scale Analysis of Levee Breaches and Failures. In: *Water* 12 (1), p. 1–22. DOI: 10.3390/w12010119.

PAOLA, C.; VOLLER, V. R. (2005): A generalized Exner equation for sediment mass balance. In: *J. Geophys. Res.* 110 (F4), n/a-n/a. DOI: 10.1029/2004JF000274.

PAPPENBERGER, F.; MATGEN, P.; BEVEN, K. J.; HENRY, J.-B.; PFISTER, L.; FRAIPONT, P. (2006): Influence of uncertain boundary conditions and model structure on flood inundation predictions. In: *Advances in Water Resources* 29 (10), p. 1430–1449. DOI: 10.1016/j.advwatres.2005.11.012.

PAQUIER, A.; BÉRAUD, C. (2010): Validating a simplified model for flood hazard downstream levees. In: Andreas Dittrich (Ed.): River Flow 2010. Proceedings of the 5th International Conference on Fluvial Hydraulics. International Conference on Fluvial Hydraulics. Braunschweig, Germany. Karlsruhe: Bundesanst. für Wasserbau, p. 591–597.

PAQUIER, A.; RECKING, A. (2004): Advances on breach models by Cemagref during IMPACT Project. In: IMPACT Project (Ed.): Investigation of Extreme Flood Processes and Uncertainty. 4th IMPACT Project Workshop. Zaragoza, ESP, 3-5 November, p. 12, last checked on 14.05.2020.

PENG, M.; ZHANG, L. M. (2015): Breaching of Changkai Levee in June 2010 in Jiangxi Province, China.

PIASECKI, MICHAEL (Ed.) (2015): Proceedings of the 11th International Conference on Hydroinformatics (HIC 2014): Informatics and the Environment: Data and Model Integration in a Heterogeneous Hydro World. International Conference on Hydroinformatics. New York, USA, 17 - 21 August 2014. INTERNATIONAL CONFERENCE ON HYDROINFORMATICS; HIC. 4 Bände. Red Hook, NY: Curran.

PONTILLO, M.; SCHMOCKER, L.; GRECO, M.; HAGER, W. H. (2010): 1D numerical evaluation of dike erosion due to overtopping. In: *Journal of Hydraulic Research* 48 (5), p. 573–582. DOI: 10.1080/00221686.2010.507005.

POPESCU, I.; JONOSKI, A.; VAN ANDEL, S. J.; ONYARI, E.; MOYA QUIROGA, V. G. (2010): Integrated modelling for flood risk mitigation in Romania: case study of the Timis–Bega River basin. In: *International Journal of River Basin Management* 8 (3-4), p. 269–280. DOI: 10.1080/15715124.2010.512550.

RAHMAN, M.; VERHOEVEN, R.; BREBBIA, C. A. (Eds.) (2002): Advances in fluid mechanics IV. Southampton: WIT (International series on advances in fluid mechanics, 1353-808X, 32).

RANZI, R.; BARONTINI, S.; MAZZOLENI, M.; FERRI, M.; BACCHI, B. (2012): Levee breaches and “geotechnical uncertainty" in flood risk mapping. Online available at https://www.researchgate.net/publication/247768635_Levee_breaches_and_geotechnical_uncertainty_in_flood_risk_mapping/link/00463528541721db8b000000/download?_tp=eyJjb250ZXh0Ijp7InBhZ2UiOiJwdWJsaWNhdGlvbiIsInByZXZpb3VzUGFnZSI6bnVsbH19, last checked on 07.12.2024.

RIFAI, I.; ERPICUM, S.; ARCHAMBEAU, P.; VIOLEAU, D.; PIROTTON, M.; EL KADI ABDERREZZAK, K.; DEWALS, B. (2017): Overtopping induced failure of noncohesive, homogeneous fluvial dikes. In: *Water Resour. Res.* 53 (4), p. 3373–3386. DOI: 10.1002/2016WR020053.

RISHER, P.; GIBSON, S. (2016): Applying Mechanistic Dam Breach Models to Historic Levee Breaches. In: *E3S Web Conf.* 7, p. 3002. DOI: 10.1051/e3sconf/20160703002.

RODI, W. (1993): Turbulence models and their application in hydraulics. A state-of-the-art review. 3. Editions. Rotterdam: Balkema (IAHR monograph series).

ROGER, S. (2011): Hybride Modellierung deichbruchinduzierter Strömungen für ein idealisiertes Breschennahfeld an Fließgewässern. Doctoral Thesis. RWTH AACHEN UNIVERSITY, Aachen. Institute of Hydraulic Engineering and Water Resources Management. Online available at http://publications.rwth-aachen.de/record/459436/files/3876.pdf.

ROGER, S.; BÜSSE, E.; KÖNGETER, J. (2007): Dike-break induced flood wave propagation. In: Philippe Gourbesville, Jean Cunge und Vincent Guinot (Eds.): Hydroinformatics 2006: Proceedings of the 7th International Conference. International Conference on Hydroinformatics. Nice, France, 4 - 8 September, 2006. Singapore: Research Publishing.

ROGER, S.; DEWALS, B. J.; ERPICUM, S.; SCHWANENBERG, D.; SCHÜTTRUMPF, H.; KÖNGETER, J.; PIROTTON, M. (2009): Experimental and numerical investigations of dike-break induced flows. In: *Journal of Hydraulic Research* 47 (3), p. 349–359. DOI: 10.1080/00221686.2009.9522006.

ROGER, S.; KÖNGETER, J.; SCHÜTTRUMPF, H.; ERPICUM, S.; ARCHAMBEAU, P.; PIROTTON, M. ET AL. (2010): Hybrid modelling of dike-break induced flows. In: Andreas Dittrich (Ed.): River Flow 2010. Proceedings of the 5th International Conference on Fluvial Hydraulics. International Conference on Fluvial Hydraulics. Braunschweig, Germany. Karlsruhe: Bundesanst. für Wasserbau, p. 523–531. Online available at https://hdl.handle.net/20.500.11970/99685.

SAMMEN, S. S.; MOHAMED, T. A.; GHAZALI, A. H.; EL-SHAFIE, A. H.; SIDEK, L. M. (2017): Generalized regression neural network for prediction of peak outflow from dam breach. In: *Water Resour Manage* 31 (1), p. 549–562. DOI: 10.1007/s11269-016-1547-8.

SCHOBEIRI, M. T. (2010): Fluid mechanics for engineers. Berlin, Heidelberg: Springer Berlin Heidelberg.

SEABOLD, S.; PERKTOLD, J. (2010): Statsmodels: Econometric and statistical modeling with python. In: S. van der Walt und J. Millman (Eds.): Proceedings of the 9th python in science conference. Python in Science Conference. Austin, Texas, June 28 - July 3 2010: SciPy (Proceedings of the Python in Science Conference), p. 92–96. Online available at https://www.statsmodels.org/stable/index.html.

SELLMEIJER, H.; LA CRUZ, J. L. DE; VAN BEEK, V. M.; KNOEFF, H. (2011): Fine-tuning of the backward erosion piping model through small-scale, medium-scale and IJkdijk experiments. In: *European Journal of Environmental and Civil Engineering* 15 (8), p. 1139–1154. DOI: 10.1080/19648189.2011.9714845.

SELLMEIJER, J. B. (1988): On the mechanism of piping under impervious structures. Doctoral thesis. DELFT TECHNICAL UNIVERSTY, Delft, The Netherlands.

SELLMEIJER, J. B.; KOENDERS, M. A. (1991): A mathematical model for piping. In: *Applied Mathematical Modelling* 15 (11-12), p. 646–651. DOI: 10.1016/S0307-904X(09)81011-1.

SEMMENS, S. N.; ZHOU, W. (2019): Evaluation of environmental predictors for sand boil formation: Rhine–Meuse Delta, Netherlands. In: *Environ Earth Sci* 78 (15), p. 1–11. DOI: 10.1007/s12665-019-8464-0.

SGEM2015 (Ed.) (2015): 15th International Multidisciplinary Scientific GeoConference, Water Resources. Forest, Marine and Ocean Ecosystems. 15th International Multidisciplinary Scientific GeoConference SGEM2015, June 18, 2015: Stef92 Technology (SGEM International Multidisciplinary Scientific GeoConference EXPO Proceedings).

SHAHIN, M. M. A. (1993): An overview of reservoir sedimentation in some African river basins. In: Richard F. Hadley und T. Mizuyama (Eds.): Sediment problems: Strategies for monitoring, prediction, and control. Proceedings of an international symposium. Yokohama, Japan, 19-21 July. International Association of Hydrological Sciences. Wallingford: International Association of Hydrological Sciences (IAHS Publication, 217), p. 93–100.

SHARIF, Y. A.; ELKHOLY, M.; HANIF CHAUDHRY, M.; IMRAN, J. (2015): Experimental study on the piping erosion process in earthen embankments. In: *J. Hydraul. Eng.* 141 (7), p. 4015012. DOI: 10.1061/(ASCE)HY.1943-7900.0001019.

SHEWCHUK, J. R. (1996): Triangle: Engineering a 2D quality mesh generator and delaunay triangulator. In: M. C. Lin und D. Manocha (Eds.): Applied computational geometry: towards geometric engineering, Vol. 1148: Springer-Verlag (Lecture Notes in Computer Science, 1148), p. 203–222. Online available at https://www.cs.cmu.edu/~quake/tripaper/triangle0.html, last checked on 26.04.2022.

SHUSTIKOVA, I.; NEAL, J. C.; DOMENEGHETTI, A.; BATES, P. D.; VOROGUSHYN, S.; CASTELLARIN, A. (2020): Levee breaching: A new extension to the LISFLOOD-FP model. In: *Water* 12 (4), p. 942. DOI: 10.3390/w12040942.

SILLS, G. L.; VROMAN, N. D.; WAHL, R. E.; SCHWANZ, N. T. (2008): Overview of New Orleans levee failures: Lessons learned and their impact on national levee design and assessment. In: *J. Geotech. Geoenviron. Eng.* 134 (5), p. 556–565. DOI: 10.1061/(ASCE)1090-0241(2008)134:5(556).

SMITH, JANE MCKEE (Ed.) (2002): Proceedings of the 28th international conference. Solving coastal conundrums. Proceedings of the 28th International Conference. Cardiff, Wales, 7 – 12 July 2002. COASTAL ENGINEERING 2002 (ICCE 2002). River Edge, NJ: World Scientific.

SWARTENBROEKX, C.; SOARES-FRAZÃO, S.; STAQUET, R.; ZECH, Y. (2010): Two-dimensional operator for bank failures induced by water-level rise in dam-break flows. In: *Journal of Hydraulic Research* 48 (3), p. 302–314. DOI: 10.1080/00221686.2010.481856.

TABRIZI, A. A. (2016): Modeling embankment breach due to overtopping. Doctoral dissertation. UNIVERSITY OF SOUTH CAROLINA. Online available at https://scholarcommons.sc.edu/etd/3958, last checked on 21.08.2020.

TADESSE, Y.; FRÖHLE, P. (2015): An integrated approach to simulate flooding due to river dike breach. In: Michael Piasecki (Ed.): Proceedings of the 11th International Conference on Hydroinformatics (HIC 2014): Informatics and the Environment: Data and Model Integration in a Heterogeneous Hydro World. International Conference on Hydroinformatics. New York, USA, 17 - 21 August 2014. International Conference on Hydroinformatics; HIC. 4 Bände. Red Hook, NY: Curran, p. 418–425. Online available at https://academicworks.cuny.edu/cc_conf_hic/55.

TADESSE, Y.; FRÖHLE, P. (2017): Modelling of river dike breach type physical test flow with Telemac-2D. In: C. Dorfmann und G. Zenz (Eds.): Proceedings of the 24th TELEMAC-MASCARET User Conference. Graz University of Technology, Austria, 17 - 20 October. Graz University of Technology. Graz, Austria: Verlag der Technischen Universität Graz, p. 107–112.

TADESSE, Y. B.; FRÖHLE, P. (2020): Modelling of flood inundation due to levee breaches: Sensitivity of flood inundation against breach process parameters. In: *Water* 12 (12), p. 3566. DOI: 10.3390/w12123566.

THOMPSON, A.; GUO, Y.; MOIN, S. (2008): Uncertainty analysis of a two-dimensional hydrodynamic model. In: *Journal of Great Lakes Research* 34 (3), p. 472–484. DOI: 10.3394/0380-1330(2008)34[472:UAOATH]2.0.CO;2.

TOLA, S. Y.; SHETTY, A. (2021): Land cover change and its implication to hydrological regimes and soil erosion in Awash River basin, Ethiopia: a systematic review. In: *Environ Monit Assess* 193 (12), p. 836. DOI: 10.1007/s10661-021-09599-6.

TÓTH, S.; NAGY, L. (2006): Dyke failures in Hungary of the past 220 years. In: J. Marsalek, Gheorghe Stancalie und Gabor Balint (Eds.): Transboundary floods. Reducing risks through flood management. Dordrecht: Springer (NATO science series. Series IV, Earth and environmental sciences v. 72), p. 247–258.

U.S. ARMY CORPS OF ENGINEERS (USACE) (2000): Design and construction of levees (Manual No. 1110-2-1913), last checked on 05.11.2019.

U.S. DEPT. OF THE INTERIOR BUREAU OF RECLAMATION (U.S. BUREAU OF RECLAMATION) (1988): Downstream hazard classifciation guidelines. Denver, Colorado (Acer technical

memorandum, 11). Online available at https://www.google.com/url?sa=t&rct=j&q=&esrc=s&source=web&cd=&ved=2ahUKEwioqK_v-b7uAhWPH-wKHRyGC44QFjAAegQIAhAC&url=https%3A%2F%2Fwww.arcc.osmre.gov%2Fresources%2Fimpoundments%2FUSBR-TechMemo11-DownstreamHazardClassificationGuidelines1988.pdf&usg=AOvVaw31nc5EbIFu9SYPSCienGkN, last checked on 07.12.2024.

VACONDIO, R.; AURELI, F.; FERRARI, A.; MIGNOSA, P.; DAL PALÙ, A. (2016): Simulation of the January 2014 flood on the Secchia River using a fast and high-resolution 2D parallel shallow-water numerical scheme. In: *Natural Hazards* 80 (1), p. 103–125. DOI: 10.1007/s11069-015-1959-4.

VAN BAARS, S.; VAN KEMPEN, I. M. (2009): The causes and mechanisms of historical dike failures in The Netherlands. European Water Association (EWA) (E-Water).

VAN BEEK, V. M.; DE BRUIJN, H. T. J.; KNOEFF, J. G.; BEZUIJEN, A.; FÖRSTER, U. (2010): Levee failure due to piping: A full-scale experiment. In: S. E. Burns, S. K. Bhatia, C. M. C. Avila und B. E. Hunt (Eds.): Proceedings of the 5th International Conference on Scour and Erosion (ICSE-5). San Francisco, USA., November 7-10. Reston, Va.: American Society of Civil Engineers, p. 283–292. Online available at https://hdl.handle.net/20.500.11970/100310, last checked on 25.02.2020.

VAN BEEK, V. M.; KNOEFF, H.; SELLMEIJER, H. (2011): Observations on the process of backward erosion piping in small-, medium- and full-scale experiments. In: *European Journal of Environmental and Civil Engineering* 15 (8), p. 1115–1137. DOI: 10.1080/19648189.2011.9714844.

VAN DER WALT, S.; MILLMAN, J. (Eds.) (2010): Proceedings of the 9th python in science conference. Python in Science Conference. Austin, Texas, June 28 - July 3 2010: SciPy (Proceedings of the Python in Science Conference). Online available at https://doi.org/10.25080/Majora-92bf1922-012.

VAN EMELEN, S.; SOARES-FRAZÃO, S.; RIAHI-NEZHAD, C. K.; HANIF CHAUDHRY, M.; IMRAN, J.; ZECH, Y. (2012): Simulations of the New Orleans 17th Street Canal breach flood. In: *Journal of Hydraulic Research* 50 (1), p. 70–81. DOI: 10.1080/00221686.2011.642578.

VIERO, D. P.; D'ALPAOS, A.; CARNIELLO, L.; DEFINA, A. (2013): Mathematical modeling of flooding due to river bank failure. In: *Advances in Water Resources* 59, p. 82–94. DOI: 10.1016/j.advwatres.2013.05.011.

VISSER, P. J. (1998): Breach growth in sand-dikes. DELFT UNIVERSITY OF TECHNOLOGY, Delft, The Netherlands. Faculity of Civil Engineering, Hydraulic and Geotechnical Engineering Division. Online available at http://resolver.tudelft.nl/uuid:3721e23b-d34c-45a9-8b36-e5930462d8e2.

VOLZ, C. (2013): Numerical simulation of embankment breaching due to overtopping. Doctoral thesis. ETH ZURICH.

VOLZ, C.; ROUSSELOT, P.; VETSCH, D.; FAEH, R. (2012): Numerical modelling of non-cohesive embankment breach with the dual-mesh approach. In: *Journal of Hydraulic Research* 50 (6), p. 587–598. DOI: 10.1080/00221686.2012.732970.

VOROGUSHYN, S.; MERZ, B.; APEL, H. (2009): Development of dike fragility curves for piping and micro-instability breach mechanisms. In: *Nat. Hazards Earth Syst. Sci.* 9 (4), p. 1383–1401. DOI: 10.5194/nhess-9-1383-2009.

VOROGUSHYN, S.; MERZ, B.; LINDENSCHMIDT, K.-E.; APEL, H. (2010): A new methodology for flood hazard assessment considering dike breaches. In: *Water Resour. Res.* 46 (8), p. 125. DOI: 10.1029/2009WR008475.

WAHL, T. (1998): Prediction of embankment dam breach parameters. Literature Review and Needs Assessment. Dam Safety Research Report. U.S. Department of the Interior, Bureau of Reclamation, Dam Safety Office (DSO-98-004). Online available at https://www.nrc.gov/docs/ML0901/ML090150051.pdf, last checked on 07.09.2019.

WAHL, T. L. (2004): Uncertainty of predictions of embankment dam breach parameters. In: *J. Hydraul. Eng.* 130 (5), p. 389–397. DOI: 10.1061/(ASCE)0733-9429(2004)130:5(389).

WAHL, T. L. (2010): Dam breach modeling – an overview of analysis methods. Las Vegas, NV, June 27- July 1, 2010. In: Joint Federal Interagency Conference on Sedimentation and Hydrologic Modeling. Las Vegas, NV, June 27 - July 1.

WEI, H.; YU, M.; WANG, D.; LI, Y. (2016): Overtopping breaching of river levees constructed with cohesive sediments. In: *Nat. Hazards Earth Syst. Sci.* 16 (7), p. 1541–1551. DOI: 10.5194/nhess-16-1541-2016.

WILLIS, T.; WRIGHT, N.; SLEIGH, A. (2019): Systematic analysis of uncertainty in 2D flood inundation models. In: *Environmental Modelling & Software* 122, p. 104520. DOI: 10.1016/j.envsoft.2019.104520.

WU, W. (2013): Simplified physically based model of earthen embankment breaching. In: *J. Hydraul. Eng.* 139 (8), p. 837–851. DOI: 10.1061/(ASCE)HY.1943-7900.0000741.

XIAO, Y.; CAO, H.; LUO, G. (2019): Experimental investigation of the backward erosion mechanism near the pipe tip. In: *Acta Geotech.* 14 (3), p. 767–781. DOI: 10.1007/s11440-019-00779-w.

YALÇIN, O. G. (2021): Applied neural networks with TensorFlow 2. API Oriented Deep Learning with Python. 1st ed. 2021. Berkeley CA: Apress; Imprint: Apress.

YU, M.; WEI, H.; LIANG, Y.; ZHAO, Y. (2013): Investigation of non-cohesive levee breach by overtopping flow. In: *Journal of Hydrodynamics, Ser. B* 25 (4), p. 572–579. DOI: 10.1016/S1001-6058(11)60398-4.

ZHANG, J.; LI, Y.; XUAN, G.; WANG, X.; LI, J. (2009): Overtopping breaching of cohesive homogeneous earth dam with different cohesive strength. In: *Sci. China Ser. E-Technol. Sci.* 52 (10), p. 3024–3029. DOI: 10.1007/s11431-009-0275-1.

ZHANG, JIAN-MIN; ZHANG, LIMIN; WANG, RUI (Eds.) (2020): Dam breach modelling and risk disposal. Cham, 2020. Cham: Springer International Publishing. Online available at 10.1007/978-3-030-46351-9.

ZHANG, L.; CHANG, D.; PENG, M.; XU, Y. (2016a): Dam failure mechanisms and risk assessment. Singapore: John Wiley & Sons. Online available at http://search.ebscohost.com/login.aspx?direct=true&scope=site&db=nlebk&AN=1252117.

ZHANG, LIMIN; PENG, M.; CHANG, D.; XU, YAO (Eds.) (2016b): Dam failure mechanisms and risk assessment: John Wiley & Sons, Ltd.

ZHAO, G. (2016): Breach growth in cohesive embankments due to overtopping. doctoral thesis. DELFT UNIVERSITY OF TECHNOLOGY. Online available at https://repository.tudelft.nl/islandora/object/uuid%3Aee435ef7-f71c-493c-812b-68cf1e39aa33/datastream/OBJ/download.

ZHU, Y. (2006): Breach growth in clay-dikes. Doctoral thesis. TECHNISCHE UNIVERSITEIT DELFT, Enschede. Civil Engineering and Geosciences.

List of Tables

List of Figures

List of Acronyms

ANN	*Artificial neural network*
API	*Application programming interface*
ASCE	*American Society of Civil Engineers*
BCE	*Björnsen Consulting Engineers*
BD	*Breach duration*
BL	*Final levee breach levels*
BP	*Breach location*
BT	*Breach start time*
BW	*Breach width*
CCD	*Charge-Coupled Device*
CFL	*Courant-Friedrichs-Lewy*
CL	*Crest level*
DEM	*Digital elevation model*
DNS	*Direct numerical solution*
EDF R&D	*Electricité de France Research and Development*
ESRI	*Environmental Systems Research Institute, Inc.*
EU	*European Union*
FOSM	*First order second moment*
GIS	*Geographic information system*
GRNN	*Generalised regression artificial neural network*
H:V	*Horizontal to vertical*
ILPD	*International Levee Performance Database*
KHD	*Koka hydropower dam*
LDA	*Laser-Doppler Anemometer*
MAE	*Mean absolute error*
MLP	*Multilayer perceptrons*
MSE	*Mean squared error*
MWE	*Ministry of Water and Energy (Ethiopia)*
n.a.	*Not applicable*

NBI	*Nile basin initiative*
NRCC	*National Research Council Canada*
NS	*Navier-Stokes*
PEM	*Point estimate method*
RANS	*Reynolds Averaged Navier-Stokes*
RMSE	*Root mean square error*
SGD	*Stochastic gradient descent*
TETAZCOMP	*Free surface gradient compatibility*
UNDP	*United Nations Development Programme*
USCS	*Unified soil classification system*
WL	*Water level*
WSSF	*Wonji Shoa Sugar Factory*

Appendix 1
An example of BREACHES DATA FILE

```
# Number of BREACHES
 3
# Breach 1, this breach is an example for breach initiation option 1
# Width of Polygon defining the breaches
50.000
# Option for breach initiation
1
# Start time of breach initiation
1339200.0
# Breach duration in seconds (0.0 = instantaneous)
3600.0
# Levee lowering option
2
# Final level of breach
1545.7
# Number of points on the levee axis where the breach will appear
4
# Coordinates of the mesh nodes on the levee axis
525931.750000 935888.000000
525932.437500 935889.375000
525933.062500 935890.687500
525933.687500 935892.062500
# Breach 2, this breach is an example for breach initiation option 2
# Width of Polygon defining the breaches
50.000
# Option for breach initiation
2
# Breach duration in seconds (0.0 = instantaneous)
3600.0
# Levee lowering option
2
# Final level of breach
1545.700
# Control level, Water level initiating the breach
1548.700
# Number of points on the levee axis where the breach will appear
6
# Coordinates of the mesh nodes on the levee axis
525940.187500 935905.625000
525940.812500 935906.937500
525941.437500 935908.312500
525942.125000 935909.687500
525942.750000 935911.000000
525943.375000 935912.375000
```

```
# Breach 3, this breach is an example for breach initiation option 3
# Width of Polygon defining the breaches
50.0
# Option for breach initiation
3
# Breach duration in seconds (0.0 = instantaneous)
3600.0
# Levee lowering option
2
# Final level of the breach
1545.700
# Global mesh node number of the point controlling the breach
 33818
# Water level initiating the breach at the point controlling the breach
1548.700
# Number of points on the levee axis where the breach will appear
5
# Coordinates of the mesh nodes on the levee axis
525937.937500 935947.375000
525937.062500 935948.562500
525936.187500 935949.812500
525935.375000 935951.062500
525934.500000 935952.250000
```

Appendix 2

Steering file used for the simulations of the August 1996 Wonji levee breach flooding

```
/-----------------------------------------------------
/               STEERING FILE OF TELEMAC 2D
/-----------------------------------------------------
BOUNDARY CONDITIONS FILE         : rev04_Awash_Koka2Awash.cli
GEOMETRY FILE                    : geo_rev04_Awash_Koka2Awash.slf
RESULTS FILE                     : res_rev04_Awash_Koka2Awash.slf
LIQUID BOUNDARIES FILE           : rev04_Awash_Koka2Awash.qls
STAGE-DISCHARGE CURVES FILE      : rev04_Awash_Koka2Awash.slq
SECTIONS INPUT FILE              : rev04_Awash_Koka2Awash.sec
SECTIONS OUTPUT FILE             : rev04_Awash_Koka2Awash_out.sec
/
TITLE = 'rev04_Awash_Koka2Awash'
VARIABLES FOR GRAPHIC PRINTOUTS  = 'U,V,H,S,B'
GRAPHIC PRINTOUT PERIOD  = 900
LISTING PRINTOUT PERIOD  = 900
MASS-BALANCE             = YES
TIME STEP                = 1.0
DURATION                 = 2246400.0
INFORMATION ABOUT SOLVER = YES
ORIGINAL DATE OF TIME    = 1996;08;08
ORIGINAL HOUR OF TIME    = 12;00;00
/-----------------------------------------------------
/  INITIAL CONDITIONS
/-----------------------------------------------------
COMPUTATION CONTINUED = NO
INITIAL CONDITIONS = 'CONSTANT ELEVATION'
INITIAL ELEVATION      = 1535.0
/-----------------------------------------------------
/  BOUNDARY CONDITIONS
/-----------------------------------------------------
STAGE-DISCHARGE CURVES = 1;0
BREACH                 = YES
BREACHES DATA FILE     = rev04_Awash_Koka2Awash.dkb
/-----------------------------------------------------
/  PHYSICAL PARAMETERS
/-----------------------------------------------------
TURBULENCE MODEL               = 1
VELOCITY DIFFUSIVITY           = 2.0
LAW OF BOTTOM FRICTION         = 5
FRICTION COEFFICIENT           = 0.10
WATER DENSITY                  = 1000.0
```

```
/-----------------------------------------------------
/  NUMERICAL PARAMETERS
/-----------------------------------------------------
EQUATIONS                    = 'SAINT-VENANT FE'
DISCRETIZATIONS IN SPACE     = 11;11
FREE SURFACE GRADIENT COMPATIBILITY      = 0.9
TREATMENT OF THE LINEAR SYSTEM   = 2
SOLVER                       = 1
SOLVER OPTION                = 2
SOLVER ACCURACY              = 1.0E-6
MAXIMUM NUMBER OF ITERATIONS FOR SOLVER  = 100
NUMBER OF SUB-ITERATIONS FOR NON-LINEARITIES = 1
TIDAL FLATS                  = YES
OPTION FOR THE TREATMENT OF TIDAL FLATS     = 1
TREATMENT OF NEGATIVE DEPTHS     = 1
THRESHOLD FOR NEGATIVE DEPTHS    = 0.0
ADVECTION                    = YES
TYPE OF ADVECTION            = 1;5
SUPG OPTION                  = 0;0
CONTINUITY CORRECTION        = YES
MASS-LUMPING ON H            = 1.0
H CLIPPING                   = NO
COMPATIBLE COMPUTATION OF FLUXES = YES
&ETA
```

Appendix 3

Parameters used to calculate the critical hydraulic gradient using equation (1).

Parameter	Meaning	Used value (reference)
L	Seepage length [m]	15
d_{70}	Grain size for which 70% (by weight) of the soil is finer [m]	$4.30*10^{-04}$ (Sellmeijer et al. 2011)
ρ_s	Density of the sand [kg/m³]	2600 (Sellmeijer et al. 2011)
ρ_w	Density of water [kg/m³]	1000
η	White's drag coefficient [-]	0.25 (Sellmeijer et al. 2011)
θ	Angle of repose of sand [°]	37 (Sellmeijer et al. 2011)
D	Thickness of the sand layer under the embankment or the foundation [m]	1
ν	Kinematic viscosity of water [m²/s]	10^{-6}
g	Acceleration due to gravity [m/s²].	9.81
k	Hydraulic conductivity of sand (m/s)	$1.76*10^{-04}$ (Sellmeijer et al. 2011)

27

WASSERBAU
River and Coastal Engineering

DOI: 10.15480/882.14128

TUHH
Hamburg
University of
Technology